СИБИРСКИЙ ЖУРНАЛ НАУКИ И ТЕХНОЛОГИЙ
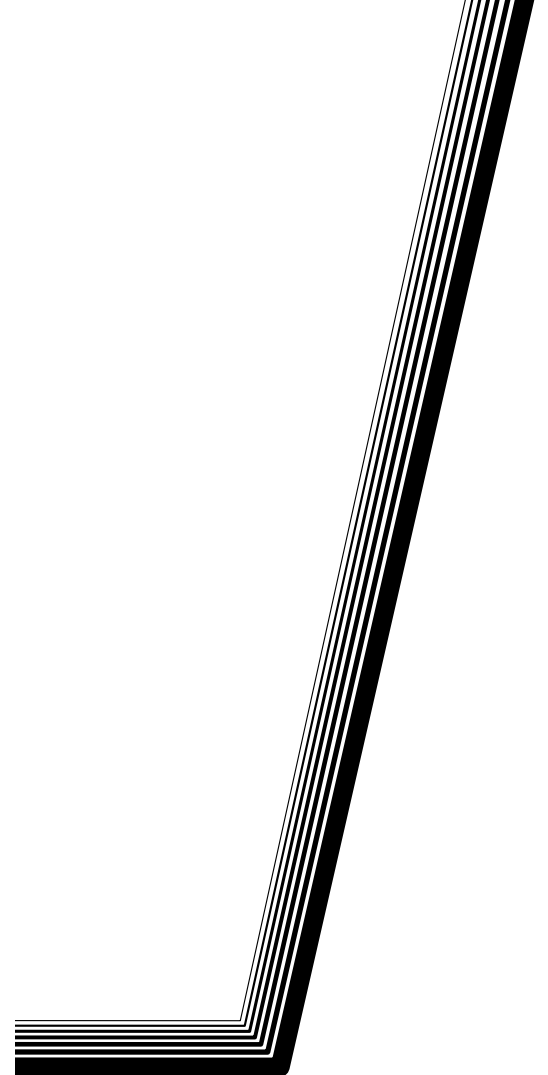
SIBERIAN JOURNAL OF SCIENCE AND TECHNOLOGY

Том
Vol. **21**, № **3**

СИБИРСКИЙ ЖУРНАЛ НАУКИ И ТЕХНОЛОГИЙ

Том 21, № 3

СИБИРСКИЙ ЖУРНАЛ НАУКИ И ТЕХНОЛОГИЙ

Том 21, № 3

СОДЕРЖАНИЕ

CONTENTS

PART 1. INFORMATICS, COMPUTER TECHNOLOGY AND MANAGEMENT

PART 2. AVIATION AND SPACECRAFT ENGINEERING

PART 3. TECHNOLOGICAL PROCESSES AND MATERIAL SCIENCE

ИНФОРМАТИКА,
ВЫЧИСЛИТЕЛЬНАЯ
ТЕХНИКА И УПРАВЛЕНИЕ

INFORMATICS,
COMPUTER TECHNOLOGY
AND MANAGEMENT

MATHEMATICAL MODEL OF RELIABILITY OF INFORMATION PROCESSING COMPUTER APPLIANCES FOR REAL-TIME CONTROL SYSTEMS

A. V. Aab[1], P. V. Galushin[2], A. V. Popova[1*], V. A. Terskov[1]

[1]Reshetnev Siberian State University of Science and Technology
31, Krasnoyarskii rabochii prospekt, Krasnoyarsk, 660037, Russian Federation
[2]Siberian Law Institute of Ministry of Internal Affairs of the Russian Federation
20, Rokossovsky st., Krasnoyarsk, 660131, Russian Federation
*E-mail: anastasiya.popowa@mail.ru

One of the main characteristics of computer appliances for processing real-time information is reliability.

The reliability of software is understood as the property of this software to perform specified functions, maintaining its characteristics within the established limits under certain operating conditions.

Software reliability is determined by its reliability and recoverability.

Reliability of software is a property to maintain its performance when using it for processing information in the information system. The reliability of the software is estimated by the probability of its operation without failures under certain environmental conditions during a given observation period.

The development of real-time systems requires a large amount of resources for design and testing. One of the solutions to this problem is mathematical modeling of computer appliances. This allows more flexible design of real-time systems with the specified reliability, taking into account the limitations on price and development time, and also opens the possibility of more flexible optimization of computer appliances for real-time control systems.

To develop a mathematical model of the reliability of computer appliance for real-time systems, it is necessary to take into account the provision of a given level of reliability, with reasonable development costs.

There are many methods for improving software reliability, but the most promising and effective methods are redundancy, which is achieved using N-version programming.

To increase the reliability of the hardware of the computer appliance, it is also necessary to use redundancy and redundancy, which includes multiprocessor and provision of different buses and independent RAM.

This paper discusses existing approaches to improving the reliability of hardware and software, proposes a model of reliability of a computer appliance, which is understood as the product of the probability of failure-free operation of hardware and the probability of error-free operation of software.

In addition, new formulas are proposed for the steady state probabilities of the hardware states of a multiprocessor computer appliance with heterogeneous processors, which give the same result as the existing ones, but require fewer computations.

The paper concludes with a question about the possibility of optimizing the reliability of computer appliances based on the developed model, and indicates optimization methods that can be used to solve this problem.

Keywords: reliability, software reliability, real-time systems, mathematical model, multiversion programming.

МАТЕМАТИЧЕСКАЯ МОДЕЛЬ НАДЁЖНОСТИ АППАРАТНО-ПРОГРАММНЫХ КОМПЛЕКСОВ ОБРАБОТКИ ИНФОРМАЦИИ ДЛЯ СИСТЕМ УПРАВЛЕНИЯ РЕАЛЬНОГО ВРЕМЕНИ

А. В. Ааб[1], П. В. Галушин[2], А. В. Попова[1*], В. А. Терсков[1]

[1]Сибирский государственный университет науки и технологий имени академика М. Ф. Решетнева
Российская Федерация, г. Красноярск, 660037, просп. им. газ. «Красноярский рабочий», 31
[2]Сибирский юридический институт МВД России
Российская Федерация, г. Красноярск, 660131, ул. Рокоссовского, 20
*E-mail: anastasiya.popowa@mail.ru

Одной из главных характеристик аппаратно-программных систем обработки информации реального времени является надёжность.

Под надёжностью программного обеспечения (ПО) понимается свойство этого обеспечения выполнять заданные функции, сохраняя свои характеристики в установленных пределах при определённых условиях эксплуатации.

Надёжность ПО определяется его безотказностью и восстанавливаемостью.

Безотказность ПО – это свойство сохранять работоспособность при использовании его для обработки информации в информационной системе. Безотказностью программного обеспечения оценивается вероятность его работы без отказов при определённых условиях внешней среды в течение заданного периода наблюдения.

Разработка и проектирование систем реального времени требует большого количества ресурсов на проектирование и тестирование. Одним из решений данной проблемы является математическое моделирование аппаратно-программных комплексов. Это позволяет более гибко проектировать системы реального времени с заданной надёжностью с учётом ограничений по цене и времени разработки, а также открывает возможность более гибкой оптимизации аппаратно-программных систем реального времени.

Для разработки математической модели надёжности аппаратно-программного комплекса систем реального времени необходимо учитывать обеспечение заданного уровня надёжности при целесообразных затратах на разработку.

Существует много методов повышения надёжности программного обеспечения, но наиболее перспективный и эффективный метод – это избыточность, которая достигается за счёт использования мультиверсионного программирования.

Для повышения надёжности аппаратной части комплекса также необходимо использовать избыточность и резервирование, что включает в себя мультипроцессорность и обеспечение разных шин и независимой оперативной памяти.

В данной статье рассматриваются существующие подходы к повышению надёжности аппаратного и программного обеспечения, предлагается модель надёжности аппаратно-программного комплекса, которая понимается как произведение вероятности безотказной работы аппаратного обеспечения и вероятности безошибочной работы программного обеспечения.

Кроме того, предлагаются новые формулы для вероятностей состояний аппаратного обеспечения многопроцессорного вычислительного комплекса с разнородными процессорами в установившемся режиме, дающие тот же результат, что существующие, но требующие меньше вычислений.

В заключении статьи ставится вопрос о возможности оптимизации надёжности аппаратно-программных комплексов на основе построенной модели, указываются методы оптимизации, которые могут быть использованы при решении данной задачи.

Ключевые слова: надёжность, программное обеспечение, системы реального времени, математическая модель, мультиверсионное программирование.

Introduction. Reliability is one of the main characteristics of real-time hardware and software systems for processing information [1–3].

Reliability of software is understood as the ability of this software to perform specified functions, while maintaining its characteristics within established limits under certain operating conditions.

The reliability of the software is determined by its faultlessness and recoverability. Faultlessness of software is a property to maintain operability when using it to process information in an information system (IS). The faultlessness of the software is the probability of its operation without failures under certain environmental conditions during a given observation period.

Real-time systems development requires a lot of design and testing resources. One of the solutions to this problem is mathematical modeling of hardware and software systems. This allows for more flexible design of real-time systems with a given reliability, taking into account the limitations on price and development time, and also opens up the possibility of more flexible optimization of hardware and software complexes of real-time control systems.

With the development of processing power, evolutionary algorithms and neural networks, such models are becoming increasingly relevant.

To develop a mathematical model of the reliability of the hardware and software complex of real-time systems, it is necessary to take into account the provision of a given level of reliability with reasonable development costs.

Reliability of the software. The reliability of the software architecture includes both the reliability of the central system core and the reliability of the individual components provided to the user. Failure of an individual component can lead to the inoperability of this and, possibly, other software components. However, this should not lead to the inoperability of the entire system as a whole. A thorough analysis of the software architecture allows to identify the components, the errors in which have the most significant impact on the reliability of the system. Generally, these are the components most commonly used or architecturally related to many other components. There are a lot of methods for increasing the reliability of software [4; 5], but currently only the multiversion fault-tolerant programming approach is a possible alternative to testing and verification methods, providing a high level of reliability of critical software functioning [6]. It is important to realize that verification does not guarantee correctness, since the specifications and / or verification systems themselves (like any other software) may contain errors.

The use of decision support systems in multiversion programming allows us to focus on the quality of requirements at the stage of creating reliable software. However, improving software reliability characteristics using redundancy requires additional time and financial resources. Therefore, the main question at this stage is how, using redundancy in the software architecture, to maximize reliability and reduce development costs. This area includes methods of multicriteria decision making, focusing on problems with a discrete decision space. Taking into account different levels of information about the expert's preferences, a variety of methodologies for multicriteria decision support have recently been developed. The use of various methods for determining the depth of multiversion and multi-criteria decision-making when choosing an architecture makes it possible to design a software system that meets the requirements.

Depending on the number and size of the components, the conditional and unconditional probabilities of failure, access, analysis and recovery time, as well as the usage time of the components, are different. The model [7], given below, can be used to assess the reliability of software for possible architectural changes, select a reliable architecture from various options and has the following designators:

1) M – number of architectural levels in software architecture;

2) N_j – number of components at level j, $j \in \{1, ..., M\}$;

3) D_{ij} – set of component indices depending on the component i at level j, $i \in \{1, ..., N_j\}, j \in \{1, ..., M\}$;

4) F_{ij} – a failure that occurred in a component i at level j, $i \in \{1, ..., N_j\}, j \in \{1, ..., M\}$;

5) PU_{ij} – probability of using component i at level j, $i \in \{1, ..., N_j\}, j \in \{1, ..., M\}$;

6) PF_{ij} – probability of a failure in a component i at level j, $i \in \{1, ..., N_j\}, j \in \{1, ..., M\}$;

7) PL^{ij}_{nm} – the conditional probability of a failure in component m at level n when a failure occurs in a component i at level j, $i \in \{1, ..., N_j\}, j \in \{1, ..., M\}, n \in \{1, ..., N_m\}, m \in \{1, ..., M\}$;

8) TA_{ij} – relative access time to the component i at level j, $i \in \{1, ..., N_j\}, j \in \{1, ..., M\}$, defined as the ratio of the average access time to component i at level j to the number of failed components at small levels of architecture for the same time;

9) TC_{ij} – relative time to analyze failure in component i at level j, $i \in \{1, ..., N_j\}, j \in \{1, ..., M\}$, defined as the ratio of the average time of failure analysis in component i at level j, $i \in \{1, ..., N_j\}, j \in \{1, ..., M\}$, to the number of faulty components at all levels of the architecture analyzed at the same time;

10) TE_{ij} – the relative time to resolve a failure in component i at level j, $i \in \{1, ..., N_j\}, j \in \{1, ..., M\}$, defined as the ratio of the average recovery time in component i at the level j, $i \in \{1, ..., N_j\}, j \in \{1, ..., M\}$, to the number of failed components at all levels of the architecture, in which failures are eliminated at the same time;

11) TU_{ij} – relative usage time of component i at level j, $i \in \{1, ..., N_j\}, j \in \{1, ..., M\}$, defined as the ratio of the average use time of component i at the level j, $i \in \{1, ..., N_j\}, j \in \{1, ..., M\}$, to the number of components at all levels of the architecture used at the same time;

12) TR –average system downtime in a large real-time software architecture, defined as the time during which the system is unable to perform its functions;

13) *MTTF (Mean Time to Failure)* –the average time to failure in a large real-time software architecture, defined as the time during which no system failures occur.

In the architecture of real software, the average time for the appearance of a failure, that is, the time during which the software functions correctly, is [7]:

$$MTTF = \sum_{j=1}^{j=M} \sum_{i=1}^{i=N_j} \{PU_{ij} \times (1-PF_{ij}) \times [TU_{ij} +$$

$$+ \sum_{(m=1)\&(m \neq j)}^{m=M} \sum_{n=1}^{n=N_m} [(1-PL^{ij}_{nm})[TU_{nm} + \sum_{l \in D_{nm}} [(1-PL^{nm}_{lm}) \times TU_{lm}]]] +$$

$$+ \sum_{k \in D_{ij}} [(1-PL^{ij}_{kj})[TU_{kj} + \sum_{(m=1)\&(m \neq j)}^{m=M} \sum_{n=1}^{n=N_m} [(1-PL^{kj}_{nm}) \times$$

$$\times [TU_{nm} + \sum_{l \in D_{nm}} [(1-PL^{nm}_{lm}) \times TU_{lm}]]]]]\}.$$

The average downtime (recovery) of the software is [7]:

$$TR = \sum_{j=1}^{j=M} \sum_{i=1}^{i=M_j} \{PU_{ij} \times PF_{ij} \times [(TA_{ij} + TC_{ij} + TE_{ij}) +$$

$$+ \sum_{(m=1)\&(m \neq j)}^{m=M} \sum_{n=1}^{n=N_n} [PL^{ij}_{nm} \times [(TA_{nm} + TC_{nm} + TE_{nm}) +$$

$$+ \sum_{l \in D_{nm}} [PL^{nm}_{lm} \times (TA_{lm} + TC_{lm} + TE_{lm})]]]$$

$$\sum_{k \in D_{ij}} [PL^{ij}_{kj} \times [(TA_{kj} + TC_{kj} + TE_{kj}) +$$

$$+ \sum_{(m=1)\&(m \neq j)}^{m=M} \sum_{n=1}^{n=N_m} [PL^{kj}_{nm}[(TA_{nm} + TC_{nm} + TE_{nm}) +$$

$$+ \sum_{l \in D_{nm}} [PL^{nm}_{lm} \times (TA_{lm} + TC_{lm} + TE_{lm})]]]]]]\}$$

Average system downtime and average failure time can be used to predict the reliability of software in general. For the case of continuous operation of complex software (and for a real-time system, this is the most likely mode of software operation), the reliability of the software can be estimated using the availability factor *S*, calculated by the following formula:

$$S = \frac{MTTF}{MTTF + TR}.$$

The availability factor can be interpreted as the probability of correct software functioning.

The main approach to increasing the reliability of software, which is subject to increased requirements for continuity and correct functioning, is multiversion development, that is, the creation by independent developers of several versions of a software component that correspond to the same specifications, but differ in implementations. The software architecture should provide for a mechanism for forming the overall result of the operation of this software component based on the results of the work of each individual version. In [8], two main methods of building architecture when using multiversion development are given, which are abbreviated as *NVP* and *RB*.

When building a multiversion component from K versions by the multiversion programming method (*NVP*, *N*-version programming) for any K, the reliability is equal to:

$$R_{ij} = p_{ij}^v \left(1 - \prod_{k \in Z_{ij}}^K (1 - p_{ij}^k) \right),$$

where p_{ij}^v – probability of failure of the voting algorithm for component i at level j, Z_{ij} – many versions of this component, and p_{ij}^k is probability of failure of version $k \in Z_{ij}$.

When building a multiversion component from K versions using the recovery block (RB, recovery block) method, the reliability is:

$$R_{ij} = \sum_{k \in Z_{ij}}^K p_{ij}^k p_{ij}^{AT} \prod_{l=1}^{k-1} \left((1 - p_{ij}^l) p_{ij}^{AT} + p_{ij}^l (1 - p_{ij}^{AT}) \right),$$

where p_{ij}^{AT} – the probability of failure-free operation of the acceptance test for component i at level j, p_{ij}^k is probability of failure of version $k \in Z_{ij}$.

The last two formulas can be used to calculate the probabilities of failure of software components:

$$PF_{ij} = 1 - R_{ij}.$$

Hardware reliability. To increase the reliability of the hardware part of the complex, it is also necessary to use redundancy and reservation, which includes multiprocessing and the provision of different buses and independent RAM.

Each processor and bus fail at some random points in time, after which they begin to recover. Let us assume that the flows of failures and recoveries are the simplest. The bus failure rate is denoted as ν_0, the bus recovery rate is μ_0. The rate of processor failure streams is denoted by ν_i, and the rate of recovery of processors of the i type is μ_i.

Probability $P_{j_0 j_1, \ldots, j_N}$ finding the system in a state in which j_0 шин интерфейса исправны и участвуют в вычислительном процессе, а $(m_0 - j_0)$ неисправны и восстанавливаются interface buses are in good working order and participate in the computational process, and $(m_0 - j_0)$ are faulty and are being recovered, j_1 type 1 processors are operational and participate in the computational process, and $(m_1 - j_1)$ faulty and are recovering, ..., j_N processors of N type are proper and participate in the computational process, and $(m_N - j_N)$ are faulty and are recovered, is determined by the following formula [9; 10]:

$$P_{j_0, j_1, \ldots j_N} = \frac{\dfrac{k!}{\prod\limits_{i=0}^N j_i!} \prod\limits_{i=0}^N \dfrac{m_i!}{(m_i - j_i)!} \rho_i^{j_i}}{\sum\limits_{j_0, \ldots, j_N} \dfrac{k!}{\prod\limits_{i=0}^N j_i!} \prod\limits_{i=0}^N \dfrac{m_i!}{(m_i - j_i)!} \rho_i^{j_i}},$$

where $k = \sum\limits_{i=0}^N m_i$, and the summation in the denominator is carried out over all possible values of the indices $j_0, \ldots j_N$ (this will be implied in all subsequent similar

formulas). In addition, the following designation is used:

$$\rho_i = \frac{\nu_i}{\mu_i}.$$

The formula for the probabilities of states in a stationary mode can be simplified. First, we can shorten $k!$ in the numerator and denominator, and also combine the works in the numerator and denominator:

$$P_{j_0 j_1, \ldots j_N} = \frac{\prod\limits_{i=0}^N \dfrac{m_i!}{(m_i - j_i)! j_i!} \rho_i^{j_i}}{\sum\limits_{j_0, \ldots, j_N} \prod\limits_{i=0}^N \dfrac{m_i!}{(m_i - j_i)! j_i!} \rho_i^{j_i}}.$$

Now let's rewrite the denominator so that first the summation is performed, and then the multiplication:

$$P_{j_0 j_1, \ldots j_N} = \frac{\prod\limits_{i=0}^N \dfrac{m_i!}{(m_i - j_i)! j_i!} \rho_i^{j_i}}{\prod\limits_{i=0}^N \sum\limits_{j_i=0}^{m_i} \dfrac{m_i!}{(m_i - j_i)! j_i!} \rho_i^{j_i}}.$$

Each of the sums in the denominator is now the multiplication of the binomial coefficient and the corresponding power of a fixed value, and therefore can be simplified using the Newton binomial formula as follows [11]:

$$\sum_{j_i=0}^{m_i} \frac{m_i!}{(m_i - j_i)! j_i!} \rho_i^{j_i} =$$

$$= \sum_{j_i=0}^{m_i} \frac{m_i!}{(m_i - j_i)! j_i!} \rho_i^{j_i} \cdot 1^{m_i - j_i} = (\rho_i + 1)^{m_i}.$$

Thus, we finally obtain the following expression for the probabilities of the hardware states in the steady state:

$$P_{j_0, j_1, \ldots j_N} = \frac{\prod\limits_{i=0}^N \dfrac{m_i!}{(m_i - j_i)! j_i!} \rho_i^{j_i}}{\prod\limits_{i=0}^N (\rho_i + 1)^{m_i}}.$$

Simplified formulas contain fewer values than the original ones, and, therefore, allow to avoid performing some unnecessary operations (for example, multiplying both the numerator and the denominator by $k!$, which obviously does not affect the value of the expression) and require significantly fewer operations to calculate the value of the denominator than the original formulas given in [9; 10].

Knowing the minimum hardware configuration required for the real-time system software to generate control action within the intervals required by the customer, the reliability of the hardware can be calculated. Indeed, if the number of trouble-free operating memory buses and processors exceeds the minimum required, then "redundant" software components can be considered as a reserve. Then the reliability of the hardware of the real-time control system, understood as the probability of ensuring the minimum required performance of the hardware, can be calculated as the sum of the probabilities of finding the hardware in states in which the number of trouble-free

operating memory buses and processors exceeds the minimum required number:

$$G_{\text{ср}} = \sum_{\substack{M_0 \le j_0 \le m_0 \\ \dots \\ M_N \le j_N \le m_N}} P_{j_0, j_1, \dots, j_N},$$

where M_0 is the minimum number of proper memory buses required to ensure a given performance, M_i is the minimum number of serviceable processors of the i type required to ensure the specified performance.

The formula for G_{cp} involves calculating the probabilities of different states of hardware with different values of the indices $j_0, j_1, \dots, j_N$. In this case, it is not advisable to repeat the calculations that have already been performed. For example, the denominator of all formulas has the same value, and, therefore, it is sufficient to calculate it once.

In addition, since it is required to compute states with sequential values of the indices, one can use the following recurrent formulas for the degrees and binomial coefficients, following from the definitions of the degree and factorial:

$$\rho_i^{j_i+1} = \rho_i^{j_i} \cdot \rho_i,$$

$$\frac{m_i!}{(m_i - j_i - 1)!(j_i + 1)!} = \frac{m_i!}{(m_i - j_i)! j_i!} \cdot \frac{m_i - j_i}{j_i + 1}.$$

These ratios allow to calculate the probabilities for states with sequential index values with a minimum number of additional operations:

$$P_{j_0, \dots j_i+1, \dots j_N} = P_{j_0, \dots j_i, \dots j_N} \cdot \frac{m_i - j_i}{j_i + 1} \rho.$$

From this ratio, elementary transformations can be used to obtain the formula for "decreasing the index":

$$P_{j_0, \dots j_i, \dots j_N} = P_{j_0, \dots j_i+1, \dots j_N} \cdot \frac{j_i + 1}{(m_i - j_i)\rho},$$

$$P_{j_0, \dots j_i-1, \dots j_N} = P_{j_0, \dots j_i, \dots j_N} \cdot \frac{j_i}{(m_i - j_i + 1)\rho}.$$

Since the simplest form of the formula for the probabilities of states is taken in cases when all buses and processors are in proper order, or when all of them are in bad order, it is advisable to start calculating G_{cp} with the probability of a state in which all buses of the RAM and processors are working correctly:

$$P_{m_0, m_1, \dots, m_N} = \frac{\prod_{i=0}^{N} \rho_i^{m_i}}{\prod_{i=0}^{N} (\rho_i + 1)^{m_i}}$$

and then, using the "decreasing indices" formulas, sequentially calculate the remaining required state probabilities.

Another opportunity for improvement opens up if the minimum configuration that provides a given performance includes fewer hardware components than half of the components present in the system. In this case, you can calculate the sum of the probabilities of states in which

the performance is not sufficient to generate a control action within the given time constraints, and then calculate the required probability as the probability of the opposite event [12]:

$$G_{\text{ср}} = 1 - \sum_{\substack{0 \le j_0 < M_0 \\ \dots \\ 0 \le j_N < M_N}} P_{j_0, j_1, \dots, j_N}.$$

When calculating using this formula, one should start with the probability of a state in which all RAM buses and processors are faulty:

$$P_{0,0,\dots,0} = \frac{1}{\prod_{i=0}^{N} (\rho_i + 1)^{m_i}}$$

and then use the index increase formulas obtained above.

Reliability model of hardware and software complex. Finally, using the above considerations, we can combine software and hardware reliability models into a general reliability model of a multiprocessor hardware-software complex of a real-time control system with multiversion software.

Due to the abstract nature of software and the negligible probability of errors during its copying and distribution (in addition, the integrity of the software can be checked using mechanisms such as checksums), it can be considered that hardware and software failures occur independently.

Therefore, the probability of simultaneous failure-free operation of the hardware-software complex is equal to the product of the probabilities of failure-free operation of the software and hardware [12]:

$$P_F = G_{\text{ср}} \cdot S.$$

Conclusion. Thus, we have obtained a model for calculating the reliability of multiprocessor hardware and software systems of real-time systems with heterogeneous processors and multiversion software, using queuing theory and reliability theory, which allows to consider many architecture options in a short time and without significant costs typical for constructing experimental samples and reliability assessment by organizing trial operation.

The proposed mathematical model can be used to automate the design of multiprocessor hardware and software systems. In practice, they strive to ensure that the projected real-time control system has the highest possible reliability, provided that the costs of its creation and operation do not exceed the allocated funds. Thus, we come to the problem of conditional or multicriteria optimization, in which the objective function is expressed in terms of the probabilities of states calculated within the framework of the proposed model. Despite the fact that there are analytical expressions for the reliability indicators of a multiprocessor hardware-software complex, this optimization problem has a number of inconvenient features: the variables being optimized are discrete, the presence of a single extremum and properties convenient for optimization (convexity) is not guaranteed, and the volume of the search space is growing rapidly with an increase in the number of processor types.

When solving such optimization problems, evolutionary optimization methods, for example, a genetic algorithm [13], a probabilistic genetic algorithm [14] or an asymptotic probabilistic genetic algorithm [15], as well as some other "nature-inspired" optimization methods, for example, the particles swarm method [16]. The disadvantage of evolutionary optimization methods is that they have a large number of tunable parameters that can significantly affect the quality of the solutions found. Moreover, different sets of parameters can be effective for different optimization problems. Thus, the use of evolutionary optimization methods requires, as a rule, experimentation and the involvement of a specialist in the field of evolutionary optimization methods.

In order to exclude the stage of selecting an effective combination of parameters, self-tuning can be used [17; 18]. Self-adjusting optimization methods use several sets of parameters, computing resources (for simplicity, we can assume that this is the number of calculations of the objective function) which are distributed depending on the quality of the solutions obtained with their help. At the beginning of the optimization process, all parameter sets receive the same resources. Then the sets of parameters that generate the best solutions receive additional computing resources due to those that perform worse. There is a certain lower bound for the allocated resources, this is done so that any set of parameters can manifest itself in the future when conditions change, since different stages of optimization may require different values of parameters.

The study of the effectiveness of these optimization methods in solving the problem of optimizing the reliability of multiprocessor hardware and software complexes of real-time control systems with multiversion software and dissimilar processors is a possible direction for further research.

References

1. Buttazzo G. Hard Real-Time Computing Systems: Predictable Scheduling Algorithms and Applications. New York, NY, Springer, 2011. XVI+524 p.

2. Vasil'ev V. A., Legkov K. E., Levko I. V. [The real-time systems and applications]. *Informaciya i kosmos.* 2016, № 3, P. 68–70 (In Russ.).

3. CHerkesov G. N. *Nadezhnost' apparatno-programmnyh kompleksov* [Reliability of the computer appliances]. Spb., Piter Publ., 2005, 479 p.

4. Lipaev V. V. *Ekonomika proizvodstva programmnyh produktov* [The economics of the software engineering]. Moscow, SINTEG Publ., 2011, 358 p.

5. Zatuliveter Yu. S., Fishchenko E. A., Hodakovskij I. A. [The software methods for improving the reliability of structurally complex distributed computing and control processes]. *Nadezhnost'.* 2009, No. 1, P. 42–49 (In Russ.).

6. Avizienis A. The N-Version Approach to Fault-Tolerant Software. *IEEE Trans. Soft. Eng.* 1985, Vol. SE-11 (12), P. 1511–1517.

7. Kukartsev V. V., Sheenok D. A. [Optimization of the software architecture of logistics information systems]. *Logisticheskie sistemy v global'noj ekonomike.* 2013, No. 3, P. 138–145 (In Russ.).

8. Antamoshkin O. A., Degterev A. S., Rusakov M. A. et al. [The analysis of the reliability of computer appliances]. *Uspekhi sovremennogo estestvoznaniya.* 2005, No. 6, P. 44–45 (In Russ.).

9. Efimov S. N., Terskov V. A. *Rekonfiguriruemye vychislitel'nye sistemy obrabotki informacii i upravleniya* [The reconfigurable computing systems of information processing and control]. – Krasnoyarsk, KrIZHT IrGUPS Publ., 2013, 249 p.

10. Efimov S. N., Tyapkin V. N., Dmitriev D. D. et al. Methods of assessing the characteristics of the multiprocessor computer system adaptation unit. *ZHurnal Sibirskogo federal'nogo universiteta. Seriya: Matematika i fizika.* 2016, Vol. 9, No. 3, P. 288–295 (In Russ.).

11. Graham R. L., Knuth D. E., Patashnik O. Concrete Mathematics – A foundation for computer science. Reading, MA, USA, Addison-Wesley Professional, 1994, 657 p.

12. Ventcel' E. S., Ovcharov L. A. *Teoriya veroyatnostej i eyo inzhenernye prilozheniya* [Probability theory and its engineering applications]. Moscow, Vysshaya shkola Publ., 2000, 480 p.

13. Goldberg D. E. Genetic algorithms in search, optimization, and machine learning. Reading, MA, Addison-Wesley, 1989, 372 p.

14. Vorozheikin F. Yu., Gonchan T. N., Panfilov I. A. at al. Modified Probabilistic Genetic Algorithm for the Solution of Complex Constrained Optimization Problems. *Vestnik SibSAU.* 2009. No. 5 (26), P. 31–36.

15. Galushin P. V. [Design and evaluation of asymptotic probabilistic genetic algorithm]. *Zhurnal Sibirskogo federal'nogo universiteta. Seriya: Matematika i fizika.* 2012, No. 1(5), P. 49–56 (In Russ.).

16. Kovalev I. V., Solov'ev E. V., Kovalev D. I. et al. [Application of particle swarm optimization to design of N-version software composition]. *Pribory i sistemy. Upravlenie, kontrol', diagnostika.* 2013, No. 3, P. 1–6 (In Russ.).

17. Semenkin E., Semenkina M. Stochastic Models and Optimization Algorithms for Decision Support in Spacecraft Control Systems Preliminary Design. *Informatics in Control, Automation and Robotics, Lecture Notes in Electrical Engineering.* 2014, Vol. 283, P. 51–65.

18. Semenkin E., Semenkina M. Self-Configuring Genetic Programming Algorithm with Modified Uniform Crossover Operator. *Proceedings of the IEEE Congress on Evolutionary Computation.* June 10–15, 2012.

Библиографические ссылки

1. Buttazzo G. Hard Real-Time Computing Systems: Predictable Scheduling Algorithms and Applications. New York, NY, Springer, 2011. XVI+524 P.

2. Васильев В. А., Легков К. Е., Левко И. В. Системы реального времени и области их применения // Информация и космос. 2016. № 3. С. 68–70.

3. Черкесов Г. Н. Надежность аппаратно-программных комплексов. Спб. : Питер, 2005. 479 с.

4. Липаев В. В. Экономика производства программных продуктов. М. : СИНТЕГ, 2011. 358 с.

5. Затуливетер Ю. С., Фищенко Е. А., Ходаковский И. А. Программные методы повышения надеж-

ности структурно сложных распределенных вычислений и процессов управления // Надежность. 2009. №. 1. С. 42–49.

6. Avizienis A. The N-Version Approach to Fault-Tolerant Software // IEEE Trans. Soft. Eng, 1985. Vol. SE-11 (12). P. 1511–1517.

7. Кукарцев В. В., Шеенок Д. А. Оптимизация программной архитектуры логистических информационных систем // Логистические системы в глобальной экономике. 2013. № 3. С. 138–145.

8. Анализ надежности мультиверсионных архитектур аппаратно программных комплексов / О. А. Антамошкин, А. С. Дегтерев, М. А. Русаков и др. // Успехи современного естествознания. 2005. №. 6. С. 44-45.

9. Ефимов С. Н., Терсков В. А. Реконфигурируемые вычислительные системы обработки информации и управления. Красноярск : КрИЖТ ИрГУПС, 2013. 249 с.

10. Methods of assessing the characteristics of the multiprocessor computer system adaptation unit / Efimov S. N., Tyapkin V. N., Dmitriev D. D. и др. // Журнал Сибирского федерального университета. Серия: Математика и физика. 2016. Т. 9, № 3. С. 288–295.

11. Грэхем Р. Л., Кнут Д. Э., Паташник О. Конкретная математика. Математические основы информатики : 2-е изд. ; пер. с англ. М. : ООО «И.Д. Вильямс», 2010. 784 с.

12. Вентцель Е. С., Овчаров Л. А. Теория вероятностей и её инженерные приложения : 2-е изд. М. : Высшая школа, 2000. 480 с.

13. Goldberg D. E. Genetic algorithms in search, optimization, and machine learning. Reading, MA, Addison-Wesley, 1989. 372 p.

14. Vorozheikin F. Yu., Gonchan T. N., Panfilov I. A. at al. Modified Probabilistic Genetic Algorithm for the Solution of Complex Constrained Optimization Problems // Vestnik SibSAU. 2009. Iss. 5 (26). P. 31–36.

15. Галушин П. В. Разработка и исследование асимптотического вероятностного генетического алгоритма // Журнал Сибирского федерального университета. Серия: Математика и физика. 2012. № 1(5). С. 49–56.

16. Использование метода роя частиц для формирования состава мультиверсионного программного обеспечения / Ковалев И. В., Соловьев Е. В., Ковалев Д. И. и др. // Приборы и системы. Управление, контроль, диагностика. 2013. № 3. С. 1–6.

17. Semenkin E., Semenkina M. Stochastic Models and Optimization Algorithms for Decision Support in Spacecraft Control Systems Preliminary Design // Informatics in Control, Automation and Robotics, Lecture Notes in Electrical Engineering. 2014. Vol. 283. P. 51–65.

18. Semenkin E., Semenkina M. Self-Configuring Genetic Programming Algorithm with Modified Uniform Crossover Operator // Proceedings of the IEEE Congress on Evolutionary Computation. June 10–15, 2012.

Aab Andrey Vladimirovich – 2-year master's degree student; Reshetnev Siberian State University of Science and Technology.

Galushin Pavel Viktorovich – Cand. Sc., docent; Siberian Law Institute of Ministry of Internal Affairs of the Russian Federation.

Popova Anastasiya Valer'evna – 2-year master's degree student; Reshetnev Siberian State University of Science and Technology. E-mail: anastasiya.popowa@mail.ru.

Terskov Vitaly Anatolyevich – Dr. Sc., Professor; Reshetnev Siberian State University of Science and Technology.

Ааб Андрей Владимирович – магистр; Сибирский государственный университет науки и технологий имени академика М. Ф. Решетнева.

Галушин Павел Викторович – кандидат технических наук, доцент; Сибирский юридический институт МВД России.

Попова Анастасия Валерьевна – магистр; Сибирский государственный университет науки и технологий имени академика М. Ф. Решетнева. E-mail: anastasiya.popowa@mail.ru.

Терсков Виталий Анатольевич – доктор технических наук, профессор; Сибирский государственный университет науки и технологий имени академика М. Ф. Решетнева.

SOLVING BOUNDARY VALUE PROBLEMS OF EQUATIONS OF TWO-DIMENSIONAL ELASTICITY THEORY USING CONSERVATION LAWS

B. D. Annin[1], S. I. Senashov[2*], O. V. Gomonova[2]

[1]Lavrentyev Institute of Hydrodynamics SB RAS
15 Lavrentyev Prospect, Novosibirsk, 630090, Russian Federation
[2]Reshetnev Siberian State University of Science and Technology
31, Krasnoyarskii rabochii prospekt, Krasnoyarsk, 660037, Russian Federation
*E-mail: sen@sibsau.ru

The plane problem for elasticity equations is well studied. It can be explained by its importance for applications and by the fact that the equations can be reduced to the Cauchy-Riemann system. In spite of this importance, exact solutions that would describe the stress-strain state of bodies of finite dimensions are not numerous. Conservation laws for differential equations have been appeared more than a hundred years ago, but, as a rule, they were not used to solve specific problems, but were of purely academic interest. The situation changed with the development of the technique of construction of conservation laws for arbitrary systems of differential equations, and then with the use of conservation laws to solve boundary value problems of the theory of plasticity and elastic-plasticity. In this article, new conservation laws are constructed for the equations of the plane theory of elasticity in the stationary case. These laws form an infinite series, which is closely related to the elasticity equations solving. This fact made possible to reduce solving of boundary value problems, in terms of displacements, to the calculation of contour integrals along the boundary of a domain bounded by the studying elastic body. As it follows from the proposed technique, the studied area can be multiply connected, and the considered boundary can be piecewise-smooth.

Keywords: conservation laws, boundary value problem, elasticity equations.

РЕШЕНИЕ КРАЕВЫХ ЗАДАЧ УРАВНЕНИЙ ДВУМЕРНОЙ ТЕОРИИ УПРУГОСТИ С ПОМОЩЬЮ ЗАКОНОВ СОХРАНЕНИЯ

Б. Д. Аннин[1], С. И. Сенашов[2*], О. В. Гомонова[2]

[1]Институт гидродинамики имени М. А. Лаврентьева СО РАН
Российская Федерация, 630090, г. Новосибирск, просп. Академика Лаврентьева, 15
[2]Сибирский государственный университет науки и технологий имени академика М. Ф. Решетнева
Российская Федерация, 660037, г. Красноярск, просп. им. газ. «Красноярский рабочий», 31
*E-mail: sen@sibsau.ru

Плоская задача для уравнений упругости достаточно хорошо изучена. Это объясняется ее важностью для приложений и тем, что уравнения сводятся к системе Коши – Римана. Несмотря на это, точных решений, которые описывали бы напряженно-деформированное состояние тел конечных размеров, не так много. Законы сохранения для дифференциальных уравнений появились более ста лет назад, но, как правило, они не использовались для решения конкретных задач, а представляли «чисто академический» интерес. Ситуация изменилась с развитием техники построения законов сохранений для произвольных систем дифференциальных уравнений, а затем – с использованием законов сохранения для решения краевых задач теории пластичности и упруго-пластичности. В этой статье построены новые законы сохранения для уравнений плоской теории упругости в стационарном случае. Эти законы образуют бесконечную серию, которая тесно связана с решениями уравнений упругости. Именно этот факт позволил свести решение краевых задач в терминах перемещений к вычислению контурных интегралов по границе области, ограниченной изучаемым упругим телом. Из данной методики следует, что область может быть многосвязной, а граница – кусочно-гладкой.

Ключевые слова: законы сохранения, краевая задача, уравнения упругости.

Introduction. Usually, the equations of two-dimensional static elasticity are solved using the complex variable theory methods. These methods were developed by G. V. Kolosov and N. I. Muskhelishvili. The use of complex variable theory methods for solving elasticity problems requires a good knowledge of the complex variable theory technique and, as a rule, is used for areas faceted with smooth contours [1; 2]. This article proposes a method for solving the same problems using conservation laws. Apparently, for the first-time conservation laws for elasticity equations were calculated in [3; 4]. These calculations were based on the theorem of E. Noether. The found laws did not find any practical application and were of purely academic interest [5]. In [6–10] it is shown that conservation laws can be successfully used in solving boundary value problems of the theory of plasticity and elastic-plasticity. G.P. Cherepanov [11; 12] noticed that the complex variable theory methods used in solving plane problems actually go back to conservation laws. In the presented work, an endless series of new conservation laws was found. These conservation laws made it possible to obtain formulas with the help of which one can effectively reduce the boundary value problems to quadratures. The latter are curvilinear integrals over a closed contour and can be easily solved numerically for given boundary conditions in displacements.

1. Formulation of the problem. Consider the equations of two-dimensional elasticity in the stationary case

$$F_1 = (\lambda + 2\mu)u_{xx} + (\lambda + \mu)v_{xy} + \mu u_{yy} = 0,$$
$$F_2 = (\lambda + 2\mu)v_{yy} + (\lambda + \mu)u_{xy} + \mu v_{xx} = 0, \qquad (1)$$

where λ, μ are constants called Lamé parameters, u, v are components of the deformation vector, the indices below indicate the derivatives with respect to the corresponding components.

Let us find conservation laws of a special form for (1). The conservation law for the system of equations (1) is an expression of the form

$$A_x(x, y, u, v) + B_y(x, y, u, v) = \omega^1 F_1 + \omega^2 F_2, \qquad (2)$$

where ω_i some functions of x, y, which are simultaneously not identically equal to zero. The magnitudes A, B will be called the components of the conserved current. We are looking for the components of the conserved current in the form:

$$A = \alpha^1(\lambda + 2\mu)u_x + \beta^1 u_y + \gamma^1 \mu v_x + \delta^1 v_y,$$
$$B = \alpha^2 u_x + \beta^2 u_y + \gamma^2 v_x + \delta^2 v_y, \qquad (3)$$

where γ^i, δ^i are some functions depended on x, y only.

Substitute expressions (3) into (2). As a result, one can obtain a polynomial of the first degree in the variables $u_x, u_y, u_{xx}, u_{xy}, u_{yy}, v_x, v_y, v_{xx}, v_{xy}, v_{yy}$. Equating the coefficients at the derivatives in this polynomial to zero and taking into account that $\alpha^i, \beta^i, \gamma^i, \delta^i$ are functions only from x, y, one can get after exclusion ω^i, $i = 1, 2$

$$\alpha^2 = -\beta^1 + (\lambda + \mu)\gamma^1, \quad \beta^2 = \mu\alpha^1,$$
$$\gamma^2 = -\delta^1 + (\lambda + \mu)\alpha^1, \quad \delta^2 = (\lambda + 2\mu)\gamma^1,$$
$$(\lambda + 2\mu)\alpha^1_x + \alpha^2_y = 0, \quad \mu\gamma^1_x + \gamma^2_y = 0, \qquad (4)$$
$$\beta^1_x + \beta^2_y = 0, \quad \delta^1_x + \delta^2_y = 0.$$

This implies:

$$(\lambda + 2\mu)\alpha^1_x - \beta^1_y + (\lambda + \mu)\gamma^1_y = 0,$$
$$\mu\gamma^1_x - \delta^1_y + (\lambda + \mu)\alpha^1_y = 0, \qquad (5)$$

$$\beta^1_x + \mu\alpha^1_y = 0, \quad (\lambda + 2\mu)\gamma^1_y + \delta^1_x = 0. \qquad (6)$$

Substituting (6) into (5) one can obtain

$$(\lambda + 2\mu)\alpha^1_{xx} + (\lambda + \mu)\gamma^1_{xy} + \mu\alpha^1_{yy} = 0,$$
$$(\lambda + 2\mu)\gamma^1_{yy} + (\lambda + \mu)\alpha^1_{xy} + \mu\gamma^1_{xx} = 0. \qquad (7)$$

It is obvious that (7), up to notation, coincides with system (1). Therefore, α^1, γ^1 is an arbitrary smooth solution to the system of equations (1). From (3) taking into account (4), one obtains the conserved current

$$A = \alpha^1(\lambda + 2\mu)(u_x + v_y) + \gamma^1 \mu(v_x - u_y),$$
$$B = \gamma^1(\lambda + 2\mu)(u_x + v_y) + \alpha^1 \mu(v_x - u_y), \qquad (8)$$

where α^1, γ^1 is arbitrary solution of the system of equations (1).

2. Construction of solutions to the boundary value problem. It is known that

$$u = G^1 - \frac{1}{4(1-v)}(xG^1 + yG^2 + G^0)_x =$$
$$= G^1 - \omega(xG^1 + yG^2 + G^0)_x, \qquad (9)$$
$$v = G^2 - \omega(xG^1 + yG^2 + G^0)_y,$$

is the solution to the system of equations (1). Here G^i are arbitrary harmonic functions, v is Poisson's ratio, which can be expressed through the Lamé parameters.

From (9) one gets

$$u_x + v_y = (G^1_x + G^2_y)(1 - \omega/2),$$
$$-u_y + v_x = -G^1_y + G^2_x. \qquad (10)$$

Let x_0, y_0 be an arbitrary point of a domain Ω with a smooth boundary Γ. Let us assume $G^1 = \ln\left((x - x_0)^2 + (y - y_0)^2\right) = \ln r^2$, $G^2 = 0$. Then one obtains

$$u_x + v_y = 2\frac{x - x_0}{r^2}\omega, \quad -u_y + v_x = 2\frac{y - y_0}{r^2}. \qquad (11)$$

From (2), by Green's formula, follows

$$\iint_\Omega (A_x + B_y)dxdy = \oint_\Gamma -A dy + B dx =$$
$$= \oint_\Gamma -\left(\alpha^1(\lambda + 2\mu)(u_x + v_y) + \gamma^1\mu(v_x - u_y)\right)dy + \qquad (12)$$
$$+ \left(\gamma^1(\lambda + 2\mu)(u_x + v_y) + \alpha^1\mu(v_x - u_y)\right)dx = 0.$$

Now let the contour Γ_1 consist of two contours: Γ and a circle of radius ε: $(x-x_0)^2+(y-y_0)^2=\varepsilon^2$.

Assuming in (12) instead of Γ the contour $\Gamma1$ and taking into account relation (11), one can obtain

$$\oint_{\Gamma_1}-\left(\alpha^1(\lambda+2\mu)2\frac{x-x_0}{r^2}\omega-\gamma^1\mu2\frac{y-y_0}{r^2}\right)dy+$$

$$+\left(\gamma^1(\lambda+2\mu)2\frac{x-x_0}{r^2}\omega+\alpha^1\mu\left(v_x-u_y\right)\right)dx= \quad (13)$$

$$=\oint_{\Gamma}+\oint_{(x-x_0)^2+(y-y_0)^2=\varepsilon^2}=0.$$

Let's represent the equation of a circle in parametric form:

$$x-x_0=\varepsilon\cos\varphi,\ y-y_0=\varepsilon\sin\varphi,\ 0\le\varphi\le2\pi.$$

Then the last of the integrals in formula (13) will be written as follows:

$$\oint_{(x-x_0)^2+(y-y_0)^2=\varepsilon^2}=$$

$$=\int_0^{2\pi}-\left(\alpha^1\left(\lambda+2\mu\right)2\omega\cos\varphi-\gamma^1\mu2\sin\varphi\right)\cos\varphi d\varphi+ \quad (14)$$

$$+\left(\gamma^1(\lambda+2\mu)2\cos\varphi+\alpha^1\mu2\sin\varphi\right)\sin\varphi d\varphi=$$

$$=2\pi\alpha^1\left(x_0,y_0\right)\left(\mu-(\lambda+2\mu)\omega.\right.$$

In formula (14), the mean value theorem was used. Finally, from (13) one obtains

$$\frac{-1}{2\pi(\mu-(\lambda+2\mu)\omega}\oint_{\Gamma}-$$

$$-\left(\alpha^1\left(\lambda+2\mu\right)2\omega\left(\frac{x-x_0}{r^2}\right)-2\gamma^1\mu\left(\frac{y-y_0}{r^2}\right)\right)dy+ \quad (15)$$

$$+\left(\gamma^1(\lambda+2\mu)2\omega\left(\frac{x-x_0}{r^2}\right)-2\alpha^1\mu\left(\frac{y-y_0}{r^2}\right)\right)dx=$$

$$=\alpha^1\left(x_0,y_0\right).$$

Assuming now in equations (10) $G^2=\ln\left((x-x_0)^2+(y-y_0)^2\right)=\ln r^2,\ G^1=0.$ In this case, similar reasoning and calculations give a formula for $\gamma^1(x_0,y_0)$.

One obtains

$$\frac{-1}{2\pi(\mu+(\lambda+2\mu)\omega}\times$$

$$\times\oint_{\Gamma}\left(\alpha^1\left(\lambda+2\mu\right)2\omega\left(\frac{y-y_0}{r^2}\right)+2\gamma^1\mu\left(\frac{x-x_0}{r^2}\right)\right)dy+ \quad (16)$$

$$+\left(\gamma^1(\lambda+2\mu)2\omega\left(\frac{y-y_0}{r^2}\right)+2\alpha^1\mu\left(\frac{x-x_0}{r^2}\right)\right)dx=$$

$$=\gamma^1\left(x_0,y_0\right).$$

Formulas (15), (16) make it possible to calculate α^1,γ^1 at any point (x_0,y_0) in the area if the values of these functions are known on the boundary of Γ. And

since α^1,γ^1 are a solution to equations (1), one can obtain a method for constructing solutions to system (1) according to their boundary conditions. Namely, let the following boundary value problem be set: there is an area Ω with a boundary Γ. On Γ, the components of the displacement vector are given

$$u\mid_{\Gamma}=u_0(x,y),\ v\mid_{\Gamma}=v_0(x,y). \quad (17)$$

Then, based on formulas (15), (16), the solution to problem (17) for the system of equations (1) can be written in the form

$$\frac{-1}{2\pi(\mu-(\lambda+2\mu)\omega}\oint_{\Gamma}-$$

$$-\left(u_0\left(\lambda+2\mu\right)2\omega\left(\frac{x-x_0}{r^2}\right)-2v_0\mu\left(\frac{y-y_0}{r^2}\right)\right)dy+$$

$$+\left(v_0\left(\lambda+2\mu\right)2\omega\left(\frac{x-x_0}{r^2}\right)-2u_0\mu\left(\frac{y-y_0}{r^2}\right)\right)dx= \quad (18)$$

$$=u_0\left(x_0,y_0\right).$$

$$\frac{-1}{2\pi(\mu+(\lambda+2\mu)\omega}\times$$

$$\times\oint_{\Gamma}\left(u_0\left(\lambda+2\mu\right)2\omega\left(\frac{y-y_0}{r^2}\right)+2v_0\mu\left(\frac{x-x_0}{r^2}\right)\right)dy+$$

$$+\left(v_0\left(\lambda+2\mu\right)2\omega\left(\frac{y-y_0}{r^2}\right)+2u_0\mu\left(\frac{x-x_0}{r^2}\right)\right)dx= \quad (19)$$

$$=v_0\left(x_0,y_0\right).$$

Conclusion. In the article, conservation laws that depend on derivatives of the first order and linear on them are found. It is shown that two coefficients at the derivatives are solutions of the elasticity equations in the plane case. This made it possible to reduce the solution of boundary value problems in displacements to the calculation of contour integrals along the boundary of the area. The proposed technique can be easily generalized to multiply – connected domains [13–15], as well as to the three-dimensional case.

References

1. Timoshenko S. P., Goodier J. *Teoriya uprugosti* [Theory of elasticity]. Moscow, Nauka Publ., 1975, 576 p.

2. Novatsky V. *Teoriya uprugosti* [Theory of elasticity]. Moscow, Mir Publ., 1975. 872 c.

3. Olver P. Conservation laws in elasticity 1. General result. Arch. Rat. Mech. Anal. 1984, No. 85, P. 111–129.

4. Olver P. Conservation laws in elasticity11. Linear homogeneous isotropic elastostatic. Arch. Rat. Mech. Anal. 1984, No. 85, P. 131–160.

5. Rozhdestvensky B. L., Yanenko N. N. *Sistemy kvazilineynykh uravneniy* [Systems of quasilinear equations]. Moscow, Nauka Publ., 1978, 688 p.

6. Annin B. D., Bytev V. O., Senashov S. I. *Gruppovye svoystva uravneniy uprugosti I plastichnosti* [Group properties of equations of elasticity and plasticity]. Novosibirsk, Nauka Publ., 1983, 143 p.

7. Senashov S. I., Gomonova O. V., Yakhno A. N. *Matematicheskiye voprosy dvumernykh uravneniy ideal-*

noy plastichnosti [Mathematical problems of two-dimensional equations of ideal plasticity]. Krasnoyarsk, 2012, 137 p.

8. Kiryakov P. P., Senashov S. I., Yakhno A. N. *Prilozheniye simmetriy i zakonov sokhraneniya k resheniyu differentsialnykh uravneniy* [Application of symmetries and conservation laws to solving differential equations]. Novosibirsk, 2001, 192 p.

9. Senashov S. I., Vinogradov A. M. Symmetries and conservation laws of 2-dimensional ideal plasticity. *Proc. Edinburg Math. Soc.* 1988, P. 415–439.

10. Vinogradov A. M. Krasilshchik I. S., Luchagin V. V. *Simmetrii i zakony sokhraneniya* [Symmetries and conservation laws]. Moscow, Factor Publ., 1996, 461 p.

11. Annin B. D., Cherepanov G. P. *Uprugoplasticheskaya zadacha* [Elastic-plastic problem]. Nocosibirsk, Nauka Publ., 1983, 126 p.

12. Cherepanov G. P. *Mekhanika khrupkogo razrusheniya* [Mechanics of fragile fracture]. Moscow, Nauka Publ., 1974, 640 p.

13. Senashov S. I., Savostyanova I. L. [Elastic state of a plate with holes of arbitrary shape]. *Vestnik Chuvashskogo gosudarstvennogo pedagogicheskogo universiteta im. U. Ya. Yakovleva. Seriya: Mekhanika predelnogo sostoyaniya*. 2016, No. 3 (29), P. 128–134 (In Russ.).

14. Senashov S. I., Filyushina E. V. [Conservation laws of the plane theory of elasticity]. *Vestnik SibGAU.* 2014, No. 1(53), P. 79–81 (In Russ.).

15. Senashov S. I., Filyushina E. V. *Uprugoplasticheskiye zadachi dlya ortotropnykh sred* [Elastic-plastic problems for orthotropic media]. Krasnoyars, 2016, 116 p.

Библиографические ссылки

1. Тимошенко С. П., Гудьер Дж. Теория упругости. М. : Наука, 1975. 576 с.

2. Новацкий В. Теория упругости. М. : Мир, 1975. 872 с.

3. Olver P. Conservation laws in elasticity 1. General result. Arch. Rat. Mech. Anal. 1984, Vol. 85, P. 111–129.

4. Olver P. Conservation laws in elasticity 11. Linear homogeneous isotropic elastostatic. Arch. Rat. Mech. Anal. 1984, Vol. 85, P. 131–160.

5. Рождественский Б. Л., Яненко Н. Н. Системы квазилинейных уравнений. М. : Наука, 1978. 688 с.

6. Аннин Б. Д., Бытев В. О., Сенашов С. И. Групповые свойства уравнений упругости и пластичности. Новосибирск : Наука, 1983. 143 с.

7. Сенашов С. И., Гомонова О. В., Яхно А. Н. Математические вопросы двумерных уравнений идеальной пластичности / Сиб. гос. аэрокосмич. ун-т. Красноярск, 2012. 137 с.

8. Киряков П. П., Сенашов С. И., Яхно А. Н. Приложение симметрий и законов сохранения к решению дифференциальных уравнений. Новосибирск : Изд-во СО РАН, 2001. 192 с.

9. Senashov S. I., Vinogradov A. M. Symmetries and conservation laws of 2-dimensional ideal plasticity // Proc. Edinburg Math.Soc. 1988. P. 415–439.

10. Виноградов А. М., Красильщик И. С., Лычагин В. В. Симметрии и законы сохранения. М. : Фактор, 1996. 461 с.

11. Аннин Б. Д., Черепанов Г. П. Упругопластическая задача. Новосибирск : Наука, 1983. 126 с.

12. Черепанов Г. П. Механика хрупкого разрушения. М. : Наука, 1974. 640 с.

13. Сенашов С. И., Савостьянова И. Л. Упругое состояние пластины с отверстиями произвольной формы // Вестник Чувашского гос. пед. ун-та им. И. Я. Яковлева. Серия: Механика предельного состояния. 2016. № 3 (29). С. 128–134.

14. Сенашов С. И., Филюшина Е. В. Законы сохранения плоской теории упругости // Вестник СибГАУ. 2014. № 1(53). С. 79–81.

15. Сенашов С. И., Филюшина Е. В. Упругопластические задачи для ортотропных сред / Сиб. гос. аэрокосмич. ун-т. Красноярск, 2017. 116 с.

Annin Boris Dmitrievich – Dr. Sc., Professor, academician of the Russian Academy of Sciences, head of Department; Lavrentyev Institute of Hydrodynamics SB RAS.

Senashov Sergey Ivanovich – Dr. Sc., Professor, head of the Department; Reshetnev Siberian State University of Science and Technology. E-mail: sen@sibsau.ru.

Gomonova Olga Valeryevna – Cand. Sc., associate Professor; Reshetnev Siberian State University of Science and Technology.

Аннин Борис Дмитриевич – доктор физико-математических наук, профессор, академик РАН, заведующий отделом; Институт гидродинамики имени М. А. Лаврентьева СО РАН.

Сенашов Сергей Иванович – доктор физико-математических наук, профессор, заведующий кафедрой; Сибирский государственный университет науки и технологий имени академика М. Ф. Решетнева. E-mail: sen@sibsau.ru.

Гомонова Ольга Валерьевна – кандидат физико-математических наук, доцент; Сибирский государственный университет науки и технологий имени академика М. Ф. Решетнева.

INTERPRETATION OF ANT ALGORITHM FOR SOLVING THE PROBLEM OF THE TECHNICAL IMPACT PROGRAM CALENDAR PLANNING

A. S. Lifar'

Reshetnev Siberian State University of Science and Technology
31, Krasnoyarskii rabochii prospekt, Krasnoyarsk, 660037, Russian Federation
E-mail: Alifar15@mail.ru

Many strategically important sectors of the domestic industry are at the stage of transition to an investment approach to asset management. One of these industries is hydropower, where the current maintenance planning system needs new methods to deliver more efficient results. In general, the planning system for the main equipment (technical impact system) maintenance and repair can be formulated as a scheduling problem. The ant algorithm is of great interest from the point of view of solving the scheduling technical impact problem. Based on the specifics of planning, implementation and factors affecting the maintenance process, a modification of the ant algorithm is proposed. The mathematical description is a methodology for calculating parameters, basic elements of the graph, optimization criteria and constraints. A preparatory stage was also introduced into the solution algorithm, which determines the initial state of the equipment at the vertex K_0. The functional model of the technical impact planning process presented in the article can be used to develop a software package within the framework of an innovative approach to asset management for hydropower companies.

Keywords: technical impact system, ant algorithm, scheduling.

ИНТЕРПРЕТАЦИЯ МУРАВЬИНОГО АЛГОРИТМА ДЛЯ РЕШЕНИЯ ЗАДАЧИ КАЛЕНДАРНОГО ПЛАНИРОВАНИЯ ПРОГРАММЫ ТЕХНИЧЕСКОГО ВОЗДЕЙСТВИЯ

А. С. Лифарь

Сибирский государственный аэрокосмический университет имени академика М. Ф. Решетнева
Российская Федерация, 660037, г. Красноярск, просп. им. газ. «Красноярский рабочий», 31
E-mail: Alifar15@mail.ru

Многие стратегически значимые отрасли отечественной промышленности находятся на этапе перехода к инвестиционному подходу к управлению активами. Одной из таких отраслей является гидроэнергетика, где на текущий момент система планирования технического обслуживания и ремонта нуждаются в применении новых методов, дающих более эффективные результаты. В общем виде система планирования технического обслуживания и ремонта основного оборудования (система технического воздействия) может быть сформулирована в виде задачи календарного планирования. Большой интерес с точки зрения решения задачи календарного планирования технического воздействия представляет муравьиный алгоритм. На основе специфики планирования, реализации и факторов, влияющих на процесс технического обслуживания, предложена модификация муравьиного алгоритма. Математическое описание представляет собой методику расчета параметров, основных элементов графа, критериев оптимизации и ограничений. В алгоритм решения также был введен подготовительный этап, который определяет начальное состояние оборудование в вершине K_0. Функциональная модель процесса планирования технического воздействия, представленная в статье, может быть использована для разработки программного комплекса в рамках инновационного подхода управления активами гидроэнергетических компаний.

Ключевые слова: система технического воздействия, муравьиный алгоритм, календарное планирование.

Problem statement. General formulation of the problem. Many strategically important sectors of the domestic industry are at the stage of technical renewal of fixed assets, which entails a transition to an investment approach to asset management [1]. First of all, this approach is focused on improving the accuracy of assessing the techni-

cal condition of equipment, but it does not exclude the development of effective planning systems for technical impact – maintenance and repair of main equipment (hereinafter – MRO).

One of these industries is hydropower, where an index system for assessing the state of the main hydropower equipment has been developed and adopted at the moment [2–4]. At the same time, the MRO planning system remains at the level of regulatory management, that is, scheduled preventive maintenance with a fixed overhaul interval.

Thus, the existing principles of the formation of a MRO planning system based on data on the average operating time in hours for one calendar year, the standard turnaround time between overhauls and the calendar duration of the repair cycle [5; 6], are insufficient and require the use of new methods that provide more efficient results.

Problem research statement. The features of MRO planning in hydropower include:

– equipment repair planning should include the development of long-term (from 5 years), annual and monthly plans for the main equipment repair;

– the system of maintenance and repair should provide for three stages of equipment functioning: the stage of maintaining the operable state (maintenance), the stage of scheduled maintenance and the stage of scheduled overhaul;

– high requirements for the regulation of repair work and terms, including due to the coordination of plans for repair work with SO UES JSC and its branches [7; 8];

– accounting of all operation resources, including material, labour and financial;

– ensuring effective planning of repair works, on the one hand, for obsolete hydropower equipment in operation, on the other hand, for newly commissioned hydraulic units.

In general, the system for planning maintenance and repair of the main equipment of hydroelectric power plants is reduced to solving the problem of scheduling repairs of technological equipment of an enterprise. At present, the problem is fairly well-known, and different methods are used to solve it: mathematical programming, combinatorial methods, statistical and heuristic methods [9].

In this work, it was necessary to investigate the possibility of adapting the ant algorithm method to automate MRO planning taking into account the specifics of the hydropower industry and to develop a functional model of the planning process, including the principles of an investment approach to asset management and automation of the MRO planning system.

Mathematical model. Mathematical model. Let us formulate the mathematical problem setting of scheduling maintenance and repairs for the main equipment of hydroelectric power plants (hereinafter referred to as HPPs).

In general, the ant colony optimization algorithm (ant colony optimization, ACO) is a heuristic that uses the idea of agents imitating the real behaviour of ants. Ants solve the problem of finding pathways to food with the help of chemical regulation – pheromones, which they leave in the path of movement. The more ants have

passed along one path, the more pheromone, the sooner the ant will prefer this path to others.

An analysis of the literature [9–15] devoted to methods for solving the scheduling problem allowed us to conclude that the ant algorithm is the most optimal, since it:

– is quite effective with a small number of nodes;

– less susceptible to suboptimal initial decisions;

– allows you to analyze permutations of the same tasks within the same process.

In the context of the considered task of adapting the ant algorithm, the following parameters were determined, on which the quality of the solution depends:

1. The ρ coefficient affects the volatility of the pheromone. The coefficient takes values from 0 (no evaporation) to 1 (evaporates to the minimum level).

2. Coefficients α and β affect the operation of the algorithm, where α is the dependence on the level of pheramone, β is the dependence on the "quality" of the arc (weight of the arc), while: if $\alpha > \beta$, then the frequency of use has a greater influence on the ant's choice of path; if $\alpha < \beta$, then the quality of the next step (arc weight) has the greatest influence; if $\alpha = \beta$, there is a balanced relationship between the quality of the track and the degree of its operation; if $\alpha = 0$, then there is a heuristic based only on the quality of passage between successive points (ignorance of the pheromone level on the path); if $\beta = 0$, then there is a heuristic based only on the amount of pheromone (this is the path attendance factor); if $\alpha = \beta = 0$, then the decision is made uniformly and regardless of the amount of pheromone or the quality of the next step [10].

Thus, having specified the amount of pheromone (τ) and the weight of the arc (V) for the k-th arc, the probability of transition along the arc k takes the form:

$$P_k = \frac{\tau_k^{\alpha} \cdot V_k}{\sum \left(\tau_k^{\alpha} \cdot V_k \right)},$$

where i-th step, $i = 1,2,3,\ldots K$.

According to [5], the objects of repair at hydroelectric power plants can be: equipment (hydraulic turbine, hydrogenerator, transformer, pump, electric motor, diesel, valve, device, etc.); installations (hydro-turbine, hydrogenerator, transformer). However, the concept of investment asset management singles out a hydraulic unit as a piece of equipment as a key object of management. Let us introduce a description of the set of hydroelectric units at hydroelectric power plants:

$$G = \{G_c\}, c = \overline{1,c},$$

where is the G_c – th hydroelectric unit at the HPP, c is the number of hydroelectric units.

The planning period is on average 1, 5 or 10 years and will take the form:

$$t \in \{1, T\},$$

where T is the duration of the planning period. Let us assume that the minimum planning step is one year.

As noted earlier, the main equipment of a hydroelectric power station can be in three states: under maintenance (MOT), under current repair (CR) or under overhaul (TO); therefore, the vertex of the graph (K) will be characterized by one of three states (fig. 1).

The weight of the arc is determined by the aggregate indicator of the hydraulic unit, which characterizes the condition of the equipment when passing the peak K+1:

$$V_k = \left(AI_{K+1} \right)^{\beta},$$

where AI_K is the cumulative indicator of the c-th hydraulic unit at the current step.
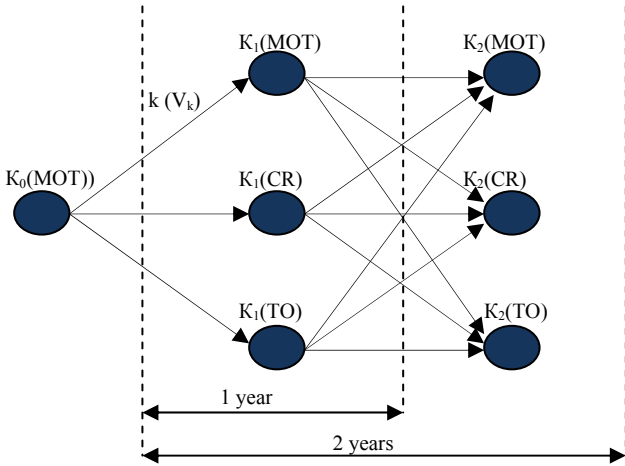
Fig. 1. Solution search graph example

Рис. 1. Пример графа поиска решения

The aggregate indicator of the hydraulic unit is determined by the product of functional indicators characterizing different aspects of the repair process (see table), taking into account the weight determined by the method of expert assessments.

$$AI = W_{\text{ТП}} \left(RR \cdot RPN \right) * W_{\text{ЭП}} \left(Z_r + Z_{lp} \right),$$

where W_i is the weight of the functional indicator.

Based on the possible directions of the company's technical policy, the following optimization criteria can be used to solve the scheduling problem. The first optimization criterion will be to minimize economic indicators along the way:

$$\text{ЭП} = \sum_{k=1}^{N} \text{ЭП}_k \to \min .$$

The second optimization criterion will be the achievement of the maximum technical indicators of the hydroelectric unit of the HPP:

$$\text{ТП} = \sum_{k=1}^{N} \text{ТП}_k \to \max .$$

In the classical model, after the ant successfully passes the route, it leaves a trace on all the traversed edges, which is inversely proportional to the length of the traversed path; in our implementation, the pheromone value will increase by the specified values in two cases – if the ant has chosen a composition that satisfies the constraints (for example, when optimizing in terms of economic indicators – restrictions on the minimum permissible residual resource) and in the case when the composition replaces the optimal solution. This change was made for reasons

of the same number of edges passed by all ants (by the number of modules, each arc is a specific combination of versions in the module) and the absence of the length indicator, which was replaced by the weight indicator. Thus, the restrictions are:

– the minimum admissible residual resource at the final vertex of the graph $(K + n)$

$$RR_{K+n} \geq RR_{\min} ;$$

– the maximum allowable total cost of repair work

$$\sum_{k=1}^{N} \text{ЭП}_k \leq \text{ЭП}_{\max} .$$

A preparatory stage was also introduced into the solution algorithm, which determines the initial state of the equipment at the vertex K_0 and is calculated based on the technical state index [2]:

$$\text{ИТS}_G = \frac{\sum_i \left(P_i \cdot \text{ИТS}_i \right)}{\sum_i P_i} ,$$

where ИТS_i is the index of the technical condition of the i-th functional unit included in the hydraulic unit; P_i is the reduction index (for hydro turbines / hydro generators – active electric power).

Functional model. To improve the efficiency of MRO planning processes, it is necessary to solve the problem of their automation and develop a program that takes into account the parameters, criteria and limitations. Its functionality should provide input of initial data (technical and financial indicators), modelling of the process of repair maintenance of both one unit and a group of units, the possibility of making changes to the original model for carrying out simulation experiments and the availability of tools for analysing and evaluating the obtained experimental results. The functional diagram of the system for planning maintenance and repairs is shown in fig. 2.

It is important to note that the first stage of optimization is implemented for each hydroelectric unit separately, with the determination of the sequence of performing types of repairs by year, along the entire planning corridor.

The second stage involves the construction of an aggregate MRO schedule for hydroelectric units (on average, about 12 hydroelectric units operate at HPPs), broken down by months and taking into account the flood and peak periods of operation of hydraulic units.

The parameters of the technical condition of the equipment, selected for the assessment of the technical condition, enter the unit for assessing the technical condition, where they are mathematically processed in accordance with [2–4]. The results obtained in the form of an index of technical condition make it possible to determine the starting points of the graph for each hydraulic unit.

The modelling block includes a method for calculating the weight of graph links and a system of constraints. The result of modelling is a graph, where the vertices are the state of the equipment (the type of technical impact on it), and the links are characterized by the aggregate indicator of the hydraulic unit.
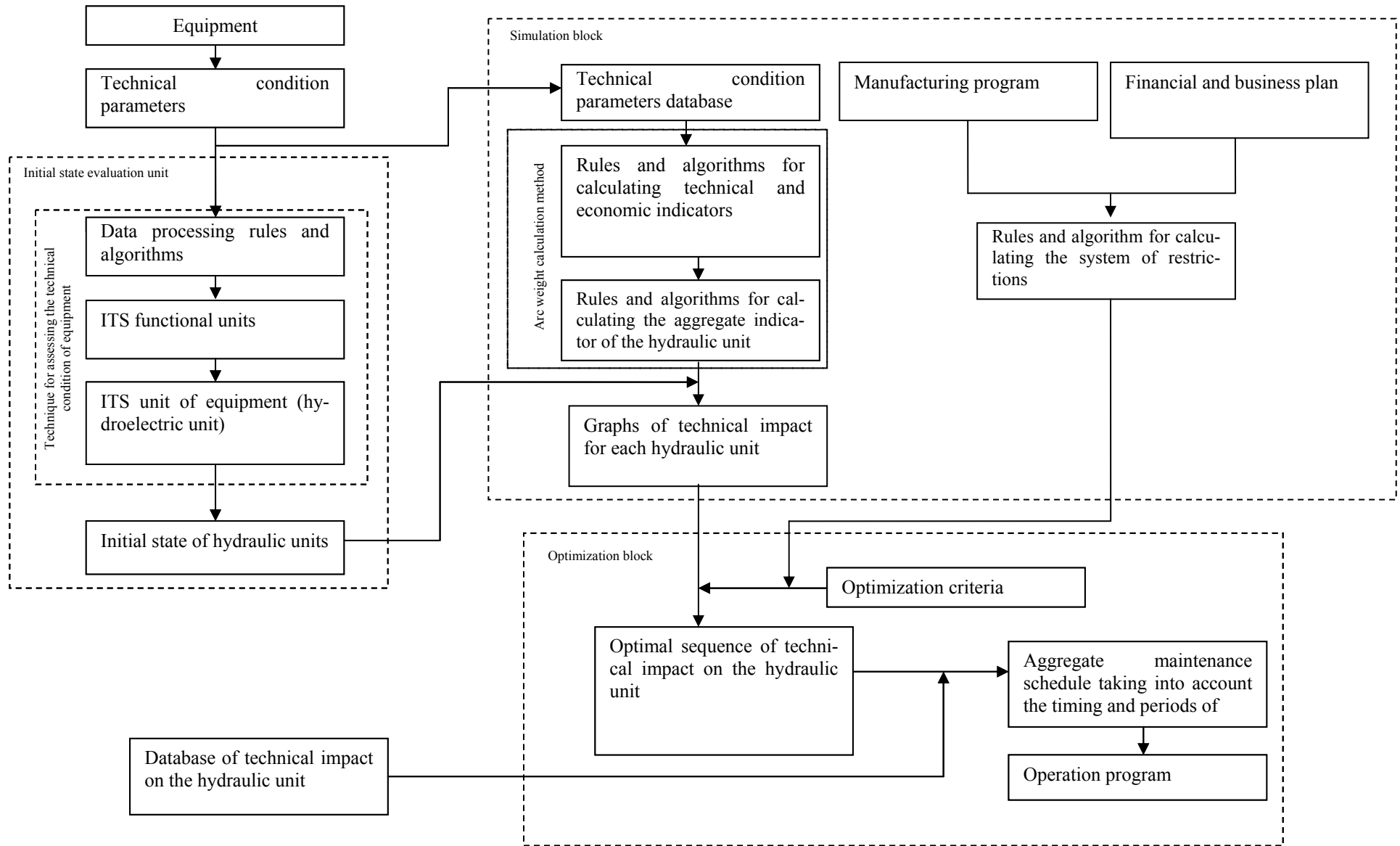
Fig. 2. Functional diagram of the system for maintenance and repairs planning

Рис. 2. Функциональная схема системы планирования технического обслуживания и ремонтов

Repair process indicators

Functional indicators	Private functional indicators	Unit of measurement	Symbol	Calculation formula
Technical indicators (TI)	Residual resource		RR	The sum of the residual life of the main units of the hydroelectric unit after repair (maintenance) at the top K+1
	Criticality index		RPN	RPN = SOD, where S is the severity of the consequences of failure of a piece of equipment, O is the probability of equipment failure within a certain period of time, D is the probability that the failure will not be detected before the manifestation of its consequences [16].
Economic indicators (EI)	Regulatory repair (maintenance) costs	Thousand rub.	Z_r	The amount of expenses for the implementation of repair work
	Lost profit	Thousand rub.	Z_{lp}	Number of days of equipment downtime due to repair *Amount of funds not received due to insufficient supply of electricity per day

Type of technical impact	PERIODS				
	2021	2022	2023	2024	2025
Maintenance (MOT)					
Current repair (CR)					
Thorough overhaul (TO)					
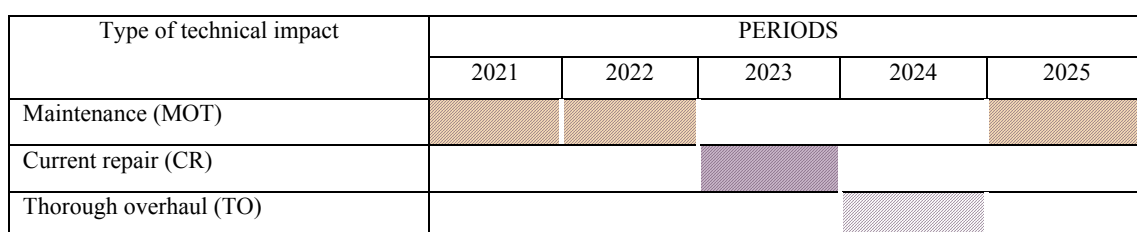
Fig. 3. Gantt chart by type of technical impact

Рис. 3. График Ганта по видам технического воздействия

Type of technical impact	PERIODS				
	2021	2022	2023	2024	2025
Maintenance (MOT)					
Current repair (CR)					
Thorough overhaul (TO)					
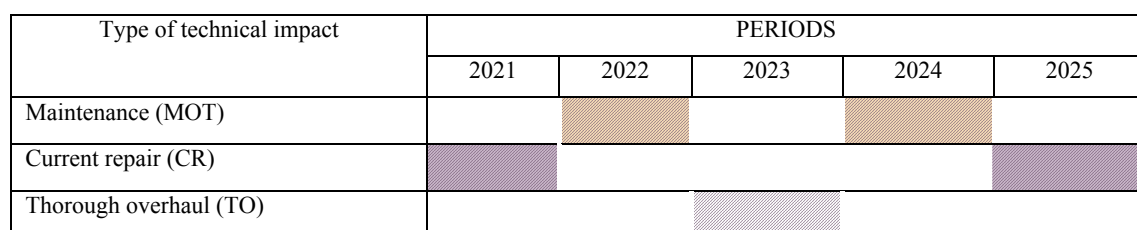
Fig. 4. Planned schedule by type of technical impact

Рис. 4. Плановый график по видам технического воздействия

In accordance with the technical policy adopted in the company (ensuring maximum technical performance of equipment or minimizing the cost of the equipment life cycle), the necessary option is selected, which is the most optimal, taking into account all the conditions and criteria. Based on the results of optimization calculations, which are based on the ant algorithm, an aggregate maintenance schedule is formed, containing the terms and types of technical impacts for all hydraulic units for any planning period.

Experimental research. The software implementation of the method was used when planning the repair cycle for the period from 2021 to 2025 for the hydroelectric unit of the station, which is part of the largest Russian private energy company, JSC EuroSibEnergo.

The following indicators were used as input parameters: a list of possible links in the graph (possible transitions from one state of an object to another); link weight, which is calculated from such equipment parameters as the cost of repairs, lost profit due to equipment downtime, equipment criticality index and residual resource.

It is important to note that the criterion was the minimization of economic indicators, while the limitation is the minimum allowable residual resource at the final vertex of the graph.

The output data is a five-year technical impact program, presented in the form of a Gantt chart (by type of technical impact) (fig. 3).

In comparison with the planned repair work schedule adopted at the hydroelectric power station (fig. 4), the

technical impact program, obtained on the basis of the ant algorithm, provided a reduction in the total economic indicators (the cost of repair work and lost profits due to equipment downtime) by 5 %. Saving for the group of costs for repair work amounted to 1,175.8 thousand rubles subject to condition RR2025 > 0.9.

Conclusion. The ant algorithm makes it possible to successfully solve scheduling problems, including planning a maintenance and repair program for the main hydropower equipment. The article formulates a mathematical statement of the problem of scheduling repairs and a functional model of the process of planning maintenance and repair. The results presented in the article can be used to develop a software package as part of an innovative approach to asset management for hydropower companies.

References

1. Technical policy of RusHydro Group (Annex to protocol of the Board of Directors dated 10.04.2020 (date of 09.04.2020) No. 307 (In Russ.). Available at: http://www.rushydro.ru/upload/iblock/5d0/Tehnicheskaya-politika.pdf (accessed: 20.06.2020).

2. About complex determination of indicators of technical and economic condition of electric power facilities, including indicators of physical wear and energy efficiency of electric grid facilities, and on monitoring of such indicators: decree of the Government of the Russian Federation of December 19, 2016 no. 1401 (In Russ.). Available at: https://russrules.ru/news/osnovnye-pravila-oformleniya-bibliog.html (accessed: 20.07.2020).

3. Indicator of the technical condition of electric power facilities (In Russ.). Available at: https://minenergo.gov.ru/node/11201 (accessed: 25.07.2020).

4. *STO 17330282.27.140.001–2006. Gidroelektrostantsii. Metodiki otsenki tekhnicheskogo sostoyaniya osnovnogo oborudovaniya* [Hydroelectric power Stations. Methods for evaluating the technical condition of the main equipment]. Available at: http://www.rushydro.ru/upload/iblock/83a/001_STO-17330282.27.140.001-2006.pdf (accessed: 25.07.2020).

5. *STO RusHydro 02.01.62–2012 Gidroelektrstantsii. Remont i tekhnicheskoe obsluzhivanie oborudovaniya, zdaniy i sooruzheniy. Oragnizatsiya proizvodstvennykh protsessov. Normy i trebovaniya* [Hydroelectric power Station. Repair and maintenance of equipment, buildings and structures. Organization of production processes. Standards and requirements]. Available at: http://www.rushydro.ru/upload/iblock/15c/062_STO-RusGidro-02.01.062-2012_Remont-i-TO-zdanij-i-sooruzhenij-GES.pdf (accessed: 01.08.2020).

6. *GOST 27.310–95 Nadezhnost' v tekhnike. Analiz vidov, posledstviy i kritichnosti otkazov. Osnovnye polozheniya* [Reliability in technology. Analysis of the types, consequences, and criticality of failures. Basic provisions]. Available at: http://www.ohranatruda.ru/ot_biblio/normativ/data_normativ/29/29151/index.php (accessed: 22.05.2020).

7. RF Federal "Low about safety of hydraulic structures" from 21.07.1997 № 117-FZ (the last edition) (In Russ.). Available at: http://www.consultant.ru/document/cons_doc_LAW_15265/ (accessed: 02.06.2020).

8. Strategy of development of the RusHydro group for the period up to 2020 with a perspective up to 2025 (In Russ.). Available at: http://www.rushydro.ru/upload/ iblock/206/Strategiya-RusGidro.pdf (accessed: 16.05.2020).

9. Sekaev V. G., Matryonin P. V. [Using the ant colony method to solve calendar planning tasks]. *Sbornik nauchnyh trudov NGTU*. 2011, P. 109–118 (In Russ.).

10. Mieczysław Drabowski, Edward Wantuch Ant Colony Optimization – Techniques and Applications. Available at: https://www.intechopen.com/books/ant-colony-optimization-techniques-and-applications/scheduling-in-manufacturing-systems-ant-colony-approach (accessed: 27.06.2020).

11. Shtovba S. D. [Ant algorithm]. *Matematika v prilozheniyakh*. 2003, No. 4(4), P. 70–75 (In Russ.).

12. Myshenkov K. S., Romanov A. Yu. [Method for solving the problem of scheduling repairs of technological equipment of an enterprise using a genetic algorithm]. *Nauka i obrazovanie*. 2011, No. 9, P. 1–10 (In Russ.).

13. Andriyan K.E., Kursin D.A. [Analysis and planning of maintenance and repair of a complex object based on its functional state]. *Nauka i obrazovanie*. 2011, No. 8, P. 1–5 (In Russ.).

14. Artyomov I. I., Simonov A. S., Denisov N. E. [Predicting the reliability and running-in time of process equipment based on the function of the failure flow parameter] (In Russ.). Available at: https://cyberleninka.ru/article/v/prognozirovanie-nadyozhnosti-i-dlitelnosti-prirabotki-tehnologicheskogo-oborudovaniya-po-funktsii-parametra-potoka-otkazov (accessed: 05.07.2020).

15. Rodionova V. N., YAgolkovskaya E. N. [Organization of operation and maintenance of equipment at the enterprise]. *Ekonominfo*. 2017, No. 4, P. 9–13(In Russ.).

16. GOST R 5190.12–2007. *Menedzhment riska. Metod analiza vidov i posledstviy otkazov.* [State Standard R 5190.12-2007. Risk management. Failure modes and consequences analysis method]. Moscow, Standartinform Publ., 2008. 35 p.

Библиографические ссылки

1. Техническая политика Группы РусГидро (Приложение к Протоколу СД от 10.04.2020 (дата проведения 09.04.2020) № 307 [Электронный ресурс]. URL: http://www.rushydro.ru/upload/iblock/5d0/Tehnicheskaya-politika.pdf (дата обращения: 20.06.2020).

2. «О комплексном определении показателей технико-экономического состояния объектов электроэнергетики, в том числе показателей физического износа и энергетической эффективности объектов электросетевого хозяйства, и об осуществлении мониторинга таких показателей»: постановление Правительства РФ от 19 декабря 2016 г. № 1401 [Электронный ресурс]. URL: https://russrules.ru/news/osnovnye-pravila-oformleniya-bibliog.html (дата обращения: 20.07.2020).

3. Показатель технического состояния объектов электроэнергетики (физический износ) [Электронный

ресурс]. URL: https://minenergo.gov.ru/node/11201 (дата обращения: 25.07.2020).

4. СТО 17330282.27.140.001–2006 «Гидроэлектростанции. Методики оценки технического состояния основного оборудования» [Электронный ресурс]. URL: http://www.rushydro.ru/upload/iblock/83a/001_STO-17330282.27.140.001-2006.pdf (дата обращения: 25.07.2020).

5. СТО РусГидро 02.01.62–2012 «Гидроэлектростанции. Ремонт и техническое обслуживание оборудования, зданий и сооружений. Организация производственных процессов. Нормы и требования» [Электронный ресурс]. URL: http://www.rushydro.ru/upload/iblock/15c/062_STO-RusGidro-02.01.062-2012_Remont-i-TO-zdanij-i-sooruzhenij-GES.pdf (дата обращения: 01.08.2020).

6. ГОСТ 27.310–95 «Надежность в технике. Анализ видов, последствий и критичности отказов. Основные положения» [Электронный ресурс]. URL: http://www.ohranatruda.ru/ot_biblio/normativ/data_normativ/29/29151/index.php (дата обращения: 22.05.2020).

7. ФЗ «О безопасности гидротехнических сооружений» от 21.07.1997 № 117-ФЗ (последняя редакция) [Электронный ресурс]. URL: http://www.consultant.ru/document/cons_doc_LAW_15265/ (дата обращения: 02.06.2020).

8. Стратегия развития группы РусГидро на период до 2020 г. с перспективой до 2025 г. [Электронный ресурс]. URL: http://www.rushydro.ru/upload/iblock/206/Strategiya-RusGidro.pdf (дата обращения: 16.05.2020).

9. Секаев В. Г., Матренин П. В. Использование метода колонии муравьев для решения задач календарного планирования // Сб. науч. тр. НГТУ. 2011. С 109–118.

10. Mieczysław Drabowski, Edward Wantuch Ant Colony Optimization – Techniques and Applications [Электронный ресурс]. URL: https://www.intechopen.com/books/ant-colony-optimization-techniques-and-applications/scheduling-in-manufacturing-systems-ant-colony-approach (дата обращения: 27.06.2020).

11. Штовба С. Д. Муравьиные алгоритмы // Математика в приложениях. 2003. № 4(4). С. 70–75.

12. Мышенков К. С., Романов А. Ю. Метод решения задачи календарного планирования ремонтов технологического оборудования предприятия с использованием генетического алгоритма // Наука и образование. 2011. № 9. С. 1–10.

13. Андриян К. Э., Курсин Д. А. Анализ и планирование технического обслуживания и ремонта сложного объекта на основе его функционального состояния // Наука и образование. 2011. № 8. С. 1–5.

14. Артемов И. И., Симонов А. С., Денисов Н. Е. Прогнозирование надежности и длительности приработки технологического оборудования по функции параметра потока отказов [Электронный ресурс]. URL: https://cyberleninka.ru/article/v/prognozirovanie-nadyozhnosti-i-dlitelnosti-prirabotki-tehnologicheskogo-oborudovaniya-po-funktsii-parametra-potoka-otkazov (дата обращения: 05.07.2020).

15. Родионова В. Н., Яголковская Е. Н. Организация эксплуатации и технического обслуживания оборудования на предприятии // Экономинфо. 2017. № 4. С. 9–13.

16. ГОСТ Р 51901.12–2007. Менеджмент риска. Метод анализа видов и последствий отказов. М. : Стандартинформ, 2008. 35 с.

Lifar' Aleksandra Stanislavovna – applicant, Reshetnev Siberian State University of Science and Technology. E-mail: alifar15@mail.ru.

Лифарь Александра Станиславовна – соискатель, Сибирский государственный университет науки и технологии имени академика М. Ф. Решетнева. E-mail: alifar15@mail.ru.

OPTIMIZATION CONTROL ACTIONS FOR THE ELECTROLYTIC METHOD OF ALUMINIUM PRODUCTON

A. V. Makeev[1], T. V. Piskazhova[2], P. M. Gofman[3]

[1]OOO "RUSAL ETC"
37, Pogranichnikov St., Krasnoyarsk, 660067, Russian Federation
[2]Siberian Federal University, SNFMMS
95, Krasnoyarskii rabochii prospekt, Krasnoyarsk, 660025, Russian Federation
[3] Reshetnev Siberian State University of Science and Technology
31, Krasnoyarskii rabochii prospekt, Krasnoyarsk, 660037, Russian Federation
*E-mail: grasser@mail.ru

The most common indicator of the aluminium production process managing efficiency is the cost of the metal production, but this concept includes a lot of components. First, this is the cost of raw materials and electricity in this region, as well as the labour cost per ton of products, consumption coefficients of raw materials and energy, capital costs for construction and repairs, waste disposal cost, environmental payments, etc. At the same time, there is no single functional of the process quality, depending on technological parameters, that is, the problem of complete and relatively strict mathematical process optimization as a whole is currently not solvable, not only because of its volume, but because of the lack of a complete efficiency model. In this study, particular efficiency criteria are considered, the improvement of which is aimed at the optimization model of control actions developed by the authors, which are selected based on the possible levers of the current automated process control system (APCS) for aluminium electrolysis. All tests were carried out on Virtual cell software without transfer to a real control object.

Keyword: aluminium production, process parameter optimization, automated process control system (APCS), Virtual cell.

ОПТИМИЗАЦИЯ УПРАВЛЯЮЩИХ ВОЗДЕЙСТВИЙ ПРИ ЭЛЕКТРОЛИТИЧЕСКОМ СПОСОБЕ ПОЛУЧЕНИЯ АЛЮМИНИЯ

А. В. Макеев[1], Т. В. Пискажова[2], П. М. Гофман[3]

[1]ООО «РУСАЛ ИТЦ»
Российская Федерация, 660067, г. Красноярск, ул. Пограничников, 37
[2]Сибирский федеральный университет, ИЦМиМ
660025, г. Красноярск, просп. им. газ. «Красноярский рабочий», 95
[3]Сибирский государственный университет науки и технологий имени академика М. Ф. Решетнева
660037, г. Красноярск, просп. им. газ. «Красноярский рабочий», 31
*E-mail: grasser@mail.ru

Наиболее общим показателем эффективности управления процессом получения алюминия является себестоимость произведенного металла, но это понятие включает в себя много составляющих. Прежде всего это стоимость сырья и электроэнергии в данном регионе, а также стоимость трудозатрат на тонну продукции, расходные коэффициенты сырья и энергии, капитальные затраты на строительство и ремонт, стоимость утилизации отходов, экологические выплаты и т.д. При этом отсутствует единый функционал качества процесса, зависящий от технологических параметров, то есть задача полной и относительно строгой математической оптимизации процесса в целом в настоящее время представляется не решаемой не только из-за ее объемности, а из-за отсутствия полной модели эффективности. В рамках данного исследования рассмотрены частные критерии эффективности, на улучшение которых направлена разработанная авторами оптимизационная модель управляющих воздействий, которые выбраны исходя из возможных рычагов действующей автоматизированной системы управления технологическим процессом (АСУТП) электролиза алюминия. Все испы-

тания проводились на программном обеспечении «Виртуальный электролизер» без передачи на реальный объект управления.

Ключевые слова: получение алюминия, оптимизация параметров процесса, управляющие воздействия АСУТП, Виртуальный электролизер.

Introduction. Mathematical optimization procedures are used in control systems to select the best one or more actions from the range of their admissible values. The best impacts are understood as allowing achieving the minimum or maximum of the objective function, that is, when choosing the best complex impact on the process, it is necessary to consider three components:

– selection of specific impacts and restrictions on them;

– optimization method;

– target function.

There are a huge number of optimization methods, ranging from simple methods – brute force, coordinate descent, passing to methods of medium complexity – gradient, simplex and ending with genetic algorithms [1; 2]. It should be noted that this study does not provide an accepted scientific classification of methods, but only talks about methods that can be applied to the current task – optimization of control actions in the electrolytic method of aluminium production.

The technical and economic indicators of the electrolysis process efficiency are the power consumption per ton of aluminium produced the specific consumption of carbon and fluorides, as well as the current efficiency [3–7]. Consumption factors are related to the current efficiency – the closer the amount of actually obtained metal to the theoretically possible, the lower the consumption of raw materials and energy in conditions of the same design and technology, but there may be some peculiarities, for example, the design may have a high current efficiency with good MHD index, but a large energy consumption due to increased heat loss.

We can consider such goals to achieve as a given melt temperature and cryolite ratio (CR) – an indicator of the electrolyte chemical composition, assuming that the technological personnel have already determined the effectiveness of the assigned values, and the optimization goal can be set to reduce the CR root-mean-square deviation (RMSD) and the electrolyte temperature from these target values.

Based on the foregoing, groups of criteria have been identified, according to which optimization is possible:

– RMSD of electrolyte temperature from a given target value;

– CR RMSD from a given target value;

– technological parameter target value achievement at the end of the optimization period;

– specific energy consumption for aluminium production minimization;

– current output maximization.

There is a division into multi-criteria and single-criteria optimization with different methods of finding a local or global extremum, but we will assume that the objective function is composed in such a way that it has one minimum or maximum and includes our requirements for the technological process.

Description of the optimization method. To search for optimal influences, a gradient optimization method was chosen – the Cauchy method [8], which is based on the formula:

$$x^{(k+1)} = x^{(k)} - \alpha \cdot \nabla f(x^{(k)}), \qquad (1)$$

where the descent step α is a given positive parameter. Descent direction is determined by the components of the gradient vector $\nabla f(x^{(k)})$. Formula (1) assumes descent in the case of an n-dimensional vector of actions:

$$x^{(k)} = (x_1^k, x_2^k, x_3^k), \qquad (2)$$

where x_i^k – various control actions, at each descent step or when finding a gradient. The gradient for the case of three variables (in our case, three influences) is written as follows:

$$\nabla f(x) = i \cdot \frac{\partial f}{\partial x_1} + j \cdot \frac{\partial f}{\partial x_2} + k \cdot \frac{\partial f}{\partial x_3}. \qquad (3)$$

The method has two disadvantages: it becomes necessary to choose a suitable descent step, and the method is also characterized by slow convergence to the minimum point due to the smallness of the gradient in the vicinity of this point.

The main advantage of this method is its stability – with a sufficiently small length of the iteration step, the inequality $f(x^{(k+1)}) \leq f(x^{(k)})$. There is a theorem on sufficient conditions for the convergence of the method with a constant step [9]. Taking this property into account, the Cauchy method can significantly reduce the value of the objective function when moving from points located at significant distances from the minimum point.

In our case, the advantage of this method prevails over its disadvantages. The optimization model based on the coordinate descent method was implemented earlier, the operation of which revealed drawbacks: low search speed and going to the local extremum, in addition, with an increase in the number of impacts, the speed of work significantly slows down, since the method goes through steps separately for each impact, therefore the gradient method is more appropriate.

The step was chosen experimentally according to the sensitivity of the objective function, and a very close approach to the minimum point is not needed – the calculation accuracy should not significantly exceed the measurement accuracy. Often, one descent (in the direction of the initial gradient) is sufficient to obtain the minimum of the objective function with sufficient accuracy.

Formula (1) assumes that the gradient can be calculated at each step of descent, but the following method is practically implemented – the gradient is calculated on the multidimensional initial cross of actions and then descent is carried out in the direction of the calculated antigradient vector until the optimized technological parameter reaches the goal, or until the RMSD of this parameter

from the target stops decreasing. In the first case, the procedure is exited, and the optimization is considered to be successfully completed; in the second case, at the last point of descent, where there was a minimum RMSD, a new cross for all influences is built and a search for a new gradient is performed.

The control actions, on the basis of which the optimization procedure can be performed, are as follows:
– aluminium fluoride addition;
– set voltage;
– series current;
– metal level;
– electrolyte level.

The first three actions can be carried out by the automated process control system; the levels of melts are regulated by the technological personnel on the APCS instructions.

Virtual cell software method implementation. Virtual cell software is a physical and mathematical model that simulates the operation of an electrolytic cell for the aluminium production and is designed to study the dynamics of processes occurring in it [10–13]. This program is intended for process support personnel in order to assess the reaction of the reduction cell to control actions adequately.

The developed optimization procedure implementation was carried out in Virtual cell software in order not to harm the real control object, to evaluate all transient processes of technological parameters under complex influences and to eliminate all possible shortcomings before the implementation of this model in APCS.

At the moment, the control system already has an Electrolyte composition stabilization module [14; 15], which includes optimization for controlling the cryolite ratio (CR), but we want to expand the functionality with additional control actions and parameters for optimization, as well as target functions.

Let us describe the practical implementation of the method in Virtual cell software in terms of two influences – the addition of AlF_3 and the specified voltage; the calculation of the remaining effects in the software implementation is carried out similarly.

Fig. 1 shows a menu of initial conditions for the calculation which are requested from the APCS database for a specific reduction cell. After all calculations, the recommendations will also be transferred for the same reduction cell to the upper APCS level.

In the optimization interface (fig. 2) there is a choice between two methods – Coordinate method and Gradient method. The electrolyte temperature was chosen as the optimized parameter. The initial control actions values for fluorine and voltage additions, as well as the criterion for the completion of the optimization, are also set by the user in the interface. In this case, the following additives were selected: 5 kg of AlF_3 and 50 mV of the set voltage, as well as the criterion for exiting the optimization – reaching the minimum RMSD temperature from the target, respectively.

The calculation begins with the construction of a cross (fig. 3), on the vertices of which are the selected impacts with a given value. During the descent, the steps in the directions will change, but the cross always counts with

the initially specified additions. Next, the root-mean-square deviation of the electrolyte temperature from the target (RMSD T) is calculated at cross four points, as well as in its middle.

Then, we calculate the gradient consisting of partial derivatives numerically (using the finite difference method):

$$DIF\_AlF_3 = (RMSD(\text{T1})\text{-}RMSD(\text{T2})) / (2 \cdot \Delta AlF_3); \quad (4)$$

$$DIF\_U = (RMSD(\text{T3})\text{-}RMSD(\text{T4})) / (2 \cdot \Delta U). \quad (5)$$

We check the difference of the gradient from zero with the specified accuracy. The vector length must be nonzero

$$Modgrad = \sqrt{(DIF\_AlF_3)^2 + (DIF\_U)^2}.$$

If it is not zero, we calculate the direction of descent to the minimum in the inner loop, otherwise, exit from optimization. Inner loop:

$$\Delta\Delta AlF_3^k = \Delta\Delta AlF_3^{k-1} - step \cdot DIF\_AlF_3 \cdot \Delta AlF_3; \quad (6)$$

$$\Delta\Delta U^k = \Delta\Delta U^{k-1} - step \cdot DIF\_U \cdot \Delta U. \quad (7)$$

$\Delta\Delta AlF_3$, $\Delta\Delta U$ are the steps of the internal descent, at the first descent step they are equal to $\Delta\Delta AlF_3$ and ΔU, or zero, then they are recalculated. Deltas of actions, found by formulas (6)–(7), are added to the current values of raw materials and stress addition

$$AlF_3^k = AlF_3^0 + \Delta\Delta AlF_3^k; \quad (8)$$

$$U^k = U^0 + \Delta\Delta U^k \quad (9)$$

and we calculate RMSD T, working out these actions during the set optimization days in Virtual cell software. RMSD T should decrease and during the first calculation using formulas (8) – (9) it should be less than RMSD T0. Compare with the previous value in this inner loop, it should be done:

$$RMSD(T^k) < RMSD(T^{k-1}). \quad (10)$$

We set Step to 1 / Modgrad. Further, during debugging for use in the control system algorithms, the step for each action can be set separately.

There are two ways to exit the inner loop:
– RMSD has ceased to decrease, then we need to turn to formulas (4) and (5) and recalculate the cross, gradient, and start the inner cycle again, but the cross will be in a new place, that is, in the middle of the cross, point T0 is now the initial values of AlF_3^0 and U^0 will be assigned to the last values found by formulas (8) and (9);
– the temperature deviation from the target value is within the specified accuracy, for example, less than 0.5 degrees, then the optimization are completed.

There should be an exit from the loop optimization procedure: the RMSD in the middle of the last crosses are compared, or the last three RMSD in the descent, if they are equal, then it is necessary to exit the optimization and stop at the last effect calculation. The looping is associated with the fact that the procedure, when choosing the actions, reaches the imposed restrictions, for example, the addition of aluminium fluoride cannot be less than zero, and this is required to increase the calculated CR.

Visualization of the optimization block in Virtual cell software. When optimization is activated, a new implemented method: the gradient method (fig. 4) and the Optimization tab with two graphs become available in the results display interface window.

The optimization progress is shown on the left graph: the magnitudes of impacts and the achieved values of the optimized parameter for each experiment are displayed. On this graph, we can observe which side the optimization is moving, calculating the impact magnitude to achieve the target value of the optimized parameter.

For example, according to fig. 2, the optimized parameter was chosen: **electrolyte temperature** (target 952 °C), and the effects: **AlF₃ addition** and **voltage setting**. In experiment No. 1 (according to fig. 4), the impact values were as follows: AlF$_3$ addition = 35 kg and voltage setting = 4.23 V, while the optimized parameter (electrolyte temperature) reached 958 °C; in experiment No. 2, the values of the actions were: AlF$_3$ addition = 35 kg and voltage setting = 4.28 V, the optimized parameter reached 960 °C, etc. The cross calculation ended in experiment 5, and experiments 6 and 7 were steps towards the descent.
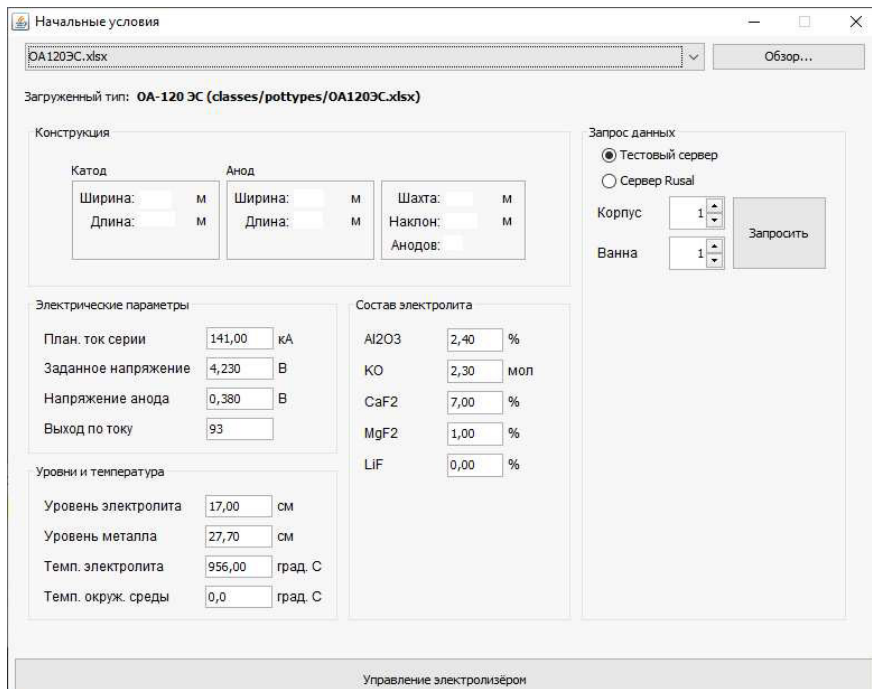
Fig. 1. Initial conditions interface

Рис. 1. Интерфейс начальных условий
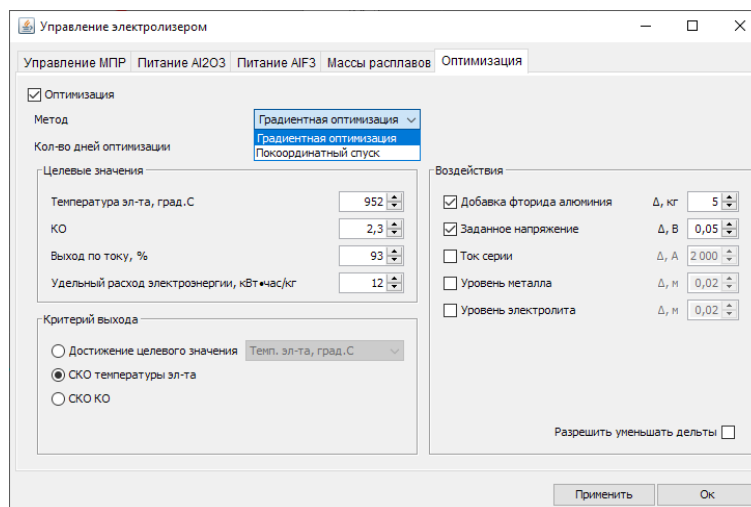
Fig. 2. Optimization interface in the Virtual cell software

Рис. 2. Интерфейс оптимизации в ПО «Виртуальный электролизёр»
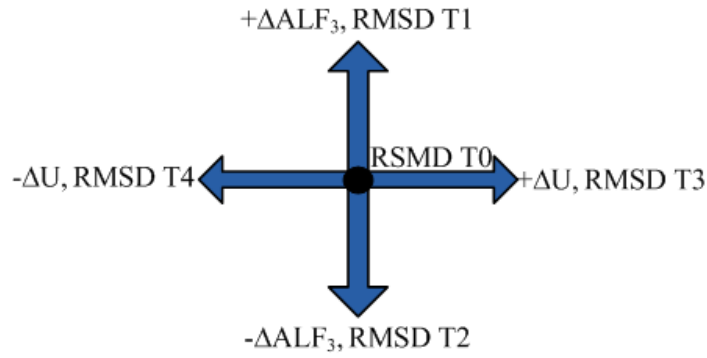
Fig. 3. Cross impacts for optimization

Рис. 3. Крест воздействий для оптимизации
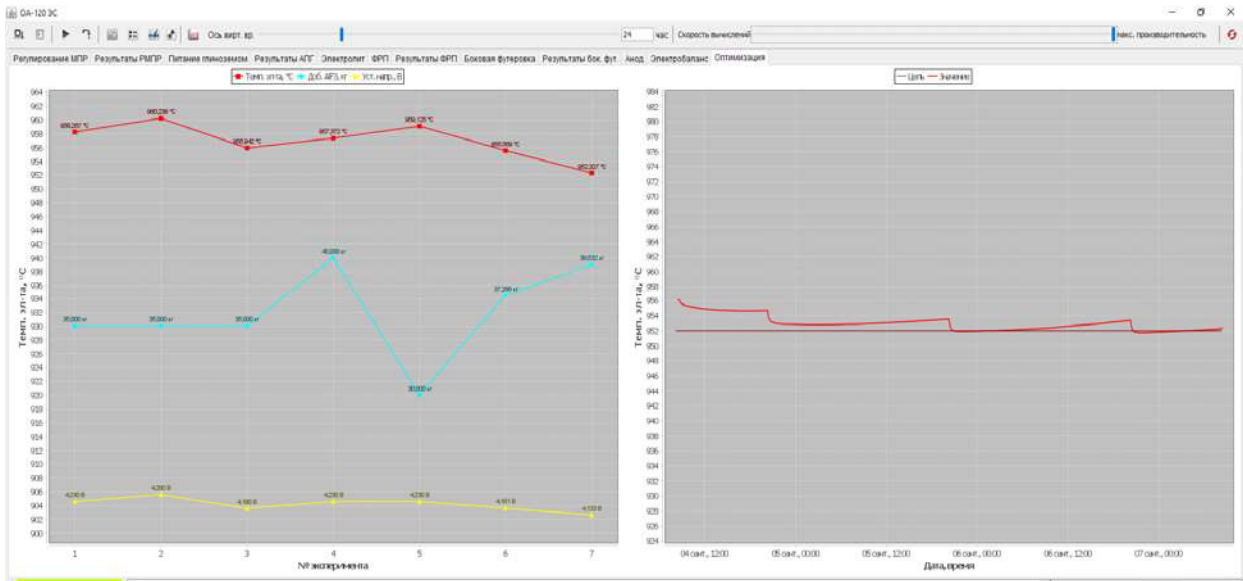
Fig. 4. Optimization tab

Рис. 4. Вкладка «Оптимизация»

Fig. 5. Optimization conditions in the test No. 2

Рис. 5. Условия оптимизации в тесте № 2

The graph is drawn and supplemented until the optimization reaches the goal, while in the case of gradient optimization, the goal can be achieved, for example, in experiment No. 7, but the optimization will continue a few more steps forward. If the optimization indicators do not improve, all subsequent experiments after the 7th will be removed from the graph and the optimal values of the parameters for achieving the goal will be seen in the last experiment No. 7.

The right graph displays the transient process of the optimized parameter (fig. 4). The graph is redrawn for each experiment, and at the end of the optimization, a transient process is displayed on it, corresponding to the experiment in which the optimization goal was achieved. We can see in detail the value of the graph at any time point in virtual time by hovering the mouse cursor over the desired location.

All subsequent tests are performed under the initial conditions indicated in fig. 5–7, the goals and optimization parameters change. In the next test No. 2, we will perform the optimal increase in the electrolyte tempera-

ture only due to the AlF_3 addition. Fig. 5 shows optimization conditions.

In fig. 6 and 7 shows the choice of reducing the daily AlF3 addition from 35 to 15 kg to increase the electrolyte temperature from 956 to 962 degrees. In contrast to test No. 1, the daily consumption and daily supplement at the beginning of the calculation was 35 kg. On the left graph in fig. 4, in experiments 1 and 2, the algorithm determined where to go, and then, in 3 steps of descent, we reached the set temperature.

Test No. 3 represents optimization with three control actions. In fig. 8 shows the selected effects to reduce the electrolyte temperature from 956 to 950 degrees. Unlike test No. 1, the program here reduced the dose of aluminium fluoride, reduced the voltage and raised the height of the metal by 4 cm, which can be seen in the results output in fig. 9. In fig. 10 the first seven calculations (experiments) made a three-dimensional cross, and then down to point 11 were carried out, then the program began to build a new cross, and at one of the new cross points it reached the specified accuracy.
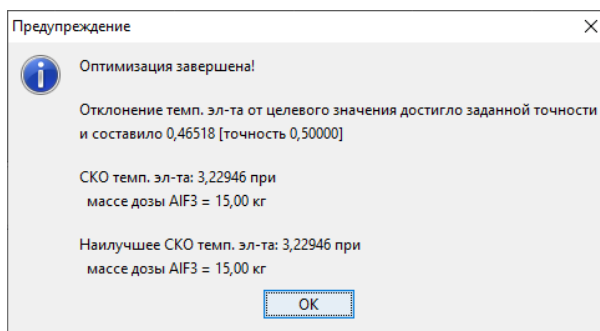
Fig. 6. Optimization results for the test No. 2

Рис. 6. Результаты оптимизации по тесту № 2
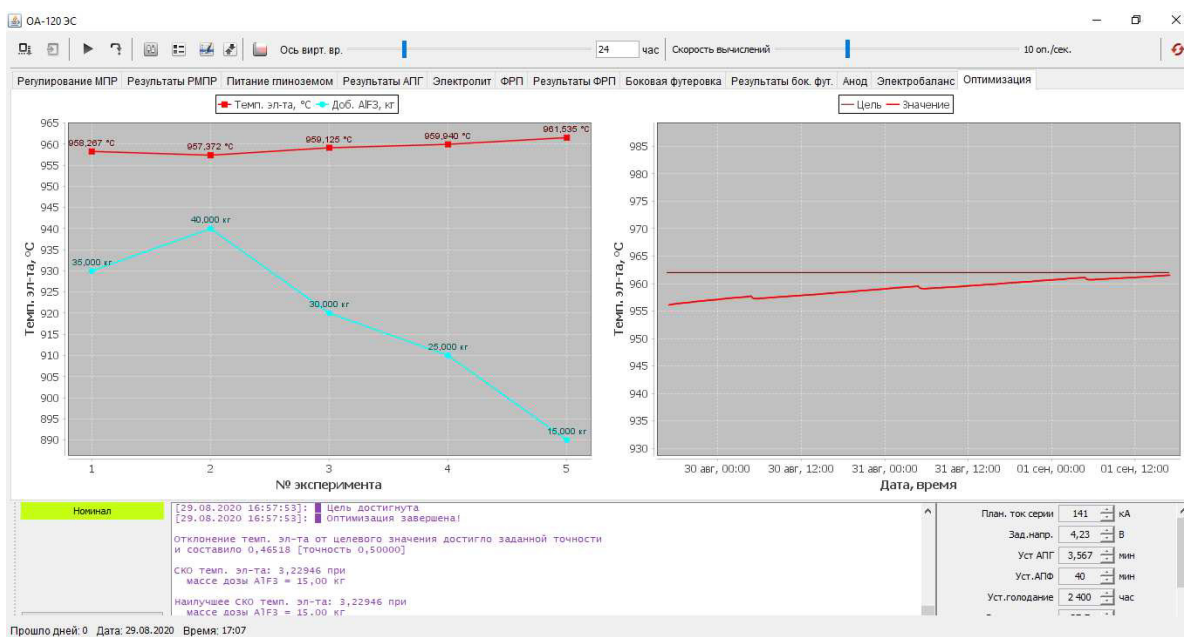
Fig. 7. Optimization procedure visualization in the calculation No. 2

Рис. 7. Визуализация процедуры оптимизации при расчете № 2
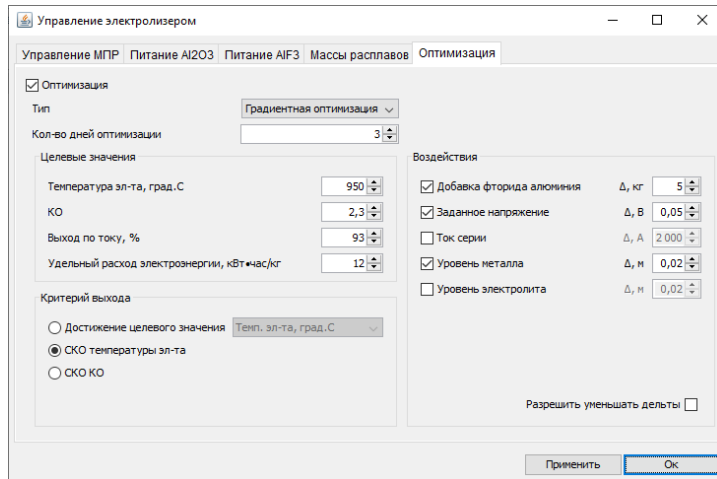
Fig. 8. Optimization conditions in the test No. 3

Рис. 8. Условия оптимизации в тесте № 3
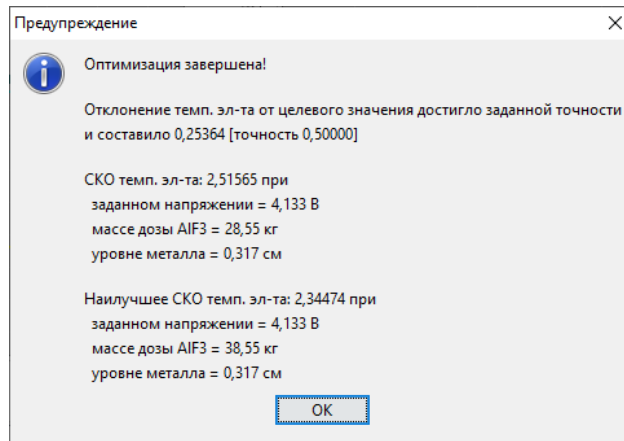
Fig. 9. Optimization result for three control actions

Рис. 9. Результат оптимизации при трех управляющих воздействиях
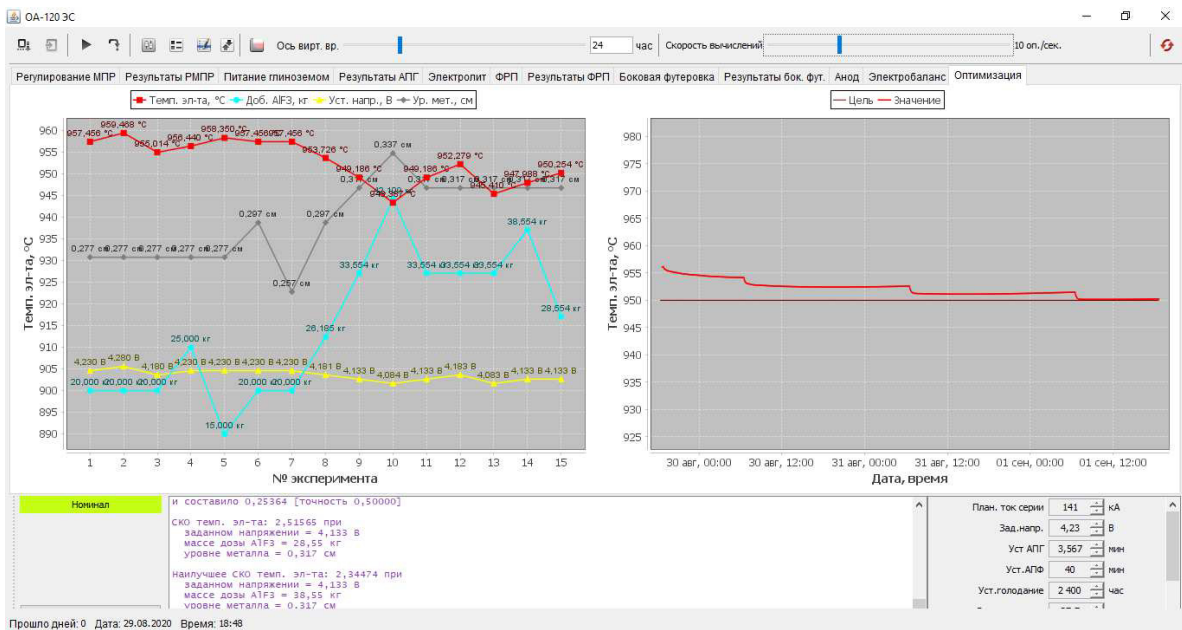
Fig. 10. Interface of optimization results with three influences, test No. 3

Рис. 10. Интерфейс результатов оптимизации при трех воздействиях, тест № 3

Conclusion. In the study, the new algorithm for calculating the complex control action by the gradient descent method was developed, software implemented and tested to improve the speed and accuracy of calculations in Virtual cell software. An interface for visualizing the operation of the optimization unit and its settings was developed. The progress of the optimization calculations is visible to the user, as well as the optimized parameter behaviour.

The developed optimization model, when introduced into the control system, will improve the control quality of the technological process of aluminium production by the electrolytic method, reduce the specific power consumption and reduce the number of electrolysers with a disturbed technological operation mode. The group of the described target functions adds variability in possible ways to optimize certain technological parameters, but for practical use in the control system algorithms, it is more important to achieve the target parameter and this will be taken into account during implementation.

References

1. Glebov N. I., Kochetkov Yu. A., Plyasunov A. V. *Metody optimizacii* [Optimization Methods]. Novosibirsk, NGU Publ., 2000, 312 p.

2. Nogin V. D., Protod'yakonov I. O., Evlampiev I. I. *Osnovy teorii optimizacii* [Fundamentals of optimization theory]. Moscow, Vysshaya shkola Publ., 2000, 214 p.

3. Galevskij G. V., Kulagin N. M., Mincis M. Ya., Sirazutdinov G. A. *Metallurgiya alyuminiya. Tekhnologiya, elektrosnabzhenie, avtomatizaciya* [Metallurgy of aluminium. Technology, power supply, automation]. Moscow, Flinta, Nauka Publ., 2008, 529 p.

4. Vetyukov M. M., Tsyplakov A. M., Shkolnikov S. N. *Elektrometallurgiya alyuminiya i magniya* [Electrometallurgy of aluminum and magnesium]. Moscow, Metallurgiya Publ., 1987, 320 p.

5. Mintsis M. Ya., Polyakov P. V., Sirazutdinova G. A. *Elektrometallurgiya alyuminiya* [Electrometallurgy of aluminum]. Novosibirsk, Nauka Publ., 2001, 368 p.

6. Bonnardel O., Homsi P. Process for regulating the temperature of the bath of an electrolytic pot for the production of aluminium. U.S. Patent No. 5,882,499. 1999.

7. Marois Marc-Andre, Bertrand Clement, Desilets Martin, Coulombe Marie-Michelle, Lacroix Marcel. Comparision of two different numerical methods for prediction the formation of the side ledge in aluminium electrolysis cell. *Light Metals*. 2009, P. 563–568.

8. Goncharov V. A. *Metody optimizacii* [Optimization methods]. Moscow, Yurayt, Vysshee obrazovanie Publ., 2010, 186 p.

9. Spirin N. A., Lavrov V. V., Rybolovlev V. Yu. et al. *Matematicheskoe modelirovanie metallurgicheskih processov v ASU TP* [Mathematical modeling of metallurgical processes in automated process control systems]. Ekaterinburg, UIPC Publ., 2014, 558 p.

10. Belolipeckiy V. M., Piskazhova T. V. *Matematicheskoe modelirovanie processa elektroliticheskogo polucheniya alyuminiya dlya resheniya zadach upravleniya tekhnologiey* [Mathematical modeling of the process of electrolytic production of aluminum for solving problems of technology management]. Krasnoyarsk, Sibirskiy federal'nyy universitet Publ., 2013, 271 p.

11. Certificate No. 2017612828 on state registration of a computer program. Educational and consulting program "Virtual electrolyzer", version 2.0. / Piskazhova T. V., Zavadyak A.V., Puzanov I. I., Tolkachev N. M., Makeev A. V.; zareg. in the register of computer programs 03 March 2017.

12. Piskazhova T. V. [*Method for optimal control of the chemical composition of the electrolyte in the production of aluminum*]. *Vestnik SibGAU.* 2010, No. 3 (29), P. 153–158.

13. Stevens McFadden Fiona J., Geoffrey P. B., Austin P. C., Welch B. J. Application of advanced process control to aluminium reduction cell – a review. Light Metals. 2002, P. 1213–1220.

14. Dupuis M., Lacroix R. Development of a 2D+ dynamic model of an aluminum reduction cell. *Proc. 38th conf. Light Metals, CIM, Quebec*. 1999. P. 41.

15. Wang Z. et al. Studies on waste heat recovery in aluminum electrolysis. Book of papers of the ninth international congress "Non-ferrous metalsand minerals". 2017. P. 209–226.

Библиографические ссылки

1. Глебов Н. И., Кочетков Ю. А., Плясунов А. В. Методы оптимизации. Новосибирск : Изд-во НГУ, 2000. 312 с.

2. Ногин В. Д., Протодьяконов И. О., Евлампиев И. И. Основы теории оптимизации. М. : Высшая школа, 2000. 214 с.

3. Металлургия алюминия. Технология, электроснабжение, автоматизация : 3-е изд., перераб. и доп. / Г. В. Галевский, Н. М. Кулагин, М. Я. Минцис, Г. А. Сиразутдинов. М. : Флинта ; Наука, 2008. 529 с.

4. Ветюков М. М., Цыплаков А. М., Школьников С. Н. Электрометаллургия алюминия и магния. М. : Металлургия, 1987. 320 с.

5. Минцис М. Я., Поляков П. В., Сиразутдинова Г. А. Электрометаллургия алюминия : монография. Новосибирск : Наука, 2001. 368 с.

6. Bonnardel O., Homsi P. Process for regulating the temperature of the bath of an electrolytic pot for the production of aluminium. U.S. Patent No. 5,882,499. 1999.

7. Comparision of two different numerical methods for prediction the formation of the side ledge in aluminium electrolysis cell / Marois Marc-Andre, Bertrand Clement, Desilets Martin, Coulombe Marie-Michelle, Lacroix Marcel. // Light Metals. 2009. P. 563–568.

8. Гончаров В. А. Методы оптимизации. М. : Юрайт ; Высшее образование, 2010. 186 с.

9. Математическое моделирование металлургических процессов в АСУ ТП / Н. А. Спирин, В. В. Лавров, В. Ю. Рыболовлев и др. Екатеринбург : УИПЦ, 2014. 558 с.

10. Белолипецкий В. М., Пискажова Т. В. Математическое моделирование процесса электролитического получения алюминия для решения задач управле-

ния технологией : монография. Красноярск : Сиб. федер. ун-т, 2013. 271 с.

11. Свидетельство № 2017612828 о государственной регистрации программы для ЭВМ. Учебно-консультационная программа «Виртуальный электролизер», версия 2.0. / Пискажова Т. В., Завадяк А. В., Пузанов И. И., Толкачев Н. М., Макеев А. В. ; зарег. в реестре программ для ЭВМ 03 марта 2017 г.

12. Пискажова Т. В. Способ оптимального управления химическим составом электролита при получении алюминия // Вестник СибГАУ. 2010. № 3 (29). С. 153–158.

13. Application of advanced process control to aluminium reduction cell – a review / Stevens McFadden Fiona J., P. B. Geoffrey, P. C. Austin, B. J. Welch // Light Metals. 2002. P. 1213–1220.

14. Dupuis M., Lacroix R. Development of a 2D+ dynamic model of an aluminum reduction cell // Proc. 38th conf. Light Metals, CIM, Quebec. 1999. P. 41.

15. Studies on waste heat recovery in aluminum electrolysis / Zhaowen Wang, Bingliang Gao, Youjian Yang, Wenju Tao, Fengguo Liu, Zhongning Shi, Xianwei Hu // Book of papers of the ninth international congress "Non-ferrous metalsand minerals". 2017. P. 209–226.

Makeev Anton Vladimirovich – manager of Process Control System Development Unit; «RUSAL ETC». E-mail: grasser@mail.ru.

Piskazhova Tatiana Valerievna – Dr. Sc., Professor; Siberian Federal University. E-mail: piskazhova@yandex.ru.

Gofman Pavel Mikhailovich – Cand. Sc., associate professor; Reshetnev Siberian State University of Science and Technology. E-mail: gofmanpm@sibsau.ru.

Макеев Антон Владимирович – менеджер отдела разработки АСУТП АП; ООО «РУСАЛ ИТЦ». E-mail: grasser@mail.ru.

Пискажова Татьяна Валериевна – доктор технических наук, профессор кафедры автоматизации производственных процессов в металлургии; Институт цветных металлов и материаловедения, Сибирский федеральный университет. E-mail: piskazhova@yandex.ru.

Гофман Павел Михайлович – кандидат технических наук, доцент, заведующий кафедрой автоматизации производственных процессов; Сибирский государственный университет науки и технологий имени академика М. Ф. Решетнева. E-mail: gofmanpm@sibsau.ru.

EFFICIENCY IMPROVING OF EMERGENCY MONITORING AND FORECASTING BASED ON THE INFORMATION SYSTEM

I. N. Pozharkova

Siberian Fire and Rescue Academy EMERCOM of Russia
1, Severnaya St., Zheleznogorsk, 662972, Russian Federation
E-mail: pozharkova@mail.ru

The article is devoted to the automated information system modification to solve monitoring and forecasting problems of natural and man-made emergencies in order to increase the efficiency of its functioning, namely, to increase the execution speed of the main operations, to reduce the error probability. Monitoring and forecasting of emergencies are among the priorities in the field of population from emergencies protection, as the prevention and elimination of their consequences are carried out on the basis of these tasks. At the same time, the data collection speed, processing and analysis largely determine the efficiency of the obtained results. The existing system of monitoring and forecasting of natural and man-made emergencies, its functional model in IDEF0 notation, characteristic features, advantages and disadvantages are considered. The existing system can be improved by automating a number of tasks related to the processing, transmission and storage of large data amounts, including real time data, as well as the generation of consolidated reports on the results of monitoring and forecasting of various objects. The information architecture of the solution reviewed and the corresponding database model form the basis of the proposed solution. The IDEF0 model of emergency monitoring and forecasting has been introduced taking into account the proposed modification of the automated information system. The main operation execution time comparative analysis based on the initial and modified automated information system (AIS) using the existing hardware confirms the effectiveness of the proposed solution. Data exchange and generation automation of consolidated reports on multiple monitoring objects will simplify analysis of the obtained results and solutions development based on them aimed at prevention of natural and man-made emergencies, as well as elimination of their consequences.

Keywords: automated information system (AIS), emergency monitoring and forecasting, automation, data conversion.

ПОВЫШЕНИЕ ЭФФЕКТИВНОСТИ РЕШЕНИЯ ЗАДАЧ МОНИТОРИНГА И ПРОГНОЗИРОВАНИЯ ЧРЕЗВЫЧАЙНЫХ СИТУАЦИЙ НА ОСНОВЕ ИНФОРМАЦИОННОЙ СИСТЕМЫ

И. Н. Пожаркова

Сибирская пожарно-спасательная академия ГПС МЧС России
Российская Федерация, 662972, г. Железногорск, ул. Северная, 1
E-mail: pozharkova@mail.ru

Статья посвящена модификации автоматизированной информационной системы решения задач мониторинга и прогнозирования чрезвычайных ситуаций природного и техногенного характера с целью повышения эффективности ее функционирования, а именно: повышения скорости выполнения основных операций, снижения вероятности возникновения ошибок. Мониторинг и прогнозирование чрезвычайных ситуаций являются одними из приоритетных направлений в сфере обеспечения защиты населения от ЧС, так как предотвращение и ликвидация их последствий осуществляются на основе решения данных задач. При этом, скорость сбора, обработки и анализа данных во многом определяют эффективность полученных результатов. В статье рассматривается существующая система мониторинга и прогнозирования чрезвычайных ситуаций природного и техногенного характера, ее функциональная модель в нотации IDEF0, характерные особенности, достоинства и недостатки. Предлагается совершенствование системы путем автоматизации ряда задач, связанных с обработкой, передачей и хранением больших объемов данных, поступающих, в том числе, и в режиме реального времени, а также с формированием сводных отчетов по результатам мониторинга и прогнозирования для различных объектов. Рассмотрена информационная архитектура предлагаемого решения, соответ-

ствующая модель базы данных. Представлена модель решения задач мониторинга и прогнозирования чрезвычайных ситуаций с учетом предлагаемой модификации автоматизированной информационной системы. Проводится сравнительный анализ времени выполнения основных операций на основе исходной и модифицированной АИС при использовании существующего аппаратного обеспечения, подтверждающий эффективность предлагаемого решения. Предлагаемая автоматизация обмена данными и генерации сводных отчетов по множеству объектов мониторинга позволит упростить анализ полученных результатов и выработку на их основе решений, направленных на предотвращение чрезвычайных ситуаций природного и техногенного характера, а также ликвидацию их последствий.

Ключевые слова: автоматизированная информационная система, мониторинг и прогнозирование чрезвычайных ситуаций, автоматизация, конвертация данных.

Introduction. The main purpose of monitoring and forecasting systems for emergencies is to monitor, control and anticipate dangerous phenomena and processes that occur in the technological sphere and nature, as well as the dynamics of their development. Forecasting allows preventing emergencies, determining their scale and organizing effective measures to eliminate them. In the Russian Federation, the general procedure for the functioning of the emergency monitoring and forecasting systems is determined by the Order No. 94 of the Ministry of Civil Defence, Emergency Situations and Natural Disaster Response of 4 March 2011 approving the Regulations on the Functional Subsystem for Monitoring, Laboratory Control and Forecasting of Emergencies of the Unified State Emergency Management System [1].

Russian physical and geographical characteristics largely determine the wide variety of emergencies occurring on its territory. Therefore, constant monitoring of a significant number of objects is required. Based on the data obtained as a result of such monitoring, the tasks of forecasting emergency situations, as well as their prevention and elimination are solved [2]. For this, various technical, software and informational support is used. The technical support of the monitoring task is based on the equipment of stations, observation systems, computer and network equipment, communication lines, etc. Monitoring data for each observation objects comes from various automated information systems; each system has its own format for storing and outputting data, which greatly complicates their processing for further use: solving forecasting problems, making decisions, compiling reports, etc. At the same time, the number of different information systems for forecasting for each type of emergency is small, while many of them are implemented on the basis of the All-Russian Centre for Monitoring and Forecasting "Antistikhiya" of the EMERCOM of Russia, and therefore have a unified format of input and output data, which simplifies their subsequent processing.

The original system description. Fig. 1 shows the IDEF0-model [3] for solving monitoring and forecasting emergencies problems, which are implemented on the solution with partial automation basis [2] in the form of separate applications and systems for data processing and analysis.

Data collection takes place in an automated mode, but the tasks of storing, analysing data and forecasting emergency situations with the generation of a preliminary solution are partially implemented manually (fig. 2–4).

The following subtasks, presented in fig. 2–4, are partially or completely solved manually:

– data recording. The readings of some sensors from the monitoring objects are presented in the form of graphic or sound data; their transfer to the computer memory for subsequent processing is carried out manually;

– data conversion. For storage in the database, the available information must be brought to a single format corresponding to the given structure, which is also partially done manually;

– converting data into a given AIS form. To solve the problems of monitoring and forecasting based on automated information systems, it is necessary to bring the input data to a given format, which may be different for diverse applications. The corresponding operation is also carried out partially manually;

– consolidation report formation. Reports obtained on the basis of data processing in different AIS are presented in the form of various format separate documents. The report synthesis of a given form and a conclusion on the basis of the analysis performed is also done manually;

– preliminary solution development. This task is solved manually by responsible persons on the basis of the obtained forecasts, as well as existing regulations.

Consequently, a significant part of the tasks solved manually are associated with the processing of a large data amount (recording, converting, combining, etc.), including real time data. This affects the speed, accuracy and, as a consequence, the implementation effectiveness of the listed and related operations, which in the case of rapidly developing emergencies requiring an urgent solution can be critical. Therefore, it is advisable to improve the quality of the existing information system by automating the above functions.

The main goals of the information system for monitoring and forecasting emergency situation modification are:

– increasing the speed of monitoring and forecasting emergencies solving problems;

– reducing the errors associated with the human factor probability when solving the problem of monitoring and forecasting emergencies;

– improving the efficiency of monitoring and forecasting emergencies solving problems.

To achieve the goals, the following tasks are automated:

– data conversion: reduction to a unified format corresponding to a specific data structure [4; 5], coming from various monitoring objects, for their further storage in the database [6];

– data conversion into the form provided by the AIS: reduction to the necessary format, which is determined by

the AIS requirements for the structure of input information [7; 8] and data stored in the database;

– formation of a consolidated report: a report synthesis of a given form [9–11] based on output information from various AIS, presented as separate documents of different formats.

Existing system modification. Despite the identified deficiencies, the existing solution to the problems of monitoring and forecasting emergencies is quite effective, i.e. making significant changes to its structure is impractical. In addition, this approach may require partial suspension of the current system functioning, which is unacceptable.

Therefore, it is advisable to develop the existing AIS by integrating [12] a subsystem into it that automates the above tasks.
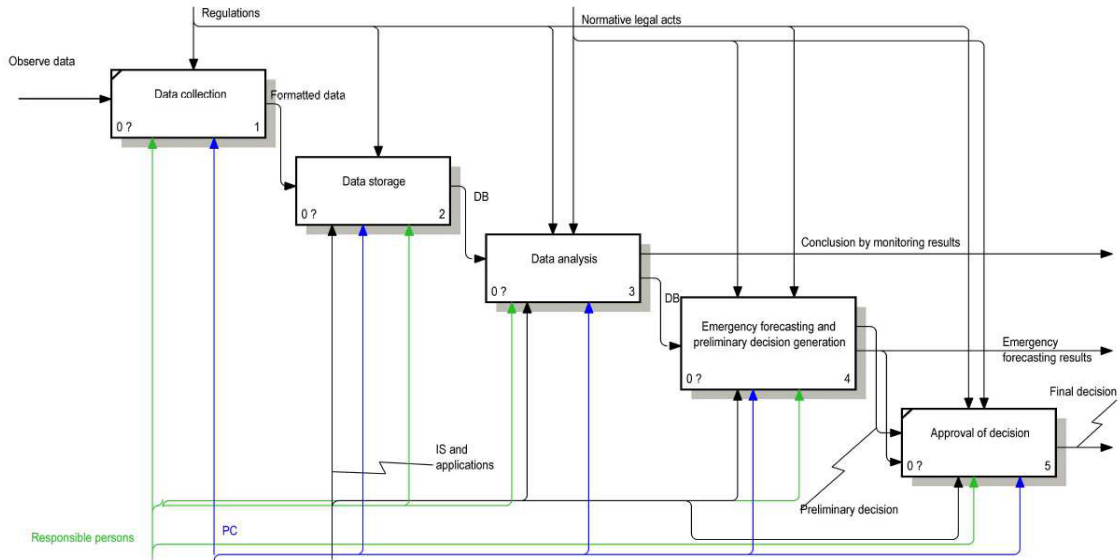
Fig. 1. Emergency monitoring and forecasting model

Рис. 1. Модель решения задачи мониторинга и прогнозирования чрезвычайных ситуаций
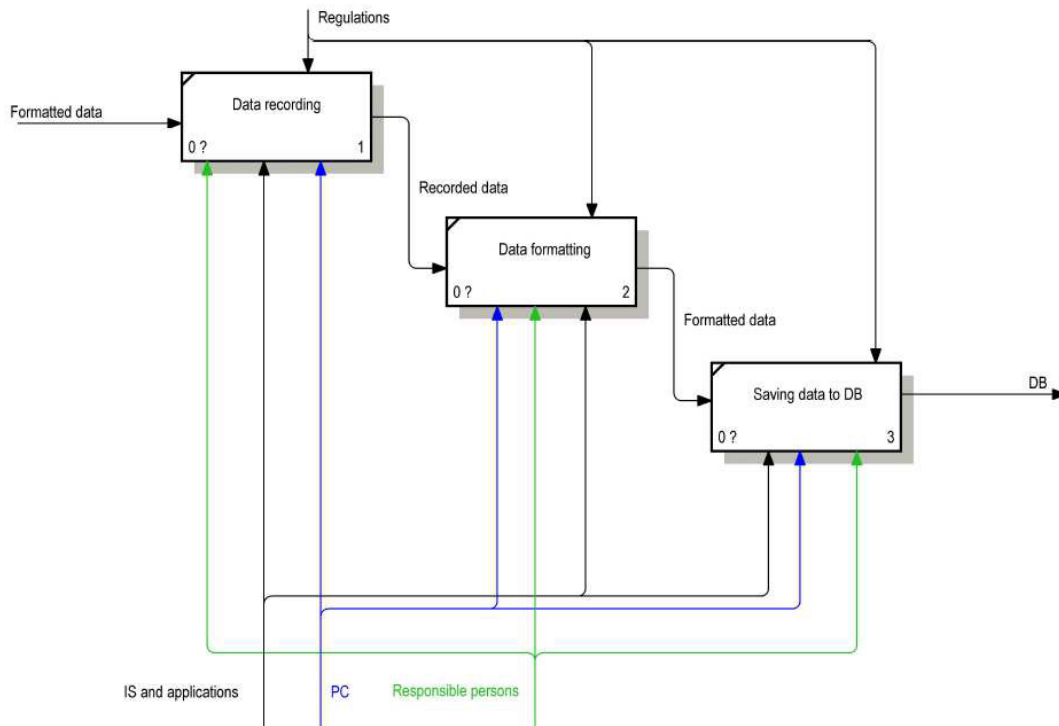
Fig. 2. Data storage solution model decomposition

Рис. 2. Декомпозиция модели решения задачи хранения данных
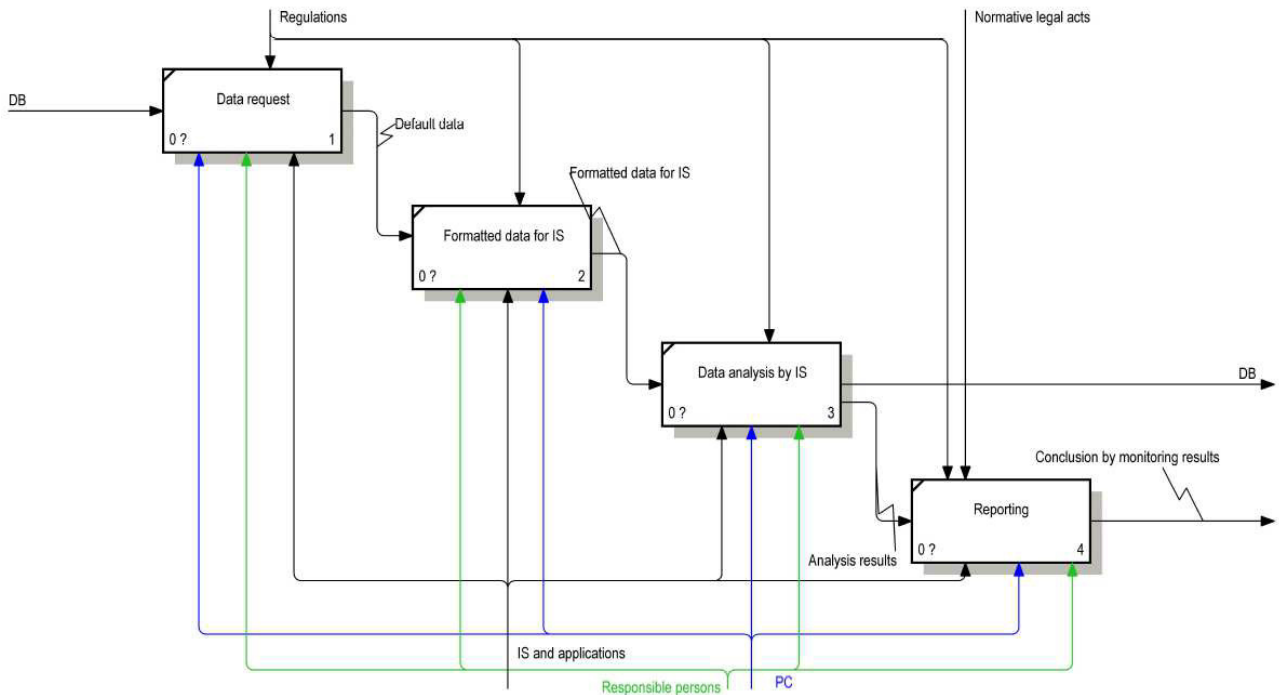
Fig. 3. Data analysis solution model decomposition

Рис. 3. Декомпозиция модели решения задачи анализа данных
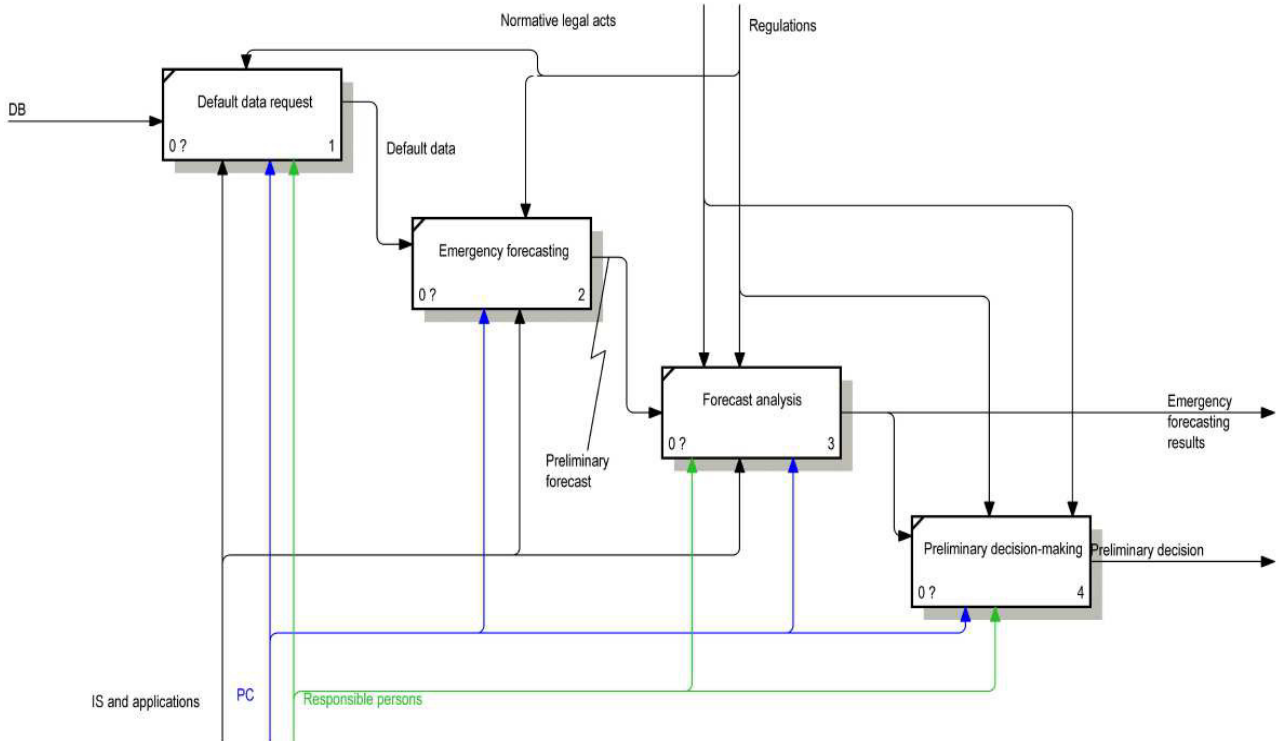
Fig. 4. Problem solution model for emergency forecasting and generation
of preliminary solution decomposition

Рис. 4. Декомпозиция модели решения задачи прогнозирования ЧС
и генерации предварительного решения
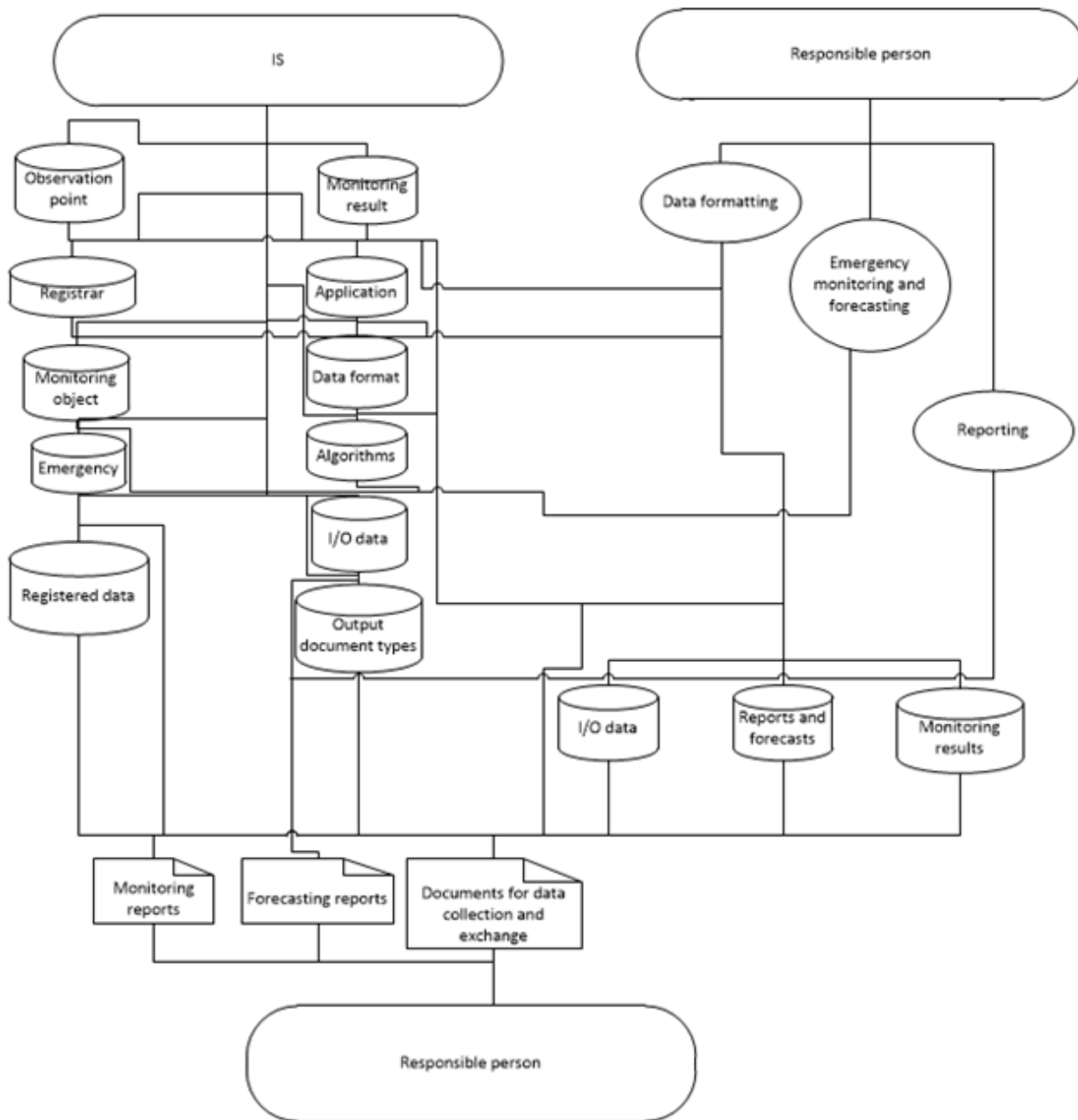
Fig. 5. AIS modified information structure for emergency monitoring and forecasting

Рис. 5. Информационная структура модифицированной АИС мониторинга
и прогнозирования чрезвычайных ситуаций

Fig. 5 shows the information structure [13] of the AIS corresponding fragment.

The basis of the automated system is the database that stores information necessary to solve problems of monitoring and forecasting emergencies, as well as modules that implement the main functions: data conversion, report generation. The database model [14] is shown in fig. 6.

The form and frequency of the basic documents formation are determined [15].

Fig. 7 shows the functional model for solving problems of monitoring and forecasting emergencies using the modified system.

The data collection solution tasks and decision approval have not changed, however, the automation degree of storage tasks, data analysis and emergency forecasting with preliminary solution generation has significantly increased (fig. 8–10).

The following subtasks, presented in fig. 8–10, are still partially or completely solved manually:
– data recording;
– preliminary solution development.

The following tasks are automated, with insignificant human involvement:
– data conversion;
– data conversion into a required AIS form;
– consolidated report formation.
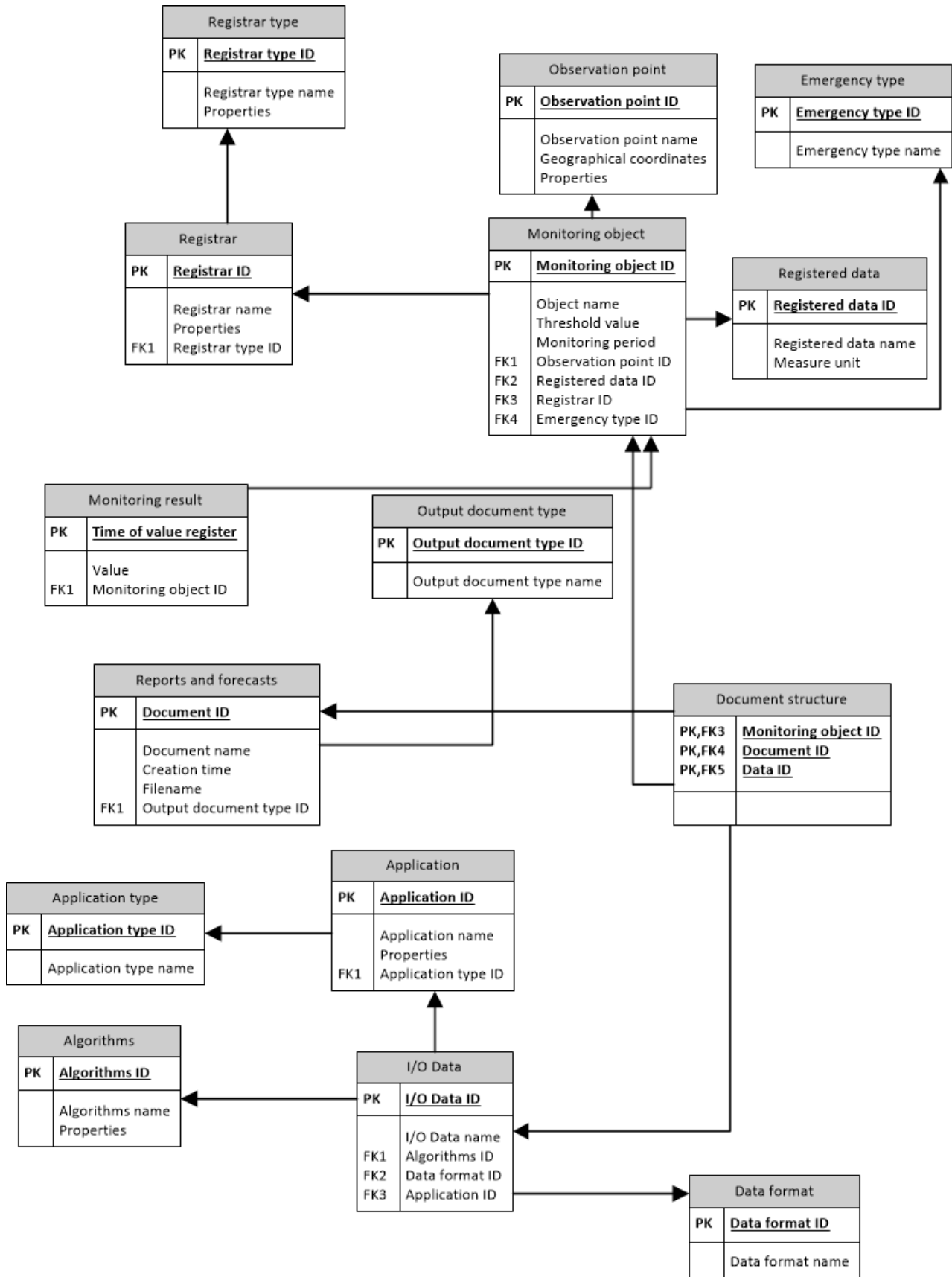
Fig. 6. Database model for the automated emergency monitoring and forecasting system

Рис. 6. Модель базы данных автоматизированной системы мониторинга
и прогнозирования чрезвычайных ситуаций
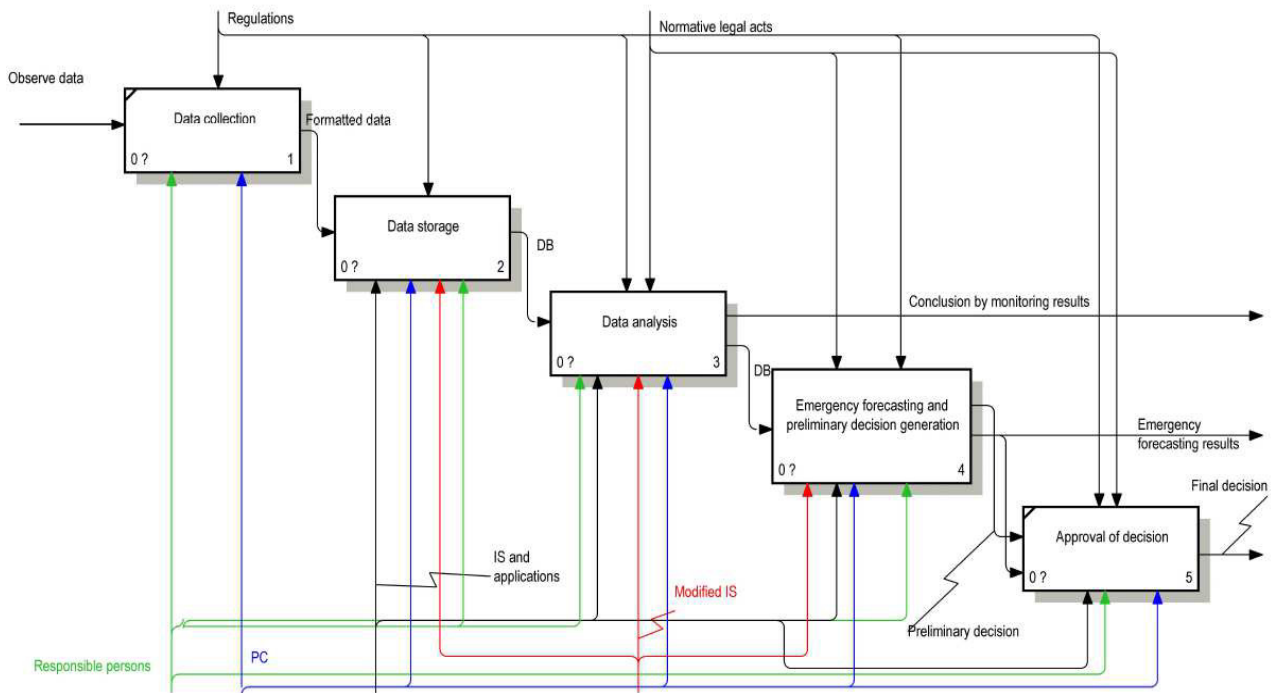
Fig. 7. Model for emergency monitoring and forecasting using the modified system

Рис. 7. Модель решения задачи мониторинга и прогнозирования чрезвычайных ситуаций
с использованием модифицированной системы
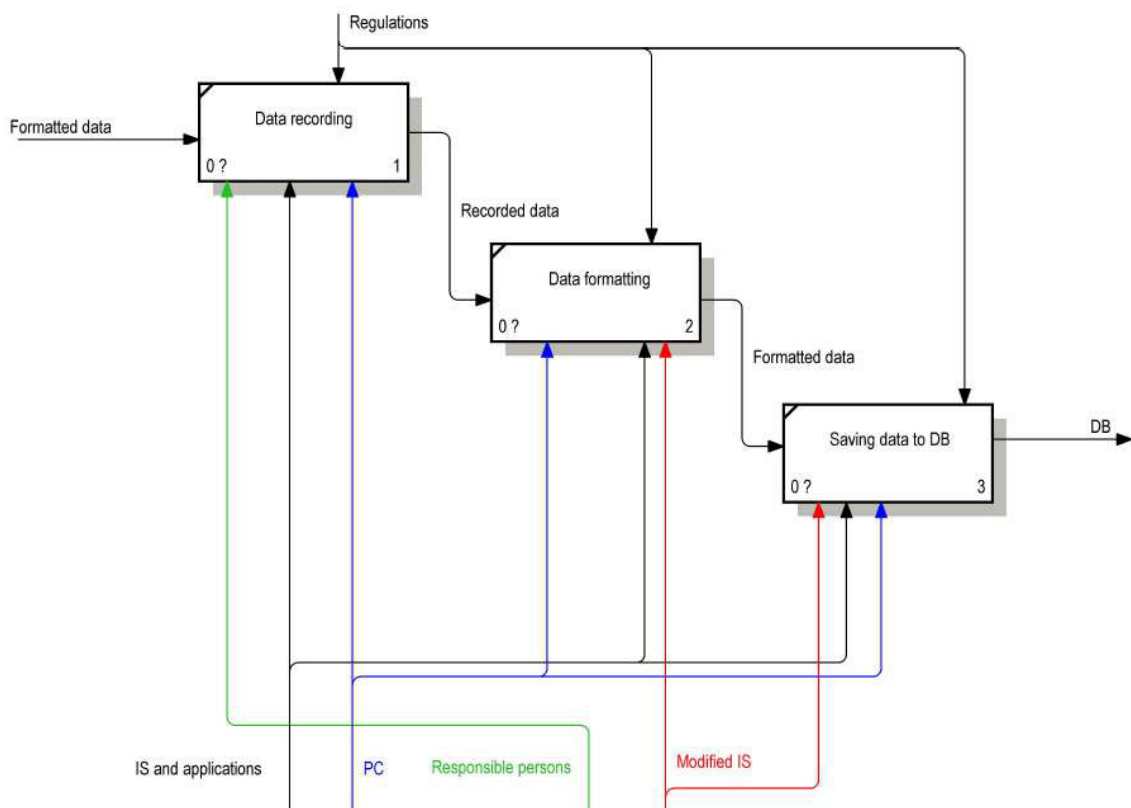
Fig. 8. The storage solution model using the modified system decomposition

Рис. 8. Декомпозиция модели решения задачи хранения данных
с использованием модифицированной системы
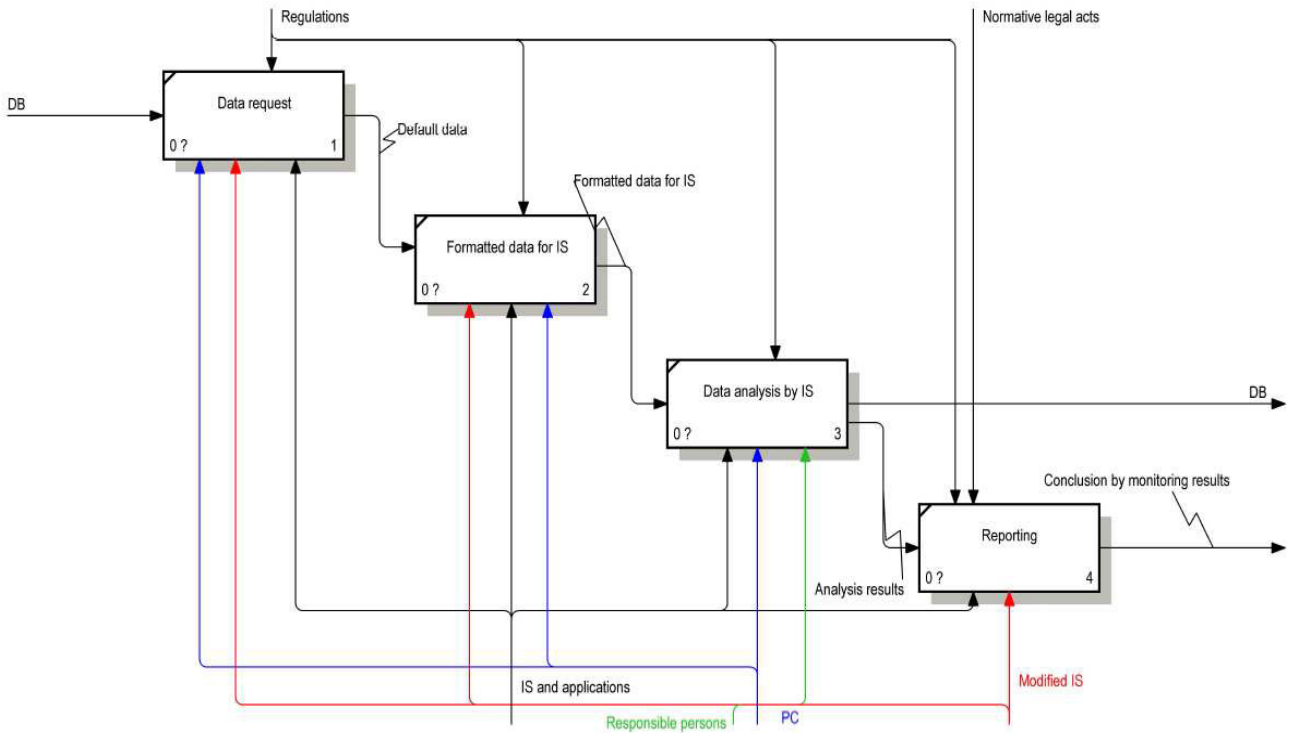
Fig. 9. Data analysis solution model using the modified system decomposition

Рис. 9. Декомпозиция модели решения задачи анализа данных
с использованием модифицированной системы
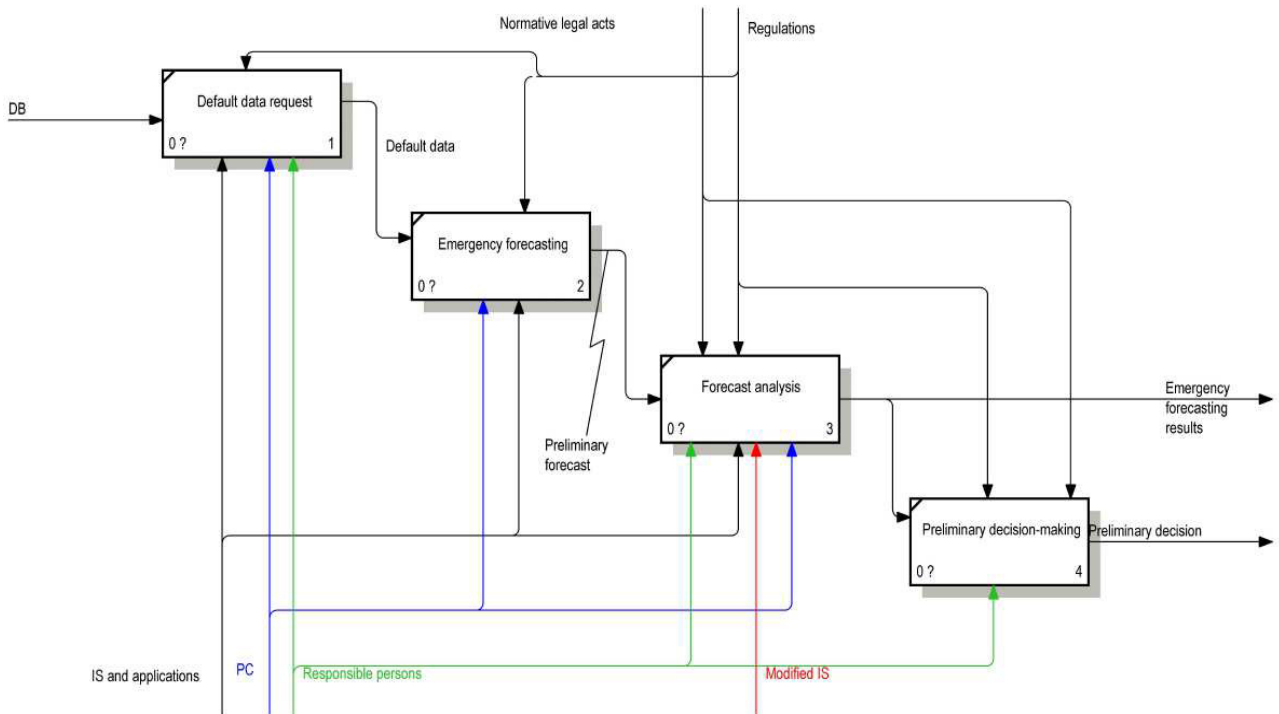
Fig. 10. The solution model of the emergency prediction and generation problem
of a preliminary solution using modified system decomposition

Рис. 10. Декомпозиция модели решения задачи прогнозирования ЧС и генерации
предварительного решения с использованием модифицированной системы

**Comparative analysis of the various operations execution time when solving monitoring
and forecasting emergencies problems**

No.	The operation name	Average execution time using the original system, s	Average execution time using the modified system, s
1	Data conversion by one parameter with writing to the database	12.4	Less than 0.001
2	Data conversion for AIS by one parameter	6.8	Less than 0.001
3	Consolidated report formation on emergency monitoring	312.8	Less than 0.001
4	Consolidated emergency forecasting report formation	248.2	Less than 0.001
5	One document completion for collection and exchange of information on emergencies	141.6	Less than 0.001

Comparative analysis of the original and modified systems. The significant part of the tasks associated with processing a large data amount (recording, converting, combining, etc.), including real time data, can be automated based on the modified information system. This has a positive effect on the speed, accuracy of data implementation and related operations. Table shows data on the execution time of basic operations based on the original and modified automated system using existing hardware.

The use of the modified automated system can significantly increase the speed of performing basic operations related to storing, processing and analysing data. With numerous operations, especially in case of rapidly developing emergencies, the use of automation can significantly increase the solving tasks efficiency.

Conclusion. According to the study, the main conclusions are:

– the task of monitoring and forecasting emergencies is one of the priorities in the security field, while its solution is associated with the collection and processing of large amounts of information. Consequently, in order to increase the implementation efficiency of these processes, it is advisable to use automated information systems, which will significantly increase the speed of data processing, analysis and decision-making based on them;

– the emergencies monitoring and forecasting implementation analysis showed that the significant part of the tasks solved manually are associated with the processing of a large amount of data (recording, conversion, merging, etc.), including real time data. This affects the speed, accuracy and, as a result, the efficiency of the data implementation and related operations, which can be critical in the case of rapidly developing emergencies requiring an urgent solution. Therefore, it was concluded that it is advisable to automate the above functions performance;

– on the basis of the modified system for monitoring and forecasting emergency situations, a significant part of the tasks can be automated, which has a positive effect on the corresponding functions implementation speed and accuracy. The comparative analysis of the manual basic operations execution time and execution time of a modified system using the existing hardware showed the significant increase in the speed of solving problems associated with storing, processing and analysing data. This indicates the high efficiency of the proposed solution.

References

1. Order No. 94 of the Ministry of Civil Defence, Emergency Situations and Natural Disaster Response of 4 March 2011 approving the Regulations on the Functional Subsystem for Monitoring, Laboratory Control and Forecasting of Emergencies of the Unified State Emergency Management System.

2. Pozharkova I. N., Ziablicki A. M. Analysis of the system of monitoring and forecasting of emergency situations of the Republic of Altai as an object of automation. *Collection of materials of the All-Russian scientific and practical conference "Monitoring, modeling and forecasting of natural hazards and emergencies"*. Zheleznogorsk, 2019. P. 156–160.

3. Systems engineering fundamentals. Available at: https://ocw.mit.edu/courses/aeronautics-and-astronautics/16-885j-aircraft-systems-engineering-fall-2005/readings/sefguide_01_01.pdf (accessed: 14.1.2020).

4. Mineharu S., Hiroko N. Raw-to-repository characterization data conversion for repeatable, replicable, and reproducible measurements. *Journal of Vacuum Science & Technology*. 2019, Vol. 12, P. 125–144.

5. Lei Zh., Li-Gang S. Research on data preprocess in data mining. *Computer science and engineering*. 2018, Vol. 7, P. 314–328.

6. Marz N., Warren D. Big Data. Principles and practices for building scalable real-time data processing systems. Moscow, Williams Publ., 2018, 582 p.

7. Malik K., Farhan M. Big-data: transformation from heterogeneous data to semantically-enriched simplified data. *Multimedia Tools and Applications*. 2016, Vol. 75, P. 12727–12747.

8. Yong-Min L., Won-Bog L. The Development of Protocol for Construction of Smart Factory. *Journal of IKEEE*. 2019, Vol. 23, P. 1096–1099.

9. Perry D., Parsons N., Costa M. 'Big data' reporting guidelines how to answer big questions, yet avoid big problems. *The Bone & Joint Journal*. 2014, Vol. 96-B, P. 7–32.

10. Taleb I., Dssouli R. Big Data Pre-processing: A Quality Framework. *IEEE International Congress on Big Data*. 2015, P. 737–751.

11. Alberti-Alhtaybat L. Big Data and corporate reporting: impacts and paradoxes. *Accounting, Auditing & Accountability Journal*. 2015, Vol. 5, P. 85–102.

12. Henningsson S., Yetton P., Wynne P. A review of information system integration in mergers and acquisi-

tions. *Journal of Information Technology*. 2018, Vol. 33, P. 255–303.

13. Dughmi S. Algorithmic information structure design. *ACM SIGecom Exchanges*. 2017, Vol. 2, P. 244–252.

14. Teorey T., Lightstone S., Nadeau T. Database Modeling and Design: Logical Design. Morgan Kaufmann, 2011. 333 p.

15. Resolution of the Government of the Russian Federation No. 334 24 March 1997, 2017 On the Procedure for the Collection and Exchange in the Russian Federation of Information in the Field of Protection of the Population and Territories from Natural and Manmade Emergencies.

Библиографические ссылки

1. Приказ Министерства Российской Федерации по делам гражданской обороны, чрезвычайным ситуациям и ликвидации последствий стихийных бедствий от 4 марта 2011 г. № 94 «Об утверждении Положения о функциональной подсистеме мониторинга, лабораторного контроля и прогнозирования чрезвычайных ситуаций единой государственной системы предупреждения и ликвидации чрезвычайных ситуаций».

2. Пожаркова И. Н., Зяблицкий А. М. Анализ системы мониторинга и прогнозирования ЧС Республики Алтай как объекта автоматизации // Мониторинг, моделирование и прогнозирование опасных природных явлений и чрезвычайных ситуаций : сб. материалов Всерос. науч.-практ. конф. Железногорск, 2019. С. 156–160.

3. Systems engineering fundamentals. [Электронный ресурс]. URL: https://ocw.mit.edu/courses/aeronautics-and-astronautics/16-885j-aircraft-systems-engineering-fall-2005/readings/sefguide_01_01.pdf (дата обращения: 14.1.2020).

4. Mineharu S., Hiroko N. Raw-to-repository characterization data conversion for repeatable, replicable, and reproducible measurements // Journal of Vacuum Science & Technology. 2019. Vol. 12. P. 125–144.

5. Lei Zh., Li-Gang S. Research on data preprocess in data mining // Computer science and engineering, 2018. Vol. 7. P. 314–328.

6. Марц Н., Уоррен Д. Большие данные. Принципы и практика построения масштабируемых систем обработки данных в реальном времени. М. : Вильямс, 2018. 582 с.

7. Malik K., Farhan M. Big-data: transformation from heterogeneous data to semantically-enriched simplified data // Multimedia Tools and Applications. 2016. Vol. 75. P. 12727–12747.

8. Yong-Min L., Won-Bog L. The Development of Protocol for Construction of Smart Factory // Journal of IKEEE. 2019. Vol. 23. P. 1096–1099.

9. Perry D., Parsons N., Costa M. 'Big data' reporting guidelines how to answer big questions, yet avoid big problems // The Bone & Joint Journal. 2014. Vol. 96-B, P. 7–32.

10. Taleb I., Dssouli R. Big Data Pre-processing: A Quality Framework // IEEE International Congress on Big Data. 2015. P. 737–751.

11. Alberti-Alhtaybat L. Big Data and corporate reporting: impacts and paradoxes // Accounting, Auditing & Accountability Journal. 2015. Vol. 5. P. 85–102.

12. Henningsson S., Yetton P., Wynne P. A review of information system integration in mergers and acquisitions // Journal of Information Technology. 2018. Vol. 33. P. 255–303

13. Dughmi S. Algorithmic information structure design // ACM SIGecom Exchanges. 2017. Vol. 2. P. 244–252.

14. Teorey T., Lightstone S., Nadeau T. Database Modeling and Design: Logical Design. Morgan Kaufmann. 2011. 333 p.

15. Постановление Правительства РФ от 24 марта 1997 г. №334 «О Порядке сбора и обмена в Российской Федерации информацией в области защиты населения и территорий от чрезвычайных ситуаций природного и техногенного характера».

Pozharkova Irina Nikolaevna – Cand. Sc., the associate professor, professor of department of technical examinations and criminalistics; Siberian Fire and Rescue Academy EMERCOM of Russia. E-mail: pozharkova@mail.ru.

Пожаркова Ирина Николаевна – кандидат технических наук, доцент, профессор кафедры инженерно-технических экспертиз и криминалистики; Сибирская пожарно-спасательная академия» Государственной противопожарной службы Министерства Российской Федерации по делам гражданской обороны, чрезвычайным ситуациям и ликвидации последствий стихийных бедствий. E-mail: pozharkova@mail.ru.

6-APERIODIC WORDS OVER THE THREE-LETTER ALPHABET

V. I. Senashov

Institute of Computational Modelling of Siberian Branch of RAS
50/44, Akademgorodok, Krasnoyarsk, 660036, Russian Federation
E-mail: sen1112home@mail.ru

The work is devoted to the study of sets of aperiodic words over a finite alphabet. A set of such words can be considered as some kind of finite formal language. W. Burnside raised the issue of local finiteness of periodic groups. The negative answer was given only sixty years later by E. S. Golod. Soon S. V. Aleshin, R. I. Hryhorczuk, V. I. Sushchanskii constructed more examples confirming the negative answer to Burnside's question. Finiteness of the free Burnside group of period n was established for periods two and three (W. Burnside), for period four (W. Burnside, I. N. Sanov), for period six (M. Hall). The infinity of such a group, for odd indicators exceeding 4381, is established in the work of P. S. Novikov and S. I. Adyan (1967), and for odd indicators exceeding 664 in the book by S. I. Adian (1975). A more intuitive version of the proof for odd $n > 10^{10}$ was proposed by A. Yu. Olshansky (1989). In this article, we consider the set of 6-aperiodic words. In the monograph by S. I. Adyan (1975) it was shown the proof of S. E. Arshon (1937) theory that there are infinitely many three-aperiodic words of any length in the two-letter alphabet. In the book of A. Y. Olshansky (1989), a proof of the infinity of the set of six-aperiodic words is given and an estimate of the number of such words of any given length is obtained. Here we try to estimate the function of the number of six-aperiodic words of any given length in a three-letter alphabet. The results obtained can be useful for encoding information in space communication sessions.

Keywords: locally finite group, word, aperiodicity, estimate, formal language.

6-АПЕРИОДИЧЕСКИЕ СЛОВА НАД ТРЕХБУКВЕННЫМ АЛФАВИТОМ

В. И. Сенашов

Институт вычислительного моделирования СО РАН
Российская Федерация, 660036, г. Красноярск, Академгородок, 50/44
E-mail: sen1112home@mail.ru

Работа посвящена изучению множеств апериодических слов над конечным алфавитом. Множество таких слов можно рассматривать как некоторый конечный формальный язык. У. Бернсайд задал вопрос о локальной конечности периодических групп. Отрицательный ответ был получен лишь через шестьдесят лет Е. С. Голодом. Вскоре С. В. Алешиным, Р. И. Григорчуком, В. И. Сущанским были построены еще примеры, подтверждающие отрицательный ответ на вопрос Бернсайда. Конечность свободной бернсайдовской группы периода n установлена в разное время для периодов два и три (У. Бернсайд), для периода четыре (У. Бернсайд; И. Н. Санов), для периода шесть (М. Холл). Бесконечность такой группы, для нечетных показателей, превышающих 4381, установлена в работе П. С. Новикова – С. И. Адяна (1967), а для нечетных показателей, превышающих 664, – в монографии С. И. Адяна (1975). Геометрический метод доказательства для нечетных показателей, превышающих 10^{10}, принадлежит А. Ю. Ольшанскому (1989). В данной статье рассматриваем множество 6-апериодических слов. l-апериодическим словом называется слово X, не содержащее нетривиальных подслов типа Y^l. В книге С. И. Адяна (1975) имеется обоснование С. Е. Аршона (1937) того, что в двухбуквенном алфавите имеется бесконечно много три-апериодических слов любой длины. В книге А. Ю. Ольшанского (1989) приведено доказательство бесконечности множества шесть-апериодических слов и получена оценка количества таких слов любой данной длины. Здесь мы хотим оценить функцию количества шесть-апериодических слов любой данной длины в алфавите из трех букв. Полученные результаты могут быть полезны при кодировании информации в сеансах космосвязи.

Ключевые слова: локально конечная группа, слово, апериодичность, оценка, формальный язык.

Introduction. The paper is devoted to the study of sets of aperiodic words over a finite alphabet. The set of such words can be considered as some finite formal language.

The group $B(d,n)$ with d generators and an identical relation $x^n = 1$ is called *a free Burnside group of rank d and period n*.

The finiteness of a free Burnside group is established at different times for period two (the trivial case), for period three by W. Burnside, for period four by W. Burnside for two generating elements; by I. N. Sanov for an arbitrary number of generating elements, and for period six by M. Hall.

William Burnside one hundred and twenty years ago raised the question of local finiteness of groups, with the identity $x^n = 1$ [1]. This problem is known as the Burnside's one. A group is called locally finite if any of its finitely generated subgroups is finite.

A negative answer to the Burnside problem was obtained in 1968 in the works of P. S. Novikov and S. I. Adyan [2–4]. The proof of the infinity of the group $B(d,n)$, with the number of generators greater than or equal to two, for odd exponents exceeding 4380 was given in [2–4], and for odd periods exceeding 665 in S. I. Adyan monograph [5].

More detailed results on the Burnside problem can be found in the work of S. I. Adyan [6].

Theorems about non-repetitive words in a three-letter alphabet and 3-aperiodic words of any length in a two-letter alphabet were proved by A. Thue in 1906 [7] (see also lemma 1 in [6]). In the article by S. E. Arshon in 1937 [8], the existence of an *n*-digit asymmetric non-repetitive sequence for an alphabet of at least three letters is proved. In the monograph of S. I. Adyan [5] on pages 13–16, by means of Arshon's method [8] it was proved that there are infinite 3-aperiodic sequences in an alphabet of two characters. The work [9] belongs to the same theory. In the monograph of A. Yu. Olshansky [9] proved the infinity of the set of 6-aperiodic words in the two-letter alphabet and obtained an estimate of the number of such words of any given length.

A report on the topic of aperiodic words was made by the author at the conference "Reshetnev Readings" [10], then research on this issue was continued: in [11] A. Yu. Olshansky's assessment of the number of 6-aperiodic words in the two-letter alphabet was improved.

In this article, we study the set of 6-aperiodic words in the three-letter alphabet. The results obtained can be useful for encoding information in space communication sessions. Previously we also considered 5-periodic words [12] and 12-aperiodic words [13].

Main result. For ease of reading, we first give a few necessary definitions.

Definition. *A periodic word with period H* is any subword of some word H^p, $p > 0$.

For example, *ababa* is a periodic word with the period *ab* or *ba*.

Definition. *An l-aperiodic word* is a word X that does not contain non-trivial subwords of type Y^l.

S. I. Adyan [4] proved that in the two-letter alphabet there is an infinite set of arbitrarily long 3-aperiodic words.

We also considered the problem of the existence of arbitrarily long words, free of squares, over the three-letter alphabet [8].

A. Yu. Olshansky [9] considered a set of 6-aperiodic words and obtained an estimate of the function $f(n)$ of the number of such words of length *n*: there are arbitrarily long 6-aperiodic words and the number $f(n)$ of such words of length *n* is greater than $(\frac{3}{2})^n$ in the two-letter alphabet. A. Yu. Olshansky [11] improved this estimate of the number of 6-aperiodic words over the two-letter alphabet.

We are interested in estimating the number of 6-aperiodic words in the three-letter alphabet.

When getting the estimate, we apply the same method as A. Yu. Olshansky used [9].

Theorem. There are arbitrarily long 6-aperiodic words and the number $f(n)$ of such words of length *n* is greater than $(\frac{5}{2})^n$ in the three-letter alphabet.

Theorem proving. Let $\{a, b, c\}$ be the alphabet. In this alphabet, we will consider 6-aperiodic words. First, we prove the inequality $f(n+1) > (5/2)f(n)$ using the method of mathematical induction.

Consider the case $n = 1$: $f(2) > \frac{5}{2} \cdot f(1)$, where $f(1) = 3$, $f(2) = 9$. It means that the base of induction is proved.

A 6-aperiodic word of length $n+1$ can be obtained by adding the letters *a, b,* or *c* to the right of the 6-aperiodic word of length *n*. In this way $3f(n)$ words X of length $n+1$ are obtained.

Some of these words may contain A^6 degrees. Then estimate the number of such extra options.

When attributed to the right, the only identity of $X \equiv YA^6$ form is obtained, since otherwise the beginning of the length *n* of the word X with the length $n+1$ contains A^6. For the words A of length 1 (only three such words), there are less than $3f(n-5)$ words of $X \equiv YA^6$ form, where the word Y is 6-aperiodic and $|Y| = n - 5$:

$$(\underbrace{\ldots\ldots}_{n-5} \; \underbrace{aa\ldots a}_{5}) \, a,$$

$$(\underbrace{\ldots\ldots}_{n-5} \; \underbrace{bb\ldots b}_{5}) \, b,$$

$$(\underbrace{\ldots\ldots}_{n-5} \; \underbrace{cc\ldots c}_{5}) \, c.$$

Obviously, there are 9 words A of length 2. The corresponding words of the $X \equiv YA^6$ type of length $n+1$ are less than $9f(n-11)$, where the word Y is 6–aperiodic of length $n-11$.

Continuing the reasoning in the same way, we have:

$$f(n+1) > 3f(n) - 3f(n-5) -$$
$$- 3^2 f(n-11) - 3^3 f(n-17) - \ldots$$

Since by the inductive assumption

$$f(n) > (5/2)^k \cdot f(n-k),$$

so

$$f(n+1) > 3f(n) - (3(5/2)^{-5} f(n) +$$
$$+ 3^2(5/2)^{-11} f(n) + 3^3(5/2)^{-17} f(n) + ...).$$

Transform the resulting inequality:

$$f(n+1) > f(n)(3 - (3(5/2)^{-5} + 3^2(5/2)^{-11} + 3^3(5/2)^{-17} + ...).$$

Since $\sqrt[6]{3} < 5/2$, so the geometric progression on the right side of the inequality is decreasing with the ratio $3(5/2)^{-6}$.

Then estimate the second factor of the right part S using the geometric progression formula

$$S = 3 - \frac{3(5/2)^{-5}}{1 - 3(5/2)^{-6}}.$$

We need to prove that $S > 5/2$.

Transform this inequality:

$$\frac{3 - 9(5/2)^{-6} - 3(5/2)^{-5} + 3(5/2)^{-5} - 5/2}{1 - 3(5/2)^{-6}} > 0.$$

After simplification we get:

$$\frac{3 - 9(5/2)^{-6} - 5/2}{1 - 3(5/2)^{-6}} > 0.$$

Since $1 - 3(5/2)^{-6} > 0$, it remains to check the correctness of the inequality:

$$3 - 9(5/2)^{-6} - 5/2 > 0.$$

We are convinced of its correctness by direct calculation. Hence, it is proved that the inequality $f(n+1) > 5/2 f(n)$ exists for any natural *n*. The theorem is proved.

Conclusion. The problem of estimating the number of aperiodic words is still being studied. The set of 6–aperiodic words in the three-letter alphabet is considered and an estimate is obtained for the function of the number of such words of any given length.

References

1. Burnside W. [On an unsettled question in the theory of discontinuous groups]. *Quart. J. Pure. Appl. Math.* 1902, Vol. 33, P. 230–238.

2. Novikov P. S., Adyan S. I. [On infinite periodic groups]. *Izv. AN SSSR, Ser. mat.* 1968, No. 1 (32), P. 212–244 (In Russ.).

3. Novikov P. S., Adyan S. I. [On infinite periodic groups. II]. *Izv. AN SSSR, Ser. mat.* 1968, No. 2 (32), P. 251–524 (In Russ.).

4. Novikov P. S., Adyan S. I. [On infinite periodic groups. III]. *Izv. AN SSSR, Ser. mat.* 1968, No. 3 (32), P. 709–731 (In Russ.).

5. Adyan S. I. *Problema Bernsayda i tozhdestva v gruppakh* [The Burnside Problem and Identities in Groups]. Moscow, Nauka Publ., 1975, 336 p.

6. Adyan S. I. [Burnside's problem and related questions]. *Uspekhi Mat. sciences.* 2010. Vol. 65, Issue. 5 (395), P. 5–60 (In Russ.).

7. Thue A. Uber unendliche Zeichenreih. Norcke Vid. Selsk. skr., I Mat. Nat. Kl. Christiania. 1906. Bd. 7. P. 1–22.

8. Arshon S. E. [Proof of existence of n-unit infinite asymmetric sequences]. *Mat. sb.* 1937, No. 4(2 (44)), P. 769–779 (In Russ.).

9. Olshansky A. Yu. Geometriya opredelyayushchikh sootnosheniy v gruppakh [Geometry of defining relations in groups]. Moscow, Nauka Publ., 1989. 448 p.

10. Senashov V. I. [Aperiodic words]. *Reshetnevskiye chteniya: materialy XIX Mezhdunar. nauch.-prakt. konf., posvyashch. 55-letiyu Sib. gos. aerokosmich. un-ta im. akad. M. F. Reshetneva* [Reshetnev Readings: materials of XIX Intern. scientific and practical. conf. for 55th anniversary of Sib. State. Aerokosmich. Univ. Acad. M. F. Reshetnev] (10-14 Nov. 2015, Krasnoyarsk). Krasnoyarsk, 2015, part 2, P. 132–133 (In Russ.).

11. Senashov V. I. [Improved estimates of the number 6-aperiodic words of fixed length]. *Vestnik SibGAU.* 2016, Vol. 17, No. 2, P. 168–172 (In Russ.).

12. Senashov V. I. [Estimation of the number of 5-aperiodic words]. *Vestnik Tuvinskogo gos. un-ta. Tekhn. i fiz.-mat. nauki.* 2017, No. 3, P. 132–138 (In Russ.).

13. Senashov V. I. [Estimation of the number of 12-aperiodic words of fixed length]. *Vestnik SibGAU.* 2017, Vol. 18, No. 1, P. 93–96 (In Russ.).

Библиографические ссылки

1. Burnside W. On an unsettled question in the theory of discontinuous groups // Quart. J. Pure. Appl. Math. 1902. Vol. 33. P. 230–238.

2. Новиков П. С., Адян С. И. О бесконечных периодических группах // Изв. АН СССР, сер. мат. 1968. № 1 (32) . С. 212–244.

3. Новиков П. С., Адян С. И. О бесконечных периодических группах. II // Изв. АН СССР, сер. мат. 1968. № 2 (32). С. 251–524.

4. Новиков П. С., Адян С. И. О бесконечных периодических группах. III // Изв. АН СССР, сер. мат. 1968. Т. 32, № 3. С. 709–731.

5. Адян С. И. Проблема Бернсайда и тождества в группах. М. : Наука. 1975. 336 с.

6. Адян С. И. Проблема Бернсайда и связанные с ней вопросы // Успехи мат. наук. 2010. Т. 65, Вып. 5 (395). С. 5–60.

7. Thue A. Uber unendliche Zeichenreih // Norcke Vid. Selsk. skr., I Mat. Nat. Kl. Christiania. 1906. Bd. 7. P. 1–22.

8. Аршон С. Е. Доказательство существования n-значных бесконечных асимметричных последовательностей // Мат. сб. 1937. № 4 (2 (44)). С. 769–779.

9. Ольшанский А. Ю. Геометрия определяющих соотношений в группах. М. : Наука. 1989. 448 с.

10. Сенашов В. И. Апериодические слова // Решетневские чтения : материалы XIX Междунар. науч.-практ. конф., посвящ. 55-летию Сиб. гос. аэрокосмич. ун-та им. акад. М. Ф. Решетнева (10–14 нояб. 2015, г. Красноярск) : в 2 ч. / под общ. ред. Ю. Ю. Логиинова ; Сиб. гос. аэрокосмич. ун-т. Красноярск, 2015. Ч. 2. С. 132–133.

11. Сенашов В. И. Улучшение оценки количества 6-апериодических слов фиксированной длины // Вестник СибГАУ. 2016. Т. 17, № 2. С. 168–172.

12. Сенашов В. И. Оценка количества 5-апериодических слов // Вестник Тувинского гос. ун-та. Техн. и физ.-мат. науки. 2017. № 3. С. 132–138.

13. Сенашов В. И. Оценка количества 12-апериодических слов фиксированной длины // Вестник СибГАУ. 2017. Т. 18, № 1. С. 93–96.

Senashov Vladimir Ivanovich – Dr. Sc., professor, leader researcher of Institute of Computational Modelling of SB RAS. E-mail: sen1112home@mail.ru.

Сенашов Владимир Иванович – доктор физико-математических наук, профессор, ведущий научный сотрудник; Институт вычислительного моделирования СО РАН. E-mail: sen1112home@mail.ru.

AUTOMATED SETTING OF REGULATORS FOR AUTOMATED PROCESS CONTROL SYSTEMS IN THE SIMINTECH VISUAL MODELING SYSTEM

V. V. Ustimenko*, A. V. Chubar, L. A. Mikhaylenko

Siberian Federal University
79, Svobodny Av., Krasnoyarsk, 660041, Russian Federation
*E-mail: zeya1998@mail.ru

For successful technological process in automated control systems it is necessary to maintain technological parameters constantly at the required level, which is ensured by the use of automated process control systems (APCS). The classical solution of this problem is the application of control devices of various types, the choice of which directly depends on the system under consideration and the requirements to it. The leading position among the automatic control system regulators for the last decades belongs to the proportional-integral-differentiating (PID) regulator, which efficiency of application in the technological process is defined by the speed and accuracy of its work. These qualities directly depend on the correct setting of the regulator parameters. The synthesis of regulators requires using of modern computer-aided design systems. The article presents the method of automatic setting of PID-regulator of the dynamic system of high order with negative feedback on the example of automatic room temperature control system. The modern Russian environment of dynamic simulation of technical systems SimInTech applied at a number of nuclear, oil refining and aerospace enterprises is used as the environment for system model development, as well as the process of its analysis and optimization. The main components of the system and transfer functions of its elements are presented. The step-by-step description of the process of project construction from standard software blocks and submodels, interacting through a single database with the use of built-in programming language, is described. The use of the built-in block of SimInTech visual simulation environment optimization for automated search of PID-regulator parameters is described in details and illustrated. The advantages and disadvantages of this adjustment method revealed during the project implementation are listed.

Keywords: modeling, PID-regulator, automatic control system, SimInTech.

АВТОМАТИЗИРОВАННАЯ НАСТРОЙКА РЕГУЛЯТОРОВ ДЛЯ АСУТП В СРЕДЕ ВИЗУАЛЬНОГО МОДЕЛИРОВАНИЯ SIMINTECH

В. В. Устименко*, А. В. Чубарь, Л. А. Михайленко

Сибирский федеральный университет
Российская Федерация, 660041, г. Красноярск, просп. Свободный, 79
*E-mail: zeya1998@mail.ru

Для успешного протекания технологического процесса требуется постоянное поддержание технологических параметров на требуемом уровне, что обеспечивается применением автоматизированных систем управления технологическими процессами (АСУТП). Классическим решением данной задачи является применение управляющих устройств различного типа, выбор которых напрямую зависит от рассматриваемой системы и предъявляемых к ней требований. Лидирующую позицию среди регуляторов АСУТП последние десятилетия занимает пропорционально-интегрально-дифференцирующий (ПИД) регулятор, эффективность применения которого в технологическом процессе определяется быстродействием и точностью его работы. Данные качества напрямую зависят от правильности настройки параметров регуляторов, для синтеза которых необходимо использование современных систем автоматизированного проектирования. В работе рассматривается метод автоматизированной настройки ПИД-регулятора динамической системы высокого порядка с обратной связью на примере системы автоматического регулирования температуры в помещении. В качестве среды разработки модели системы, а также процесса ее анализа и оптимизации используется современ-

ная российская среда динамического моделирования технических систем SimInTech, используемая на ряде предприятий атомной, нефтеперерабатывающей и аэрокосмической отраслей. Приведены основные компоненты системы, передаточные функции ее элементов. Дано поэтапное описание процесса создания проекта из типовых блоков и субмоделей программного обеспечения, взаимодействующих через единую базу данных сигналов с применением встроенного языка программирования. Подробно описано и проиллюстрировано использование встроенного блока оптимизации среды визуального моделирования SimInTech для автоматизированного поиска параметров регулятора ПИД-типа. Перечислены выявленные в ходе реализации проекта преимущества и недостатки данного метода настройки.

Ключевые слова: моделирование, ПИД-регулятор, АСУТП, SimInTech.

Introduction. Design of control systems is an important component of modern technological production. For a long time regulators have been acting as the basis for managing technological processes. Their main task is to maintain the value of the system parameter at the level set by technology for the successful flow of the technological process as a whole. The choice of regulator type is diverse: from the simplest two-position to self-adjusting microprocessor regulators.

Traditionally, proportional-integral-differentiating (PID) regulators are used in process control systems. PID regulation is a fundamental element of the management process in continuous operation. PID-type control devices are widely used in the field of automation due to their longevity, flexibility, high functionality and reliability. PID-regulators are universal in application, suitable for solving most practical problems, they are easy to implement and have a low cost. Their applications range from household devices to nuclear and aerospace industries.

However, in practice a significant proportion of control problems are associated with incorrect configuration of PID-regulators: the accuracy and speed of the system as a whole depends on the correct setting of the regulator coefficients. It means that the task of parametric synthesis of control devices is an urgent task.

The task of parametric synthesis for the specified control objects is reduced to determining the optimal parameters of the regulator, which meet the required operating conditions of the system, as well as the requirements for the quality and accuracy of control.

Currently, a number of methods, algorithms and rules allows speeding up and simplifying the task of setting up regulators [1–4]. These methods are usually divided into two broad categories: methods aimed at ensuring the quality requirements of regulation, or selection methods, in which the system operator must match the desired operator as accurately as possible [5]. Recently, regulators that can calculate the "correct" parameters when the device is connected to the system have become very popular [6]. Some of the methods for setting up regulators were considered in previous works [7–9].

In this paper, we consider the process of automated search for parameters of a PID-type control device included in the control loop. The object of regulation is a heated room. The model of the automatic control system (ACS) of room temperature is implemented in the Russian environment of dynamic modeling of technical systems *SimInTech*.

The algorithm of PID-regulator work. The PID-regulator is a parallel connection of typical links of P-, I- and D-regulators [10]. The transfer function of a PID-regulator is the sum of the transfer functions of each type of regulator:

$$W_{PID} = K_p + \frac{1}{T_i \cdot p} + T_d \cdot p \,,$$

where K_p – the regulator gain coefficient or the transmission coefficient; $K_i = \dfrac{1}{T_i}$ – the integration constant; $K_d = T_d$ – the differentiation constant.

There is no static error in PID-regulator system and they are of high performance. Regulators of this type provide a relatively high quality of regulation of objects that have a large transition delay (for example, heat exchange and mass transfer devices), as well as in cases where the load in the control objects changes frequently and quickly.

It should be noted that if the adjustment coefficients of the PID-type control device are set inaccurately, it might have worse indicators than the two-position regulator and even go into self-oscillation mode.

Automatic room temperature control system. In general, the automatic temperature control system in the room is shown in fig. 1.

The object of regulation in the system under consideration is a heated room. The indoor temperature θ is a controlled value; the air temperature θ_k coming from the heater is a regulating (controlling) effect; external factors *f* are a disturbing effect.

The sensing device (sensitive element) in this control system is a thermal resistor R_d included in the bridge circuit. The thermal resistor also performs the functions of a comparing device. An amplifier provides the amplification of the ΔU signal (mismatch signal) of the measuring bridge circuit. The amplified signal U_d provides rotation of the two-phase prime engine, which changes the amount of movement of the valve (flap) on the steam supply pipeline to the heater, which achieves a change in the air temperature at the outlet of the heater regulating the effect on the control object.

The initial data of the system is in [11]. The control system model has the following transfer functions:

$$W_r(p) = \frac{1}{400 \cdot p + 1}$$ – transfer function of the object of

regulation according to the regulatory effect;

$$W_d(p) = \frac{0.2}{400 \cdot p + 1}$$ – transfer function of the object of

regulation according to the disturbing effect;

$W_s(p) = 0.2$ – transfer function of the sensor;

$W_m(p) = \dfrac{10}{0.5 \cdot p + 1}$ – transfer function of a magnetic amplifier;

$W_e(p) = \dfrac{0.002}{p \cdot (0.08 \cdot p + 1)}$ – engine transfer function in conjunction with the valve;

$W_h(p) = \dfrac{10}{20 \cdot p + 1}$ – transfer function of the heater.

Main requirements for the quality of automatic control system. The main task of the regulator in the system under consideration is to maintain the technological parameter and the room temperature at a given level while minimizing the influence of external disturbing influences.

The system has the following requirements:

– working out the set value without an error in a settled mode;

– transition time – no more than 500 seconds;

– number of vibrations – no more than one, its amplitude should not exceed 5 % of the set value.

Simulation of ACS in the environment *SimInTech* and setting the coefficients of PID-regulator. The Russian SimInTech modeling environment was chosen as the system development environment for its analysis and optimization [12–14].

The initial complex dynamics model implemented in this software can be simplified. This provides verification of the basic principles of operation of the simulated object and its control system. As the design progresses, its individual parts can be refined and supplemented to match the real object in as much detail as possible.

To create a complex mathematical model, models of the main subsystems (submodels) implemented as separate projects are combined into a single package [15]. To link projects to each other, the signals database is used, which is a file database that contains all the necessary variables for the projects to work. These variables are used to describe the model, visually represent the modeling process on video frames, exchange data with external modules etc.

As a programming language, this software uses the built-in C language to write scripts that perform manipulations with schema objects as they are calculated.

The ACS scheme implemented in the *SimInTech* visual modeling environment is shown in fig. 2. The control object is placed in a submodel consisting of standard blocks, the composition of which is shown in fig. 3.

In the "calculation of transient parameters" submodel, which is shown in fig. 4, automatic calculation of time indicators of control quality is performed: the control time and the maximum of the controlled value. In the script, basing on the data obtained (the steady value and its maximum) the overshooting value is calculated.

The calculation of the control time – the time for which the value of the system reaches a new steady value is as follows: the mismatch signal module (control error) is applied to the middle (logical) input port of the key. Given that the complete process attenuation occurs at $t \to \infty$, the duration of the transition process is limited to the moment when the controlled value begins to deviate from the steady value by less than 5 %. Based on this, if the mismatch signal exceeds the specified five percent set point, the current model time (signal from the lower input port) is transmitted to the key output. If the control signal is less than the set point, the same signal is transmitted to the key output, but delayed by one integration step (the signal from the upper input port). Thus, after the calculation is completed, the variable «determining the control time» will contain the value of the transition time.

All variables calculated during operation are recorded in the signal database. An example of a project signal database is shown in fig. 5.

Detailed information about the database structure of the project (tab. 1).

In the *SimInTech* visual modeling environment, the PID regulator is represented by a separate block of the "Discrete" library – "Discrete PID-regulator". When implementing the ACS scheme with an embedded PID-regulator, shown in fig. 6, only the macroblock "Control object" is modified: the regulator, which parameter setting is the task of this work, takes place after the comparison device.
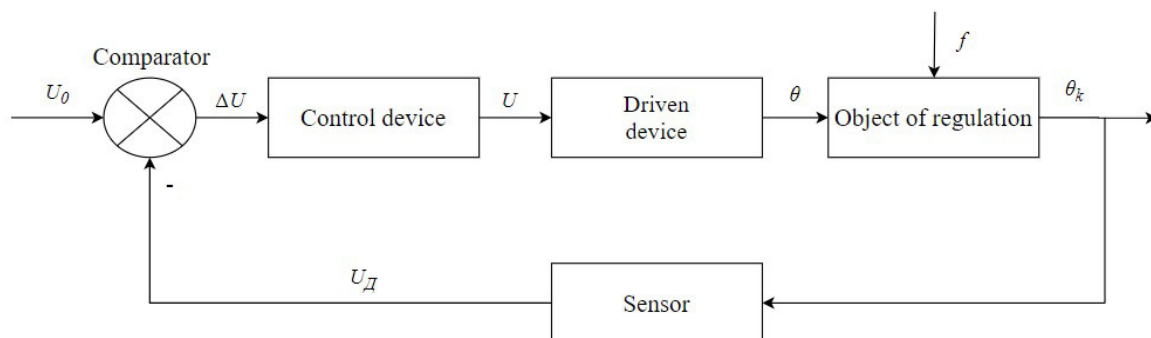
Fig. 1. Functional chart of automatic control system of room temperature

Рис. 1. Функциональная схема САР температуры в помещении
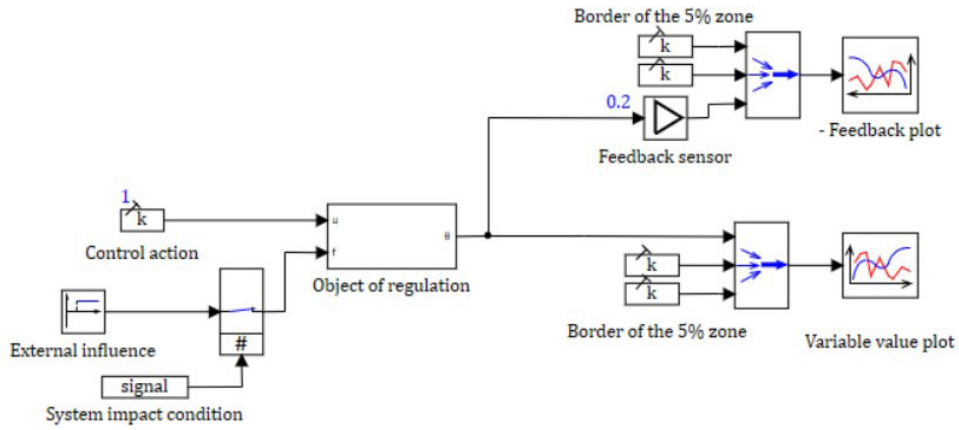
Fig. 2. The automatic control system in the SimInTech environment

Рис. 2. Система автоматического регулирования, введенная в схемное окно SimInTech
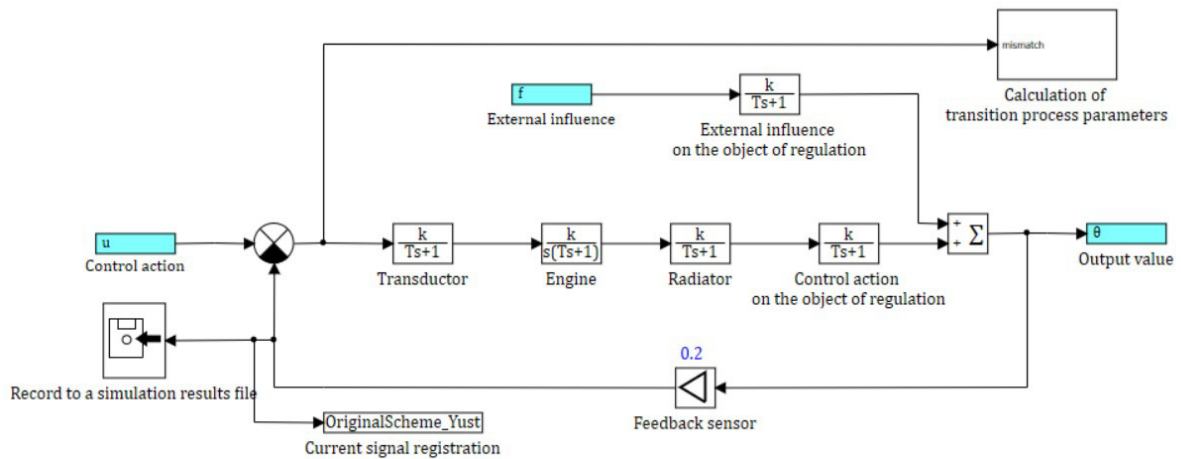
Fig. 3. Composition of the «Control object» substructure

Рис. 3. Состав субструктуры «Объект управления»
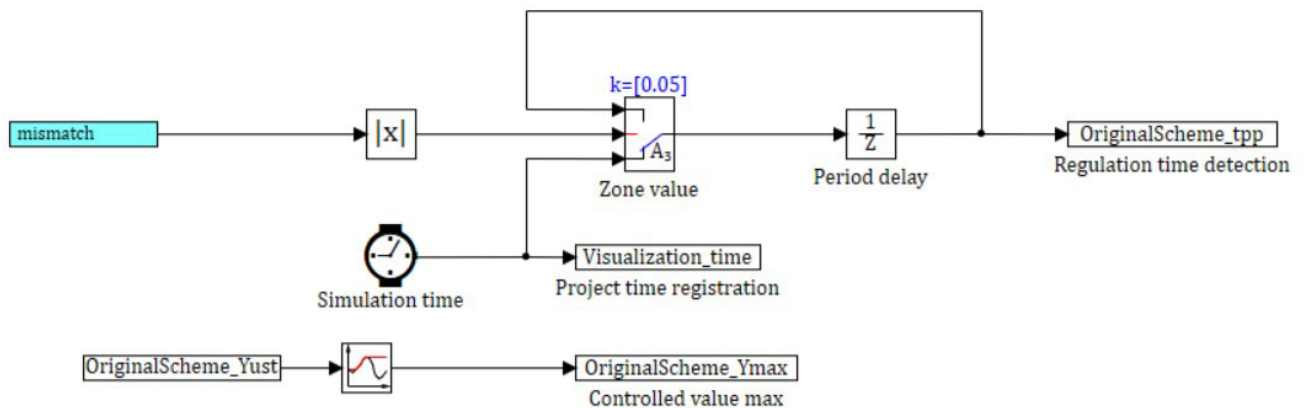
Fig. 4. Composition of the substructure "Calculation of transition process parameters"

Рис. 4. Состав субструктуры «Вычисление параметров переходного процесса»
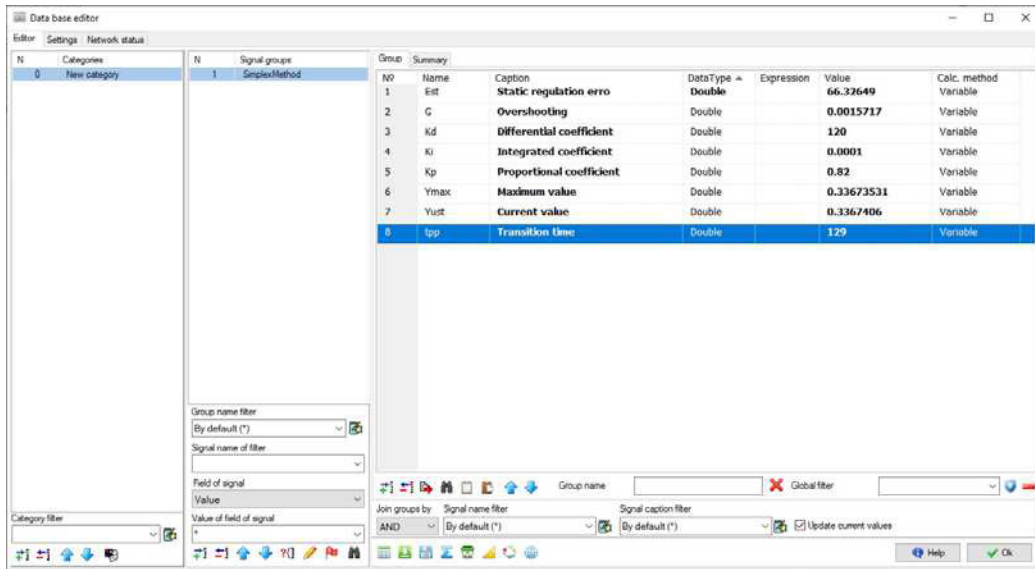
Fig. 5 Design of the Signal Database of the Package

Рис. 5. Внешний вид базы данных сигналов пакета
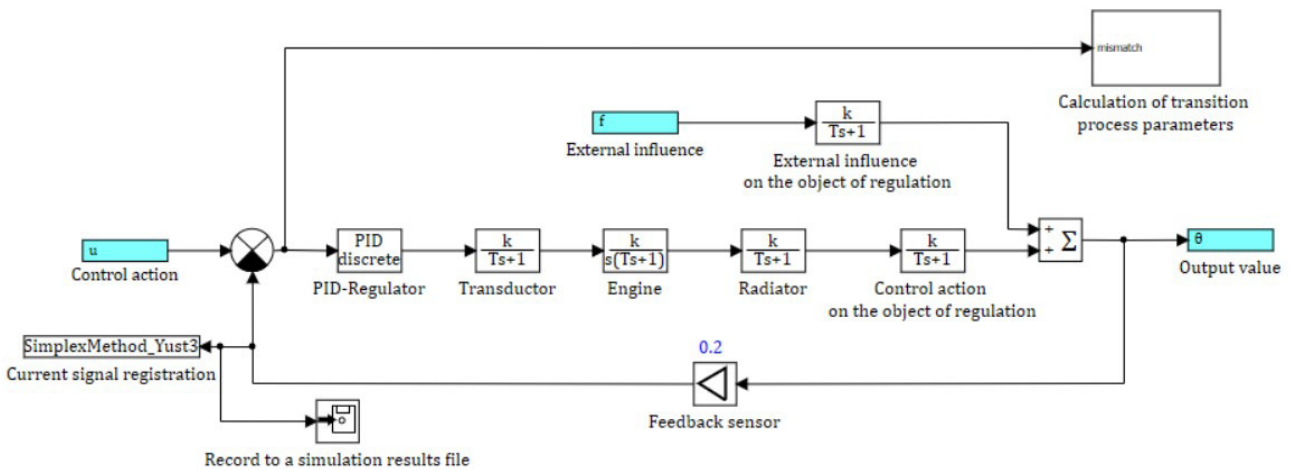
Fig. 6. The automatic control system model with discrete PID regulator

Рис. 6. Модель САР с дискретным ПИД-регулятором

Table 1

The list of signals of the project database

Name	Caption	Data type
tpp	Transition time	double
$Y_{\max}$	Maximum value	double
$Yust$	Current value	double
Est	Statistic regulation error	double
G	Overshooting	double
K_p	Proportional coefficient of regulator	double
K_i	Integrated coefficient of regulator	double
K_d	Differential coefficient of regulator	double

The regulator block will be accessed via the signal database: for this purpose, the corresponding variable from the signal database is specified in the properties of the control device block opposite to each of the components of the PID-regulator. The values of the regulator coefficients will change automatically, which allows accessing this object from any project in the package.

In the dynamic environment *SimInTech* created a special block "Optimizer", located in the library "Analysis and optimization", which allows you to perform an automated search for such values of variable parameters of the ACS, in which the dynamic characteristics of the ACS (and the transition process, in particular) meet one or more conditions (criteria) "optimalities". The scheme of the system with the parameter optimization block is shown in fig. 7.

The following algorithms are used as optimization methods that can be implemented in this block [13]:

1) Search – 2: an algorithm for dividing the step in half for one optimized parameter ($n = 1$) and an algorithm for converting the direction matrix for ($n > 1$) is implemented. Next, we consider the multidimensional search algorithm.

2) Search – 4: implements a quadratic interpolation algorithm for one optimized parameter ($n = 1$) and an algorithm for rotation and stretch-compression transformations ($n > 1$).

3) Simplex method: the "deformable polyhedron" method of Nedler and Mead is used, in which a function of n independent variables is minimized using ($n + 1$) vertices of the deformable polyhedron. Each vertex can be identified by the vector x. The vertex (point) at which the value of $f(x)$ is maximal is projected through the center of gravity (centroid) of the remaining vertices. Improved (smaller) values of the objective function are found by sequentially replacing the point with the maximum value of $f(x)$ with more "good" points until the minimum of $f(x)$ is found.

The main task of using the "Optimizer" block is to correctly configure the required data, including:

– names of variable parameters, limits of their change and calculation error;

– names of local criteria and acceptable limits of their values;

– calculated optimization method and its settings.

Look at the process of configuring the parameters of the optimization block in details [13].

The optimization parameters are the transition time *tpp* and the maximum value *Ymax* during the transition process. Accordingly, the optimization should be calculated for the entire transition process, so in the "Parameter optimization mode" select "full transition process".

Using the properties "Maximum values of block outputs" and "Minimum values of block outputs", we limit the search range for optimal system parameters. The proportional and integral components will vary in the range [0.0001; 5], the differential – in the range [0.0001; 300].

In the "Absolute accuracy of selecting output values" property, we specify the accuracy when calculating the optimized parameters.

The "Initial increment of outputs" property sets the first increment step when selecting optimum values. The larger the step, the faster the selected values change at the beginning of the search for the optimum, but there is a chance that the optimal value will be skipped. Set a step equal to "Absolute accuracy of selecting output values», it slows down the calculation, but guarantees the search with the specified accuracy.

The "Minimum values of input optimization criteria" and "Maximum values of input optimization criteria" properties define the acceptable range of optimization criteria. According to the requirements imposed on the

system when setting the task for the synthesis of the regulator, the value of overshoot should not exceed 5 % of the set value, the transition time when working out the task should not exceed 500 s. Thus, the minimum values of the optimization criteria are as follows: $Y_{max} = 0.95$; $tpp = 0$ s. The maximum values of the optimization criteria are: $Y_{max} = 1.05$; $tpp = 500$ s.

The simplex method is chosen as the optimization method.

The "Initial approximation of outputs of the block" property sets the vector of initial values of the optimized parameters. In this case, the optimized parameters are the coefficients of the PID-regulator. Add approximate values of the regulator parameters calculated by the Ziegler–Nichols method to this property [16]. The result of configuring the properties of the "Optimizer" block is shown in fig. 8.

The setup procedure in the Ziegler-Nichols method has the following steps:

1. Experimental study of the system: the studied system with a given object of regulation is supplied with a proportional regulator, the gain coefficient K_p of which vary as long as at the output of the system the oscillations with constant amplitude are not set.

2. Fixing of values: the value of the transmission coefficient of the regulator, at which the system is at the boundary of stability and the period T^* of steady-state oscillations in the system, is fixed and denoted by K_p^*.

3. Values of the PID-regulator parameters are calculated using the formulas given in tab. 2.

This method is based on the use of data obtained experimentally on a real object and the use of stability reserves [15].

Experimental results of the study. The proportional coefficient $K_p^* = 1.242$ was determined experimentally, at which oscillations with a constant amplitude are established in the system. From the graph, we determine the oscillation period $T^* = 577$ s.

Required parameters of the PID-regulator, according to table 2 have the following values:

$K_p = 0.7450$;
$K_i = 0.0025$;
$K_d = 53.755$.

Add data to the properties of the «Optimizer» block and configure parameters using the built-in tools of the *SimInTech* environment.

Graphs of the transition process without the use of the controller and with the application controller of the PID type, the coefficients of which were obtained from calculations of the unit "Optimizer" is shown in fig. 9.

For better comparison of the quality of the transition process, the designed in the course of work indicators of quality of regulation are summarized in tab. 3.

Table 2

PID-regulator parameters

Type	K_p	K_i	K_d
PID-regulator	$0.60 \cdot K_p^*$	$\dfrac{1.2 \cdot K_p^*}{T^*}$	$0.075 \cdot K_p^* \cdot T^*$
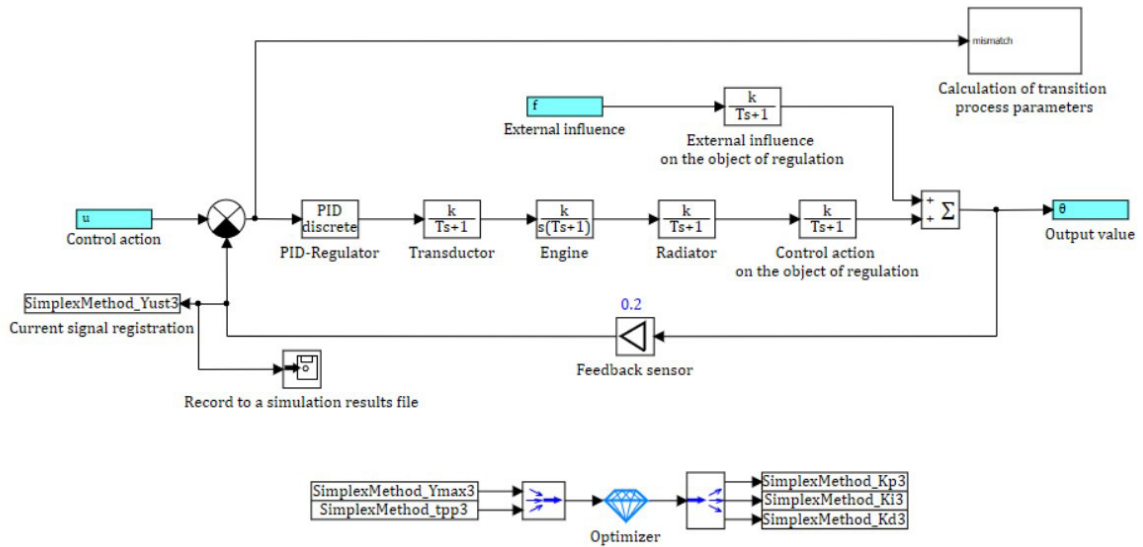
Fig. 7. The automatic control system model with optimizer

Рис. 7. Модель САР с оптимизатором

Fig. 8. Properties of the "Optimizer" block

Рис. 8. Свойства блока «Оптимизатор»

Table 3

Comparison of the quality of the transition process indicators

Parameter	Original scheme	PID-regulator scheme
Regulation time t_{reg}, s	11907	410
Maximum value Y_{max}	1.9	1.04
Second maximum value $Y_{max\,2}$	1.8	–
Overshooting σ, %	90.7	4
Attenuation D	0.11	1

343
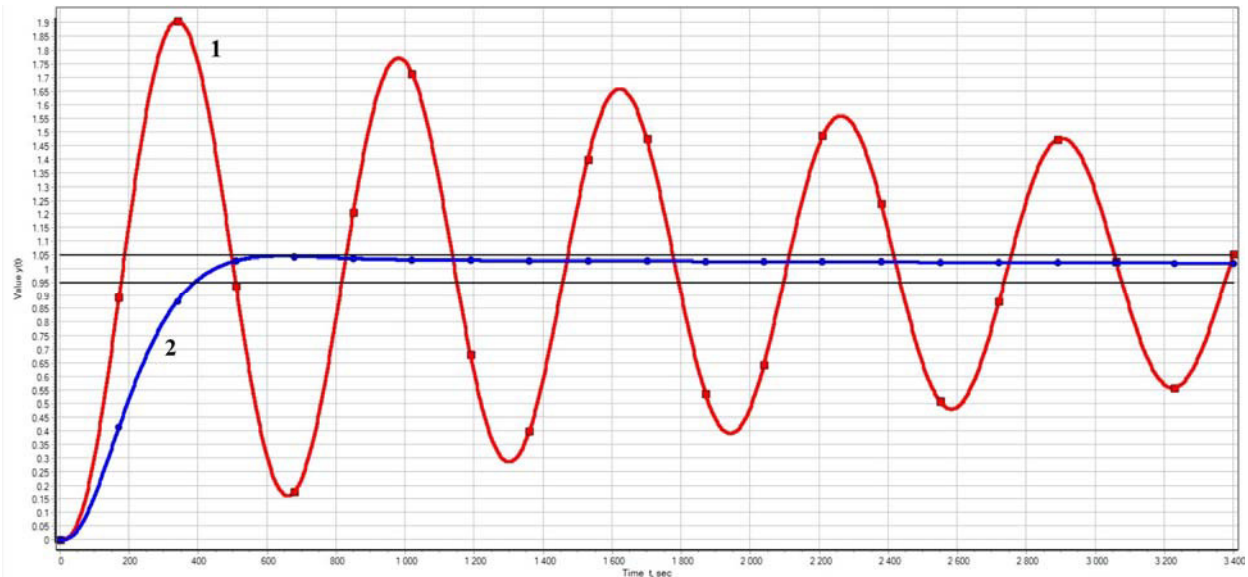
Fig. 9. Comparison of the automatic control system transition diagrams,
where *1* is the original circuit, *2* is the circuit with the tuned PID regulator

Рис. 9. Сравнение графиков переходного процесса САР:
1 – исходная схема, *2* – схема с настроенным ПИД-регулятором

From the graphs of the ACS transition process and control quality indicators presented in fig. 9 and tab. 3, respectively, we can conclude that it is advisable to use control devices in technological process control systems. The automated search for controller parameters using the built-in *SimInTech* dynamic modeling environment fully meets the system requirements: the process parameter, in this case, the room temperature, is maintained at the set level, the set value is processed without error in the steady-state mode, the transition time is reduced compared to the original scheme and is less than 500 seconds, there are no fluctuations. The system is stable and efficient.

Automated adjustment of PID-regulator parameters using *SimInTech's* built-in tools has the advantage that the algorithm will work until it makes parameter settings that meet the required optimality criteria or, if this is not possible, selects such regulator coefficients so that the quality of system regulation is as close as possible to the required level. Moreover, several optimization methods are available, which allows to choose the best one for the designed system.

This method does not require the direct presence of the operator, it only sets the necessary operating conditions for the block, however, the configuration process can take a long time.

At the same time, the "Optimizer" in the *SimInTech* environment can be used to configure the parameters of control devices and dynamic systems of various types. The main thing is to set the optimality criteria and initial approximations of the output variables correctly.

Conclusion. In this paper, in the environment of dynamic modeling of *SimInTech* technical systems using standard blocks of general technical software libraries, a model of an automation object is developed and imple-

mented – a dynamic system with feedback on the example of an automatic temperature control system in a room. The application of such development environment tools as a database and a programming language is described.

The system includes a proportional-integral-differentiating regulator, which is a parallel connection of P-, I- and D-regulators in the form of a single block "Discrete PID-regulator".

An automated search for PID-regulator parameters was performed using the built-in tools of the development environment – using the "Optimizer" block, a detailed description of the application and settings of which is described in this paper. The advantages and disadvantages of the configuration method identified during the project implementation are described.

The results of the ACS simulation, as well as the system with the control device, are confirmed by time graphs and mathematical calculations. The quality indicators of the system control process are compared based on the following indicators: control time, maximum value of the controlled value, overshoot, attenuation.

Based on the results of system modeling, the feasibility of using *SimInTech* tools to determine the coefficients of a PID-type control device was evaluated. Conclusions are made about the effectiveness of this method: the system meets the requirements for it in full. It is possible to use the *SimInTech* model parameter optimization block for dynamic systems of different orders and control devices of different composition from the one under consideration.

References

1. Denisenko V. [PID Regulators: construction and modification principles. Part 1]. *Sovremennye tekhnologii avtomatizatsii*. 2006, No. 4, P. 66–74 (In Russ.).

2. Denisenko V. [PID Regulators: construction and modification principles. Part 2]. *Sovremennye tekhnologii avtomatizatsii.* 2007, No. 1, P. 78–88 (In Russ.).

3. Denisenko V. [PID Regulators: implementation issues. Part 1]. *Sovremennye tekhnologii avtomatizatsii.* 2007, No. 4, P. 86–97 (In Russ.).

4. Denisenko V. [PID Regulators: implementation issues. Part 2]. *Sovremennye tekhnologii avtomatizatsii.* 2008, No. 1, P. 86–97 (In Russ.).

5. Gebel E., Pastukhova E. *Teoriya avtomatizatsii tekhnologicheskikh protsessov opasnykh proizvodstv: uchebnoe posobie* [The theory of automation of technological processes of dangerous productions: training manual]. 2017, Omskii gosudarstvennyi tekhnicheskii universitet Publ., P. 59–61 (In Russ.).

6. Leva A., Cox C., Ruano A. Hands-on PID autotuning: a guide to better utilisation. *IFAC Professional Brief.* P. 84. Available at: https://www.ifac-control.org/publications/list-of-professional-briefs/pb_final_ levacox-ruano.pdf/view (accessed 28.08.2020).

7. Ustimenko V. V., Chubar A. V., Myznikova V. A. [Fuzzy Regulators Construction in the SimInTech Environment]. *Kosmicheskie apparaty i tekhnologii.* 2019, No.1(27), P. 22–27 (In Russ.).

8. Ustimenko V. V., Chubar A. V., Myznikova V. A. [Using of fuzzy regulators in dynamic systems]. *Aktualnye problemy aviatsii i kosmonavtiki: materialy V Mezhdunarodnoi nauchno-prakticheskoi konferentsii, posvyashchennoi Dnyu kosmonavtiki* [Actual problems of aviation and cosmonautics: materials of the V International scientific-practical conference dedicated to the Day of Cosmonautics]. Krasnoyarsk, 2019, Vol. 1, P. 593–594 (In Russ.).

9. Ustimenko V. V., Chubar A. V., Rusin D. S. [Application of the genetic algorithm to optimization of a system of controlling of an autonomous object parameters with using an environment of dynamic modelling SimInTech]. *Robototekhnika i iskusstvennyi intellekt: materialy XI Vserossiiskoi nauchno-tekhnicheskoi konferentsii s mezhdunarodnym uchastiem* [Proceedings of the X Vseross. scientific and technical conference with int. participation "Robotics and artificial intelligence"]. Krasnoyarsk, 2019, P. 261–266 (In Russ.).

10. Entsiklopediya ASUTP [Encyclopedia APCS] (In Russ.). Available at: https://www.bookasutp.ru/Chapter5_1.aspx (accessed 28.08.2020).

11. Kartashov B. A., Shabaev E. A., Kozlov O. S. et al. *Sreda dinamicheskogo modelirovaniya tekhnicheskikh sistem SimInTech: Praktikum po modelirovaniyu sistem avtomaticheskogo regulirovaniya: uchebnoe posobie* [He environment of dynamic simulation of technical systems SimInTech: Workshop on modeling systems of automatic regulation: a training manual]. Moscow, DMK Press Publ., 2017, P. 241–243.

12. Spravochnaya sistema SimInTech [SimInTech help system] (In Russ.). Available at: http://help.simintech.ru/#o_simintech/o_simintech.html (accessed 28.08.2020).

13. Khabarov S., Shilkina M. *Osnovy modelirovaniya tekhnicheskikh sistem. Sreda SimInTech: uchebnoe posobie* [Basics of modeling technical systems. SimInTech Environment: a training manual]. Moscow, Lan Publ., 2019, 120 p.

14. Monakhov O. *Pakety prikladnykh programm MVTU, MATLAB, SIMINTECH i ikh primenenie v uchebnom protsesse na spetsial'nosti "Upravlenie v tekhnicheskikh sistemakh": Uchebno-metodicheskoe posobi.* [Application packages of MSTU, MATLAB, SIMINTECH and their application in the educational process on the specialty "Management in technical systems": Educational and methodical aids]. Moscow, Rossiiskii universitet transporta Publ., 2019, 92 p.

15. Pozharkova I. N., Chubar A. V., Grishchenko I. A. etc. [Process simulation in SimInTech visual simulation environment]. *Sibirskii pozharno-spasatelnyi vestnik.* 2018, No. 2, P. 29–37 (In Russ.).

16. Vadutov O. *Nastroika tipovykh regulyatorov po metodu Tsiglera–Nikol'sa: metodicheskie ukazaniya k vypolneniyu laboratornoi raboty dlya studentov, obuchayushchikhsya po napravleniyam 210100 "Elektronika i nanoelektronika" i 201000 «Biotekhnicheskie sistemy i tekhnologii»* [Setting of typical regulators by the Ziegler-Nicolls method: methodological guidelines for laboratory work for students studying in the areas of 210100 "Electronics and nanoelectronics" and 201000 "Biotechnical systems and technologies"]. Toms, Tomskii politekhnicheskii universitet Publ., 2014, P. 5–7.

Библиографические ссылки

1. Денисенко В. ПИД-регуляторы: принципы построения и модификации. Ч. 1 // Современные технологии автоматизации. 2006. № 4. С. 66–74.

2. Денисенко В. ПИД-регуляторы: принципы построения и модификации. Ч. 2 // Современные технологии автоматизации. 2007. № 1. С. 78–88.

3. Денисенко В. ПИД-регуляторы: вопросы реализации. Ч. 1 // Современные технологии автоматизации. 2007. № 4. С. 86–97.

4. Денисенко В. ПИД-регуляторы: вопросы реализации. Ч. 2 // Современные технологии автоматизации. 2008. № 1. С. 86–97.

5. Гебель Е., Пастухова Е. Теория автоматизации технологических процессов опасных производств. Омск : Изд-во ОмГТУ, 2017. С. 59–61.

6. Leva A., Cox C., Ruano A. Hands-on PID autotuning: a guide to better utilisation. IFAC Professional Brief, P. 84. Available at: https://www.ifac-control.org/publications/list-of-professional-briefs/pb_final_ levacox-ruano.pdf/view (accessed 28.08.2020).

7. Устименко В., Чубарь А., Мызникова В. Построение нечетких регуляторов для систем управления автономных объектов в среде SimInTech // Космические аппараты и технологии. 2019. № 1(27). С. 22–27.

8. Устименко В., Чубарь А., Мызникова В. Применение нечетких регуляторов в динамических системах / Актуальные проблемы авиации и космонавтики : материалы V Междунар. науч.-практ. конф., посвященной Дню космонавтики / СибГУ им. М. Ф. Решетнева. Красноярск, 2019. Т. 1. С. 593–594.

9. Устименко В. Чубарь А., Русин Д. Применение генетического алгоритма для оптимизации парамет-

ров системы управления автономным объектом с использованием среды динамического моделирования SimInTech // Робототехника и искусственный интеллект : материалы XI Всерос. науч.-техн. конф. с междунар. участием / Сиб. федер. ун-т. Красноярск, 2019. С. 261–266.

10. Энциклопедия АСУТП [Электронный ресурс]. URL: https://www.bookasutp.ru/Chapter5_1.aspx (дата обращения: 28.08.2020).

11. Среда динамического моделирования технических систем SimInTech : Практикум по моделированию систем автоматического регулирования / Б. А. Карташов, Е. А. Шабаев, О. С. Козлов и др. М. : ДМК Пресс, 2017. С. 241–243.

12. Справочная система SimInTech [Электронный ресурс]. URL: http://help.simintech.ru/#o_simintech/o_simintech.html (дата обращения 28.08.2020).

13. Хабаров С., Шилкина М. Основы моделирования технических систем. Среда SimInTech. СПб. : Лань. 2019. 120 с.

14. Монахов О. Пакеты прикладных программ МВТУ, MATLAB, SIMINTECH и их применение в учебном процессе на специальности «Управление в технических системах». М. : РУТ (МИИТ), 2019. 92 с.

15. Моделирование технологического процесса в среде визуального моделирования SimInTech / И. Н. Пожаркова, А. В. Чубарь, И. А. Грищенко и др. // Сибирский пожарно-спасательный вестник. 2018. № 2. С. 29–37.

16. Вадутов О. Настройка типовых регуляторов по методу Циглера–Никольса: методические указания к выполнению лабораторной работы для студентов, обучающихся по направлениям 210100 «Электроника и наноэлектроника» и 201000 «Биотехнические системы и технологии». Томск : Изд-во Томского политех. ун-та, 2014. С. 5–7.

Ustimenko Valeriya Vladimirovna – Master; Siberian Federal University. E-mail: zeya1998@mail.ru.
Chubar Aleksei Vladimirovich – Cand. Sc., docent, head of research automated process control system lab; Siberian Federal University. E-mail: alexchub@mail.ru.
Mikhailenko Lyudmila Andreevna – Master; Siberian Federal University. E-mail: ll-oda@mail.ru.

Устименко Валерия Владимировна – магистрант; Сибирский федеральный университет. E-mail: zeya1998@mail.ru.
Чубарь Алексей Владимирович – кандидат технических наук, доцент, руководитель научно-учебной лаборатории АСУТП; Сибирский федеральный университет. E-mail: alexchub@mail.ru.
Михайленко Людмила Андреевна – магистрант; Сибирский федеральный университет. E-mail: ll-oda@mail.ru.

MODELS AND ALGORITHMS FOR AUTOMATIC GROUPING OF OBJECTS BASED ON THE K-MEANS MODEL

G. Sh. Shkaberina*, L. A. Kazakovtsev, R. Li

Reshetnev Siberian State University of Science and Technology
31, Krasnoyarskii rabochii prospekt, Krasnoyarsk, 660037, Russian Federation
*E-mail: z_guzel@mail.ru

The paper is devoted to the study and development of new algorithms for automatic grouping of objects. The algorithms can improve the accuracy and stability of the result of solving practical problems, such as the problems of identifying homogeneous batches of industrial products. The paper examines the application of the k-means algorithm with the Euclidean, Manhattan, Mahalanobis distance measures for the problem of automatic grouping of objects with a large number of parameters. A new model is presented for solving problems of automatic grouping of industrial products based on the k-means model with the Mahalanobis distance measure. The model uses a training procedure by calculating the averaged estimate of the covariance matrix for the training sample (sample with pre-labeled data). A new algorithm for automatic grouping of objects based on an optimization model of k-means with the Mahalanobis distance measure and a weighted average covariance matrix calculated from a training sample is proposed. The algorithm allows reducing the proportion of errors (increasing the Rand index) when identifying homogeneous production batches of products based on the results of tests. A new approach to the development of genetic algorithms for the k-means problem with the use of a single greedy agglomerative heuristic procedure as the crossover operator and the mutation operator is presented. The computational experiment has shown that the new mutation procedure is fast and efficient in comparison with the original mutation of the genetic algorithm. The high rate of convergence of the objective function is shown. The use of this algorithm allows a statistically significant increase both in the accuracy of the result (improving the achieved value of the objective function within the framework of the chosen mathematical model for solving the problem of automatic grouping), and in its stability, in a fixed time, in comparison with the known algorithms of automatic grouping. The results show that the idea of including a new mutation operator in the genetic algorithm significantly improves the results of the simplest genetic algorithm for the k-means problem.

Keywords: automatic grouping, k-means, Mahalanobis distance, genetic algorithm.

МОДЕЛИ И АЛГОРИТМЫ АВТОМАТИЧЕСКОЙ ГРУППИРОВКИ ОБЪЕКТОВ НА ОСНОВЕ МОДЕЛИ К-СРЕДНИХ

Г. Ш. Шкаберина, Л. А. Казаковцев, Ж. Ли

Сибирский государственный университет науки и технологий имени академика М. Ф. Решетнева
Российская Федерация, 660037, г. Красноярск, просп. им. газ. «Красноярский рабочий», 31
*E-mail: z_guzel@mail.ru

Работа посвящена исследованию и разработке новых алгоритмов автоматической группировки объектов, которые позволяют повысить точность и стабильность результата решения практических задач, например, таких как задача выделения однородных партий промышленной продукции. В статье исследуется применение алгоритма k-средних с Евклидовым, Манхэттенским, Махаланобиса мерами расстояния для задачи автоматической группировки объектов с большим количеством параметров. Представлена новая модель для решения задач автоматической группировки промышленной продукции на основе модели k-средних с мерой расстояния Махаланобиса. Данная модель использует процедуру обучения путем вычисления усредненной оценки ковариационной матрицы для обучающей выборки (выборка с предварительно размеченными данными). Предложен новый алгоритм автоматической группировки объектов, основанный на оптимизационной модели k-средних

с мерой расстояния Махаланобиса и средневзвешенной ковариационной матрицей, рассчитанной по обучающей выборке. Алгоритм позволяет снизить долю ошибок (повысить индекс Рэнда) при выявлении однородных производственных партий продукции по результатам тестовых испытаний. Представлен новый подход к разработке генетических алгоритмов для задачи k-средних с применением единой жадной агломеративной эвристической процедуры в качестве оператора скрещивания и оператора мутации. Вычислительный эксперимент показал, что новая процедура мутации является быстрой и эффективной по сравнению с исходной мутацией генетического алгоритма, показана высокая скорость сходимости целевой функции. Применение данного алгоритма позволяет статистически значимо повысить точность результата (улучшить достигаемое значение целевой функции в рамках выбранной математической модели решения задачи автоматической группировки), а также его стабильность за фиксированное время по сравнению с известными алгоритмами автоматической группировки. Результаты показывают, что идея включения нового оператора мутации в генетическом алгоритме значительно улучшает результаты простейшего генетического алгоритма для задачи k-средних.

Ключевые слова: автоматическая группировка, k-средних, расстояние Махаланобиса, генетический алгоритм.

Introduction. Automatic grouping (AG) involves dividing a set of objects into subsets (groups) so that objects from one subset are more similar to each other than to objects from other subsets according to some criterion. General characteristics of the object and the methods by which the division took place are taken into account in the process of grouping objects of a certain set into certain groups (subsets).

To exclude the emergence of unreliable electrical radio products intended for installation in the on-board equipment of a spacecraft with a long period of active existence, the entire electronic component base passes through specialized technical test centers [1; 2]. These centers perform operations of full incoming inspection of electrical radio products, additional verification tests, diagnostic non-destructive testing and selective destructive physical analysis. Detection of initial homogeneous production batches of electrical radio products from shipped batches is an important stage during testing [1].

The k-means model is one of the best known cluster analysis models. The goal is to find k points (centers) X_1, …, X_k in d-dimensional space, such that the sum of the squared distances from known points (data vectors) A_1, …, A_N to the nearest of the required points (centers) reaches a minimum [3]:

$$\arg\min F(X_1,...,X_k) = \sum_{i=1}^{N} \min_{j \in \{1,k\}} \left\| X_j - A_i \right\|^2 . \quad (1)$$

Initially it is necessary to predict the number of groups (subsets) in the k-means algorithm. In addition, the result obtained depends on the initial choice of centers. The distance function and its definition also play an important role in the problem of dividing the set under study into groups.

The first genetic algorithm for solving the discrete p-median problem was proposed by Hosage and Goodchild [4]. The algorithm [5] gives fairly accurate results. However, the rate of convergence of the objective function is very slow. In their work O. Alp, E. Erkut, Z. Drezner [6] presented a faster simple genetic algorithm with a special recombination procedure, which also gives accurate results. These algorithms solve discrete problems. The authors of the work "Genetic algorithm-based clustering technique" [7] encode solutions (chromosomes) in their

GAs as sets of centroids, represented by their coordinates (vectors of real numbers) in a multidimensional space.

The analysis of the literature has shown that the existing solutions in the field of AG of multidimensional objects either have high accuracy, or ensure the stability of the result with multiple runs of the algorithm, or have high speed of operation, but do not combine all these qualities at the same time. To date, algorithms for k-means and k-medians have been developed only for the most common distance measures (Euclidean, Manhattan). However, taking into account the feature space peculiarities of a specific practical problem when choosing a distance measure can lead to increasing the accuracy of AG objects. In the presented work, we use the Rand Index (RI) [8] as a measure of the clustering accuracy.

It is extremely difficult to improve the AG result of multidimensional objects with increased requirements for the accuracy and stability of the result using known algorithms without a significant increase in time costs. When solving practical problems of the AG of multidimensional data, for example, the problems of identifying homogeneous batches of industrial products, the adequacy of the models and, as a result, the accuracy of the AG of industrial products are questionable. It is still possible to develop algorithms that further improve the result based on the chosen model, for example, the k-means model.

In a multidimensional feature space, there is often a correlation between individual features and groups of features. The use of correlation dependences can be used by moving from search in the space with the Euclidean or rectangular metric to search in the space with the Mahalanobis metric [9–11]. The square of the Mahalanobis distance D_M is defined as follows:

$$D_M(X) = (X - \mu)^T C^{-1} (X - \mu) , \quad (2)$$

where X is the vector of values of the measured parameters, μ is the vector of mean values (for example, the center of the cluster), C is the covariance matrix.

The aim of the study in the presented work is to improve the accuracy and stability of the result of solving problems in automatic grouping of objects.

The idea of the work is to use the Mahalanobis distance measure with the averaged estimate of the covariance matrix in the k-means problem to reduce the proportion of the AG error in comparison with other known al-

gorithms, and also to use the mutation operator as a part of the genetic algorithm to improve the accuracy and stability of the solution according to the achieved value of the objective function in a fixed execution time in comparison with known algorithms for separating objects.

Initial data. The study was carried out on the data of testing the batches of integrated circuits [12], intended for installation in space vehicles. The tests were carried out in a specialized center for technical tests. The data is a set of parameters for electrical radio products (ERP). The original batch of ERI belongs to different homogeneous batches, in accordance with the manufacturer's marking. The total number of products is 3987. In each batch, the product is described by 205 measured parameters. Batch 1 contains 71 products, batch 2 – 116 products, batch 3 – 1867 products, batch 4 – 1250 products, batch 5 – 146 products, batch 6 – 113 products, and batch 7 – 424 products.

The algorithm of k-means with the Mahalanobis distance with an averaged estimate of the covariance matrix over the training sample. The computational results of experiments on automatic grouping of industrial products with *k*-medoid and *k*-means models, in which the Mahalanobis metric is applied, show an increase in clustering accuracy with automatic grouping into 2–6 clusters and a small number of objects and informative features [13].

Instead of the covariance matrix from (2), it was proposed to calculate the averaged estimate of the covariance matrix for homogeneous batches of products (according to pre-labeled data) using the training sample:

$$C = \frac{1}{n}\sum_{j=1}^{k} C_j n_j , \qquad (3)$$

where n_j is the number of objects (products) in the *j*-th batch, n is the total sample size, C_j are the covariance matrices of individual batches of products.

In this paper, we propose an algorithm for automatic grouping of objects based on the *k*-means model with the adjustment of the Mahalanobis distance measure parameter (covariance matrix) based on the training sample:

The algorithm of 1. *k*-means with the Mahalanobis distance with averaged estimate of the covariance matrix

Step 1. Using the *k*-means method with Euclidean distance, divide the sample into a certain number of *k* clusters (here *k* is some expert estimate of the possible number of homogeneous groups, not necessarily accurate);

Step 2. Calculate the center μ_i for each cluster. The center is defined as the arithmetic mean of all points in the cluster

$$\mu_i = \frac{1}{m}\sum_{j=1}^{m} X_{ji} , \qquad (4)$$

where *m* is the number of points, X_j is a vector of values of one measured parameter (*j* = 1...*m*);

Step 3. Calculate the averaged estimate of the covariance matrix (3). If the averaged estimate of the covariance matrix is degenerate, go to step 4, otherwise go to step 5;

Step 4. Increase the number of clusters by $(k + 1)$ and repeat steps 1 and 2. Form new clusters with the squared Euclidean distance:

$$D(X_j, \mu_i) = \sum_{i=1}^{n}(X_{ji} - \mu_i)^2 , \qquad (5)$$

where *n* is the number of parameters. Return to step 3 with a new training example (set).

Step 5. Match each point to the nearest centroid using the square of the Mahalanobis distance (2) with the averaged estimate of the covariance matrix *C* (3) to form new clusters.

Step 6. Repeat the algorithm from step 2 until the clusters stop changing.

The paper presents the results of three groups of experiments on the data of industrial product samples.

The first group. The training sample corresponds to the working sample for which the clustering was carried out.

The second group. The training and working samples are not the same. In practice, a test center can use retrospective data on deliveries and testing of products of the same type as a training sample.

The third group. The training and working samples also do not match, but the results of the automatic grouping of products (*k*-means in the multistart mode with the Euclidean metric) were used as the training sample.

In each group of experiments, for each working sample, the *k*-means algorithm was run 30 times with each of the five clustering models studied.

DM1 model – *k*-means with the Mahalanobis distance, the covariance matrix is calculated for the entire training sample.

DC model – *k*-means with a distance similar to the Mahalanobis distance, but using a correlation matrix instead of a covariance matrix.

DM2 model – *k*-means with Mahalanobis distance, with averaged estimate of the covariance matrix.

DR model – *k*-means with the Manhattan distance.

DE model – *k*-means with the Euclidean distance.

For each model, the minimum (Min), maximum (Max), average (Average) values, standard deviation (Std.Dev) of the Rand index (RI) and the objective function, as well as the values of the coefficients of variation (V) and the range (R) of the target functions (tab. 1) are calculated.

It was found that the new *DM2* model with an averaged estimate of the covariance matrix shows the best accuracy among the presented models in almost all series of experiments according to the Rand index (RI) and in all cases it exceeds the *DE* model, where the Euclidean distance is used. The experiments also showed that in most cases the coefficient of variation of the objective function values is higher for the *DE* model, where the Euclidean measure of distance is used, and also that the coefficient of the range of the objective function values has the highest values for the *DM2* model, where the Mahalanobis distance measure with an averaged estimate of the covariance matrix is used.

The results of a computational experiment on the data of the 1526IE10_002 microcircuit (3987 data vectors with a dimension of 68), the training sample consists of 10 batches, the third group, the working sample is made up of 7 batches of products)

V-series	Rand index (RI)					Objective function				
	Model					Model				
	DM1	DC	DM2	DR	DE	DM1	DC	DM2	DR	DE
Max	0.767	0.658	0.749	0.740	0.735	255886	379167	281265	18897	6494.62
Min	0.562	0.645	0.696	0.703	0.705	250839	36997	274506	17785	5009.42
Average	0.632	0.650	**0.725**	0.714	0.719	252877	37178	277892	18240	5249.95
Std .Dev	0.047	0.003	0.016	0.008	0.006	1164.5	152.8	2358.9	452.7	366.5
V						0.461	0.411	0.849	2.482	**6.981**
R						5047	920	**6759**	1112	1485

Therefore, multiple attempts to run the *k*-means algorithm or to use other algorithms based on the *k*-means model (for example, *j*-means [14] or greedy heuristic algorithms [15]) are required to obtain consistently good values of the objective function.

Genetic cross-mutation algorithm for the *k*-means problem. The new algorithm improves the accuracy of solving the *k*-means problem and the stability of the result in a fixed limited execution time. In this chapter, by the accuracy of the algorithm we mean exclusively the achieved value of the objective function, without taking into account the indicators of the model adequacy and the correspondence of the algorithm results to the actual (real) separation of objects, if known.

A very limited set of possible mutation operators is known for genetic algorithms for solving the *k*-means problem with real coding of solutions. For example, the authors of the work "Genetic algorithm-based clustering technique" [7] encode solutions (chromosomes) in their GAs as sets of centroids represented by their coordinates (vectors of real numbers) in a multidimensional space. Each chromosome undergoes mutation with a fixed probability μ. The procedure (operator) of mutation is as follows.

Algorithm 2 3.1 Initial GA mutation procedure for the *k*-means problem

Step 1. Generation of a random number $b \in (0,1]$ with uniform distribution;

Step 2. IF $b < \mu$, then the chromosome mutates. If the position of the current centroid is υ, then after mutation it becomes:

$$\upsilon \leftarrow \begin{cases} \upsilon \pm 2 \times b \times \upsilon, & \upsilon \neq 0, \\ \upsilon \pm 2 \times b, & \upsilon = 0. \end{cases}$$

The signs "+" and "–" have the same probability. The centroid coordinates are shifted randomly.

In our work we replaced this mutation procedure for the *k*-means problem with the following procedure.

Algorithm 3 3.2 GA cross mutation procedure for the k-means problem

Step 1. Generating a random initial solution $S = \{X_1 ... X_k\}$;

Step 2. Applying the k-means algorithm to S to obtain the local optimum S';

Step 3. Applying a simple crossover procedure for the mutated individual S' from the population and S to obtain a new solution S'';

Step 4. Applying the k-means algorithm to S'' to obtain local optimum S'';

Step 5. IF $F(S'') < F(S')$, **THEN** $S' \leftarrow S''$.

The proposed procedure is used with a mutation probability of 1 after each crossover operator.

The results of running the original algorithm 2, described with a mutation probability of 0.01, and its version with algorithm 3 as a mutation operator are shown in the figure (population size $N_{POP} = 20$). The new mutation procedure is fast and efficient in comparison with the original mutation of the genetic algorithm; a high convergence rate of the objective function has been shown.

Greedy genetic algorithms and many other evolutionary algorithms for the *k*-means problem do without mutation. The idea of a greedy agglomerative heuristic procedure is to combine two known solutions into one unacceptable solution with an excessive number of centroids, and then the number of centroids is successively reduced. The centroid which shows the smallest increase in the objective function value (1) is removed at each iteration.

Algorithm 4. Basic greedy agglomerative heuristic procedure

It is given: the initial number of clusters K, the required number of clusters k, $k < K$, the initial solution $S = \{X_1,...,X_K\}$, where $|S| = K$.

STEP 1. Improve the initial solution by the *k*-means algorithm

WHILE $K > k$

CYCLE for each $i' \in \{\overline{1, K}\}$ perform:

STEP 2. $S' \leftarrow S\{X_i'\}$. Improve the solution S' by the *k*-means algorithm and store the corresponding obtained values of the objective function (1) as variables $F_i' \leftarrow F\{X'\}$.

END OF CYCLE

STEP 3. Select the subset S_{elim} from the centers n_{elim}, $S_{elim} \in S$, $|S_{elim}| = n_{elim}$ with the minimum value of the corresponding variables F_i'. $n_{elim} = \max\{1, 0.2 \cdot (|S|-k)\}$.

STEP 4. Get a new solution $S \leftarrow S / S_{elim}$, $K = K - 1$. Improve the solution by the k-means algorithm.

END WHILE

The initial solution S can also be obtained by combining two known solutions. Algorithms 5 and 6 modify the initial solution by the second known solution. In fact, Greedy procedure 1 supplements the first set in turn with each element from the second set. Greedy procedure 2 combines both sets.

Algorithm 5. Greedy procedure 1 with partial join

It is given: Two sets of cluster centers $S' = \{X'_1,...,X'_K\}$ и $S'' = \{X''_1,...,X''_K\}$

Cycle: for each $i' \in \{\overline{1, K}\}$

Step 1. Combine S' and one element from the set $S'' : S \leftarrow S \cup \{X''_1,...,X''_K\}$.

Step 2. Run Algorithm 3.3 with the initial solution S and save the result.

END OF CYCLE

Step 3. Revert the best solutions saved in Step 2.

Algorithm 6. Greedy procedure 2 with full set union

It is given: Two sets of cluster centers $S' = \{X'_1,...,X'_K\}$ and $S'' = \{X''_1,...,X''_K\}$

Step 1. Combine two sets of cluster centers $S \leftarrow S' \cup S''$.

Step 2. Run Algorithm 3 3.3 with the initial solution S.

The basic genetic algorithm (GA) for k-means problems is described as follows:

Algorithm 7. GA with the alphabet of real numbers for the k-means problem

It is given: Initial population size N_{POP}

STEP 1. Choose N_{POP} of initial solutions $S_1,...,S_{N_{POP}}$, where $|S_i|=k$, and $\{S_1,...,S_{N_{POP}}\}$ is a randomly selected subset of the set of data vectors. Improve each initial solution by the k-means algorithm and store the corresponding obtained values of the objective function (1) as variables $f_k \leftarrow F(S_k), k = \overline{1, N_{POP}}$.

CYCLE

STEP 2. IF the stop condition is met, **THEN** STOP. Return the solution $S_{i^*}, i^* \in \{\overline{1, N_{POP}}\}$ with the minimum value f_{i^*}.

STEP 3. Randomly select 2 indices $k_1, k_2 \in \{\overline{1, N_{POP}}\}$, $k_1 \neq k_2$.

STEP 4. Start crossing procedure: $S_c \leftarrow Crossingover(S_{k_1}, S_{k_2})$.

STEP 5. Start mutation procedure: $S_c \leftarrow Mutation(S_c)$.

STEP 6. Start the chosen selection procedure to change the population set.

END OF CYCLE

The following algorithm is proposed At STEP 6.

Algorithm 8. Selection procedure

STEP 1. Randomly select 2 indices $k_4, k_5 \in \{\overline{1, N_{POP}}\}$, $k_4 \neq k_5$.

STEP 2. IF $f_{k_4} > f_{k_5}$ **THEN** $S_{k_4} \leftarrow S_c$, $f_{k_4} \leftarrow F(S_c)$, **ELSE** $S_{k_5} \leftarrow S_c$, $f_{k_5} \leftarrow F(S_c)$.

A GA with greedy heuristic for p-medians and k-means problems can be described as follows.

Algorithm 9. A GA with greedy heuristic for p-medians and k-means problems (modifications GA-FULL, GA-ONE и GA-MIX)

It is given: Population size N_{POP}.

Step 1. Set $N_{iter} \leftarrow 0$. Choose a set of initial solutions $\{S_1,...,S_{N_{POP}}\}$, where $|S_i| = k$. Improve each initial solution by the k-means algorithm and store the corresponding obtained values of the objective function (1) as variables $f_k \leftarrow F(S_k), k = \overline{1, N_{POP}}$. In this work the initial value of the population is $N_{POP} = 5$.

Cycle

Step 2. IF the stop condition is met, **THEN** STOP. Return the solution $S_{i^*}, i^* \in \{\overline{1, N_{POP}}\}$ with the minimum value f_{i^*}, **ELSE** set the population size as follows: $N_{iter} \leftarrow N_{iter} + 1$; $N_{POP} \leftarrow \max\{N_{POP,}[\sqrt{1 + N_{iter}}]\}$; **IF** N_{POP} has changed, **THEN** generate a new one $S_{N_{POP}}$ as described in Step 1.

Step 3. Randomly select 2 indices $k_1, k_2 \in \{\overline{1, N_{POP}}\}$, $k_1 \neq k_2$.

Step 4. Run Algorithm 5 (for GA-ONE*) or Algorithm 6 (for GA-FULL*) with solutions S_{k_1} and S_{k_2}. For GA-MIX* Algorithm 5 or Algorithm 6 are chosen at random with equal probability. Get a new solution S_c.

Step 5. $S_c \leftarrow Mutation(S_c)$ By default the mutation procedure is not used.

Step 6. Run Algorithm 5

END OF CYCLE

* GA-ONE is a genetic algorithm with greedy heuristic with partial union, GA-FULL is a genetic algorithm with greedy heuristic with full union; GA-MIX is a random choice of algorithms 5 or 6

This algorithm uses a dynamically growing population. In our new version of Step 5, the cross mutation operator looks like this.

Algorithm 10. A cross mutation operator for Step 5 of Algorithm 9 (modifications GA-FULL-MUT, GA-ONE-MUT and GA-MIX-MUT)

Step 1. Run the k-means algorithm for a randomly selected initial solution to obtain solution S'.

Step 2. Run Algorithm 5 (for GA-ONE) or Algorithm 6 (for GA-FULL) with solutions S_c and S''. Get a new solution S_c'.

Step 3. If $F(S_c') < F(S_c)$, **THEN** $S_c \leftarrow S_c'$.

Computational experiments with datasets from the Machine Learning Repository, Basic Benchmark repositories, as well as with data from industrial product samples (tab. 2) were carried out. New modifications of three GAs (GA-FULL-MUT, GA-ONE-MUT and GA-MIX-MUT) were compared with the well-known *j*-means and *k*-means algorithms (in multistart mode), GA without mutation (GA-FULL, GA-ONE and GA-MIX), automatic grouping algorithms for the k-means problem with combined application of search algorithms with alternating randomized neighborhoods formed by applying greedy agglomerative heuristics (*k*-GH-VNS1, *k*-GH-VNS2, *k*-GH-VNS3) and also for the *j*-means (*j*-means GH-VNS1, *j*-means

GH-VNS2) problem. 30 attempts were made to run each algorithm for all datasets. For each algorithm, the minimum (Min), maximum (Max), average (Average) values and the standard deviation (Std.Dev.) of the objective function were calculated.

The best values of the new algorithms (*) are highlighted in bold, the best values of the known algorithms are indicated in italics, the most achieved values of the objective function are underlined (tab. 2). The Mann-Whitney U-test ($\uparrow\downarrow\updownarrow$) and Student's t-test ($\Uparrow\Downarrow\Updownarrow$) were used to confirm the statistical significance of the advantages ($\uparrow\Uparrow$) and disadvantages ($\downarrow\Downarrow$) of the new algorithms over the known algorithms.

The performed computational experiments show that GA with a greedy agglomerative crossover operator with a new idea of the mutation procedure is superior to GA without mutation in terms of the obtained value of the objective function.
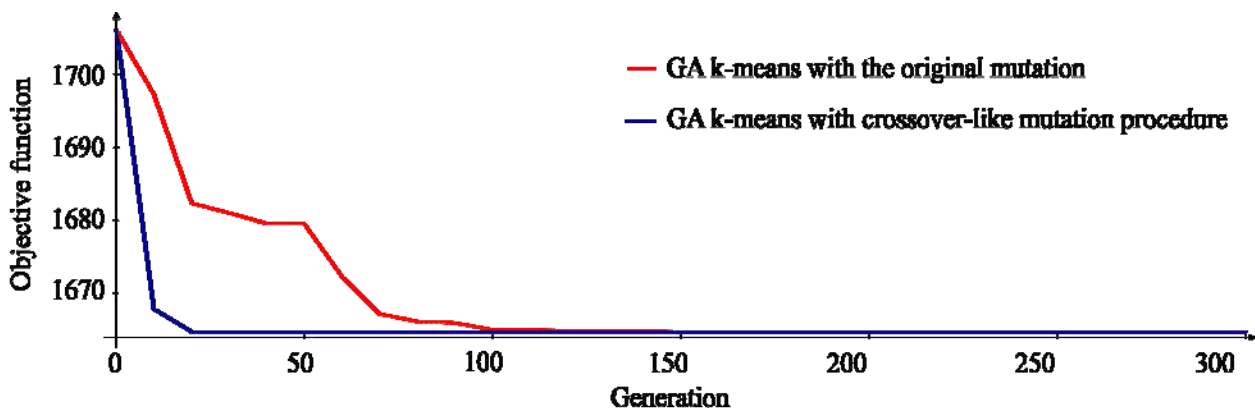
Results for data set Mopsi-Joensuu (6014 data vectors of dimension 2), 300 clusters, time limit 3 minutes

Результаты для набора данных Mopsi-Joensuu (6014 векторов данных размерностью 2), 300 кластеров, 3 минуты

Table 2

Results of computational experiments for the Europe dataset (169309 data vectors of dimension 2), 30 clusters, 4 hours

Algorithm	Objective function value			
	Min	Max	Average	Std.Dev.
j-means	7.51477E+12	7.60536E+12	7.56092E+12	29.764E+9
k-means	7.54811E+12	7.57894E+12	7.56331E+12	13.560E+9
k-GH-VNS1	*7.49180E+12*	7.49201E+12	*7.49185E+12*	*0.073E+9*
k-GH-VNS2	7.49488E+12	7.52282E+12	7.50082E+12	9.989E+9
k-GH-VNS3	7.49180E+12	7.51326E+12	7.49976E+12	9.459E+9
j-means-GH-VNS1	7.49180E+12	7.49211E+12	7.49185E+12	0.112E+9
j-means-GH-VNS2	7.49187E+12	7.51455E+12	7.4962E+12	8.213E+9
GA-FULL-MUT*	7.49293E+12	7.49528E+12	7.49417E+12	0.934E+9
GA-MIX-MUT*	7.49177E+12	7.49211E+12	7.49186E+12	0.117E+9
GA-ONE-MUT*$\uparrow\Uparrow$	**7.49177E+12**	7.49188E+12	**7.49182E+12**	**0.042E+9**

Conclusion. The proposed new model of automatic grouping of industrial products and a new algorithm based on an optimization model of k-means with Mahalanobis distances and a trained covariance matrix can reduce the proportion of errors (increase the Rand index) when identifying homogeneous production batches of products. The presented new genetic algorithm for the k-means problem with the original idea of using one procedure as the crossover operator and the mutation operator demonstrates a more accurate and stable result of the objective function value in a fixed execution time.

References

1. Orlov V. I., Kazakovtsev L. A., Masich I. S., Stashkov D. V. *Algoritmicheskoe obespechenie podderzhki prinyatiya reshenii po otboru izdelii mikroelektroniki dlya kosmicheskogo priborostroeniya* [Algorithmic support of decision-making on selection of microelectronics products for space industry]. Krasnoyarsk, 2017, 225 p.

2. Kazakovtsev L. A., Antamoshkin A. N. [Greedy heuristic method for location problems]. *Vestnik SibGAU.* 2015, Vol. 16, No. 2, P. 317–325 (In Russ.).

3. MacQueen J. Some methods for classification and analysis of multivariate observations. *Proc. Fifth Berkeley Symp. Math. Stat. Probab.* 1967, Vol. 1, P. 281–297.

4. Hosage C. M., Goodchild M. F. Discrete Space Location-Allocation Solutions from Genetic Algorithms. *Annals of Operations Research.* 1986, Vol 6, P. 35–46. http://doi.org/10.1007/bf02027381

5. Bozkaya B., Zhang J., Erkut E. A Genetic Algorithm for the p-Median Problem, Drezner Z., Hamacher H. (eds,), Facality Location: Applications and Theory, *Springer, Berlin,* 2002.

6. Alp O., Erkut E., Drezner Z. An Efficient Genetic Algorithm for the p-Median Problem. *Annals of Operations Research.* 2003, Vol. 122, P. 21–42. doi: 10.1023/A:1026130003508

7. Maulik U., Bandyopadhyay S. Genetic Algorithm-Based Clustering Technique. *Pattern Recognition.* 2000, Vol. 33, No. 9, P. 1455–1465. doi: 10.1016/S0031-3203(99)00137-5

8. William M. Rand. Objective Criteria for the Evaluation of Clustering Methods. *Journal of the American Statistical Association.* 1971, Vol. 66, No. 336, P. 846–850.

9. De Maesschalck R., Jouan-Rimbaud D., Massart D. L. The Mahalanobis distance. *Chem Intell Lab Syst.* 2000, Vol. 50, No. 1, P. 1–18. doi: 10.1016/S0169-7439(99)00047-7

10. McLachlan G. J. Mahalanobis Distance. *Resonance.* 1999, Vol. 4, No. 20. doi: 10.1007/BF02834632.

11. Xing E. P., Ng A. Y., Jordan M. I., Russel S. Distance metric learning with application to clustering with side-information. *Advances in Neural Information Processing Systems.* 2003, Vol. 15, P. 505–12.

12. Orlov V. I., Fedosov V. V. ERC clustering dataset, 2016. http://levk.info/data1526.zip

13. Orlov V. I., Shkaberina G. Sh., Rozhnov I. P., Stupina A. A., Kazakovtsev L. A. [Application pf clustering algorithm wirh special distance measures for the problem of automatic grouping of electronic and radio devices]. *Control systems and information technologies.* 2019, Vol. 3, No. 3, P. 42–46 (In Russ.).

14. Hansen P., Mladenovic N. J-means: a new local search heuristic for minimum sum of squares clustering. *Pattern recognition.* 2001, Vol. 34, No. 2, P. 405–413.

15. Kazakovtsev L. A., Antamoshkin A. N. Genetic Algorithm with Fast Greedy Heuristic for Clustering and Location Problems. *Informatica.* 2014, Vol. 38, No. 3, P. 229–240.

Библиографические ссылки

1. Алгоритмическое обеспечение поддержки принятия решений по отбору изделий микроэлектроники для космического приборостроения / В. И. Орлов, Л.А. Казаковцев, И.С. Масич и др. ; Сиб. гос. аэрокосмич. ун-т. Красноярск, 2017. 225 с.

2. Казаковцев Л. А., Антамошкин А. Н. Метод жадных эвристик для задач размещения // Вестник СибГАУ. 2015. Т. 16, № 2. С. 317–325.

3. MacQueen J. Some methods for classification and analysis of multivariate observations // Proc. Fifth Berkeley Symp. Math. Stat. Probab. 1967. Vol. 1. P. 281–297.

4. Hosage C. M., Goodchild M. F. Discrete Space Location-Allocation Solutions from Genetic Algorithms // Annals of Operations Research. 1986. Vol 6. P. 35–46. http://doi.org/10.1007/bf02027381

5. Bozkaya B., Zhang J., Erkut E. A Genetic Algorithm for the p-Median Problem // Drezner Z., Hamacher H. (eds,), Facality Location. Applications and Theory, Springer, Berlin, 2002.

6. Alp O., Erkut E., Drezner Z. An Efficient Genetic Algorithm for the p-Median Problem // Annals of Operations Research. 2003. Vol. 122. P. 21–42. http://doi.org/10.1023/A:1026130003508

7. Maulik U., Bandyopadhyay S. Genetic Algorithm-Based Clustering Technique // Pattern Recognition. 2000. Vol. 33, No. 9. P. 1455–1465. https://doi.org/10.1016/S0031-3203(99)00137-5

8. William M. Rand. Objective Criteria for the Evaluation of Clustering Methods // Journal of the American Statistical Association. 1971. Vol. 66, No. 336. P. 846–850.

9. De Maesschalck R., Jouan-Rimbaud D., Massart D. L. The Mahalanobis distance // Chem Intell Lab Syst. 2000. Vol 50, No. 1. P 1–18. doi: 10.1016/S0169-7439(99)00047-7

10. McLachlan G J. Mahalanobis Distance // Resonance. 1999. Vol 4, No. 20. doi: 10.1007/BF02834632.

11. Distance metric learning with application to clustering with side-information / E. P. Xing, A. Y. Ng,

M. I. Jordan and et al. // Advances in Neural Information Processing Systems. 2003. Vol. 15. P. 505–512.

12. Орлов В. И., Федосов В. В. Набор данных электрорадиоизделий. 2016 [Электронный ресурс]. URL: http://levk.info/data1526.zip.

13. Применение алгоритмов кластеризации с особыми мерами расстояния для задачи автоматической группировки электрорадиоизделий / В. И. Орлов, Г. Ш. Шкаберина, И. П. Рожнов и др. // Системы управления и информационные технологии. 2019. № 3 (77). С. 42–46.

14. Hansen P., Mladenovic N. J-means: a new local search heuristic for minimum sum of squares clustering // Pattern recognition. 2001. Vol. 34, No. 2. P. 405–413.

15. Kazakovtsev L. A., Antamoshkin A. N. Genetic Algorithm with Fast Greedy Heuristic for Clustering and Location Problems // Informatica. 2014. Vol. 38, No. 3. P. 229–240.

Shkaberina Guzel Shariphanovna – Associate Professor of the Department of Information and Control System; Reshetnev Siberian State University of Science and Technology. E-mail: z_guzel@mail.ru.
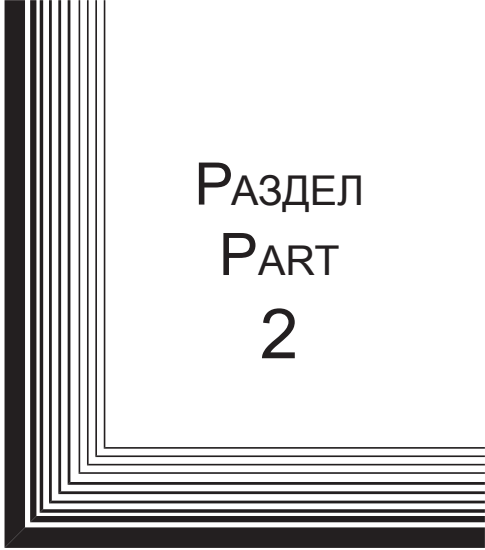
Kazakovtsev Lev Aleksandrovich – Dr. Sc., the Head of the Department of Systems Analysis and Operations Research; Reshetnev Siberian State University of Science and Technology. E-mail: levk@bk.ru.

Li Rui – graduate student of the Department of Systems Analysis and Operations Research; Reshetnev Siberian State University of Science and Technology. E-mail: 646601833@qq.com.

Шкаберина Гузель Шарипжановна – доцент кафедры информационно-управляющих систем; Сибирский государственный университет науки и технологий имени академика М. Ф. Решетнева. E-mail: z_guzel@mail.ru.

Казаковцев Лев Александрович – доктор технических наук, доцент, заведующий кафедрой системного анализа и исследования операций; Сибирский государственный университет науки и технологий имени академика М. Ф. Решетнева. E-mail: levk@bk.ru.

Ли Жуя – аспирант кафедры системного анализа и исследования операций; Сибирский государственный университет науки и технологий имени академика М. Ф. Решетнева. E-mail: 646601833@qq.com.

АВИАЦИОННАЯ
И РАКЕТНО-
КОСМИЧЕСКАЯ ТЕХНИКА

AVIATION
AND SPACECRAFT
ENGINEERING

THE INFLUENCE OF THE METHOD OF FUEL SUPPLY INTO THE COMBUSTION CHAMBER ON THE QUALITY OF MIXING AND ON THE CARBON OXIDE FORMATION

A. V. Baklanov

Kazan National Research Technical University named after A. N. Tupolev − KAI
10, Marx St., Kazan, 420111, Russian Federation
E-mail: andreybaklanov@bk.ru

The burning of fuel in the combustion chamber of a gas turbine engine (GTE) is accompanied by formation of toxic substances. The most dangerous among them are carbon oxides that have a detrimental effect on humans and environment. In this regard the article is solving the urgent problem of determining the optimal method of gaseous fuel supplying in GTE combustion chamber to ensure low carbon-oxide emissions.

The paper presents the design features of injectors that work with a separate supply of air and fuel. Natural gas is used as fuel. One of the considered injectors provides jet fuel supply by means of a perforated spray, and another one provides twisted fuel supply by means of a swirler built into the fuel channel. The main geometric parameters of the injectors are given as well, such as the size of the swirler, the number of blades, and the diameter of the output nozzle.

In this regard the quality of air-fuel mixture preparation in a swirl jet in the outlet of the burner with two types of injector is defined. It is found that the best quality of mixing is ensured by the injector with jet spray.

The design of a heat pipe simulator, in which the tested nozzle is placed, is considered. The design of a stand installation designed for testing injectors in a heat pipe simulator, as well as the modes under which these tests were carried out, are presented. The results were obtained in a heat pipe simulator with installed jet injectors and injectors with a swirling fuel jet. An analysis was conducted, which resulted in conclusions about the effectiveness of using jet injectors. According to the conducted research, the parameters of the injector with a swirling fuel jet are characterized by the presence of high values of CO levels in the combustion products, which is explained by the extremely low quality of mixing fuel with air and, consequently, low efficiency of fuel combustion. Jet fuel injection has low CO values, which indicates good quality of mixing fuel with air and high efficiency of a combustion process. As a result, we have received recommendations on setting the selected type of injectors in a full-size combustion chamber.

Keywords: combustion chamber of gas-turbine engine, emission reduction, diffusion combustion, injector, burner, mixing.

ВЛИЯНИЕ СПОСОБА ПОДАЧИ ТОПЛИВА В КАМЕРУ СГОРАНИЯ НА КАЧЕСТВО СМЕШЕНИЯ И ОБРАЗОВАНИЕ ОКСИДА УГЛЕРОДА

А. В. Бакланов

Казанский национальный исследовательский технический университет им. А. Н. Туполева – КАИ
Российская Федерация, 420111, г. Казань, ул. К. Маркса, 10
E-mail: andreybaklanov@bk.ru

Сжигание топлива в камере сгорания газотурбинного двигателя сопровождается образованием токсичных веществ. Особую опасность среди них представляют окислы углерода, оказывающие вредное воздействие на человека и окружающую среду. В связи с этим в статье решается актуальная задача по определению оптимального способа подачи газообразного топлива в камеру сгорания ГТД для обеспечения низкого выброса СО.

В работе представлены особенности конструкции форсунок, которые работают с раздельной подачей воздуха и топлива. В качестве топлива используется природный газ. Одна из рассмотренных форсунок обеспечивает струйную подачу топлива при помощи перфорированного распылителя, а другая – закрученную подачу топлива при помощи завихрителя, встроенного в топливный канал. Также приведены основные геометрические параметры форсунок, такие как размеры завихрителя, количество лопаток, диаметр выходного сопла.

Произведено определение качества подготовки топливовоздушной смеси в закрученной струе на выходе из горелок с двумя типами форсунок. Установлено, что наилучшее качество смешения обеспечивает форсунка со струйным распылом топлива.

Рассмотрена конструкция имитатора жаровой трубы, в который помещается испытываемая форсунка. Представлена конструкция стендовой установки, предназначенной для испытания форсунок в имитаторе жаровой трубы, а также режимы, при которых данные испытания проводились. Получены результаты в имитаторе жаровой трубы с установленными струйными форсунками и форсунками с подачей закрученной топливной струи. Проведен анализ, по результатам которого сделаны выводы об эффективности применения струйных форсунок. В соответствии с проведенными исследованиями параметры форсунки с подачей закрученной топливной струи характеризуются наличием высоких значений уровня СО в продуктах сгорания, что объясняется крайне низким качеством перемешивания топлива с воздухом и, следовательно, низкой эффективностью сжигания топлива. Форсунка со струйной подачей топлива имеет низкие значения СО, что свидетельствует о хорошем качестве смешения топлива с воздухом и высокой эффективности организации горения. В результате получены рекомендации о постановке выбранного типа форсунок в полноразмерную камеру сгорания.

Ключевые слова: камера сгорания ГТД, снижение выбросов вредных веществ, диффузионное горение, форсунка, горелка, смешение.

Introduction. The quality of the preparation of air-fuel mixture in the combustion chambers of gas turbine engines largely determines the level of emissions of toxic substances, herewith the quality of mixing is ensured by the way fuel is fed into the combustion chamber [1]. For this reason, the issue of the reasonable choice of a fuel supply method and determination of its influence on the formation of toxic substances in the combustion products of gas turbine engines is relevant. The main toxic substances in the combustion of hydrocarbon fuels are nitrogen oxides and carbon monoxide [2], therefore, reducing the level of their concentration is one of the most important tasks of engine manufacturers.

The burner unit of the annular combustion chamber includes an annular plate in which swirling gas burners are installed regularly around the circumference, between the inner and outer shells of the flame tube (fig. 1). In the center of these burners there are injectors that provide fuel supply [3].

Fig. 1. Burner device of a serial combustion chamber:
1 – injector; *2* – swirler; *3* – mixing chamber;
4 – jet nozzle

Рис. 1. Схема горелочного устройства серийной КС:
1 – форсунка; *2* – завихритель; *3* – камера смешения;
4 – сопловой насадок

The fuel supplied by the gas injectors *1* along the axis of each of the burners is mixed in the mixing chamber *3* with the air flow swirling in the swirler *2*. As a result,

in the primary zone of the chamber behind the nozzle heads *4* of each of the swirling burners, flows of the fuel-air mixture are formed, these flows have paraxial circulation areas. The presence of such areas ensures the circulation of hot combustion products and active centers from the combustion zone to the base of the fresh mixture torch, which creates conditions for stable ignition and flame stabilization.

The fuel supply method can be jet in the form of fuel jets and in the form of a swirling fuel jet. This paper considers two injectors operating on gaseous fuel, which differ in the way of fuel supply [4].

The principle of operation of the first one is to supply a swirling gas stream from the center of the burner. The injector (fig. 2) includes: body *2*, screw *1* with a nut (plug) *3* and a throttling washer *4*.

Fig. 2. Centrifugal gas injector:
1 – screw; *2* – injector body; *3* – nut (plug);
4 – throttling washer

Рис. 2. Центробежная газовая форсунка:
1 – шнек; *2* – корпус форсунки; *3* – гайка (заглушка);
4 – дросселирующая шайба

The body of the injector *2* is made with an internal passage for supplying gas and with the metering holes A for gas outlet. The body has a flange with holes for attach-

ing the injector to the combustion chamber body and a threaded channel for installing the screw *1*. The throttling orifice *4* is installed to provide the required gas flow through the injector.

The injector operates in the following way: gas flows from the gas collecting main through pipelines to the injectors, passes through the fuel passage in the injector body. Getting on the blades of the screw *1*, it twists and leaves the metering holes A. Mixing with the air that goes out of the burner swirler, the gas enters the combustion chamber [4]. Such an injector can be classified as a centrifugal gas injector.

The screw installed inside the injector body (fig. 3) is a swirler with four blades twisted along a helical curve of right-hand thread, stroke – 32 mm, blade thickness – 1 mm.
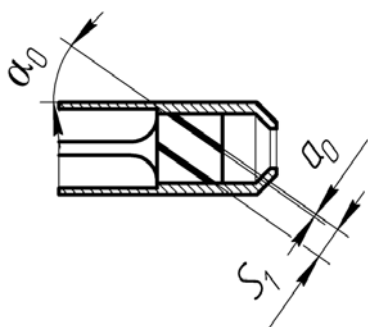
Fig. 3. Injector screw (swirler):
$D_{outer screw} = 10.5$ mm; $D_{inner screw} = 5$ mm;
$\alpha_o = 45^o$; $a_o = 4$ mm; $S_1 = 5$ mm

Рис. 3. Шнек (завихритель) форсунки:
Д$_{нар.шн.} = 10,5$ мм; Д$_{внутр.шн.} = 5$ мм; $\alpha_o = 45^o$;
$a_o = 4$ мм; $S_1 = 5$ мм

The second injector (fig. 4) differs from the first one in that the screw is excluded from the design, and at the tip of the injector there are four equally spaced holes (instead of one hole) for gas outlet [5].

To check the quality of fuel-air mixing behind the burner with a jet gas injector in comparison with a centrifugal gas injector, additional studies were carried out to determine the quality of the preparation of the fuel-air mixture at the outlet from the burners with these injectors.
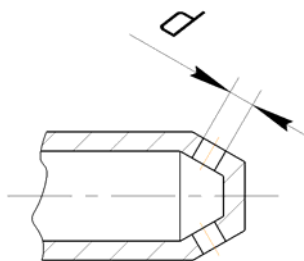
Fig. 4. Jet gas injector. Four holes
with the diameter $d = 2.9$ mm

Рис. 4. Струйная газовая форсунка.
Четыре отверстия диаметром $d = 2,9$ мм

The studies were carried out on a testing stand (fig. 5), which includes three systems: air supply, gas supply and measurement system.

The burner is placed on the test-bench equipment as follows: the injector is installed in the receiver body, to the connecting branch of which fuel is supplied. The burner is placed with the sleeve part in the orifice of the receiver cover. The fuel from the jet injectors is fed into the inner cavity of the jet nozzle, as a result, fuel-air mixture is formed at the outlet of the burner. The fuel is supplied to the propellant feed system from the cylinder manifold. Carbon dioxide (CO_2) is used as a gas to replace methane. To measure the concentration fields at the outlet of the burner, a coordinate device with a receiver of the gas analyzer called PKU-4-MK-S is installed. This device allows us to move the detector receiver axially and radially. Concentration measurements are made from the center of the burner, for which the nozzle axis "0" is taken, with further movement of the sampling instrument in both directions along the burner nozzle, across the jet every 4 mm. According to this principle, measurements are performed repetitively in seven sections: at the nozzle exit section and every 50 mm up to the distance of 300 mm [6].

The measurements of CO2 concentrations in the burner jets were also aimed at determining the distance at which the concentration pattern is equalized, as well as at fixing the rate of concentration change along the jet axis [7; 8].

To visualize the intensity of the mixing process, fig. 6 shows the characteristics of CO2 = f (r), showing in detail the change in the concentration over the cross section of the swirling jet.

According to the data in fig. 6, it can be seen that behind the burner with a centrifugal gas injector, there is no significant expansion of the mixing area, which is associated with the formation of the high flow rate of fuel gas, which leads to the high ejection ability of the jet forming a narrow flow core, in which intensive mixing of fuel with air occurs. Beyond the relative coordinate $\bar{r} = \dfrac{r_i}{r_{max}}$ corresponding to the value of 0.5, mixing does not occur, since this area contains practically no fuel.

The burner with a jet gas injector has a wide concentration field and its low level, which is explained by the volumetric recirculation zone provided by the presence of jet fuel supply, which makes it possible to mix fuel with air throughout the entire volume of the swirling jet formed behind the jet nozzle.

The quality of preparation was assessed analyzing the dependence characterizing the maximum relative deviation of concentration from the mean integral value of the concentration field [9]:

$$\bar{C} = \frac{C_{max} - C_{mi}}{C_{mi}}, \qquad (1)$$

where C_{max} – maximum value in the measured concentration field; C_{mi} – mean integral value of concentration.

In accordance with this dependence, the indicator of the ideally regular distribution of the concentration of the air-fuel mixture in the section is the value $\bar{C} = 0$.

Fig. 7 shows that the best mixing quality in all seven sections is observed for the burner with a jet gas injector. That proves the quality of the mixture preparation.

The measurements of the concentration fields behind the swirl burners confirm that the mixing process is achieved in the burner with a jet gas injector due to the jet fuel supply to the recirculation zone, and in the burner with a centrifugal gas injector due to the high ejection ability of the swirling fuel jet inside the air stream swirled in the opposite direction [10].

Further studies comprised placing the injectors into the combustion chamber in order to determine the emissions of nitrogen oxides and carbon monoxide. The compartment is 1/8 part of a full-size combustion chamber, consisting of an outer and inner shell, a flame tube with a burner unit, in which four burners with injectors are installed. The combustion can is bounded by cooling sidewalls on both sides [11].

The combustion chamber compartment is studied on a testing stand, the diagram of which is shown in fig. 8. The stand is equipped with the necessary systems for measuring and registering parameters. The stand includes a gas turbine engine (blowing engine), which is used to supply compressed air to the tested compartment of the combustion chamber 3. Air is taken from the high-pressure compressor, then it enters through the pipeline into the central line 1. Air consumption is measured by a flow meter.

The stand is equipped with a measuring section 2 with recording the readings of a pressure sensor 4, 5; the air temperature is controlled by a chromel-alumel thermocouple 6. The fuel (natural gas) is supplied through the fuel system 7 to the fuel manifold 8 of the combustion chamber compartment, and then it enters the front-line device and injectors. To measure the temperature in the outlet of the compartment, a survey rake 12 is installed at the outlet of it, the data from which is transmitted to the recording equipment 13. To determine the composition of combustion products, a gas sampling probe 9 and a line for transporting combustion products 10 to the gas analyzing equipment 11 are located at the outlet of the compartment.

The gas analyzer testo350 [12] is used to determine the CO content in combustion products.

The compartments were tested under the following conditions: Air pressure Pa = 1.37 kPa, Air flow Ga = 1.72 kg / s, Air temperature Ta = 488 K, superficial velocity speed λ = 0.28. The change in the excess air ratio was carried out by reducing the fuel consumption.

After determining the component composition of combustion products for carbon monoxide, the emission index EI_i is calculated, according to the equation [13]:

$$EI_i = \frac{\mu_i}{\mu_в}(1 - \alpha_i \cdot L_0) \cdot \chi_i \cdot 10^{-3}. \qquad (2)$$
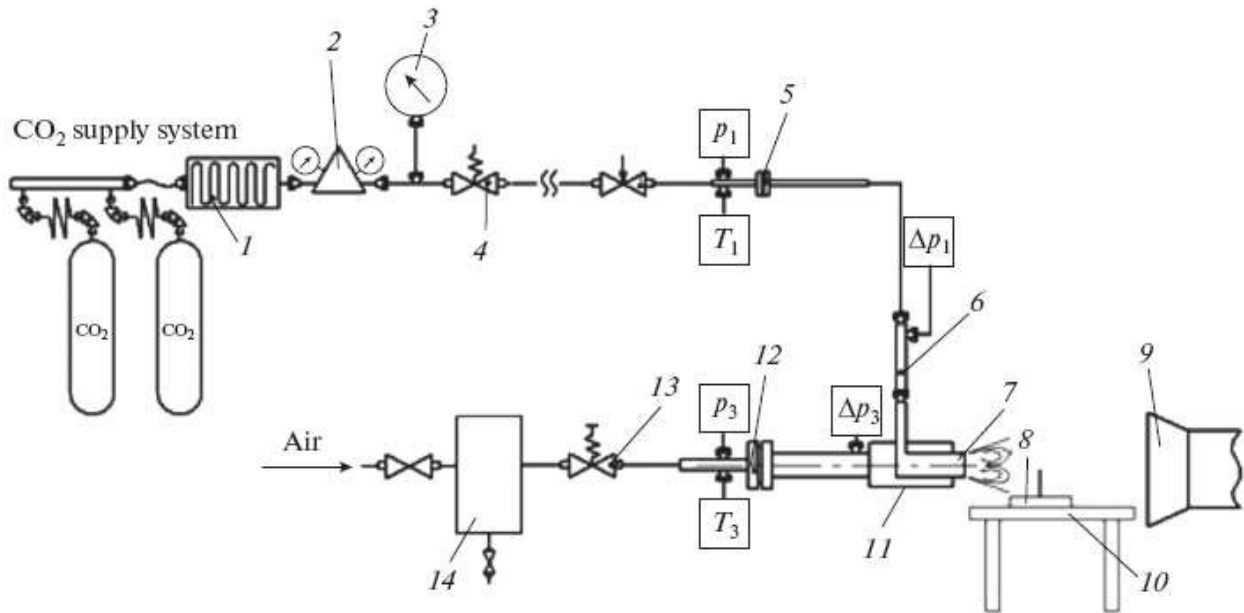
Fig. 5. Structure of test stand:
1 – Heater; *2* – outlet reducer; *3* – pressure gauge; *4* – cutoff valve; *5* – flow meter; *6* – tee joint; *7* – burner; *8* – gas analyzer;
9 – ventilation device for removing carbon dioxide from the working room; *10* – coordinate table; *11* – receiver; *12* – flow meter;
13 – electromagnetic valve; *14* – moisture separator; absolute pressure and CO_2 temperature sensors installed upstream
of the flow meter (throat); sensor for measuring pressure difference across the CO_2 path; absolute pressure
and air temperature sensors installed upstream of the flow meter; and sensor for measuring air pressure difference
installed upstream of the receiver

Рис. 5. Принципиальная схема стенда:
1 – нагреватель; *2* – выходной редуктор; *3* – манометр; *4* – отсечной клапан; *5* – расходомер; *6* – тройник;
7 – горелка; *8* – газоанализатор; *9* – вентиляционное устройство для отвода углекислого газа из рабочего помещения;
10 – координатный стол; *11* – ресивер; *12* – расходомер *13* – электромагнитный клапан; *14* – влагоотделитель

a

b
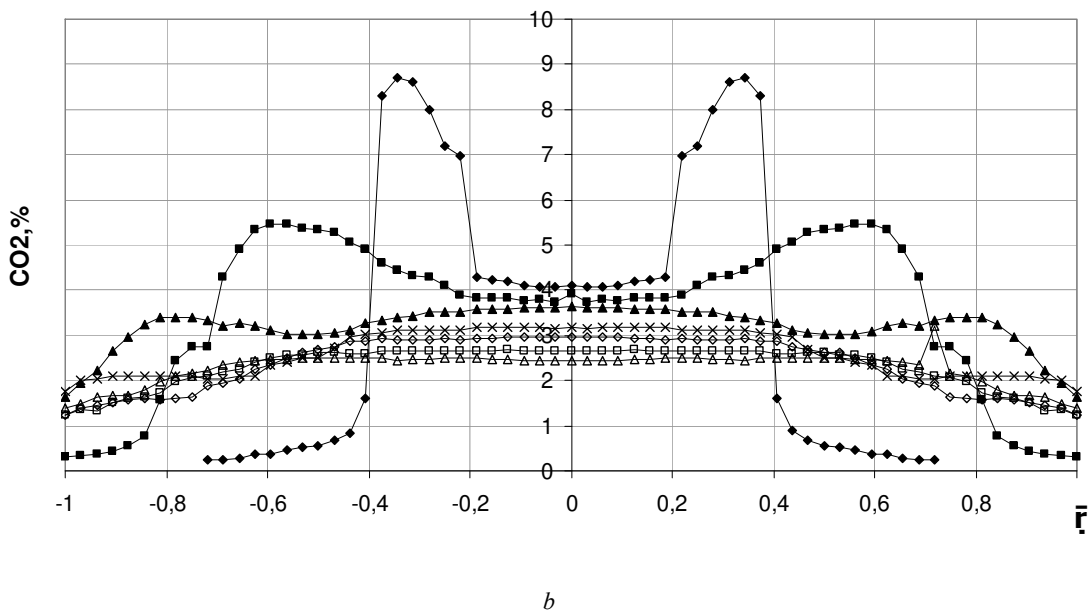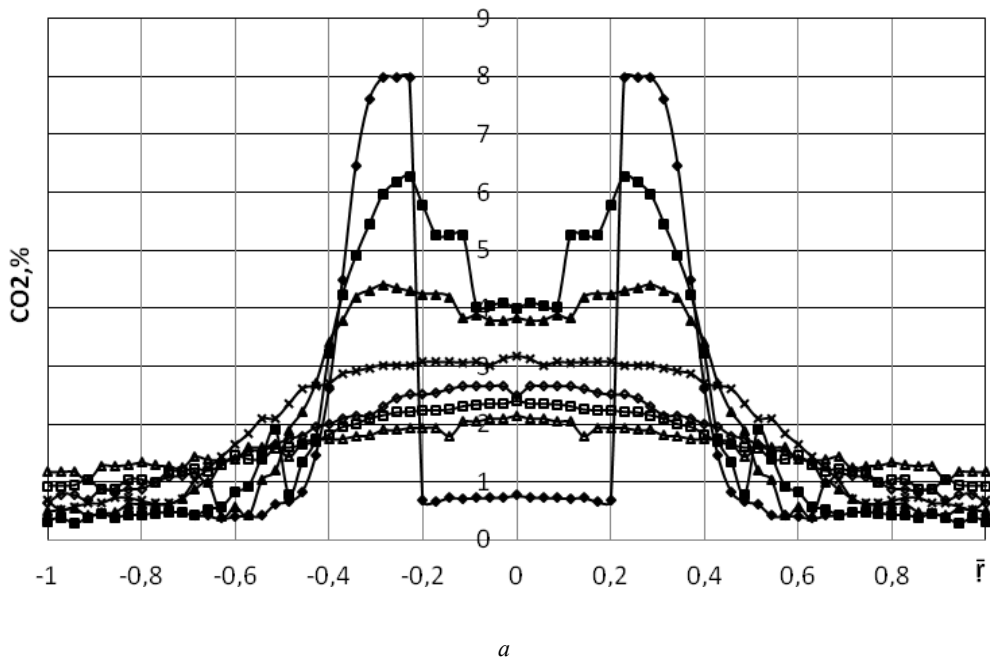
Fig. 6. Field of CO_2 concentrations in various sections of a swirling jet:
a – centrifugal gas injector (CGI); *b* – with jet injector (JI)
♦ – nozzle cut; ■ – 50 mm; ▲ – 100 mm; × – 150 mm; ◊ – 200 mm; □ – 250 mm; Δ – 300 mm

Рис. 6. Поле концентраций CO_2 в различных сечениях закрученной струи:
a – ЦБГФ; *b* – СГФ
♦ – срез сопла; ■ – 50 мм; ▲ – 100 мм; × – 150 мм; ◊ – 200 мм; □ – 250 мм; Δ – 300 мм

Where $L_0 = 16.7$ – stoichiometric coefficient of methane combustion (kg of air / kg of fuel); α_i – total or local air-to-fuel ratio; μ_i – molar mass of the determined toxic substance; $\mu_\text{в}$ – molar air mass; χ_i – volume fraction of a toxic substance (ppm). When calculating EI_i we have taken the following values of molar masses:

μco = 28.010 kg / kmol and $\mu_\text{в}$ = 28.964 kg / kmol [14; 15].

According to the results of the measurements (fig. 9), it can be seen that the value of the carbon monoxide emission index in the compartment with a jet gas injector has decreased by half compared to the compartment with a centrifugal gas injector.

The results showed that it is preferable to use gas distribution with the help of jet feed, which, in contrast to the supply of swirling fuel jets, not only increases the interface of the mixed media, but it also allows us (by appropriate orientation and range of the jets) to distribute fuel over the air flow section with the required concentration profile in the flame tube in a simple and reliable way.
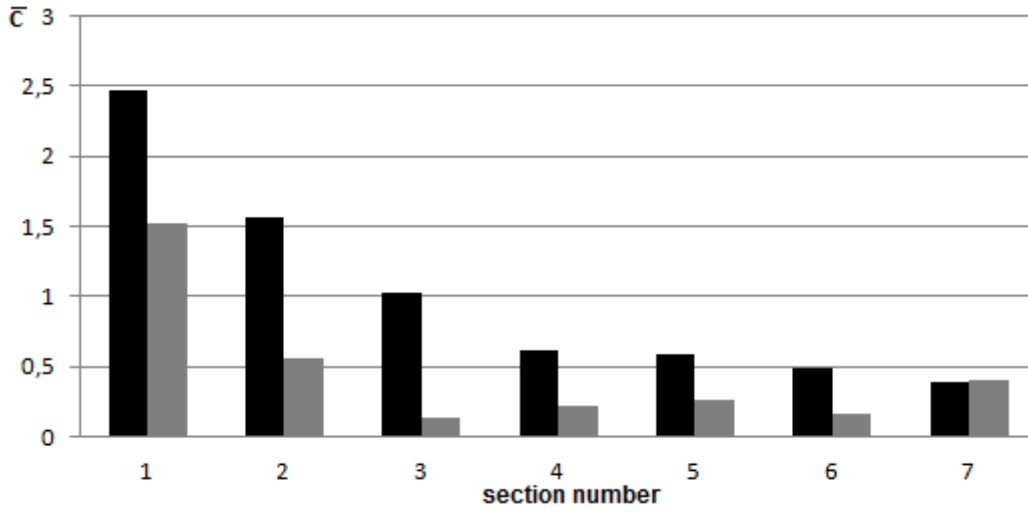
Fig. 7. The quality of the preparation of the air-fuel mixture in a swirling stream:
■ – the burner with centrifugal gas injector (CGI); ▥ – the burner with jet injector (JI)

Рис. 7. Качество подготовки топливовоздушной смеси в закрученной струе:
■ – горелка с ЦБГФ; ▥ – горелка с СГФ
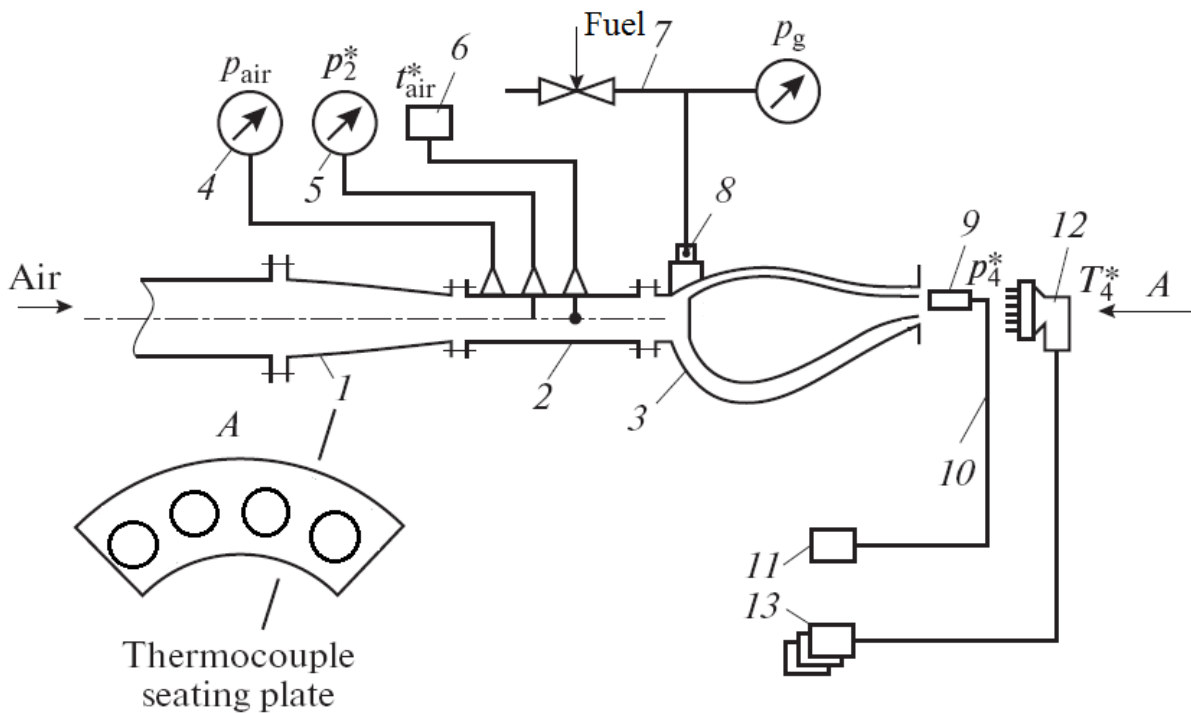
Fig. 8. Stand for testing the sections of a combustion chamber

Рис. 8. Стенд для исследования отсеков камеры сгорания
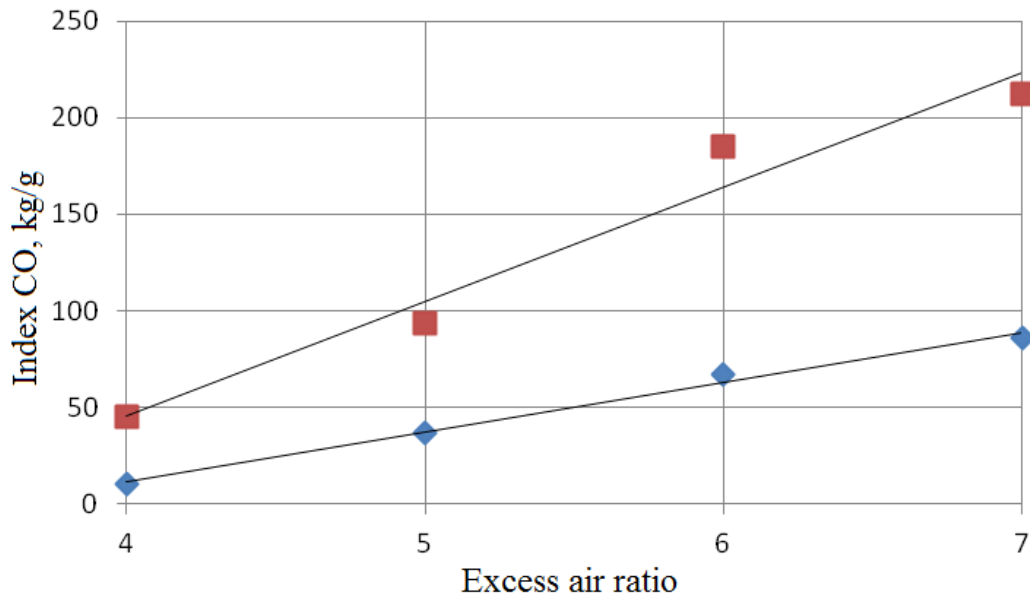
Fig. 9. CO index at the outlet of the compartment:
♦ – JI; ■ – CGI

Рис. 9. Индекс СО на выходе из отсека:
♦ – СГФ; ■ – ЦБГФ

Conclusion.

1. The organization of jet fuel supply will allow us to perform the most efficient combustion of gaseous fuel in comparison with the fuel supply with a swirling jet, which makes it possible to halve the index of carbon monoxide in the combustion products of the combustion chamber compartment.

2. Jet fuel supply provides better preparation of a fuel-air mixture.

3. It is recommended to install a jet gas injector as a measure to reduce carbon monoxide in combustion products of a gas turbine engine.

References

1. Matveev S. S., Zubrilin I. A., Orlov M. Yu., Matveev S. G., Chechet I. V. Investigation of fuel distribution in partially premixed swirled burner with pilot flame. Proceedings of the ASME Turbo Expo Turbomachinery Technical Conference and Exposition. Сер. "ASME Turbo Expo 2016: Turbomachinery Technical Conference and Exposition, GT 2016" 2016.

2. Baklanov A. V., Neumoin S. P. [A technique of gaseous fuel and air mixture quality identification behind the swirl burner of gas turbine engine combustion chamber]. *Russian Aeronautics*. 2017, Vol. 60, P. 90–96 (In Russ.).

3. Gritsenko E. A., Danilchenko V. P., Lukachev S. V. *Konvertirovanie aviatsionnykh GTD v gazoturbinnye ustanovki nazemnogo primeneniya* [Conversion of aviation gas turbine engines to land-based gas turbines]. Samara, SNTs RAN Publ., 2004, 266 p.

4. Mingazov B. G. *Kamery sgoraniya gazoturbinnykh dvigateley* [The combustion chamber of gas turbine engines]. Kazan, Izd-vo Kazan. gos. tekhn. un-ta Publ., 2004, 220 p. (In Russ.).

5. Baklanov A. V. [Controlling fuel combustion process by burner design change in gas turbine engine combustion chamber]. *Vestnik Moskovskogo aviatsionnogo instituta*. 2018, Vol. 25, No. 2, P. 73–85 (In Russ.).

6. Markushin A. N., Baklanov A. V. [Testing stands for researching the processes and maturation of low emission combusters]. *Vestnik of the Samara State Aerospace University*. 2013, No. 3(41), P. 131–138 (In Russ.).

7. Lefebvre A. H., Ballal D. R. Gas Turbine Combustion: Alternative Fuels and Emissions. Third Edition. CRC Press, 2010, 560 p.

8. Lefebvre A. H. Fuel effects on gas turbine combustion-ignition, stability, and combustion efficiency. *Am. Soc. Mech.* Eng. (Pap.); (United States). 1984, Vol. 84, No. CONF-840611.

9. Gritsenko E. A., Danilchenko V. P., Lukachev S. V. et al. *Nekotorye voprosy proektirovaniya aviatsionnykh gazoturbinnykh dvigateley* [Some issues of designing aircraft gas turbine engines]. Samara, SNTs RAN Publ., 2002, 527 p.

10. Gokulakrishnan P., Fuller C. C., Klassen M. S., Joklik R. G., Kochar Y. N., Vaden S. N., Seitzman J. M. Experiments and modeling of propane combustion with vitiation. *Combustion and Flame*. 2014, Vol. 161, No. 8, P. 2038–2053.

11. Yi T., Gutmark E. J. Real-time prediction of incipient lean blowout in gas turbine combustors. *AIAA journal*. 2007, Vol. 45, No. 7, P. 1734–1739.

12. Moses C., Roets P. Properties, Characteristics and Combustion Performance of Sasol Fully Synthetic Jet Fuel. *ASME Journal of Engineering for Gas Turbines and Power*. 2009, Vol. 131, No. 4, P. 041502-041502-17.

13. Canilo P. M., Podgornyy A. N., Khristich V. A. *Energeticheskie i ekologicheskie kharakteristiki GTD pri ispol'zovanii uglevodorodnykh topliv i vodoroda* [Energy and environmental characteristics of gas turbine engines when using hydrocarbon fuels and hydrogen]. Kiev, Nauk. Dumka Publ., 1987, P. 224.

14. Dubovkin N. F. *Spravochnik po teplofizicheskim svoystvam uglevodorodnykh topliv i ikh produktam sgoraniya* [Handbook of the thermophysical properties of hydrocarbon fuels and their combustion products]. Moscow – Leningrad, Gosenergoizdat Publ., 1962, 288 p.

15. Isserlin A. S. *Osnovy szhiganiya gazovogo topliva* [Basics of burning gas fuel]. Leningrad, Nedra Publ., 1987, 336 p.

Библиографические ссылки

1. Matveev S. S., Zubrilin I. A., Orlov M. Yu., Matveev S. G., Chechet I. V. Investigation of fuel distribution in partially premixed swirled burner with pilot flame. Proceedings of the ASME Turbo Expo Turbomachinery Technical Conference and Exposition. Сер. "ASME Turbo Expo 2016: Turbomachinery Technical Conference and Exposition, GT 2016" 2016.

2. Бакланов А. В., Неумоин С. П. Методика определения качества смешения газообразного топлива и воздуха за вихревой горелкой камеры сгорания ГТД // Известия вузов. Авиационная техника. 2017. № 1. С. 87–92.

3. Конвертирование авиационных ГТД в газотурбинные установки наземного применения / Е. А. Гриценко, В. П. Данильченко, С. В. Лукачев и др. Самара, СНЦ РАН, 2004. 266 с.

4. Мингазов Б. Г. Камеры сгорания газотурбинных двигателей. Казань : изд-во Казан. гос. техн. ун-та, 2004. 220 с.

5. Бакланов А. В. Управление процессом сжигания топлива путем изменения конструкции горелки в камере сгорания газотурбинного двигателя // Вестник Московского авиационного ин-та. 2018. Т. 25, № 2. С. 73–85.

6. Маркушин А. Н., Бакланов А. В. Испытательные стенды для исследования процессов и доводки низкоэмиссионных камер сгорания ГТД // Вестник Самарского гос. аэрокосмич. ун-та им. ак. С. П. Королёва (нац. исследовательского ун-та). 2013. № 3–1 (41). С. 131–138.

7. Lefebvre A.H., Ballal D. R. Gas Turbine Combustion: Alternative Fuels and Emissions. Third Edition. CRC Press, 2010. 560 p.

8. Lefebvre A. H. Fuel effects on gas turbine combustion-ignition, stability, and combustion efficiency // Am. Soc. Mech. Eng. (Pap.); (United States). 1984. Vol. 84, №. CONF-840611.

9. Некоторые вопросы проектирования авиационных газотурбинных двигателей / Е. А. Гриценко, В. П. Данильченко, С. В. Лукачев и др. Самара, СНЦ РАН, 2002. 527 с.

10. Gokulakrishnan P., Fuller C. C., Klassen M. S., Joklik R. G., Kochar Y. N., Vaden S. N., Seitzman J. M. Experiments and modeling of propane combustion with vitiation // Combustion and Flame. 2014. Vol. 161, № 8. P. 2038–2053.

11. Yi T., Gutmark E. J. Real-time prediction of incipient lean blowout in gas turbine combustors // AIAA journal. 2007. Vol. 45, № 7. P. 1734–1739.

12. Moses C., Roets P. Properties, Characteristics and Combustion Performance of Sasol Fully Synthetic Jet Fuel // ASME Journal of Engineering for Gas Turbines and Power. 2009, Vol. 131, No. 4. P. 041502–041502-17.

13. Канило П. М., Подгорный А. Н., Христич В. А. Энергетические и экологические характеристики ГТД при использовании углеводородных топлив и водорода. Киев : Наук. думка, 1987. 224 с.

14. Дубовкин Н. Ф. Справочник по теплофизическим свойствам углеводородных топлив и их продуктам сгорания. М. – Л. : Госэнергоиздат, 1962. 288 с.

15. Иссерлин А. С. Основы сжигания газового топлива. Л. : Недра, 1987. 336 с.

Baklanov Andrey Vladimirovich – Associate Professor; Kazan National Research Technical University named after A. N. Tupolev − KAI. E-mail: andreybaklanov@bk.ru.

Бакланов Андрей Владимирович – доцент; Казанский национальный исследовательского технический университет имени А. Н. Туполева − КАИ. Email: andreybaklanov@bk.ru.

HEAT TRANSFER IN THE CENTRIFUGAL FORCE FIELD FOR GAS TURBINES ELEMENTS

A. A. Zuev[1*], A. A. Arngold[2], E. V. Khodenkova[1]

[1]Reshetnev Siberian State University of Science and Technology
31, Krasnoyarskii rabochii prospekt, Krasnoyarsk, 660037, Russian Federation
[2]JSC "Krasnoyarsk machine-building plant"
29, Krasnoyarsky Rabochy Av., Krasnoyarsk, 660123, Russian Federation
[*]E-mail: dla2011@inbox.ru

The study of heat transfer from combustion products (CP) to the impeller and the casing of gas turbines of liquid rocket engines (LRE) is an urgent task.

The solution of the flow problem, taking into account heat transfer, in rotational flows, in the flowing parts of the turbopump units (TPU) of the rocket engine, is carried out by the following methods: numerical methods; analytical approach, when solving the equations of dynamic and temperature boundary layers; as well as using empirical dependencies. The temperature parameter of the gaseous combustion products and, as a consequence, the heat exchange between the combustion products and the structural elements of the flow part, significantly affects the working and energy characteristics of the TPU LRE.

When designing gas turbines of LRE, it is necessary to take into account the presence of heat exchange processes, the working fluid temperature distribution and the structural element temperatures in the cavities of the TPU LRE (since energy losses and viscosity depend on the temperatures of the working fluid, and also determine the flow parameters). The temperature distribution in the structural elements determines the performance and reliability of the unit.

In the case of the use of cryogenic fuel components in the TPU LRE units the heating of the component leads to the implementation of cavitation modes and a drop in operating and energy characteristics. On the other hand, a lowered temperature of the working fluid leads to an increased viscosity of the components and, as a consequence, a decrease in the efficiency of the unit (especially when using gel-like components).

When studying heat transfer in the field of centrifugal forces for elements of rocket engine gas turbines it is necessary to obtain a joint solution of the equations of dynamic and temperature boundary layers in the boundary conditions of the flow parts.

This article offers a model of the distribution of dynamic and temperature boundary layers taking into account the convective component (for the case of a gaseous working fluid, i. e. Pr < 1), which is necessary for the analytical solution and determination of the heat transfer coefficient in the boundary conditions of the flow cavities of the LRE turbine. The energy equation has been analytically obtained for the boundary conditions of the temperature boundary layer, which allows integration over the surface of any shape, which is necessary in determining the thickness of the energy loss. Taking into account the integral relation, the heat transfer law of the turbulent boundary layer for the rotation cavities is written. The equations for determining the heat transfer coefficient in the form of the Stanton criterion for rectilinear uniform and rotational flows for cases of turbulent flow regimes were obtained analytically. The obtained equations for heat transfer coefficients are in good agreement with experimental data and dependences of other authors.

Keywords: heat transfer coefficient, temperature boundary layer, turbopump unit, power parameters, turbine.

ТЕПЛООТДАЧА В ПОЛЕ ЦЕНТРОБЕЖНЫХ СИЛ ДЛЯ ЭЛЕМЕНТОВ ГАЗОВЫХ ТУРБИН

А. А. Зуев[1*], А. А. Арнгольд[2], Э. В. Ходенкова[1]

[1]Сибирский государственный университет науки и технологий имени академика М. Ф. Решетнева
Российская Федерация, г. Красноярск, 660037, просп. им. газ. «Красноярский рабочий», 31
[2] АО «Красноярский машиностроительный завод»
Российская Федерация, 660123, г. Красноярск, просп. им. газ. «Красноярский рабочий», 29
[*]E-mail: dla2011@inbox.ru

Исследование теплоотдачи от продуктов сгорания (ПС) к рабочему колесу и корпусу газовых турбин жидкостных ракетных двигателей (ЖРД) является актуальной задачей.

Решение задачи течения с учетом теплообмена при вращательных течениях в проточных частях турбонасосных агрегатов (ТНА) ЖРД осуществляется следующими способами: численными методами, аналитическим подходом при решении уравнений динамического и температурного пограничных слоев, а также с использованием эмпирических зависимостей. Параметр температуры газообразных ПС и, как следствие, теплообмен между ПС и конструктивными элементами проточной части значительно влияет на рабочие и энергетические характеристики ТНА ЖРД.

При проектировании газовых турбин ЖРД необходимо учитывать наличие теплообменных процессов, распределение температур рабочего тела и температур конструктивных элементов в полостях ТНА ЖРД (так как энергетические потери и вязкость зависят от температур рабочего тела, а также определяют параметры течения). Распределение температур в конструктивных элементах определяют работоспособность и надежность агрегата.

В случае применения криогенных компонентов топлива в агрегатах подачи ТНА ЖРД, подогрев компонента приводит к реализации кавитационных режимов и падению рабочих и энергетических характеристик. С другой стороны, пониженная температура рабочего тела приводит к повышенной вязкости компонентов и снижению КПД агрегата (особенно при использовании гелеобразных компонентов).

При исследовании теплоотдачи в поле центробежных сил для элементов газовых турбин ЖРД необходимо получить совместное решение уравнений динамического и температурного пограничных слоев в граничных условиях проточных частей.

Предложена модель распределения динамического и температурного пограничных слоев с учетом конвективной составляющей (для случая газообразного рабочего тела, т. е. Pr < 1), необходимая для аналитического решения и определения коэффициента теплоотдачи в граничных условиях проточных полостей турбины ЖРД. Аналитически получено уравнение энергии для граничных условий температурного пограничного слоя, позволяющего вести интегрирование по поверхности любой формы, необходимое при определении толщин потери энергии. С учетом интегрального соотношения записан закон теплообмена турбулентного пограничного слоя для полостей вращения. Аналитическим путем получены уравнения для определения коэффициента теплоотдачи в виде критерия Стантона для прямолинейного равномерного и вращательных течений для случаев турбулентных режимов течения. Полученные аналитические уравнения для коэффициентов теплоотдачи хорошо согласуются с экспериментальными данными и зависимостями других авторов.

Ключевые слова: коэффициент теплоотдачи, температурный пограничный слой, турбонасосный агрегат, энергетические параметры, турбина.

Introduction. Considering the features of heat transfer in the flowing parts of turbopump units (TPU) of liquid rocket engines (LRE) is an urgent task. Currently, taking into account the features of the flow with heat transfer during the implementation of the potential and vortex rotational flow in the flow parts is mainly carried out by the following methods: using empirical equations, numerical and analytical methods for solving differential equations in partial derivatives [1].

The first method does not always provide the required accuracy in calculating the hydrodynamic and thermal characteristics of rotational flows taking heat transfer into account and requires additional specifying experimental studies. As a rule, this entails quite a bit more time and material costs for setting up and conducting research.

Numerical methods are quite difficult to use when carrying out engineering calculations and require their implementation in specialized software. Numerical research methods use direct numerical simulation (DNS method) and the averaged Navier-Stokes and Reynolds equations (RANS method). The choice of method depends on the complexity of the problem and the accuracy of the results. The RANS method is often used with the k-ε and k-ω turbulence models [2–7]. The issues of heat transfer during the flow around a curved surface with a longitudinal curvature of the working fluid gaseous flow were also considered in [8–10], where cases of flow around turbine blades were investigated. In [11], convective heat transfer in a channel with periodic protrusions was studied on the basis of multiblock computational technologies based on the solution of the Reynolds equations closed by the Mentor model of shear stress transfer using the factorized finite-volume method and the energy equation on multiscale intersecting structured grids.

The analytical method allows obtaining analytical dependences applicable for engineering calculations in a

wide range of possible variations of design and operational parameters. Analytical methods, as a rule, were developed for a rectilinear uniform flow, and have a number of limitations. One of the earliest studies is the work of E. L. Knuth [12], in which the analysis is based on an extended Reynolds analogy with the transfer of heat, mass, and momentum in a developed turbulent flow in a pipe. The use of the velocity and temperature distribution profiles in the boundary layer was proposed by W. D. Rannie [13] and modified by D.L. Turcotte [14]. Turcotte sublayer analysis took into account the effect of heat transfer on turbulence. The analytical methods for determining the heat transfer coefficients proposed in [15; 16] take into account convective heat transfer in LRE chambers and are performed for a rectilinear turbulent flow. A one-dimensional analytical model for subcritical conditions was also proposed by S.R. Shine [17].

Design features of liquid rocket engine turbopump units (LRE TPU) turbines and the object of the study. During design, the diameter of the LRE TPU turbine is selected taking into account the layout and ensuring the minimum dimensions and is limited by the strength of the turbine rotor. From the analysis of adiabatic work it is known that with a selected working fluid the greatest value of adiabatic work is achieved at high temperatures and large pressure ratios.

The use of high temperatures is limited by the structure operability. LRE use uncooled turbines. Due to the design features and materials used the working fluid temperature in front of an uncooled turbine is limited, as a rule, for a reducing gas of 1000–1200 ^{0}C, for an oxidizing gas of 700–900 ^{0}C. The higher the temperature in front of the turbine can be assumed, the less pressure should be in front of the turbine. Due to the design features, LRE turbines are single-stage and rarely two-stage.

High temperatures of the working fluid lead to temperature deformations, including turbine disks [18]. When designing the flowing parts of the units and assemblies of the LRE TPU, it is necessary to take into account the change in the working fluid flow temperature along the length of the working channel, since the viscosity parameter is a function of temperature and determines the flow regime and, as a result, losses, in particular, disk friction and hydrodynamic losses in the flowing part.

The optimal level of the turbopump units (TPU) energy parameters stability is ensured in the course of development work by adjusting the geometric dimensions of parts and assembly the gas-dynamic path units, choosing technological schemes for dimensional processing, assembly and turbine testing with the involvement of static material significant amount. In this regard, the LRE TPU energy parameters' modelling represents an urgent scientific and technical problem. The parameter optimization of the workflow and the mathematical model of the propulsion system (PS) are considered by V.A. Grigoryev [19], where the analysis of models was carried out and the advantages and disadvantages for various design stages were revealed.

The requirements for the TPU design are formed on the basis of the tasks performed by the propulsion system (PS) into which the TPU is integrated as a single unit. And the requirements for the TPU design are formed on the basis of the tasks performed by the propulsion system (PS), into which the TPU is an integral part with which it is assembled as a single unit. Requirements for PS fully apply to the TPU: to ensure at all engine operating modes the supply of fuel components with the required flow rate and pressure with a high degree of reliability and efficiency; provide minimum dimensions and weight; simplicity of design and minimal cost.

The main object of study where the potential and vortex rotational flow occurs is the structural elements of the flowing parts of gas turbines of the rocket engine: inlet and outlet device, the cavity between the stator and the impeller [20].

The research problem. In the generalized problem formulation of fluid flow during heat exchange with the surface of aggregates, such as compressors, expanders, pumps of cryogenic components, etc., it is necessary to take into account the change in flow temperature along the length of the working channel, since viscosity, as a function of temperature, mainly determines the flow regime and, as a result, hydraulic losses [21].

For the case of incompressible fluid flow, it is necessary and sufficient to jointly solve the equations of motion and energy in the boundary conditions of the spatial boundary layer [22]; for a compressible fluid, the system must be supplemented with the equation of state.

The processes of heat transfer in power stations are largely similar, but there are certain differences in the analysis and derivation of heat transfer equations for the boundary conditions of the liquid propellant rocket engine. The main differences are as follows: extremely high values of heat fluxes, temperatures and pressures, the presence of high flow velocities, the initial turbulent state of flows in the core, working fluids can be in a gaseous and liquid state, surface curvature effects, the presence of density and compressibility gradients, non-stationarity heat fluxes and the presence of flow instability in the active zone of heat transfer [23].

The heat transfer law of a turbulent flow of a spatial boundary layer temperature. The integral relation of the energy equation. For Prandtl numbers less than unity (Pr < 1 is characteristic of gaseous working fluids, including combustion products), the thickness of the dynamic boundary layer is below the thickness of the temperature boundary layer, i. e., δ < δt (fig. 1). At very low Prandtl numbers (liquid metals), molecular thermal conductivity is the main mechanism of heat transfer and cannot be neglected even in a turbulent flow core. At low Prandtl numbers, thermal resistance is distributed over the entire flow section [24].

If we assume that at the boundary of the dynamic boundary layer, the temperature changes due to the transfer of velocity, and beyond its boundary – only due to molecular thermal conductivity. This assumption is in good agreement with Case's conclusions, since at very low Prandtl numbers the thickness of the dynamic boundary layer is much less than the thickness of the temperature boundary layer. Accordingly, thermal resistance is present throughout the thickness of the temperature boundary layer. Within the boundaries of the dynamic boundary layer, thermal resistance is due to turbulent heat transfer and outside the boundaries of the dynamic

boundary layer thermal resistance is due to molecular thermal conductivity.
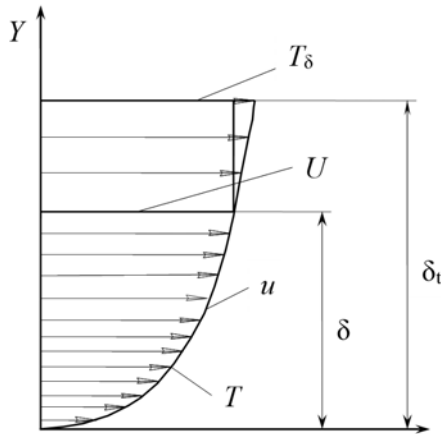
Fig. 1. Temperature distribution model
and dynamic boundary layers at Pr < 1

Рис. 1. Модель распределения температурного
и динамического пограничных слоев при Pr < 1

The equation of the thickness of the energy loss of the temperature boundary layer could be considered as [25]:

$$\delta_{t\varphi}^{**} = \int_0^{\delta_t} \frac{u}{U}\left(1 - \frac{T - T_0}{T_\delta - T_0}\right) dy . \tag{1}$$

The integration boundaries of the thickness of the energy loss (1) must be divided into two characteristic sections. The first integration section lies at the boundary of the thickness of the dynamic boundary layer δ, the second integration section lies at the boundary of the end of the thickness of the dynamic boundary layer δ to the end of the temperature boundary layer δ_t.

The thickness of the energy loss equation (1) for the distribution of the temperature model and dynamic boundary layers under consideration, with the accepted model of splitting into two characteristic integration sections, can be written as:

$$\delta_{t\varphi}^{**} = \int_0^{\delta} \frac{u}{U}\left(1 - \frac{T - T_0}{T_\delta - T_0}\right) dy + \int_\delta^{\delta_t} \frac{u}{U}\left(1 - \frac{T - T_0}{T_\delta - T_0}\right) dy . \tag{2}$$

Using equation (2), it becomes possible to determine the form of the heat transfer law for the case Pr < 1. For further use, equation (2) needs to be integrated taking into account the accepted laws of distribution of the velocity profile in the boundary layer. Next, we first consider the power-law profile, then the gradient profile.

The distribution of the dynamic boundary layer is approximated by a power function of the form

$$\frac{u}{U} = \left(\frac{y}{\delta}\right)^{\frac{1}{m}} .$$

The distribution of the temperature boundary layer is approximated by a function of the form

$$\frac{T - T_0}{T_\delta - T_0} = \left(\frac{y}{\delta_t}\right)^{\frac{1}{m}} .$$

Given the accepted model of the distribution of dynamic and temperature boundary layers and the distribution function of the parameters of the dynamic and temperature layers, we write the equation for the thickness of the energy loss:

$$\delta_{t\varphi}^{**} = \int_0^{\delta} \left(\frac{y}{\delta}\right)^{\frac{1}{m}}\left(1 - \left(\frac{y}{\delta_t}\right)^{\frac{1}{m}}\right) dy + .$$

$$+ \int_\delta^{\delta_t} \left(\frac{y}{\delta}\right)^{\frac{1}{m}}\left(1 - \left(\frac{y}{\delta_t}\right)^{\frac{1}{m}}\right) dy . \tag{3}$$

If we take into account that in the first term of equation (3), the distribution profiles of the dynamic and temperature boundary layers coincide. Then, within the boundaries of integration of the first term of equation (3), the thicknesses of the temperature and dynamic boundary layers coincide, i. e. $\delta_t = \delta$. Considering the second term of equation (3), we note that there is no change in the dynamic boundary layer along the Y axis at the integration boundaries and the flow velocity is equal to the flow velocity in the flow core. Then the distribution of the dynamic boundary layer in the second term of equation (3) can be written as

$$\frac{u}{U} = \left(\frac{y}{\delta}\right)^{\frac{1}{m}} = 1 .$$

Also, in the second term of equation (3.3), a change in the diagram of the temperature boundary layer occurs only due to molecular thermal conductivity. It should be noted that for this section of the profile diagram is as follows:

$$\frac{T - T_\delta}{T_{\delta_t} - T_\delta} = \lambda \frac{y}{\delta_t} .$$

Taking into account the condition of conjugation of the temperature and dynamic profiles for the physical model of thermal conductivity at Pr < 1 (fig. 2) with the convective component, we write:

$$\frac{T - T_0}{T_\delta - T_0} = \lambda\left(\frac{y}{\delta} - 1\right) + 1 .$$

In this case, the equation for the thickness of the energy loss, taking into account the accepted two-layer model of the distribution of the temperature boundary layer with the presence of heat transfer under the condition Pr < 1, can be rewritten as:

$$\delta_{t\varphi}^{**} = \int_0^{\delta}\left(\frac{y}{\delta}\right)^{\frac{1}{m}}\left(1 - \left(\frac{y}{\delta}\right)^{\frac{1}{m}}\right) dy + \int_\delta^{\delta_t}\left(1 - \left(\lambda\left(\frac{y}{\delta} - 1\right) + 1\right)\right) dy =$$

$$= \int_0^{\delta}\left(\frac{y}{\delta}\right)^{\frac{1}{m}}\left(1 - \left(\frac{y}{\delta}\right)^{\frac{1}{m}}\right) dy + \int_\delta^{\delta_t}\left(-\lambda\left(\frac{y}{\delta} - 1\right)\right) dy . \tag{4}$$

Let us replace the variables in the equation of the thickness of the energy loss of the temperature boundary layer (4):

$$A1 = \int_0^\delta \left(\frac{y}{\delta}\right)^{\frac{1}{m}}\left(1-\left(\frac{y}{\delta}\right)^{\frac{1}{m}}\right)dy,$$

$$A2 = \int_\delta^{\delta_t}\left(-\lambda\left(\frac{y}{\delta}-1\right)\right)dy.$$

Consider the first term of the equation:

$$A1 = \int_0^\delta \left(\frac{y}{\delta}\right)^{\frac{1}{m}}\left(1-\left(\frac{y}{\delta}\right)^{\frac{1}{m}}\right)dy = \frac{m\delta}{(m+1)(m+2)}. \quad (5)$$
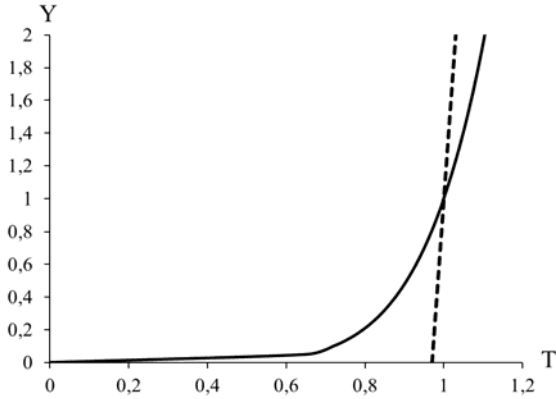
Fig. 2. The pairing of temperature and dynamic profiles
for the physical model at Pr < 1:
━━ – dynamic boundary layer with a power-law velocity
distribution; ▬▬ – temperature boundary layer

Рис. 2. Сопряжение температурного и динамического
профилей для физической модели при Pr < 1:
━━ – динамический пограничный слой со степенным
распределением скорости; ▬▬ – температурный
пограничный слой

We define the second term of the equation to determine the thickness of the energy loss of the temperature boundary layer:

$$A2 = \int_\delta^{\delta_t} -\lambda\left(\frac{y}{\delta}-1\right)dy = -\left.\frac{\delta\lambda\left(\frac{y}{\delta}-1\right)^2}{2}\right|_\delta^{\delta_t} = -\frac{\lambda(\delta-\delta_t)^2}{2\delta}. \quad (6)$$

Then the equation for the thickness of the energy loss (4) taking into account (5) and (6) can be written as

$$\delta_{t\varphi}^{**} = \frac{m\delta}{(m+1)(m+2)} - \frac{\lambda(\delta-\delta_t)^2}{2\delta}. \quad (7)$$

Taking into account that

$$\frac{\delta}{\delta_t} = x,$$

after transformations we get

$$\delta_{t\varphi}^{**} = \frac{m\delta}{(m+1)(m+2)} - \frac{\lambda\left(\delta-\frac{\delta}{x}\right)^2}{2\delta}, \quad (8)$$

or

$$\delta_{t\varphi}^{**} = \frac{m\delta}{(m+1)(m+2)} - \frac{\delta\lambda(x-1)^2}{2x^2} =$$
$$= \delta\left(\frac{m}{(m+1)(m+2)} - \frac{\lambda(x-1)^2}{2x^2}\right). \quad (9)$$

For the heat transfer law in the form of the Stanton criterion, it is necessary to determine the derivative of the temperature boundary layer on the wall of the heat transfer surface. Since the derivative does not exist formally for $m < 1$, we determine it from the accepted two-layer model of turbulence with a laminar sublayer. Given that in the laminar sublayer, the profiles of the dynamic and temperature boundary layers coincide, based on the accepted model

$$\frac{\partial}{\partial y}\left(\frac{T-T_0}{T_\delta-T_0}\right)_{y=0} = \frac{U}{\alpha_\text{л}^2 \nu}\left(\frac{\alpha_\text{л}^2 \nu}{U\delta_t}\right)^{\frac{2}{m+1}}, \quad (10)$$

we express the thickness of the dynamic boundary layer from (9):

$$\delta = \frac{\delta_{t\varphi}^{**}}{\dfrac{m}{(m+1)(m+2)} - \dfrac{\lambda(x-1)^2}{2x^2}}. \quad (11)$$

Then the temperature boundary layer thickness is defined as

$$\delta_t = \frac{\delta_{t\varphi}^{**}}{\dfrac{xm}{(m+1)(m+2)} - \dfrac{\lambda(x-1)^2}{2x}}. \quad (12)$$

Using the equation for the thickness of the energy loss (12) and performing the transformations for the derivative on the wall of the heat exchange surface of the temperature boundary layer distribution profile (10), and also taking into account the heat transfer law, we obtain

$$St = \frac{\lambda}{\rho C_p U}\cdot\frac{U}{\alpha_\text{л}^2 \nu}\left(\frac{\alpha_\text{л}^2 \nu}{U\dfrac{\delta_{t\varphi}^{**}}{\dfrac{xm}{(m+1)(m+2)} - \dfrac{\lambda(x-1)^2}{2x}}}\right)^{\frac{2}{m+1}} \quad (13)$$

or

$$St = \frac{\lambda}{\rho C_p U^{\frac{2}{m+1}}}\cdot\left(\frac{\dfrac{xm}{(m+1)(m+2)} - \dfrac{\lambda(x-1)^2}{2x}}{\alpha_\text{л}^{m-1}\nu^{\frac{m-1}{2}}}\right)^{\frac{2}{m+1}} \times$$
$$\times \frac{1}{\left(\delta_{t\varphi}^{**}\right)^{\frac{2}{m+1}}}. \quad (14)$$

Considering the distribution profile turbulization degree of the thermal and dynamic boundary layers at $m = 7$, we write

$$\text{St} = \frac{\lambda}{\rho C_p U^{0,25} \alpha_{\text{л}}^{1,5} \nu^{0,75}} \cdot \frac{1}{(\delta_{t\varphi}^{**})^{0,25}} \times$$

$$\times \left(\frac{7}{72} x - \frac{\lambda(x-1)^2}{2x} \right)^{0,25}. \quad (15)$$

For the practical implementation of the heat transfer law, it is necessary to determine the value of $\alpha_{\text{л}}$. It is found from the condition that the laminar sublayer closes with the turbulent profile [25] at $y = \delta_{\text{л}}$ and profile degree at 7:

$$\alpha_{\text{л}} = {}^{1,5}\!\!\sqrt{\frac{\left(\dfrac{xm}{(m+1)(m+2)} \right)^{0,25} \times}{\left(\left(\dfrac{xm}{(m+1)(m+2)} - \dfrac{\lambda(x-1)^2}{2x} \right) \dfrac{(m+1)}{(m+3)} \right)^{\frac{2}{m+1}} 0,012\,56}} \times \left(\left(\dfrac{xm}{(m+1)(m+2)} - \dfrac{\lambda(x-1)^2}{2x} \right) x \dfrac{(m+1)}{(m+3)} \right)^{\frac{2}{m+1}}}.$$

Now we finally get the equation for determining the laminar sublayer coefficient of the turbulent temperature boundary layer distribution profile for the admitted model:

$$\alpha_{\text{л}} = 12{,}5496 \, \text{Pr}^{\frac{1}{18}}.$$

We write the integral relation of the energy equation of the boundary layers taking into account the heat transfer law (14):

$$\frac{1}{H_\varphi} \cdot \frac{\partial}{\partial \varphi}\left(\delta_{t\varphi}^{**} \right) + \frac{1}{H_\psi} \cdot \frac{\partial}{\partial \psi}\left(\delta_{t\psi}^{**} \right) +$$

$$+ \frac{1}{H_\varphi H_\psi} \cdot \frac{\partial H_\psi}{\partial \varphi} \delta_{t\varphi}^{**} + \frac{1}{H_\varphi H_\psi} \cdot \frac{\partial H_\varphi}{\partial \psi} \delta_{t\psi}^{**} =$$

$$= \frac{\lambda}{\rho C_p U^{\frac{2}{m+1}}} \left(\frac{\dfrac{xm}{(m+1)(m+2)} - \dfrac{\lambda(x-1)^2}{2x}}{\alpha_{\text{л}}^{m-1} \nu^{\frac{m-1}{2}}} \right)^{\frac{2}{m+1}} \times$$

$$\times \frac{1}{\left(\delta_t^{**} \right)^{\frac{2}{m+1}}} - \frac{\tau_{\varphi_0}\left(1 + \varepsilon^2 \right)}{\rho C_p \left(T_\delta - T_0 \right)}. \quad (16)$$

Assuming relative characteristic thickness

$$J = \frac{1}{\varepsilon} \cdot \frac{\delta_{t\psi}^{**}}{\delta_{t\varphi}^{**}}, \quad (17)$$

we write

$$\frac{1}{H_\varphi} \cdot \frac{\partial}{\partial \varphi}\left(\delta_{t\varphi}^{**} \right) + \frac{J}{H_\psi} \cdot \frac{\partial}{\partial \psi}\left(\varepsilon \delta_{t\varphi}^{**} \right) +$$

$$+ \frac{1}{H_\varphi H_\psi} \cdot \frac{\partial H_\psi}{\partial \varphi} \delta_{t\varphi}^{**} + \frac{J}{H_\varphi H_\psi} \cdot \frac{\partial H_\varphi}{\partial \psi} \delta_{t\varphi}^{**} =$$

$$= \frac{\lambda}{\rho C_p U^{\frac{2}{m+1}}} \left(\frac{\dfrac{xm}{(m+1)(m+2)} - \dfrac{\lambda(x-1)^2}{2x}}{\alpha_{\text{л}}^{m-1} \nu^{\frac{m-1}{2}}} \right)^{\frac{2}{m+1}} \times$$

$$\times \frac{1}{\left(\delta_t^{**} \right)^{\frac{2}{m+1}}} - \frac{\tau_{\varphi_0}\left(1 + \varepsilon^2 \right)}{\rho C_p \left(T_\delta - T_0 \right)}. \quad (18)$$

We consider a rectilinear uniform flow under the following boundary conditions: $\dfrac{\partial}{\partial \psi} = 0$, $H_\psi = H_\varphi = 1$, $\dfrac{\partial H_\psi}{\partial \varphi} = \dfrac{\partial H_\varphi}{\partial \psi} = 0$ [26].

Then the integral relation of the energy equation for the rectilinear uniform flow (18) is transformed to the equation

$$\frac{\partial}{\partial \varphi} \delta_{t\varphi}^{**} = \frac{\lambda}{\rho C_p U^{\frac{2}{m+1}}} \left(\frac{\dfrac{xm}{(m+1)(m+2)} - \dfrac{\lambda(x-1)^2}{2x}}{\alpha_{\text{л}}^{m-1} \nu^{\frac{m-1}{2}}} \right)^{\frac{2}{m+1}} \times$$

$$\times \frac{1}{\left(\delta_{t\varphi}^{**} \right)^{\frac{2}{m+1}}} - \frac{\tau_{\varphi_0}\left(1 + \varepsilon^2 \right)}{\rho C_p \left(T_\delta - T_0 \right)}. \quad (19)$$

For a rotational flow realized in the cavities of energy and power-generating units, the stream line is an annular line. Let us write the integral relation of the energy equation (18) in cylindrical coordinates, taking into account that for an axisymmetric flow at $\varepsilon = \text{const}$ the relations are

$$\varphi = \alpha, \ \psi = R, \ H_\varphi = R, \ \frac{\partial H_\varphi}{\partial \psi} = \frac{\partial R}{\partial R} = 1, \ H_\psi = 1, \ \frac{\partial H_\psi}{\partial \varphi} = 0,$$

$$\frac{\partial}{\partial \varphi} = 0 \ [27; 28]:$$

$$J\varepsilon \frac{\partial}{\partial R} \delta_{t\varphi}^{**} + \frac{J\varepsilon}{R} \delta_{t\varphi}^{**} =$$

$$= \frac{\lambda}{\rho C_p U^{\frac{2}{m+1}}} \left(\frac{\dfrac{xm}{(m+1)(m+2)} - \dfrac{\lambda(x-1)^2}{2x}}{\alpha_{\text{л}}^{m-1} \nu^{\frac{m-1}{2}}} \right)^{\frac{2}{m+1}} \times$$

$$\times \frac{1}{\left(\delta_{t\varphi}^{**} \right)^{\frac{2}{m+1}}} - \frac{\tau_{\varphi_0}\left(1 + \varepsilon^2 \right)}{\rho C_p \left(T_\delta - T_0 \right)}. \quad (20)$$

The integral relation of the energy equation (20) is necessary for recording and determining the energy loss thickness of the temperature spatial boundary layer, which is included in the equation for determining the local heat transfer coefficient in the Stanton criterion form.

369

Local heat transfer under various laws of the external flow. For a rectilinear uniform flow, we neglect the dissipative term and obtain the integral relation of the energy equation (19) in the following form:

$$\frac{\partial}{\partial \varphi} \delta_{t\varphi}^{**} = \frac{\lambda}{\rho C_p U^{\frac{2}{m+1}}} \left(\frac{\dfrac{xm}{(m+1)(m+2)} - \dfrac{\lambda(x-1)^2}{2x}}{\alpha_{\text{л}}^{m-1} \nu^{\frac{m-1}{2}}} \right)^{\frac{2}{m+1}} \times$$

$$\times \frac{1}{\left(\delta_{t\varphi}^{**} \right)^{\frac{2}{m+1}}}. \qquad (21)$$

Next, we separate the variables and integrate from zero to the current value of the variables:

$$\int_0^{\delta_{t\varphi}^{**}} \left(\delta_{t\varphi}^{**} \right)^{\frac{2}{m+1}} d\delta_{t\varphi}^{**} =$$

$$= \frac{\lambda}{\rho C_p U^{\frac{2}{m+1}}} \left(\frac{\dfrac{xm}{(m+1)(m+2)} - \dfrac{\lambda(x-1)^2}{2x}}{\alpha_{\text{л}}^{m-1} \mu^{\frac{m-1}{2}}} \right)^{\frac{2}{m+1}} \int_0^{\varphi} d\varphi, \quad (22)$$

$$\delta_{t\varphi}^{**} = \left(\frac{\lambda \varphi}{\rho C_p U^{\frac{2}{m+1}}} \right)^{\frac{m+1}{3+m}} \times$$

$$\times \left(\frac{\dfrac{xm}{(m+1)(m+2)} - \dfrac{\lambda(x-1)^2}{2x}}{\alpha_{\text{л}}^{m-1} \nu^{\frac{m-1}{2}}} \right)^{\frac{2m+2}{(m+1)(m+3)}} \left(\frac{3+m}{m+1} \right)^{\frac{m+1}{3+m}}. \quad (23)$$

Taking into account the heat transfer law equation (14) and the resulting equation for the thickness of the energy loss (23), we write:

$$\mathrm{St} = \frac{\dfrac{\lambda}{\rho C_p U^{\frac{2}{m+1}}} \left(\dfrac{\dfrac{xm}{(m+1)(m+2)} - \dfrac{\lambda(x-1)^2}{2x}}{\alpha_{\text{л}}^{m-1} \nu^{\frac{m-1}{2}}} \right)^{\frac{2}{m+1}}}{\left[\left(\dfrac{\lambda \varphi}{\rho C_p U^{\frac{2}{m+1}}} \right)^{\frac{m+1}{3+m}} \times \left(\dfrac{\dfrac{xm}{(m+1)(m+2)} - \dfrac{\lambda(x-1)^2}{2x}}{\alpha_{\text{л}}^{m-1} \nu^{\frac{m-1}{2}}} \right)^{\frac{2m+2}{(m+1)(m+3)}} \cdot \left(\dfrac{3+m}{m+1} \right)^{\frac{m+1}{3+m}} \right]^{\frac{2}{m+1}}}.$$

$$(24)$$

After transformations and considering equations for the Prandtl criteria $\left(\mathrm{Pr} = \dfrac{\mu C_p}{\lambda} \right)$ and Reynolds $\left(\mathrm{Re} = \dfrac{\rho U \varphi}{\mu} \right)$, we obtain an equation for determining the local heat transfer coefficient in the form of the Stanton criterion of a rectilinear uniform flow with a power-law distribution profile of the velocity and temperature diagrams at Pr < 1:

$$\mathrm{St} = \frac{1}{\mathrm{Pr}^{\frac{m+1}{m+3}}} \left(\frac{\left(\dfrac{xm}{(m+1)(m+2)} - \dfrac{\lambda(x-1)^2}{2x} \right)(m+1)}{\alpha_{\text{л}}^{m-1}(m+3) \mathrm{Re}_U} \right)^{\frac{2}{m+3}}. \quad (25)$$

Then we will consider the rotational flow. Neglecting the dissipative term in the integral relation of the energy equation (20), we obtain

$$J\varepsilon \frac{\partial}{\partial R}\left(\delta_{t\varphi}^{**} \right) + \frac{J\varepsilon}{R} \delta_{t\varphi}^{**} - \frac{\lambda}{\rho C_p U^{\frac{2}{m+1}}} \times$$

$$\times \left(\frac{\dfrac{xm}{(m+1)(m+2)} - \dfrac{\lambda(x-1)^2}{2x}}{\alpha_{\text{л}}^{m-1} \nu^{\frac{m-1}{2}}} \right)^{\frac{2}{m+1}} \cdot \frac{1}{\left(\delta_{t\varphi}^{**} \right)^{\frac{2}{m+1}}} = 0. \quad (26)$$

We take into account that the rotational flow is realized according to the law of a solid body $\left(\dfrac{U}{R} = \omega = \mathrm{const} \right)$ and then equation (26) is transformed to

$$\frac{\partial}{\partial R} \delta_{t\varphi}^{**} + \frac{\delta_{t\varphi}^{**}}{R} - \frac{\lambda}{J\varepsilon \rho C_p \omega^{\frac{2}{m+1}}} \times$$

$$\times \left(\frac{\dfrac{xm}{(m+1)(m+2)} - \dfrac{\lambda(x-1)^2}{2x}}{\alpha_{\text{л}}^{m-1} \nu^{\frac{m-1}{2}}} \right)^{\frac{2}{m+1}} \cdot \frac{1}{R^{\frac{2}{m+1}} \left(\delta_{t\varphi}^{**} \right)^{\frac{2}{m+1}}} = 0. \quad (27)$$

We introduce the intermediate notation:

$$\delta_{t\varphi}^{**} = y,$$

$$B = \frac{\lambda}{J\varepsilon \rho C_p \omega^{\frac{2}{m+1}}} \left(\frac{\dfrac{xm}{(m+1)(m+2)} - \dfrac{\lambda(x-1)^2}{2x}}{\alpha_{\text{л}}^{m-1} \nu^{\frac{m-1}{2}}} \right)^{\frac{2}{m+1}}.$$

Then

$$\frac{dy}{dR} + \frac{y}{R} - \frac{B}{R^{\frac{2}{m+1}} y^{\frac{2}{m+1}}} = 0.$$

This equation is solved by the substitution method, where $y = u\vartheta$:

$$\frac{du}{dR}\vartheta + \frac{d\vartheta}{dR}u + u\frac{\vartheta}{R} = \frac{B}{u^{\frac{2}{m+1}}\vartheta^{\frac{2}{m+1}}R^{\frac{2}{m+1}}},$$

$$u\left(\frac{d\vartheta}{dR} + \frac{\vartheta}{R}\right) + \vartheta\frac{du}{dR} = \frac{B}{u^{\frac{2}{m+1}}\vartheta^{\frac{2}{m+1}}R^{\frac{2}{m+1}}}.$$

The function ϑ must satisfy the condition $\frac{d\vartheta}{dR} + \frac{\vartheta}{R} = 0$, then $\vartheta = \frac{1}{R}$, where

$$u = \sqrt[\frac{m+3}{m+1}]{\frac{BR^2(m+3)}{2(m+1)}},$$

$$y = \delta_{t\varphi}^{**} = \frac{1}{R}\sqrt[\frac{m+3}{m+1}]{\frac{BR^2(m+3)}{2(m+1)}} =$$

$$= \sqrt[\frac{m+3}{m+1}]{\frac{BR^2(m+3)}{2(m+1)}}R^{\left(\frac{m-1}{m+1}\right)}, \qquad (28)$$

$$\delta_{t\varphi}^{**} = \sqrt[\frac{m+3}{m+1}]{\frac{\dfrac{\lambda}{J\varepsilon\rho C_p\omega^{\frac{2}{m+1}}} \times \left(\dfrac{\dfrac{xm}{(m+1)(m+2)} - \dfrac{\lambda(x-1)^2}{2x}}{\alpha_{\text{л}}^{m-1}\nu^{\frac{m-1}{2}}}\right)^{\frac{2}{m+1}}\cdot(m+3)}{2(m+1)}}\cdot R^{\frac{m-1}{m+1}}.$$

With the provision for the heat transfer law equations (14) and the resulting equation for the energy loss thickness (28), we determine the Stanton criterion for rotational flow according to the law of a solid body of the power-law distribution profile of the temperature boundary layer and Pr < 1:

$$\text{St} = \cfrac{\cfrac{\lambda}{J\varepsilon\rho C_p U^{\frac{2}{m+1}}}\left(\cfrac{\cfrac{xm}{(m+1)(m+2)} - \cfrac{\lambda(x-1)^2}{2x}}{\alpha_{\text{л}}^{m-1}\nu^{\frac{m-1}{2}}}\right)^{\frac{2}{m+1}}}{\sqrt[\frac{m+3}{m+1}]{\left[\cfrac{\lambda}{J\varepsilon\rho C_p\omega^{\frac{2}{m+1}}} \times \left(\cfrac{\cfrac{xm}{(m+1)(m+2)} - \cfrac{\lambda(x-1)^2}{2x}}{\alpha_{\text{л}}^{m-1}\nu^{\frac{m-1}{2}}}\right)^{\frac{2}{m+1}}\cfrac{(m+3)}{2(m+1)}R^{\frac{m-1}{m+1}}\right]^{\frac{2}{m+1}}}}.$$

$$(29)$$

After the transformation and considering Prandtl's criteria $\left(\text{Pr} = \frac{\mu C_p}{\lambda}\right)$ and Reynold's $\left(\text{Re} = \frac{\rho U\varphi}{\mu}\right)$, the local heat transfer coefficient in the form of the Stanton criterion for rotational flow according to the law of a solid body for the case Pr < 1 can be defined as:

$$\text{St} = \frac{1}{\text{Pr}^{\frac{m+1}{m+3}}}\left(\frac{2J\varepsilon}{\alpha_{\text{л}}^{m-1}\text{Re}}\frac{(m+1)}{(m+3)}\right)^{\frac{2}{m+3}} \times$$

$$\times \left(\frac{xm}{(m+1)(m+2)} - \frac{\lambda(x-1)^2}{2x}\right)^{\frac{2(m+3)-4}{(m+1)(m+3)}}. \qquad (30)$$

Next, the rotational flow will be considered, which is carried out according to the free vortex law $(UR = C = \text{const})$, in this case, the energy equation integral relation (26) takes the form

$$\frac{d\delta_{t\varphi}^{**}}{dR} + \frac{\delta_{t\varphi}^{**}}{R} - \frac{\lambda}{J\varepsilon\rho C_p C^{\frac{2}{m+1}}} \times$$

$$\times \left(\frac{\dfrac{xm}{(m+1)(m+2)} - \dfrac{\lambda(x-1)^2}{2x}}{\alpha_{\text{л}}^{m-1}\nu^{\frac{m-1}{2}}}\right)^{\frac{2}{m+1}} \cdot \frac{R^{\frac{2}{m+1}}}{\left(\delta_{t\varphi}^{**}\right)^{\frac{2}{m+1}}} = 0. \quad (31)$$

After replacement:

$$\delta_{t\varphi}^{**} = y,$$

$$D = \frac{\lambda}{J\varepsilon\rho C_p C^{\frac{2}{m+1}}}\left(\frac{\dfrac{xm}{(m+1)(m+2)} - \dfrac{\lambda(x-1)^2}{2x}}{\alpha_{\text{л}}^{m-1}\nu^{\frac{m-1}{2}}}\right)^{\frac{2}{m+1}},$$

we solve the equation (31) similarly to the case of rotational flow according to the law of a solid body for Pr < 1 by substitution $y = u\vartheta$, where

$$\vartheta = \frac{1}{R}, \quad u = \frac{D^{\frac{m+1}{m+3}}R^2}{2^{\frac{m+1}{m+3}}}. \qquad (32)$$

Then the energy loss thickness is determined as

$$\delta_{t\varphi}^{**} = \left(\frac{D}{2}\right)^{\frac{m+1}{m+3}}R, \qquad (33)$$

or, after substitution:

$$\delta_{t\varphi}^{**} = \left[\frac{\lambda}{J\varepsilon\rho C_p C^{\frac{2}{m+1}}} \times \left(\frac{\dfrac{xm}{(m+1)(m+2)} - \dfrac{\lambda(x-1)^2}{2x}}{\alpha_{\text{л}}^{m-1}\nu^{\frac{m-1}{2}}}\right)^{\frac{2}{m+1}}\bigg/2\right]^{\frac{m+1}{m+3}}\cdot R. \quad (34)$$

Substituting the equation for determining the energy loss thickness (34) in the equation of the heat transfer law (14), we obtain

$$St = \frac{\dfrac{\lambda}{\rho C_p U^{\frac{2}{m+1}}}\left(\dfrac{\dfrac{xm}{(m+1)(m+2)}-\dfrac{\lambda(x-1)^2}{2x}}{\alpha_{\text{л}}^{m-1}\nu^{\frac{m-1}{2}}}\right)^{\frac{2}{m+1}}}{\left(\left[\dfrac{\lambda}{J\varepsilon C_p C^{\frac{2}{m+1}}}\times\left(\dfrac{\dfrac{xm}{(m+1)(m+2)}-\dfrac{\lambda(x-1)^2}{2x}}{\alpha_{\text{л}}^{m-1}\nu^{\frac{m-1}{2}}}\right)^{\frac{2}{m+1}}/2^{\frac{m+1}{m+3}}\right]^{\frac{m+1}{m+3}}\cdot R\right)^{\frac{2}{m+1}}}.$$

(35)

After transformations and with regard to the Prandtl $\left(Pr = \dfrac{\mu C_p}{\lambda}\right)$ and Reynolds criteria $\left(Re = \dfrac{\rho U \varphi}{\mu}\right)$, we determine the local heat transfer coefficient in the form of the Stanton criterion for rotational flow according to the law of the free vortex for the case Pr < 1:

$$St = \frac{1}{Pr^{\frac{m+1}{m+3}}}\times$$

$$\times\left(\frac{2J\varepsilon}{\alpha_{\text{л}}^{m-1}Re}\left(\frac{xm}{(m+1)(m+2)}-\frac{\lambda(x-1)^2}{2x}\right)\right)^{\frac{2}{m+3}}.$$ (36)

Thus, the equations for the local heat transfer coefficient are determined in the form of the Stanton criterion for various laws of the external flow for the power-law profile of the velocity distribution in the boundary layer for the case Pr < 1.

In fig. 3 shows the influence of the Prandtl criterion on friction and heat transfer according to various studies [29]. In the range of Prandtl number values Pr > 1, the obtained theoretical dependences for dimensionless heat transfer coefficients in the form of Stanton criteria, taking into account the integral relation of the energy equation, are in good agreement with the results of other authors. Cf represents the friction coefficient.

The heat transfer coefficient in the form of the Nusselt criterion is a product of the criteria of Stanton, Reynolds and Prandtl $Nu = St\,Re\,Pr$.

The distribution graph of the dimensionless heat transfer coefficient in the form of the Nusselt criterion for turbulent rotational flow according to the solid body law with the Prandtl criterion Pr = 0.7 is shown in fig. 4. The theoretical dependence determined by the model with a convective component gives the best agreement with the results of experimental studies and does not exceed 3.5 %. Also, the best convergence of the results determined by the model with the convective component is given by the theoretical dependence obtained by the affine-like model and the theoretical dependence obtained by J. M. Owen [30] and do not exceed 1.5 and 2.66 % respectively.

Discrepancy of theoretical data obtained by theoretical dependence using a model with a convective component with a dependence obtained by I. V. Shevchuk [31] accounted for 9.5 %. A discrepancy with the dependence obtained L. A. Dorfman [32] is 16.7 %.
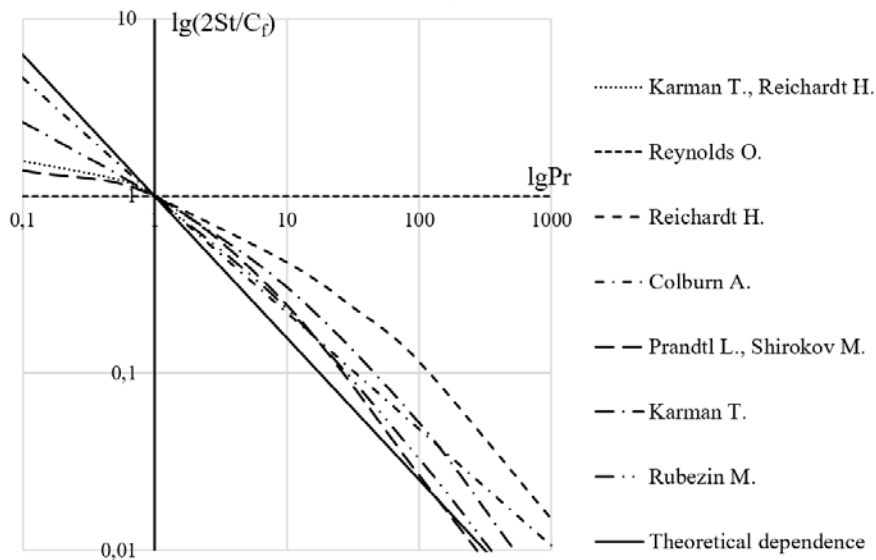
Fig. 3. Comparison of various theories of the analogy between friction and heat transfer in turbulent flows at Re = 10^7

Рис. 3. Сравнение различных теорий аналогии между трением и теплообменом в турбулентных потоках при Re = 10^7
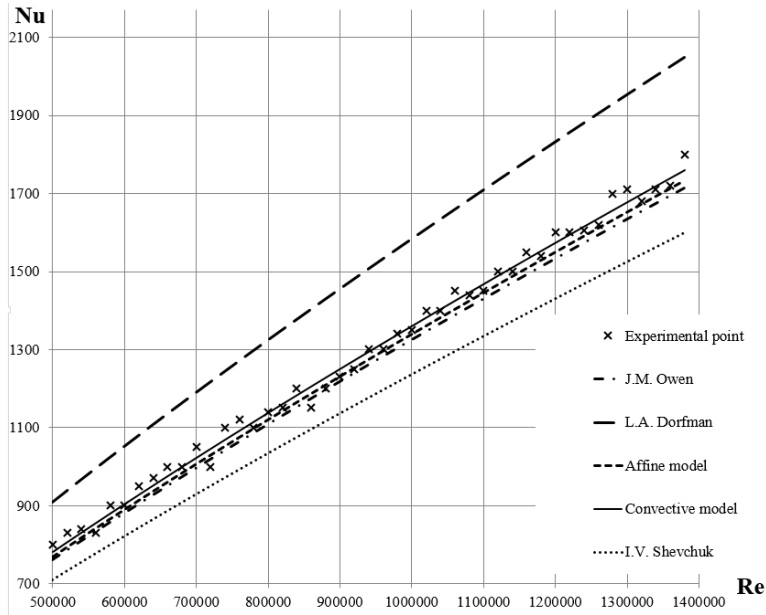
Fig. 4. The dependence of the dimensionless heat transfer coefficient
of turbulent rotational flow according to the law of a solid body at Pr = 0.7

Рис. 4. Зависимость безразмерного коэффициента теплоотдачи турбулентного
вращательного течения по закону твердого тела при Pr = 0,7
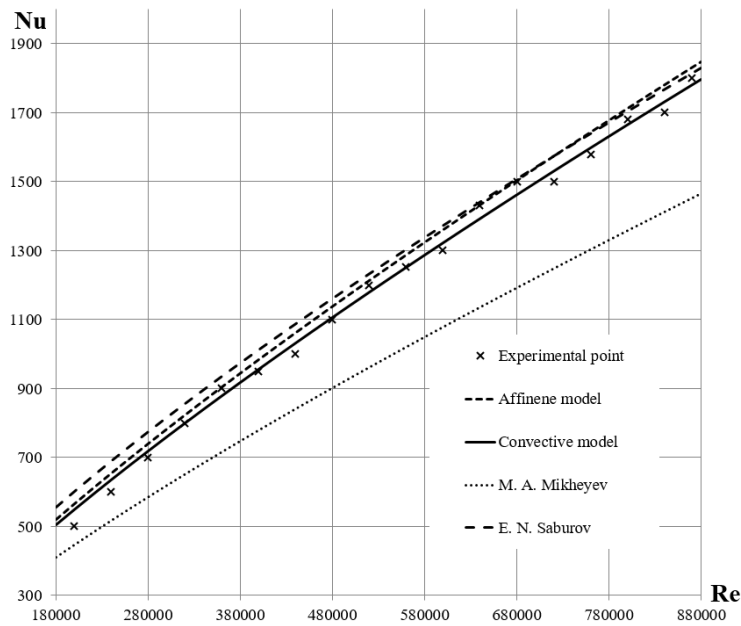
Fig. 5. The dependence of the dimensionless heat transfer coefficient
of a turbulent rotational flow according to the free vortex law at Pr = 0.7

Рис. 5. Зависимость безразмерного коэффициента теплоотдачи турбулентного
вращательного течения по закону свободного вихря при Pr = 0,7

In fig. 5 shows a distribution graph of the dimensionless heat transfer coefficient in the form of the Nusselt criterion for the turbulent potential rotational flow according to the law of the free vortex under the Prandtl criterion Pr = 0.7. The theoretical dependence, which was determined by the model with a convective component, is

in good agreement with the results of experimental studies and does not exceed 5 %.

The discrepancy between the theoretical data obtained from the theoretical dependence using the model with the convective component and the model with affine-like profiles does not exceed 3.5 %. The theoretical depend-

ences obtained from the distribution models of the temperature and dynamic boundary layers with a convective component and with affine-like profiles at Pr = 0.7 give fairly close results, due to the close similarity of the distribution of the temperature and dynamic layers, and are close to the case Pr = 1.

From the fig. 5 graph we can conclude that the obtained theoretical dependences are in the region determined by other authors, but the comparison of the results is not correct, since the theoretical dependences were obtained for other boundary conditions of the potential rotational flow according to the law of the free vortex.

The obtained theoretical dependencies and the dependences of other authors are in the same range and are suitable for engineering calculations and data analysis. It should be noted that the boundary conditions of flow and heat transfer, such as speed, viscosity, density and temperature gradient of the working fluid and heat transfer surface, significantly affect the dimensionless heat transfer coefficient in the form of the Nusselt criterion.

Conclusion. The integral relationship of the energy equation of the spatial boundary layer temperature, allowing integration over the surface of any shape, which is necessary to determine the energy loss thickness, was obtained. The equations for determining the energy loss thickness of the spatial boundary layer temperature are necessary to determine the local heat transfer coefficients for typical flow cases taking into account heat transfer.

The equations for determining the local heat transfer coefficient in the form of the Stanton criterion for a rectilinear uniform flow, a rotational flow according to the law of a solid body, and a free vortex rotational flow of a power-law profile of the dynamic and temperature boundary layer distribution parameters for the case Pr < 1 were obtained analytically.

The analytical equations for the heat transfer coefficients are in good agreement with the experimental data and dependences of other authors.

References

1. Voiskunski J. I., Faddeev, Y. I., Fedyaevsky K. K. *Gidromekhanika* [Hydromechanics]. Leningrad, Sudostroenie Publ., 1982, 456 p.

2. Stoll J., Straub J. Film cooling and heat transfer in nozzles. *J. Turbomach.* 1988, No. 110, P. 57–64.

3. Dellimore K. Modeling and Simulation of Mixing Layer Flows for Rocket Engine Film Cooling (Ph. D. thesis). University of Maryland at College Park, 2010.

4. Jansson L. S., Davidson L., Olsson E. Calculation of steady and unsteady flows in a film-cooling arrangement using a two-layer algebraic stress model. *Numer. Heat. Transf.* 1994, Part A 25, P. 237–258.

5. Cruz C. Experimental and Numerical Characterization of Turbulent Slot Film Cooling (Ph.D. thesis). University of Maryland at College Park, 2008.

6. Cruz C., Marshall A. Surface and gas measurements along a film cooled wall. *J. Thermophys. Heat. Transf.* 2007, No. 21, P. 181–189.

7. Betti B., Martelli E. Heat flux evaluation in oxygen/ methane thrust chambers by RANS approach. *Proceedings of the 46th AIAA/ASME/SAE/ASEE Joint Propulsion Conference, AIAA.* 2010, P. 2010–6721.

8. Ilinkov A. V., Gabdrakhmanov R. R., Takmovtsev V. V., Shchukin A. V. [Effect of centrifugal mass forces on heat transfer during air flow around a concave surface with transverse protrusions]. *Vestnik Moskovskogo aviatsionnogo institute.* 2018, Vol. 25, No. 1, P. 39–48 (In Russ.).

9. Gorelov Yu. G., Strokach E. A. [Analysis of regularities of calculation of the heat transfer coefficient from gas at the inlet edges of the nozzle blades of high-pressure turbines]. *Vestnik Moskovskogo aviatsionnogo institute.* 2016, Vol. 23, No 1, P. 80–85 (In Russ.).

10. Shcherbakov M. A., Vorobyev D. A., Maslakov S. A., Ravikovich Yu. A. [Determination of the heat transfer coefficient on the turbine blade at off-design operating conditions]. *Vestnik Moskovskogo aviatsionnogo institute.* 2013, Vol. 20, No 3, P. 95–103 (In Russ.).

11. Dreytser G. A., Isayev S. A., Lobanov I. E. [Calculation of convective heat transfer in a pipe with periodic projections]. *Vestnik Moskovskogo aviatsionnogo institute.* 2004, Vol. 11, No. 2, P. 28–35 (In Russ.).

12. Knuth E. L. The mechanism of film cooling, (Ph.D. thesis). California Institute of Technology. 1954.

13. Rannie W. D. Heat transfer in turbulent shear flow. *J. Aeronaut. Sci.* 1956, No. 23, P. 485–489.

14. Turcotte D. L. A sublayer theory for fluid injection into the incompressible turbulent boundary layer. *J. Aeronaut. Sci.* 1960, No. 27, P. 675–678.

15. Stechman R. C., Oberstone J., Howell J. C. Design criteria for film cooling for small liquid-propellant rocket engines. *J. Spacecr. Rocket.* 1969, No. 6, P. 97–102.

16. Bartz D. R. A simple equation for rapid estimation of rocket nozzle convective heat transfer coefficients, Jet. Propuls. *ARS J.* 1957, No. 27, P. 49–51.

17. Shine S. R., Kumar S. S., Suresh B. N. A new generalised model for liquid film cooling in rocket combustion chambers. *Int. J. Heat. Mass Transf.* 2012, No. 55, P. 5065–5075.

18. Elhefny A., Liang G. Stress and deformation of rocket gas turbine disc under different loads using finite element modelling. *Propulsion and Power Research.* 2013, Vol. 2, Iss. 1, P. 38–49.

19. Grigoryev V. A., Zagrebelnyy A. O., Kuznetsov S. P. [On the estimation of the mass of the power plant in the problem of optimization of the working process parameters of the aircraft turboprop engine]. *Vestnik Moskovskogo aviatsionnogo institute.* 2015. Vol. 22, No 3. P. 103–106 (In Russ.).

20. Kishkin A. A., Chernenko D. V., Chernenko E. V. [The equation of impulses of a three-dimensional boundary layer]. *Izv. vuzov. Tekhnicheskiye nauki.* 2007, No. 4, P. 35–41 (In Russ.).

21. Romanenko P. N. *Teplomassoobmen i treniye pri gradiyentnom techenii zhidkostey* [Heat and mass transfer and friction at gradient flow of liquids]. Moscow, Energy Publ., 1971, 568 p.

22. Shlikhting G. *Teoriya pogranichnogo sloya* [The theory of the boundary layer]. Moscow, Nauka Publ., 1974, 712 p.

23. Shine S. R., Shri S. Nidhi. Review on film cooling of liquid rocket engines. *Propulsion and Power Research.* 2018, No. 7, Iss. 1, P. 1–18.

24. Keys V. M. *Konvektivnyy teplo- i massoobmen* [Convective heat and mass transfer]. Moscow, Energy Publ., 1972, 448 p.

25. Kishkin A. A., Zuev A. A., Leonov V. P. [Local heat transfer in the boundary conditions of turbomachines]. *Izv. vuzov. Mashinostroyeniye.* 2015, No (658), P. 3–10 (In Russ.).

26. Tolstopyatov M. I., Zuev A. A., Kishkin A. A., Zhuikov D. A., Nazarov V. P. [Straight-line uniform flow of gases with heat transfer in power plants of aircraft]. *Vestnik SibGAU.* 2012, No. 4(44), P. 134–139 (In Russ.).

27. Kishkin A. A., Zhuykov D. A., Tolstopyatov M. I. [Flow with heat transfer in the cavities of rotation of power plants of space and aircraft]. *Vestnik SibGAU.* 2011, No. 7(40), P. 63–68 (In Russ.).

28. Kishkin A. A., Zuev A. A., Chernenko E. V., Smirnov P. N. [The rotation of the liquid over a fixed base according to the law of a solid]. *Izv. vuzov. Tekhnicheskiye nauki.* 2011, No. 1, P. 126–131 (In Russ.).

29. Chapman D. R. Kester R. H. Measurements of turbulent skin friction on cylinders in axial flow at subsonic and supersonic velocities. *JAS.* 1953, Vol. 20, P. 441–448.

30. Owen J. M., Rogers R. H. Flow and heat transfer in rotating disc systems. Rotor-stator systems. Taunton: Research Studies Press, 1989, 302 p.

31. Shevchuk I. V. Convective Heat and Mass Transfer in Rotating Disk Systems. Springer, 2009, 235 p.

32. Dorfman L. A. *Gidrodinamicheskoye soprotivleniye i teplootdacha vrashchayushchikhsya tel* [Hydrodynamic resistance and heat transfer of rotating bodies]. Moscow, Fizmatgiz Publ., 1960, 260 p.

Библиографические ссылки

1. Войткунский Я. И., Фаддеев Ю. И., Федяевский К. К. Гидромеханика. Л. : Судостроение, 1982. 456 с.

2. Stoll J., Straub J. Film cooling and heat transfer in nozzles // J. Turbomach. 1988. No. 110. P. 57–64.

3. Dellimore K. Modeling and Simulation of Mixing Layer Flows for Rocket Engine Film Cooling (Ph. D. thesis). University of Maryland at College Park, 2010.

4. Jansson L. S., Davidson L., Olsson E. Calculation of steady and unsteady flows in a film-cooling arrangement using a two-layer algebraic stress model // Numer. Heat. Transf. 1994. Part A 25. P. 237–258.

5. Cruz C. Experimental and Numerical Characterization of Turbulent Slot Film Cooling (Ph.D. thesis). University of Maryland at College Park, 2008.

6. Cruz C., Marshall A. Surface and gas measurements along a film cooled wall // J. Thermophys. Heat. Transf. 2007. No. 21. P. 181–189.

7. Betti B., Martelli E. Heat flux evaluation in oxygen/ methane thrust chambers by RANS approach // Proceedings of the 46th AIAA/ASME/SAE/ASEE Joint Propulsion Conference, AIAA. 2010. P. 2010–6721.

8. Влияние центробежных массовых сил на теплоотдачу при обтекании потоком воздуха вогнутой поверхности с поперечными выступами / А. В. Ильинков, Р. Р. Габдрахманов, В. В. Такмовцев, А. В. Щукин // Вестник Московского авиационного ин-та. 2018. Т. 25, № 1. С. 39–48.

9. Горелов Ю. Г., Строкач Е. А. Анализ закономерностей расчета коэффициента теплоотдачи от газа на входных кромках сопловых лопаток турбин высокого давления // Вестник Московского авиационного ин-та. 2016. Т. 23, № 1. С. 80–85.

10. Щербаков М. А., Воробьев Д. А., Маслаков С. А., Равикович Ю. А. Определение коэффициента теплоотдачи на пере лопатки турбины на нерасчётных режимах работы // Вестник Московского авиационного ин-та. 2013. Т. 20, № 3. С. 95–103.

11. Дрейцер Г. А., Исаев С. А., Лобанов И. Е. Расчет конвективного теплообмена в трубе с периодическими выступами // Вестник Московского авиационного ин-та. 2004. Т. 11, № 2. С. 28–35.

12. Knuth E. L. The mechanism of film cooling, (Ph.D. thesis). California Institute of Technology. 1954.

13. Rannie W. D. Heat transfer in turbulent shear flow // J. Aeronaut. Sci. 1956. No. 23. P. 485–489.

14. Turcotte D. L. A sublayer theory for fluid injection into the incompressible turbulent boundary layer // J. Aeronaut. Sci. 1960. No. 27. P. 675–678.

15. Stechman R. C., Oberstone J., Howell J. C. Design criteria for film cooling for small liquid-propellant rocket engines // J. Spacecr. Rocket. 1969. No. 6. P. 97–102.

16. Bartz D. R. A simple equation for rapid estimation of rocket nozzle convective heat transfer coefficients, Jet. Propuls // ARS J. 1957. No. 27. P. 49–51.

17. Shine S. R., Kumar S. S., Suresh B. N. A new generalised model for liquid film cooling in rocket combustion chambers // Int. J. Heat. Mass Transf. 2012. No. 55. P. 5065–5075.

18. Elhefny A., Liang G. Stress and deformation of rocket gas turbine disc under different loads using finite element modelling // Propulsion and Power Research. 2013. Vol. 2, Iss. 1. P. 38–49.

19. Григорьев В. А., Загребельный А. О., Кузнецов С. П. К вопросу оценки массы силовой установки в задаче оптимизации параметров рабочего процесса авиационного турбовинтового двигателя // Вестник Московского авиационного ин-та. 2015. Т. 22, № 3. С. 103–106.

20. Кишкин А. А., Черненко Д. В., Черненко Е. В. Уравнение импульсов трехмерного пограничного слоя // Изв. вузов. Северо-Кавказский регион. Техн. науки. 2007. № 4. С. 35–41.

21. Романенко П. Н. Тепломассообмен и трение при градиентном течении жидкостей. М. : Энергия, 1971. 568 с.

22. Шлихтинг Г. Теория пограничного слоя М. : Наука, 1974. 712 с.

23. Shine S. R., Shri S. Nidhi. Review on film cooling of liquid rocket engines // Propulsion and Power Research. 2018. Vol. 7, Iss. 1. P. 1–18.

24. Кейс В. М. Конвективный тепло- и массообмен : пер. с англ. М. : Энергия, 1972. 448 с.

25. Кишкин А. А., Зуев А. А., Леонов В. П. Локальная теплоотдача в граничных условиях турбомашин // Изв. вузов. Машиностроение. 2015. № 1 (658). С. 3–10.

26. Прямолинейное равномерное течение газов с теплоотдачей в энергетических установках летательных аппаратов / М. И. Толстопятов, А. А. Зуев, А. А. Кишкин и др. // Вестник СибГАУ. 2012. № 4(44). С. 134–139.

27. Течение с теплоотдачей в полостях вращения энергетических установок космических и летательных аппаратов / А. А. Зуев, А. А. Кишкин, Д. А. Жуйков, М. И. Толстопятов // Вестник СибГАУ. 2011. № 7(40). С. 63–68.

28. Вращение жидкости над неподвижным основанием по закону твердого тела / А. А. Кишкин, А. А. Зуев, Е. В. Черненко, П. Н. Смирнов // Изв. вузов. Северо-Кавказский регион. Техн. науки. 2011. № 1. С. 126–131.

29. Chapman D. R. Kester R. H., Measurements of turbulent skin friction on cylinders in axial flow at subsonic and supersonic velocities // JAS. 1953. Vol. 20. P. 441–448.

30. Owen J. M., Rogers R. H. Flow and heat transfer in rotating disc systems. Rotor-stator systems. Taunton: Research Studies Press, 1989. 302 p.

31. Shevchuk I. V. Convective Heat and Mass Transfer in Rotating Disk Systems. Springer, 2009. 235 p.

32. Дорфман Л. А. Гидродинамическое сопротивление и теплоотдача вращающихся тел. М. : Физматгиз, 1960. 260с.

Zuev Alexander Alexandrovich – Ph. D., associate Professor, Department of Aircraft Engines; Reshetnev Siberian State University of Science and Technologies. E-mail: dla2011@inbox.ru.

Arngold Anna Anatolievna – Department of Special Connectors and Instruments, Krasnoyarsk Machine-Building Plant. E-mail: arngoldanna@mail.ru.

Khodenkova Elga Vladimirovna – senior teacher, Technical English Department; Reshetnev Siberian State University of Science and Technologies. E-mail: zamyatinaev@sibsau.ru.

Зуев Александр Александрович – кандидат технических наук, доцент, доцент кафедры двигателей летательных аппаратов; Сибирский государственный университет науки и технологий имени академика М. Ф. Решетнева. E-mail: dla2011@inbox.ru.

Арнгольд Анна Анатольевна – начальник бюро спецсоединителей, приборов и пультов аппаратуры; АО «Красноярский машиностроительный завод». E-mail: arngoldanna@mail.ru.

Ходенкова Эльга Владимировна – старший преподаватель кафедры технического иностранного языка; Сибирский государственный университет науки и технологий имени академика М. Ф. Решетнева. E-mail: dla2011@inbox.ru.

FLOW DYNAMICS IN THE RADIAL-ANNULAR CAVITY OF TURBOMACHINES

A. A. Kishkin*, Yu. N. Shevchenko

Reshetnev Siberian State University of Science and Technology
31, Krasnoyarskii rabochii prospekt, Krasnoyarsk, 660037, Russian Federation
*E-mail:spsp99@mail.ru

This paper considers the problem of modeling a rotational flow in the radial-annular cavity of turbo machines with fixed walls. This case corresponds to the boundary conditions of the supply channel for a radial centripetal turbine. In the presented model, the flow is conventionally divided into radial and circumferential movement. The radial component of the velocity is determined by the mass flow rate from the continuity equation, the circumferential component is formed by the tangential channel supply. The main equation in the integration is the equation of the change in the momentum for the flow in the form of the Euler equation. In the case of the circumferential component of the velocity, the angular momentum law is used, assuming the potentiality of the flow and the constancy of the angular momentum within the integration step. As a result of the transformations of the motion equations, differential equations for the radial, circumferential component of velocity and static pressure are obtained, which represent a certain system of three equations in three unknowns. The system of equations allows integration under known boundary conditions at the inlet; as a result of integration, it is possible to obtain the field of distributions of velocities and pressures along the radius of the radial-annular cavity. The results of the study can be used in modeling the circumferential and radial forces on the rotor (impeller) of turbo machines.

Keywords: radial-annular cavity, turbo machine, flow dynamics, continuity equations, Euler equations, boundary conditions, impeller.

ДИНАМИКА ПОТОКА В РАДИАЛЬНО-КОЛЬЦЕВОЙ ПОЛОСТИ ТУРБОМАШИН

А. А. Кишкин*, Ю. Н. Шевченко

Сибирский государственный университет науки и технологий имени академика М. Ф. Решетнева
Российская Федерация, 660037, г. Красноярск, просп. им. газ. «Красноярский рабочий», 31
*E-mail: spsp99@mail.ru

В работе рассмотрена задача моделирования вращательного течения в радиально-кольцевой полости турбомашин с неподвижными стенками. Данный расчетный случай соответствует граничным условиям подводящего канала для радиальной центростремительной турбины. В представленной модели поток условно разделен на радиальное и окружное движение. Радиальная составляющая скорости определяется массовым расходом из уравнения неразрывности, окружная составляющая формируется тангенциальным канальным подводом. Основным уравнением при интегрировании является уравнение изменения количества движения для потока в форме уравнения Эйлера. В случае окружной составляющей скорости используется закон изменения момента количества движения при допущении потенциальности потока и постоянства момента количества движения в пределах шага интегрирования. В результате преобразований уравнений количества движения получены дифференциальные уравнения для радиальной и окружной составляющих скорости, а также для статического давления, представляющие определенную систему трех уравнений с тремя неизвестными. Система уравнений позволяет вести интегрирование при известных граничных условиях на входе, в результате интегрирования возможно получить поле распределений скоростей и давлений по радиусу радиально-кольцевой полости. Результаты исследования могут быть использованы при моделировании окружных и радиальных усилий на ротор (рабочее колесо) турбомашин.

Ключевые слова: радиально-кольцевая полость, турбомашина, динамика потока, уравнения неразрывности, уравнения Эйлера, граничные условия, рабочее колесо.

Introduction. Turbo machines of various types (pumps, compressors, turbines, expansion engines) are currently being used everywhere. While designing and constructing turbo machines, specialists often have to deal with the issue how to model the movement of liquid flow or gas flow in working cavities properly in order to assess the distribution fields of velocity and pressure, friction stresses, coefficients of losses and the overall energy efficiency of a turbo machine [1–4]. The problem of modeling is complicated by the fact that the flow has a complex spatial nature [5–6], for which it makes sense to decompose the main system of equations into two projections – radial and circumferential ones. The final form of the system of equations of motion depends on the design of the cavity of a turbo machine [7].

Herewith, we consider the problem of modeling a rotational flow in a radial-annular cavity of a turbo machine with fixed walls, which corresponds to the boundary conditions of the supply channel for a radial centripetal turbine. The approach presented in this work can be used to calculate the turbines of other types.

Research task description. The main task of the work is to obtain a system of equations that properly describe the fields of pressure and velocity distribution at the inlet into the impeller for the design case of flow in the supply device of a radial centripetal turbine. It is necessary to consider the following characteristic aspects [8–11]:

– the correct formation (without losses) of the velocity and pressure fields in front of the impeller mainly determines the value of the circumferential power of a turbine, and, as a consequence, the overall efficiency of a turbine.

– the partiality, nonuniformity of the velocity and pressure fields in this area determine the value of axial load on the turbine rotor, which reduces the resource of rolling units [12].

To solve the problem, it is necessary to transform the equations of motion together with the continuity equation in order to obtain expressions for numerical integration for the flow rate and circumferential velocity components, as well as static pressure, taking the mass velocity into consideration as an initial parameter.

Basic assumptions and design flow diagram. The radial-annular cavities of turbo machines with multidirectional flows relative to the radius R can form a confusor or diffuser flow. This flow is asymmetric, therefore, the solution is considered in cylindrical coordinates with the condition $\partial/\partial x = 0$.

There are two possible cases of flow: purely radial $C = V_R$ and radial-circumferential $C = (V_R^2 + U^2)^{0,5}$. In both cases, we use the momentum conservation equation for the mass fluid flow for the analysis. The design diagram of the radial-annular cavity is shown in figure.

The flow area in the radial direction F_R is defined as follows:

$$F_R = 2\pi R \cdot n_{oz}, \qquad (1)$$

where R is the radius of the cavity, n_{0z} is the axial clearance in the direction of the z coordinate.

The incrementation of the flow area in the radial direction:

$$dF_z = 2\pi R \cdot dR. \qquad (2)$$

The equations (1) and (2) determine the geometric parameters of the flow area at the integration step, which make it possible to find the radial velocity at a known mass flow rate of the actuation fluid.
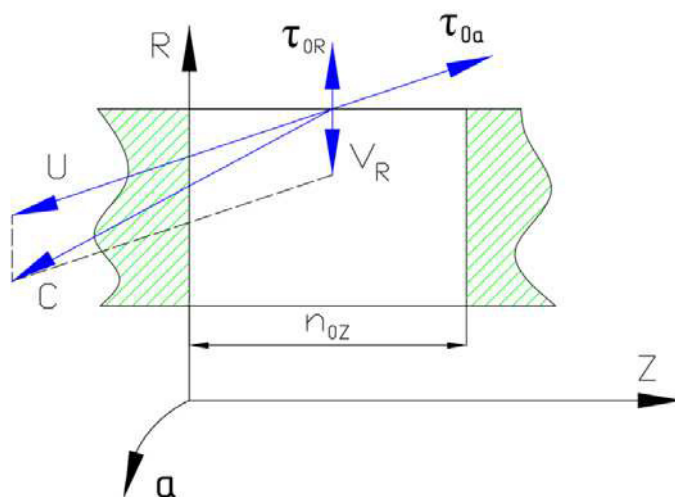
Design diagram of a radial-annular cavity:
R, Z, a – coordinates; *C, U, V_R* – velocity components; *τ_{0R}, τ_{0a}* – friction stresses in the radial and circumferential direction; *n_{0z}* – normal gap clearance

Расчетная схема радиально-кольцевой полости:
R, Z, a – координаты; *C, U, V_R* – компоненты скорости; *τ_{0R}, τ_{0a}* – напряжения трения в радиальном и окружном направлении;
n_{0z} – нормальный зазор

Mathematical model of the flow. The incrementation in the change in the momentum for the flow in differential form is determined by the equation:

$$\dot{m}\frac{dV_R}{dR}\cdot dR = \frac{d\left(p\cdot F_R\right)}{dR}\cdot dR + 2dF_z\tau_{oR}, \qquad (3)$$

where $\dot{m}$ is a mass flow; V_R is a radial velocity component; τ_{0R} is the circumferential component of the friction stress on the wall, p is a pressure quantity.

Taking (1) into consideration, the equation for the radial velocity component has the following form:

$$V_R = \frac{\dot{m}}{p\cdot F_R} = \frac{\dot{m}}{p\cdot 2\pi R n_{oz}}. \qquad (4)$$

We change the equation (3) taking (2) into consideration:

$$\dot{m}\frac{dV_R}{dR} = F_R\frac{dp}{dR} + p\frac{dF_R}{dR} + \tau_{oR}\cdot 4\pi RdR. \qquad (5)$$

We determine the derivative of the radial velocity component using the equation (4):

$$\frac{dV_R}{dR} = \frac{d}{dR}\left(\frac{\dot{m}}{p\cdot 2\pi R n_{oz}}\right) = \frac{-\dot{m}}{p\cdot 2\pi R^2 n_{oz}},$$

$$\frac{dV_R}{dR} = \frac{V_R}{R}. \qquad (6)$$

The derivative of the flow area F_R, considering (1), is determined by the following equation:

$$\frac{dF_R}{dR} = \frac{d}{dR}\left(2\pi\cdot R n_{oz}\right) = 2\pi n_{oz}. \qquad (7)$$

Taking (6) and (7) into consideration, we rewrite the equation (5) in the form:

$$\frac{-\dot{m}V_R}{R} = F_R\frac{dp}{dR} + 2\pi n_{oz}\cdot p + \tau_{oR}\cdot 4\pi R.$$

Let us distinguish the derivative dp/dR in the equation:

$$\frac{dp}{dR} = \frac{-\dot{m}}{F_R R} - \frac{2\pi n_{oz}}{F_R}\cdot p - \frac{4\pi R}{F_R}\cdot \tau_{0R}. \qquad (8)$$

Taking (1) and (4) into consideration we obtain:

$$\frac{dp}{dR} = -\frac{pV_R^2}{R} - \frac{p}{R} - \frac{2\tau_0 R}{n_{oz}}\cdot \tau_{oR}, \qquad (9)$$

or finally:

$$\frac{dp}{dR} = \frac{-\dot{m}^2}{p\cdot 4\pi^2\cdot n_{oz}^2\cdot R^3} - \frac{p}{R} - \frac{2\tau_{0R}}{n_{oz}}, \qquad (10)$$

It will be recalled that that when flowing to the center of coordinates ($-V_R$), the flow is confusor and vice versa.

For the radial flow, the system of equations (4) and (9) is sufficient, with V_R = const. For the radial flow with a circumferential component, the formula for the peripheral velocity U is required. For the potential flow $rot\ U = 0$, the following formula is satisfied:

$$U\cdot R = C_u = \text{const.} \qquad (11)$$

The formula (11) completely determines the function $U = f(R)$, however, when integrating over the radius, it is necessary to take into consideration the influence of the circumferential component of the friction stress on the wall τ_{0a}; this friction stress reduces the values of C_U for any direction of the radial velocity V_R [13].

Next we find the formula for the circumferential component of the velocity of the radial-circumferential flow. We use the law of changing the angular momentum [14–15]:

$$\dot{m}\frac{d(U\cdot R)}{dR}\cdot dR = dF_{mp}\cdot R, \qquad (12)$$

where dF_{fr} is the friction force on the elementary volume $2\pi n_{0z}\cdot dR$.

Friction force on two surfaces (see fig.):

$$dF_{mp} = 4\cdot\tau_{oa}\cdot\pi R\cdot dR, \qquad (13)$$

We take the derivative of the equation (12) and take into consideration (13):

$$\frac{dU}{dR} = -\frac{U}{R} + \frac{4\pi\tau_{oa}R}{\dot{m}},$$

$$\dot{m}\left(R\frac{dU}{dR} + U\right) = 4R\cdot\tau_{oa}\cdot 4\pi R.$$

We express the derivative:

$$\frac{dU}{dR} = -\frac{U}{R} + \frac{4\pi\tau_{oa}R}{\dot{m}}. \qquad (14)$$

Or taking $U = \omega R$ into consideration we obtain the equation:

$$\frac{d\omega}{dR} = -\frac{2\omega}{R} + \frac{4\pi\tau_{oa}}{\dot{m}}. \qquad (15)$$

Taking (11) into consideration, we finally obtain:

$$\frac{dC_u}{dR} = \frac{4\pi R^2\tau_{oa}}{\dot{m}} = \frac{2R\tau_{oa}}{n_{oz}\cdot p\cdot V_R}. \qquad (16)$$

The equations (14), (15), (16) can be integrated autonomously without knowing the change in the pressure field p.

Next, we find the formula for the static pressure for the radial-circumferential flow. We use the equation for changing the momentum for absolute speed (see fig.):

$$C = \sqrt{V_R^2 + U^2}, \qquad (17)$$

Where V_R and U are determined by the equations (4) and (11).

After transformations we obtain:

$$\dot{m}\frac{dC}{dR}\cdot dR = \frac{d\left(p\cdot F_R\right)}{dR}\cdot dR + 2\tau_{oR}\cdot dF_z, \qquad (18)$$

where $dF_z = 4\pi RdR$ is the double lateral surface of the elementary volume $dV = 2\pi R n_{0z}\cdot dR$, $F_R = 2\pi R n_{0z}$ is the flow area.

We define the derivatives of the velocities. The derivative dV_R/dR, according to the equation (6):

$$\frac{dV_R}{dR} = -\frac{V_R}{R}. \qquad (19)$$

Considering the equation (11), the derivative of the circumferential component on the elementary volume $dV = 2\pi R n_{0z} \cdot dR$ can be defined as follows:

$$\frac{dU}{dR} = -\frac{C_u}{R^2}. \qquad (20)$$

The derivative dC/dR according to the equation (17) is defined as:

$$\frac{dC}{dR} = \frac{d}{dR}\left(V_R^2 + U^2\right)^{0.5} = \frac{1}{2}\left(V_R^2 + U^2\right)^{-0.5} \cdot \frac{d}{dR}\left(V_R^2 + U^2\right)^{0.5} =$$

$$= \frac{1}{2}\left(V_R^2 + U^2\right)^{-0.5} \cdot \left(2V_R\frac{dV_R}{dR} + 2U\frac{dU}{dR}\right).$$

We take into consideration the equations (19) and (20) and continue the transformation:

$$\frac{dC}{dR} = \frac{1}{2}\left(V_R^2 + U^2\right)^{-0.5} \cdot \left(-2V_R\frac{dV_R}{dR} - 2U\frac{dU}{dR}\right),$$

$$\frac{dC}{dR} = -\frac{1}{R}\sqrt{\left(V_R^2 + U^2\right)} = -\frac{C}{R}. \qquad (21)$$

Considering (21) we transform the equation (18) into the following form:

$$-\frac{C\dot{m}}{R} = -F_R\frac{dp}{dR} + p\frac{dF_R}{dR} + 2\tau_{oR} \cdot dF_z. \qquad (22)$$

After substitution of the equations (1) and (2) we obtain, respectively:

$$\frac{dF_R}{dR} = 2\pi n_{oz}; \qquad 2dF_z = 4\pi R dR; \qquad F_R = 2\pi R n_{oz};$$

Thereupon:

$$\frac{-\dot{m}C}{R}dR = \left(F_R\frac{dp}{dR} + p\frac{F_R}{R}\right)dR + 4\tau_{oR} \cdot \pi \cdot R \cdot dR.$$

We simplify the last equation by dR, as a result we obtain:

$$\frac{-\dot{m}C}{R} = F_R\frac{dp}{dR} + p\frac{F_R}{R} + 4 \cdot \pi \cdot R \cdot \tau_{oR}. \qquad (23)$$

We express the pressure derivative:

$$-\frac{dp}{dR} = -\frac{\dot{m}}{RF_R} - p\frac{1}{R} + \frac{4 \cdot \pi \cdot R \cdot \tau_{oR}}{F_R}. \qquad (24)$$

Considering $V_R = \dot{m}/\rho F_R$, we obtain:

$$\frac{dp}{dR} = -\frac{\dot{m} \cdot C}{2\pi R^2 n_{oz}} - \frac{p}{R} - \frac{2 \cdot \tau_{0R}}{n_{oz}}. \qquad (25)$$

The equation (25) combined with the equations (4) and (17) form a closed system of equations for determining the velocity and pressure fields in the radial-annular cavity of turbo machines.

Conclusion. The mathematical model obtained in this work can be used at complex modeling of radial centripetal turbo machines for calculating the flow dynamics in inlet and outlet devices. The model determines the fields of velocity and pressure at the inlet and outlet of the rotor, which is a condition that forms the vector of radial and axial forces that determine the dynamics of the rotor, the load on the rolling units, and, as a consequence, the re-

source of a turbo machine in general. The approach presented in this work can be used to calculate the turbines of other types.

References

1. Bader P., Pschernig M., Sanz W. et al. Experimental investigation of boundary layer relaminarization in accelerated flow. *Journal of Fluids Engineering, Transactions of the ASME.* 2018, Vol. 140, Iss. 8, P. 081201.

2. Ju G., Li J., Li K. A novel variational method for 3D viscous flow in flow channel of turbomachines based on differential geometry. *Applicable Analysis.* 2020, Vol. 99, Iss. 13, P. 2322–2338.

3. Takizawa K., Tezduyar T. E., Hattori H. Computational analysis of flow-driven string dynamics in turbomachinery. *Computers and Fluids.* 2017, Vol. 142, P. 109–117.

4. Morgese G., Fornarelli F., Oresta P. et al. Fast design procedure for turboexpanders in pressure energy recovery applications. *Energies.* 2020. Vol. 13, Issue 14. P. 3669.

5. Agromayor R., Müller B., Nord L.O. One-dimensional annular diffuser model for preliminary turbomachinery design. *International Journal of Turbomachinery, Propulsion and Power.* 2019, Vol. 4, Iss. 3. DOI: 10.3390/ijtpp4030031.

6. Gregory-Smith D. G., Crossland S. C. Prediction of turbomachinery flow physics from CFD: review of recent computations of APPACET test cases. *Task quarterly.* 2001, No. 5 (4), P. 407–432.

7. Potashev A. V., Potasheva E. V. [Design of impellers of turbomachines based on the solution of inverse boundary value problems]. *Uchenyye zapiski Kazanskogo universiteta. Seriya Fiziko-matematicheskiye nauki.* 2015, No. 157 (1), P. 128–140 (In Russ.).

8. Chang H., Zhu F., Jin D., Gui X. Effect of blade sweep on inlet flow in axial compressor cascades. *Chinese Journal of Aeronautics.* 2015, Vol. 28, No. 1, P. 103–111.

9. Xu H., Chang H., Jin D., Gui X. Blade bowing effects on radial equilibrium of inlet flow in axial compressor cascades. *Chinese Journal of Aeronautics.* 2017, No. 30(5), P. 1651–1659.

10. Kudryavtsev I. A., Laskin A. S. [Aerodynamic improvement of the input devices of high-pressure cylinders of powerful steam turbines on the basis of numerical modeling]. *Nauchno-tekhnicheskiye vedomosti SPbPU. Yestestvennyye i inzhenernyye nauki.* 2016, No. 1 (238), P. 7–18 (In Russ.).

11. Krivosheev I. A., Osipov E. V. [Using experimental methods to improve the characteristics of the gas path of turbines of GTE]. *Vestnik Ufimskogo gosudarstvennogo aviatsionnogo tekhnicheskogo universiteta.* 2010, No. 14 (3 (38)), P. 3–15 (In Russ.).

12. Zhuikov D. A., Kishkin A. A., Zuev A. A. [Calculation of axial force during flow in end slots of turbomachines]. *Izvestiya vysshikh uchebnykh zavedeniy. Severo-Kavkazskiy region. Tekhnicheskiye nauki.* 2013, No. 1 (170), P. 24–27 (In Russ.).

13. Smirnov P. N., Kishkin A. A., Zhuikov D. A. [Computational modeling of flow in the cavity of a disk

pump]. *Vestnik SibGAU.* 2011, No. 4 (37), P. 196–201 (In Russ.).

14. Zuev A. A., Nazarov V. P., Arngold A. A. et al. [Disk friction in determining the power balance of turbopump units of liquid-propellant rocket engines]. *Vestnik Permskogo natsional'nogo issledovatel'skogo politekhnicheskogo universiteta. Aerokosmicheskaya tekhnika.* 2019, No. 57, P. 17–31 (In Russ.).

15. Smirnov P. N., Kishkin A. A., Zhuikov D. A. et al. [Moment of resistance of a disk rotating in a stream swirling according to the law of a rigid body]. *Izvestiya vysshikh uchebnykh zavedeniy. Severo-Kavkazskiy region. Tekhnicheskiye nauki.* 2012, No. 2, P. 36–41 (In Russ.).

Библиографические ссылки

1. Experimental investigation of boundary layer relaminarization in accelerated flow / Bader P., Pschernig M., Sanz W. et al. // Journal of Fluids Engineering, Transactions of the ASME. 2018. Vol. 140, Issue 8. P. 081201.

2. Ju G., Li J., Li K. A novel variational method for 3D viscous flow in flow channel of turbomachines based on differential geometry // Applicable Analysis. 2020. Vol. 99, Iss. 13. P. 2322–2338.

3. Takizawa K., Tezduyar T. E., Hattori H. Computational analysis of flow-driven string dynamics in turbomachinery // Computers and Fluids. 2017. Vol. 142. P. 109–117.

4. Fast design procedure for turboexpanders in pressure energy recovery applications / Morgese G., Fornarelli F., Oresta P. et al. // Energies. 2020. Vol. 13, Iss. 14. P. 3669.

5. Agromayor R., Müller B., Nord L.O. One-dimensional annular diffuser model for preliminary turbomachinery design // International Journal of Turbomachinery, Propulsion and Power. 2019. Vol. 4, Iss. 3. DOI: 10.3390/ijtpp4030031.

6. Gregory-Smith D. G., Crossland S. C. Prediction of turbomachinery flow physics from CFD: review of recent computations of APPACET test cases // Task quarterly. 2001. No. 5 (4). P. 407–432.

7. Поташев А. В., Поташева Е. В. Проектирование рабочих колес турбомашин на основе решения обратных краевых задач // Ученые записки Казанского ун-та. Серия: Физ.-мат. науки. 2015. № 157 (1). С. 128–140.

8. Chang H., Zhu F., Jin D., Gui X. Effect of blade sweep on inlet flow in axial compressor cascades // Chinese Journal of Aeronautics. 2015. Vol. 28, No. 1. P. 103–111.

9. Xu H., Chang H., Jin D., Gui X. Blade bowing effects on radial equilibrium of inlet flow in axial compressor cascades // Chinese Journal of Aeronautics. 2017. No. 30(5). P. 1651–1659.

10. Кудрявцев И. А., Ласкин А. С. Аэродинамическое совершенствование входных устройств цилиндров высокого давления мощных паровых турбин на основе численного моделирования // Научно-технические ведомости СПбПУ. Естественные и инженерные науки. 2016. № 1 (238), С. 7–18.

11. Кривошеев И. А., Осипов Е. В. Использование экспериментальных методов совершенствования характеристик газового тракта турбин ГТД // Вестник Уфимского гос. авиационного техн. ун-та. 2010. № 14 (3 (38)). С. 3–15.

12. Жуйков Д. А., Кишкин А. А., Зуев А. А. Расчет осевой силы при течении в торцевых щелях турбомашин // Известия вузов. Северо-Кавказский регион. Техн. науки. 2013. № 1 (170). С. 24–27.

13. Смирнов П. Н., Кишкин А. А., Жуйков Д. А. Расчетное моделирование течения в полости дискового насоса // Вестник СибГАУ. 2011. № 4 (37). С. 196–201.

14. Дисковое трение при определении баланса мощностей турбонасосных агрегатов жидкостных ракетных двигателей / А. А. Зуев, В. П. Назаров, А. А. Арнгольд и др. // Вестник Пермского нац. исследовательского политехн. ун-та. Аэрокосмическая техника. 2019. № 57. С. 17–31.

15. Момент сопротивления диска, вращающегося в потоке, закрученном по закону твердого тела / П. Н. Смирнов, А. А. Кишкин, Д. А. Жуйков и др. // Известия вузов. Северо-Кавказский регион. Техн. науки. 2012. № 2. С. 36–41.

Kishkin Alexander Anatolievich – Dr. Sc., professor, head of the Department of refrigeration, cryogenic engineering and conditioning; Reshetnev Siberian State University of Science and Technology. E-mail: spsp99@mail.ru.

Shevchenko Yulia Nikolaevna – head of the laboratories of the Department of refrigeration, cryogenic engineering and conditioning; Reshetnev Siberian State University of Science and Technology. E-mail: gift_23j@mail.ru.

Кишкин Александр Анатольевич – доктор технических наук, профессор, заведующий кафедрой холодильной, криогенной техники и кондиционирования; Сибирский государственный университет науки и технологий имени академика М. Ф. Решетнева. E-mail: spsp99@mail.ru.

Шевченко Юлия Николаевна – заведующий лабораториями кафедры холодильной, криогенной техники и кондиционирования; Сибирский государственный университет науки и технологий имени академика М. Ф. Решетнева. E-mail: gift_23j@mail.ru.

DEVELOPMENT OF THE HEAT PANEL OF THE SMALL SPACE APPARATUS FOR NAVIGATION SUPPORT

V. V. Kolga*, I. S. Yarkov, E. A. Yarkova

Reshetnev Siberian State University of Science and Technology
31, Krasnoyarskii rabochii prospekt, Krasnoyarsk, 660037, Russian Federation
*E-mail: kolgavv@yandex.ru

To clarify the trajectory of the spacecraft in a given orbit, the parameter of unmodeled acceleration is taken into account. Today, in the design and manufacture of a spacecraft to meet the requirements of the technical specifications for the maximum allowable values of unmodeled accelerations during the operation of on-board equipment, it is necessary to take into account the effects of asymmetric heat fluxes from the panels of the spacecraft on the deviation of its center of mass from a given orbit. This article discusses the problem of the influence of asymmetric heat fluxes from the surfaces of the spacecraft emanating from the panels $\pm Z, + Y$ (deterministic and non-deterministic component) on the level of unmodeled accelerations, which significantly affects the trajectory of the spacecraft.

In order to meet the requirements for the temperature control system in terms of ensuring efficient heat removal from the on-board equipment devices and its distribution over the surface of the instrument installation panel, it is necessary to significantly improve the technical characteristics of heat transfer and heat conduction processes in the spacecraft. The analysis of the current thermal control system in modern satellites is carried out and its shortcomings are revealed. A constructive option is proposed for creating an energy-intensive thermal panel, which allows more efficient heat removal from devices and distribution over the panel. The designed thermal panel is a flat sealed panel of a single complex design of aluminum alloy, made by the additive technology method. The dimensions of the thermal panel are limited by the structural dimensions of the working area of 3D printers. At the moment, the main dimensions reach 600-800 mm. An increase in the working area in the future will enable the installation of large-sized electronic equipment.

A two-dimensional mathematical model for calculating heat transfer processes in the designed thermal panel is presented. For the calculation, specific average values are introduced that characterize the effective cross sections for the vapor channels and the wick in the longitudinal and transverse directions, physical parameters (porosity of the wick and its degree of liquid saturation).

Keywords: spacecraft, asymmetric heat fluxes, thermal control system, unmodeled accelerations, power thermal panel.

РАЗРАБОТКА ТЕПЛОВОЙ ПАНЕЛИ МАЛОГО КОСМИЧЕСКОГО АППАРАТА НАВИГАЦИОННОГО ОБЕСПЕЧЕНИЯ

В. В. Кольга*, И. С. Ярков, Е. А. Яркова

Сибирский государственный университет науки и технологий имени академика М. Ф. Решетнева
Российская Федерация, 660037, г. Красноярск, просп. им. газ. «Красноярский рабочий», 31
*E-mail: kolgavv@yandex.ru

Для уточнения траектории движения космического аппарата по заданной орбите учитывается параметр немоделируемого ускорения. На сегодняшний день при проектировании и изготовлении космического аппарата для обеспечения требований технического задания к предельно допустимым значениям немоделируемых ускорений при работе бортовой аппаратуры, необходим учет воздействия несимметричных тепловых потоков с панелей космического аппарата на отклонение его центра масс от заданной орбиты. В данной статье рассмотрена проблема влияния ассиметричных тепловых потоков с поверхностей космического аппарата, исходящих с панелей $\pm Z, +У$ (детерминированной и недетерминированной составляющей) на величину уровня немоделируемых ускорений, что существенно влияет на траекторию движения космического аппарата.

Для обеспечения требований к системе терморегулирования в части обеспечения эффективного отвода тепла от приборов бортовой аппаратуры и распределения его по поверхности панели установки приборов необходимо значительно улучшить технические характеристики процессов теплопередачи и теплопроводности в космическом аппарате. Проведен анализ действующей системы терморегулирования в современных спутниках и выявлены её недостатки. Предложен конструктивный вариант создания энергоемкой тепловой панели, которая позволяет эффективнее отводить тепло от приборов и распределять его по панели. Спроектированная тепловая панель представляет собой плоскую герметичную панель единой сложной конструкции из алюминиевого сплава, изготовленную методом аддитивных технологий. Размеры тепловой панели ограничены конструктивными размерами рабочей зоны 3D-принтеров. На сегодняшний момент основные размеры доходят до 600–800 мм. Увеличение рабочей площади в дальнейшем даст возможность монтажа крупногабаритной радиоэлектронной аппаратуры.

Представлена двухмерная математическая модель для расчета процессов теплообмена в спроектированной тепловой панели. Для расчета вводятся удельные средние величины, характеризующие эффективные сечения для паровых каналов и фитиля в продольном и поперечном направлениях, физические параметры (пористость фитиля и степень его насыщенности жидкостью).

Ключевые слова: космический аппарат, несимметричные тепловые потоки, система терморегулирования, немоделируемые ускорения, силовая тепловая панель.

Introduction. The development of space technology at the present stage is characterized by the creation of small spacecrafts for various purposes using a denser placement of payload devices, which affects the unevenness and asymmetry of heat fluxes from the panels of the spacecraft.

Placing electrical devices with a high heat flux density on small layout areas requires solving the problem of ensuring the operating temperatures of equipment, structure and spacecraft elements within strictly limited ranges at all operating modes of the thermal control system.

To meet the requirements for ensuring the guaranteed operating temperatures of the instrument seats, it is necessary to increase the efficiency of the thermal control system (TCS) by creating an energy-intensive panel that can remove heat and efficiently distribute it over the spacecraft panel.

Taking into account the influence of asymmetry of heat fluxes from the spacecraft panels in the spacecraft motion model leads to the creation of a more accurate and more reliable computational model of the spacecraft.

To meet the requirements of the technical design specifications for the permissible level of unmodeled accelerations arising during the operation of the spacecraft onboard systems, it is necessary to take into account the effect of asymmetric heat fluxes from instrument panels on the possibility of deviating the spacecraft center of mass from a given orbit.

The accuracy of determining the parameters of the spacecraft trajectory, in addition to the obvious limitation imposed by the composition of the available measurement information, substantially depends on the degree of correspondence of the dynamic model used for the numerical integration of the spacecraft motion equations to the real set of perturbations that form its trajectory.

To date, to refine the forecast of errors in the trajectory of the spacecraft movement along the orbit, such a parameter as unmodeled acceleration is used.

The total effect of unmodeled acceleration on the accuracy of calculations of spacecraft motion is quite significant. And, although the absolute value of unmodeled accelerations does not exceed $10^{-12} \div 10^{-13}$ km/s^2, the resulting perturbations in the spacecraft coordinates can reach significant values [1]. The need to reduce the level of influence of unmodeled acceleration on the spacecraft trajectory requires the development of special measures to minimize this effect.

The problem of reducing the values of unmodeled accelerations arising from the influence of the operation of on-board systems has a high degree of relevance, since, on the one hand, it can serve to refine the already existing trajectories of spacecrafts, and on the other hand, when creating new vehicles, it will make it possible to refine and optimize the computational dynamic model, minimizing energy consumption for adjusting the working orbit (which will lead to a decrease in the total mass of spacecrafts) [2; 3].

Analysis of the current thermoregulation system. To reduce the level of unmodeled accelerations and take them into account in the computational dynamic model, we have developed an a priori model that allows us to clarify the physical processes of thermal radiation of on-board instruments and spacecraft systems, corrected and refined during flight tests. At the same time, it is necessary to take into account the correctness of setting the values of thermal and mechanical loads and the duration of the load cyclogram modes during «normal operation of the spacecraft», as well as the accuracy of the heat release cyclogram of the onboard equipment of the automatic voltage stabilization complex in terms of the absolute values of heat release and the duration of operating modes.

At the present time, the available estimate of the accuracy of the cyclograms of the heat release of the automatic voltage stabilization complex is up to 150 W and the duration of the modes is up to 4 hours.

Cyclograms are necessary to take into account the asymmetry of the spacecraft's own thermal supply, and at the same time should not exceed 10 W (short-term heat emissions) and 5 W (long-term heat emissions).

The processing of data from temperature sensors on board the spacecraft in order to calculate heat fluxes is a complex task from the methodological and computational point of view, the solution of which, taking into account the capacities of the onboard information computer complex, is not possible in space. Thus, the task of processing

measurements of temperature sensors should be solved in the ground control complex.

At present, it is not possible to meet the requirements for minimizing unmodeled accelerations by existing TCS without additional energy costs and changes in the spacecraft dimensions. The implementation of this requirement should be carried out through new layout solutions at the spacecraft level, taking into account the precise determination of the values of heat fluxes and cyclograms of heat release onboard equipment.

To date, in navigation spacecraft they use a thermal control system [4–9], which is a honeycomb panel with a liquid collector built into it. The production of a three-layer honeycomb panel (with various types of honeycomb filler) is carried out using the following technology:

– production of component parts, including honeycomb filler, skins, reinforcing and embedded elements, heat pipes;

– joining (bonding) the surface of the shelves of heat pipes with sheathing using heat-conducting glue;

– connection (bonding) of sheathing with honeycomb core and built-in embedded elements.

The assembly (bonding) of the three-layer honeycomb panel is carried out on the technological equipment (table) through a special gasket. The required pressure is provided using a vacuum bag covered with a layer of thermal insulation.

Bonding is carried out in a thermal oven for the required time at an elevated temperature (about 125 °C), which is increased stepwise to the bonding temperature, thereby providing the required exposure (about 3 hours), and then gradually cooled to ambient temperature. In particular, film glue VK-51 TU1-596-212–85 is used to bond the sheathing with honeycomb core

The analysis showed that in the manufacture of large-sized three-layer honeycomb panels with thin aluminum skins, it is first of all necessary that the technological equipment used be made with a high degree of flatness and surface cleanliness, and that spacers made of aluminum sheet were used to exclude the influence of the difference in the coefficient of thermal linear expansion between equipment and honeycomb panel.

The disadvantage of the said method is the possibility of using this technology for honeycomb panels with dimensions only up to 2000 × 3000 mm. When polymerizing large panels, it is necessary to use composite backing sheets.

Due to an increase in the overall dimensions of honeycomb panels (up to 3000 × 6000 mm), as well as a decrease in the thickness of the skins (down to 0.3 mm) used for modern spacecrafts, and the need to improve the geometric accuracy of the working surface, the use of solid large-sized sheets, on the one hand, is unprofitable, given the high cost of their manufacture and delivery, on the other hand, it does not provide the required accuracy (the overall flatness of the panel is not more than 1.5 mm, the flatness is 0.1 mm at a size of 200 × 200 mm). Such stringent requirements are due to the long period of active existence of the spacecraft (up to 15 years), the trouble-free operation of satellite instruments installed on the

working surface of the honeycomb panel through heat-conducting paste. In this case, the temperature difference between the mounting surface of the device and the casing should be minimal, therefore, the flatness of the panel should be as small as possible.

Thus, a significant disadvantage of the said method is the complexity of manufacturing and insufficiently high quality of honeycomb panels of large dimensions. Engineering approaches aimed at solving this problem lead to the need to reduce the overall dimensions of the honeycomb panel and change its design to ensure more efficient heat removal from the onboard equipment.

The calculated values of the operating temperatures of the equipment based on the results of the thermal analysis of the spacecraft must meet the requirements for the calculated uncertainty, while the calculated uncertainty is taken basing on the devices belonging to the temperature group.

The current TCS does not provide a uniform efficient heat removal from the spacecraft devices, «hot» spots with extremely high power consumption of the devices are created, the equipment overheats.

Asymmetric heat fluxes from the spacecraft surfaces, emanating from the ±Z, +Y panels (deterministic and non-deterministic components), in turn, contribute to the value of the level of unmodeled accelerations from various onboard systems, which significantly affects the spacecraft trajectory.

To solve this problem, we propose to use the heat-conducting panels developed by us, which increase the efficiency of heat removal from radio-electronic equipment on board the spacecraft and have, at the same time, much smaller dimensions. When working with such structures, it is necessary to develop a computational algorithm for assessing the removed heat fluxes under different operating modes of distribution of the heat load on the panel surface. This algorithm is necessary both at the stage of spacecraft development using such structures in the thermal control system and in determining the optimal arrangement of spacecraft instruments and equipment.

This paper presents a two-dimensional mathematical model of heat transfer in a thermal panel. On the basis of the model, an algorithm is described for assessing the performance of the panel by capillary limitation for a given distribution of heat flux density on the surface. The model allows to obtain the temperature field distribution on the panel surface.

Power thermal panel design. The power thermal panel is a flat sealed panel, which is a single complex structure of aluminum alloy, made by the method of additive technologies and consisting of two cross channels with wicks, a porous structure, closed on all sides with a thin layer of aluminum. The dimensions of the thermal panel are limited by the structural dimensions of the working area of 3D printers. At the moment, the main dimensions are up to 600–800 mm. An increase in the working area in comparison with hyper-heat-conducting panels [10], the size of which reaches 100 × 300 mm, makes it possible to install large-sized electronic equipment.
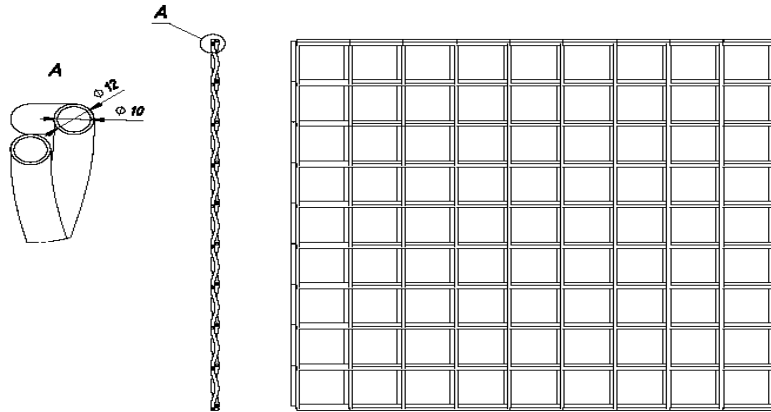
The structure of the channels inside the power thermal panel

Строение каналов внутри силовой термопанели

In this case, the internal structure of the panels is such that the coolant moves freely over the entire plane of the panel inside the cruciform channels with wicks filled with a working fluid (ammonia, water, etc.) (see fig.). Heat transfer along the panel is carried out due to the movement of the working substance in the form of vapor from the heating area to the condensation area through the vapor channels and back, in the form of a liquid through the wick. The main feature of a phase change thermal panel is a highly efficient heat removal system and an even temperature distribution over the panel surface with a difference of up to 1–2 ℃. When heated, the liquid heat transfer agent begins to evaporate and in the form of vapor moves to the evaporation zone, then condenses, moves through the wick in the form of a liquid to the heating zone, thus distributing heat over the panel. The movement of the working substance is carried out by capillary forces, which does not require the use of pumps and complex circuits for pumping coolant.

The capillary head of the wick must exceed the sum of the pressures arising in the liquid moving along the wick and in the vapor moving along the vapor channels. In the opposite case, the wick under the heat-generating element is drained, and the effective thermal conductivity of the panel drops sharply.

The technology for manufacturing a power thermal panel involves the modernization of its configuration by introducing internal vapor channels with a wick, the specific dimensions of which are unknown and are selected experimentally.

For the calculation, specific average values are introduced that characterize the effective sections for vapor channels and wick in the longitudinal and cross sections, physical parameters (porosity of the wick and the degree of its saturation with liquid).

Mathematical model. Let us introduce the values characterizing the effective longitudinal and cross sections for vapor channels and the wick [11–15]. Let us define the following values to describe the vapor move-

ment: *Svx*, *Svy* – the fraction of the effective section of the vapor channel from the total section of the panel for the longitudinal direction x and transverse y, respectively. Similarly, for describing the fluid motion: *Slx*, *Sly* – the fraction of the effective section of the wick from the total section of the panel for the longitudinal direction x and transverse y, respectively. The *Svx*, *Svy*, *Slx*, *Sly* values are dimensionless and can be from 0 to 1.

The input conditions for the problem are the heat flux to the panel surface $Q(x, y)$, where $x \in [0,H]$, $y \in [0,W]$. Values H, W are the panel length and width. It follows from the stationarity of the problem that the amount of the evaporating coolant from the wick to the vapor channels per unit area at each point of the panel is equal to $\dot{m}_1 = Q/\lambda$, where λ is the latent heat of pore formation.

For the movement of fluid in the wick, you can write the mass conservation equation:

$$\operatorname{div} \mathbf{m_l} = -\dot{m}\, l/D, \qquad (1)$$

where $\mathbf{m_l} = (m_{lx}, m_{ly})$ is the fluid mass flow inside the wick, D is the panel thickness minus the panel body wall thickness.

To describe the movement of the gas phase of the coolant, we use a formula similar to (1):

$$\operatorname{div} \mathbf{m_v} = \dot{m}\, l/D, \qquad (2)$$

where $\mathbf{m_v} = (m_{vx}, m_{vy})$ is the vapor mass flow in the vapor channels.

The panel will work successfully if the pressure difference between the gaseous and liquid phases at each point is less than the capillary pressure

$$P_c = \frac{2\sigma\cos\theta}{rc}, \qquad (3)$$

where rc is the radius of the pores of the wick, σ is the coefficient of surface tension, θ is the minimum angle of wetting of the material of the wick by the coolant.

It is possible to find the pressure distributions in the gaseous and liquid phases $P_v(x, y)$ and $P_l(x, y)$ up to a

constant. Since there is a point ($x_{\min}$, $y_{\min}$) inside the panel (in the area of the condenser) at which $P_v = P_l$ can be taken, the pressure difference between the gaseous and liquid phases can be written as follows

$$\Delta P = P_v(x, y) - P_l(x, y) -$$
$$- (P_v(x_{\min}, y_{\min}) - P_l(x_{\min}, y_{\min})). \qquad (4)$$

If max (ΔP) > P_c, then capillary forces will not be able to pull up the coolant, the wick in the panel will dry out and the panel will not work satisfactorily

Thus, the capillary condition for the panel operation can be written as follows:

$$\max(\Delta P) < P_c. \qquad (5)$$

The temperature distribution on the panel surface will be determined by the saturated vapor temperature at a given point, the heating power density and the thermal resistance of the wick layer and the panel body:

$$T(x, y) = T_s(P_v(x, y)) + Q(x, y) R, \qquad (6)$$

where $R = R_f + R_w$ is the sum of the thermal resistances of the wick and the panel body wall. The thermal resistance of the wick can be estimated: $R_f = c /k_f$, where c is the thickness of the wick (distance from the steam channel to the surface), k_f is the thermal conductivity of the wick filled with a coolant.

The thermal resistance of the wall is: $R_w = t /k_w$, where t is the wall thickness, k_w is the thermal conductivity of the panel body material.

The transfer of a laminar flow of fluid in a porous wick, depending on the type of wick, is determined either by Darcy's law (for liquids obeying the Navier-Stokes law)

$$-\Delta P - \frac{\eta}{k} \vec{u} + p \vec{f} = 0, \qquad (7)$$

div $\vec{u} = 0$, or Poiseuille's law (one of the simplest exact solutions of the Navier-Stokes equations).

$$Q = \frac{\pi R^4}{8\eta l} (P_1 - P_2) = \frac{\pi d^4}{128\eta l} -\Delta P. \qquad (8)$$

The kinetics of the liquid-vapor phase transition, i.e. the rate of evaporation and condensation can be determined using the Kn criterion (the Knudsen number). Maximum heat flux during evaporation from a flat surface to vacuum

$$q_{\max} = f \frac{LP_ж}{\sqrt{2\pi R o T_ж / \mu}}, \qquad (9)$$

where R_0 is the universal gas constant, L is the latent heat of vaporization. In some cases, the transfer of energy and matter in heat pipes can occur with partial drying of a porous wick. As a result, the calculation of the heat pipe is based on the equations of the dynamics of the flow of liquid and vapor, the description of the kinetics of phase transitions at the liquid-vapor interface, as well as the equations of energy transfer in the arteries of the tube, in the capillary-porous part (wick) and in the pipe shell itself.

The flow of fluid in the porous body of the wick should be described in more detail by Darcy's law

$$m = p_ж V_ж = - \frac{K_ж}{\mu_ж} gradP. \qquad (10)$$

By integrating this equation, we get the pressure drop at two points of the wick. Permeability $K_ж$ depends on the porosity Π of the wick and the degree of its saturation with liquid $b_ж$

$$K_ж = f(\Pi, b_ж). \qquad (11)$$

Another characteristic of a porous body is the differential curve of the distribution of surface permeability $f(K)$ (similar to the distribution curve of pores along the radius). For a homogeneous material, such a curve can be represented as a delta function of K or a linear combination of these functions

$$f(K) = \sum_{i=j}^{N} \delta Ai,$$

Ai satisfies the condition $\sum_{i=1}^{N} Ai = 1$, N is finite. (12)

If $f(K)$ cannot be represented as a finite number of functions, then the material is heterogeneous. If $f(K)$ is represented by one term, the material is homogeneous. If a material is described by two or more functions $f(K)$, then it is heterogeneous. If $f(K)$ depends on rectangular coordinates x_i ($i = 1,2,3$) and angular coordinates Ψ, θ, then the porous material is anisotropic. If there is no dependence on angular coordinates, the material is isotropic

$$P(K_1 \le K \le K_2) = \int_{K1}^{K2} f(xi\theta\psi)dxid\theta d\psi. \qquad (13)$$

Conclusion. The presented mathematical model of heat transfer processes in a thermal panel allows one to predict various modes of operation of a heat transfer device for high-temperature cycles.

Thus, the use of a new design of a thermal panel in small spacecraft will not only solve the problem of irregularity and asymmetry of heat fluxes from spacecraft panels, but also ensure the requirements of the technical specification for the limiting level of unmodeled accelerations during onboard systems operation.

References

1. Beloysov L. U. *Ocenivanie parametrov dvizheniya kosmicheskih apparatov* [Estimation of motion parameters of spacecraft]. Moscow, Fizmatlit Publ., 2002, 216 p.

2. Malahovskij E. E., Poznyak E. L., Shulyaka A. A. [Flexible controlled apparatus with disturbances from internal sources]. *Kosmicheskiye issledovaniya*. 1995, Vol. 33, No. 5, P. 538–545 (In Russ.).

3. Maximov I. A. [Problems of support of reliable operation of modern spacecraft under factors of space and technogeneous character destabilizing influence]. *Vestnik SibGAU*. 2010, Vol. 30, No. 4, P. 100–101 (In Russ.).

4. Caplin S. V., Bolychev S. A. [A system for providing thermal conditions for an experimental model of an optical-telescopic complex of a spacecraft]. *Vestnik SamGU.* 2013, No. 9/2(110), P. 236–243 (In Russ.).

5. Alekseev N. G., Zagar O. V., Kas'yanov A. O. [A system for ensuring the thermal regime of the device with temperature control in a narrow range]. *Materialy* XI *Mezhdunar. nauch. konf. "Reshetnevskie chteniya"* [Materials XI Intern. Scientific. Conf "Reshetnev reading"]. Krasnoyarsk, 2007, P. 213 (In Russ.).

6. Kosenko V. E, Zvonary V. D., Suntsov S. B., Derevyanko V. A., Vasilyev E. N., Nesterov D. A. [The use of hyper-heat-conducting structures in the development of leaky space vehicles of increased power and resource] *Materialy XVII Mezhdunarodnoy nauchnoy konferencii "Sistemnyy analiz, upravlenie i navigaciya"* [Materials XVII International Scientific Conference "System analysis, management and navigation"]. Evpatoria, 2012, P. 20–22 (In Russ.).

7. Kosenko V. E, Zvonary V. D., Suntsov S. B., Chebotarev V. E., Fatkulin R. F., Bakirov M. T., Derevyanko V. A., Makukha M. V. [The Results of Using Heat-Conductive structures in the apparatus of spacecraft]. *Materialy XXI Mezhdunarodnoy nauchnoy konferencii "Sistemnyy analiz, upravlenie i navigaciya"* [Materials XXI International Scientific Conference "System analysis, management and navigation"]. Moscow, MAI, 2016, P. 45–47 (In Russ.).

8. Meseguer J., Perez-Grande I., Sanz-Andres A. Spacecraft thermal control. Cambridge, UK: Woodhead Publishing Limited, 2012. 413p.

9. Analysis of efficiency of systems for control of the thermal regime of spacecraft / A.V. Delkov et al. *Chemical and Petroleum Engineering.* 2016, No. 9, P. 714–719.

10. Suntsov S. B., Kosenko V. E, Derevyanko V. A. *Modul' radioelektronnoj apparatury s giperteploprovodyashchim osnovaniem* [The module of electronic equipment with hyperthermally conductive]. Patent RF, no 2403692, 2009.

11. Vasilyev E. N., Derevyanko V. A., Nesterov D. A., Kosenko V. E., Chebotarev V. E. [Computational modeling of heat exchange processes in thermal control systems of spacecraft]. *Vychislitel'nyye tekhnologii.* 2009, Vol. 14, Iss. 6, P. 19–28 (In Russ.).

12. Delcov A. V., Hodenkov A. A., Zhuikov D. A. Mathematical modeling of single-phase thermal control system of the spacecraft. *Proceedings of 12th Intern. Conf. on Actual Problems of Electronic Instrument Engineering.* APEIPE 2014, P. 591–593.

13. Tanasienko F. V., Shevchenko Y. N., Delikov A. V., Kishkin A. A. [Two-dimensional thermal model of the thermal control system for nonhermetic formation spacecraft]. *Siberian Journal of Science and Technology.* 2018, Vol. 19. No. 3, P. 445–451 (In Russ.).

14. Kraev M. V., Zagar O. V., Kraev V. M., Golikovskaya K. F. *Nestacionarnye teplovye rezhimy kosmicheskih apparatov sputnikovyh system* [Non-stationary thermal conditions of spacecraft of satellite systems]. Krasnoyarsk, 2004, 280 p.

15. Faghri A. Heat Pipe Science and Technology. Taylor and Francis Group, 1995, 874 p.

Библиографические ссылки

1. Белоусов Л. Ю. Оценивание параметров движения космических аппаратов. М. : Физматлит, 2002. 216 с.

2. Малаховский Е. Е., Позняк Э. Л., Шуляка А. А. Гибкий управляемый аппарат при возмущениях от внутренних источников // Космические исследования, 1995. Т. 33, № 5. С. 538–545.

3. Максимов И. А. Проблемы обеспечения надежного функционирования современных космических аппаратов в условиях дестабилизирующего воздействия факторов космического пространства и факторов техногенного характера // Вестник СибГАУ. 2010. № 4(30). С. 100–101.

4. Цаплин С. В., Болычев С. А. Система обеспечения теплового режима экспериментальной модели оптико-телескопического комплекса космического аппарата // Вестник СамГУ. 2013. № 9/2(110). С. 236–243.

5. Алексеев Н. Г., Загар О. В., Касьянов А. О. Система обеспечения теплового режима прибора с регулированием температуры в узком диапазоне // Решетневские чтения : материалы XI Междунар. науч. конф. (10–12 ноября 2007, г. Красноярск) : в 2 ч. / Сиб. гос. аэрокосмич. ун-т. Красноярск, 2007. С. 213

6. Применение гипертеплопроводящих структур при разработке негерметичных космических аппаратов повышенной мощности и ресурса / В. Е. Косенко, В. Д. Звонарь, С. Б. Сунцов, В. А. Деревянко и др. // Системный анализ, управление и навигация : материалы XVII Междунар. науч. конф. Евпатория. 2012. С. 20–22.

7. Результаты применения гипертеплопроводящих структур в аппаратуре космических аппаратов / В. Е. Косенко, В. Д. Звонарь,С. Б. Сунцов, В. Е. Чеботарев и др. // Системный анализ, управление и навигация : материалы XXI Междунар. науч. конф. М. : МАИ. 2016. С. 45–47.

8. Meseguer J., Perez-Grande I., Sanz-Andres A. Spacecraft thermal control. Cambridge, UK: Woodhead Publishing Limited, 2012. 413p.

9. Analysis of efficiency of systems for control of the thermal regime of spacecraft / A. V. Delkov et al. // Chemical and Petroleum Engineering. 2016. No. 9. P. 714–719.

10. Патент № 2403692 Российская Федерация, МПК Н05К 1/00. Н05К 7/20. Модуль радиоэлектронной аппаратуры с гипертеплопроводящим основанием / Сунцов С. Б., Косенко В. Е., Деревянко В. А. № 2009116488/07 ; заявл. 29.04.2009 ; опубл. 10.11.2010, Бюл. № 31.

11. Вычислительное моделирование процессов теплообмена в системах терморегулирования космических аппаратов / Е. Н. Васильев, В. А. Деревянко, Д. А. Нестеров, В. Е. Косенко, В. Е. Чеботарев // Вычислительные технологии. 2009. Т. 14, вып. 6. С. 19–28.

12. Delcov A. V., Hodenkov A. A., Zhuikov D. A. Mathematical modeling of single-phase thermal control system of the spacecraft // Proceedings of 12th Intern. Conf. on Actual Problems of Electronic Instrument Engineering, APEIPE 2014. P. 591–593.

13. Двухмерная тепловая модель системы терморегулирования космических аппаратов негерметичного исполнения / Ф. В. Танасиенко, Ю. Н. Шевченко, А. В. Делков, А. А. Кишкин // Сибирский журнал науки и технологий. 2018. Т. 19, № 3. С. 445–451.

14. Нестационарные тепловые режимы космических аппаратов спутниковых систем / М. В. Краев, О. В. Загар, В. М. Краев, К. Ф. Голиковская. Красноярск, 2004. 280 с.

15. Faghri A. Heat Pipe Science and Technology. Taylor and Francis Group, 1995. 874 p.

Kolga Vadim Valentinovich – Dr. Sc., Professor; Reshetnev Siberian State University of Science and Technology. E-mail: kolgavv@yandex.ru.

Yarkov Ivan Sergeevich – Postgraduate student; Reshetnev Siberian State University of Science and Technology.

Yarkova Evgeniya Aleksandrovna – Postgraduate student; Reshetnev Siberian State University of Science and Technology. E-mail: Yarkova.sib@yandex.ru.

Кольга Вадим Валентинович – доктор педагогических наук, кандидат технических наук, профессор, профессор кафедры летательных аппаратов; Сибирский государственный университет науки и технологий имени академика М. Ф. Решетнева. E-mail: kolgavv@yandex.ru.

Ярков Иван Сергеевич – аспирант; Сибирский государственный университет науки и технологий имени академика М. Ф. Решетнева.

Яркова Евгения Александровна – аспирант; Сибирский государственный университет науки и технологий имени академика М. Ф. Решетнева. E-mail: Yarkova.sib@yandex.ru.

STUDY OF IMPELLER DESIGN PARAMETERS EFFECT ON THE AXIAL THRUST OF A CENTRIFUGAL ELECTRIC PUMP ASSEMBLY

Z. A. Kuznetsova*, M. I. Sinichenko, A. D. Kuznetsov, I. A. Kleshnina, F. K. Sin'kovskiy

JSC Academician M. F. Reshetnev Information Satellite Systems
52, Lenin St., Zheleznogorsk, Krasnoyarsk region, 662972, Russian Federation
*E-mail: u-z-a@yandex.ru

This paper discusses and estimates the effect of some design parameters on the value of axial thrust appearing during functioning of the core component of a spacecraft's (SC) thermal control subsystem – electric pump unit (EPU). The major causes of axial forces in centrifugal pumps of in-line arrangement are described and analysed. Design parameters having an effect of axial thrust value are: impeller position relatively to EPU diffuser (position was chosen based on dimension chain calculation), presence and size of discharging holes in the impeller, number and shape of impeller vanes (numbers of 14 & 16 were considered). EPU impellers with different number and shape of vanes were designed and manufactured. A series of experiments was carried out in order to research the effects of all aforementioned parameters: measurements of head vs flow curves and axial thrust values at given flow values. Each parameter's contribution in the value of axial thrust appearing during EPU functioning is evaluated. Vibration measurements were obtained and analysed for electric motor DBE 63-25-6.3 fitted with different impellers. In this study, a DLP additive process was used for impellers manufacturing, which significantly sped up the tests. Obtained results will extend knowledge of processes taking place in EPU impellers, enable choice of the aforementioned parameters at design phase so to minimise axial thrust appearing during functioning of a centrifugal EPU of a spacecraft's thermal control subsystem. Outcomes of this study are capable of improving SC reliability at all phases of its life because EPU axial thrust causes its premature loss of operability.

Keywords: centrifugal pump, pump impeller, axial thrust, spacecraft thermal control subsystem.

ИССЛЕДОВАНИЕ ВЛИЯНИЯ КОНСТРУКТИВНЫХ ПАРАМЕТРОВ РАБОЧЕГО КОЛЕСА НА ВЕЛИЧИНУ ОСЕВОЙ НАГРУЗКИ ЦЕНТРОБЕЖНОГО ЭЛЕКТРОНАСОСНОГО АГРЕГАТА

З. А. Кузнецова*, М. И. Синиченко, А. Д. Кузнецов, И. А. Клешнина, Ф. К. Синьковский

АО «Информационные спутниковые системы» имени академика М. Ф. Решетнева»
Российская Федерация, 662972, г. Железногорск Красноярского края, ул. Ленина, 52
*E-mail: u-z-a@yandex.ru

В данной статье рассматривается и оценивается влияние некоторых конструктивных параметров на величину осевой нагрузки, возникающей при работе главного элемента активной жидкостной системы терморегулирования космического аппарата (КА) – электронасосного агрегата (ЭНА). Описаны и проанализированы основные причины возникновения осевой нагрузки в центробежном насосе с «осевым» принципом компоновки. Исследовались конструктивные параметры, влияющие на величину осевой нагрузки: положение рабочего колеса относительно диффузора ЭНА (положение выбиралось из расчета размерных цепей), наличие и размер разгрузочных отверстий в рабочем колесе, количество и форма лопастей рабочего колеса (рассмотрено количество лопастей 14 и 16). Были спроектированы и изготовлены рабочие колеса ЭНА с различным количеством и формами лопастей. Проведен ряд экспериментов по исследованию влияния всех перечисленных параметров: измерение расходно-напорных характеристик и величины осевой нагрузки при достижении определенного расхода. Дана оценка вклада каждого из перечисленных параметров на величину осевой нагрузки, возникающей при функционировании рабочего колеса. Была получена и проанализирована виброизмерительная информация на электродвигателе (ЭД) ДБЭ 63-25-6.3 с установленными поочередно рабочими колесами. В данном исследовании использовалась аддитивная технология печати DLP для изготовления рабочих колес, что значительно ускорило процесс испытаний. Полученные результаты способствуют расширению знаний о процессах, происходящих в рабочем колесе, позволяют осуществить выбор вышеперечисленных параметров на этапе проекти-

рования, способных снизить величину осевой нагрузки, возникающей при работе центробежного ЭНА в системе терморегулирования КА. Результаты данной работы способны повысить надежность функционирования КА во весь срок активного существования, поскольку повышенная осевая нагрузка в ЭНА является причиной его преждевременной потери работоспособности.

Ключевые слова: центробежный насос, рабочее колесо насоса, осевая нагрузка, система терморегулирования космического аппарата.

Introduction. Currently, there is a tendency for the appearance of Platforms with a thermal power of 8 to 10 kW on the world market of telecommunication spacecraft (SC) [1]. One of the possible options for structural design of the thermal control system (TCS) of such Platforms is a monophase active TCS with a liquid coolant [2].

The most important element of this system is the electric pumping unit (EPU) [3], which provides continuous circulation of the coolant in the heat circuit, providing the thermal regime of the target and service equipment. Fail-safe operation of EPU during the entire active life of the spacecraft is a key indicator of the reliability of the entire spacecraft.

For the EPU of centrifugal type, reducing the axial thrust acting on the bearing arrangements of the pumps is one of the most important tasks of ensuring the long service life of the EPU.

This article presents the results of a study of the effect of the design parameters of the impeller of a single-stage centrifugal EPU on the axial thrust.

EPU design. The studied EPU refers to the "axial" principle of the layout: the main and standby centrifugal pumps are installed on the same axis, while the EPU housing is a single monoblock structure for both pumps, in which spiral diffusers for each pump are made in one piece [4]. In order to meet the high requirements for tightness, the pump motors are welded into the EPU housing through a bimetallic adapter. Fig. 1 shows a single-stage centrifugal EPU used in experiments in this study.

The technical parameters of such an EPU are presented in tab. 1.

Axial force in EPU. When the pump is started, an axial force of hydrodynamic origin, shown in fig. 1, begins to act on the bearing supports *3* (fig. 1) of the rotor *2*.

The presence of this force affects the durability of the bearing supports *3* of the rotor of the electric motor *2* (fig. 1). This was confirmed in the course of studies of bearings that worked out during life tests in the electric motor of EPU. Inspection of the rotor bearings showed that they have numerous traces of wear in the form of dents, traces of friction, traces of metal transfer. In the course of metallographic research, it was found that these tracks are of a fatigue nature. According to the results of the study, it was found that the position of the wear marks on the rings indicates the presence of an axial thrust during the operation of the bearings. According to [5], the nature of the formation of axial force is the difference in pressure values in cavities "A" and "B" between the impeller and the casing. The area of the outer surface of the main disc under the discharge pressure is larger than that of the cover disc, which results in a static pressure force directed towards the inlet funnel. Fig. 2 shows the direction of action of forces in the EPU impeller. In this case, the difference between F_A and F_B is always directed towards the flow entering the impeller, and it is applied to the impeller, and through it to the bearing supports of the pump rotor. Thus, based on the nature of the formation of the axial force, it follows that to reduce it, it is necessary to eliminate the difference between F_A and F_B.

The geometric parameters of the impeller of the studied EPU are shown in fig. 3.
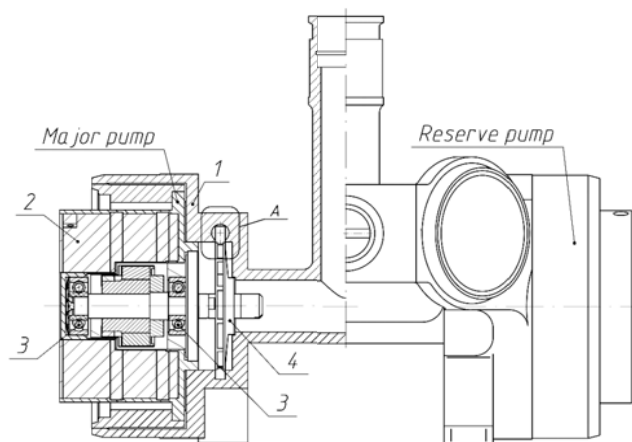
Fig. 1. Single-stage centrifugal electric pump unit:
1 – electric pump unit housing; *2* – motor; *3* – journal bearing; *4* – impeller

Рис. 1. Одноступенчатый центробежный ЭНА:
1 – корпус ЭНА; *2* – электродвигатель; *3* – радиальные подшипники; *4* – рабочее колесо

Technical parameters of EPU with standard impeller

Parameter name	Parameter value
Head (ΔP), kgf/cm^2	0.61
Flow rate (Q), m^3/s	110–150
Rotational speed of the electric motor (n), rpm	5800
Power fluid	LZ-TK-2
Axial thrust, N	> 9.8
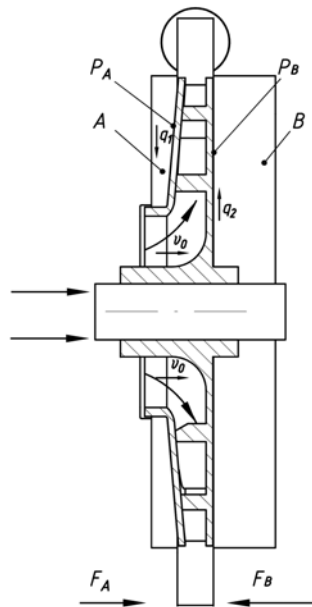
Fig. 2. The direction of the forces in the pump rotor:
A, B – pressured cavities; P_A – rotor top disk area;
P_B – disk with blades area; F_A – axial force acting from the top disk;
F_B – axial force acting from the disk with blades

Рис. 2. Направление действия сил на рабочее колесо ЭНА:
A, B – полости, где действует давление; P_A – площадь покрывного
диска рабочего колеса; P_B – площадь диска с лопатками;
F_A – осевая сила, действующая со стороны покрывного диска;
F_B – осевая сила, действующая со стороны основного диска
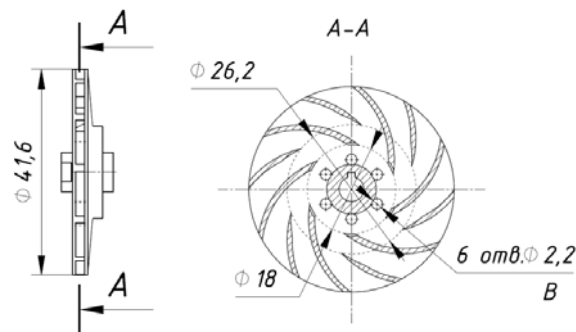
Fig. 3. Pump impeller:
B – discharging holes

Рис. 3. Рабочее колесо насоса:
B – разгрузочные отверстия

According to the calculations, the value of the acting axial thrust in an EPU of a similar design with an impeller without discharge holes is in the range from 1 to 8 N, depending on the pressure drop. According to the technical specifications for the electric motor, in order to ensure the required service life, the axial thrust should not exceed 8.7 N. In order to increase the service life of the bearing supports, we will consider ways to reduce the axial force without changing the design of the pump flow path and minimal changes in the impeller.

The influence of the position of the end of the impeller relative to the diffuser and the influence of the presence of discharging holes. One of the simplest ways to reduce the effect of axial force is to drill holes in the main impeller disc. Full unloading of the rotor will be achieved in the case $(P_B \cdot S_B) = (P_A \cdot S_A)$ [5; 6].

Taking into account the current design of the pump impeller shown in fig. 3, the total area of the discharging holes is 9 % of the area of the holes required to completely unload the rotor from the axial thrust. The position of the impeller relative to the spiral bend can affect the flow conditions of the working fluid in its vicinity. Each position of the impeller corresponds to a radial clearance X (remote element *A*, fig. 1), it affects the leakage through the front seal (q_1) and the rear seal (q_2), shown in fig. 2. In accordance with [6], any change in the gap in the seals or the nature of the movement in the sinuses causes an additional axial force due to the unbalanced part of the pressure diagram arising from the impeller geometry. Let us check experimentally the pressure values from the rear side of the electric motor at different positions of the impeller relative to the spiral bend.

Experiment № 1. Study of the position of the end of the impeller relative to the diffuser; discharge holes are present. Setting up the experiment: the pressure on the pump impeller is investigated at various pressure heads. Pump configuration: the impeller has relief holes shown in fig. 3, tests were carried out with an electric motor DBE63-25-6.3 by measuring the pressure in the bearing area (on the back of the electric motor). The impeller is installed with different clearances X (0 mm and 0.4 mm, see fig. 1) relatively to the spiral bend. These clearances are obtained from the calculation of dimensional chains. Fig. 1 shows a fragment of the EPU used in the experiment with different clearance X. The assumption is tested that at different clearances different conditions of the flow of the power fluid in the EPU impeller are presented, and at X = 0.4 mm the pressure on the back side of the impeller will be greater will lead to increased axial thrust. During the experiment, the flow-pressure characteristics of the EPU were measured [7].

Experiment № 2. Investigation of the position of the end of the impeller relatively to the diffuser, the discharge holes are closed. Setting up the experiment: similar to experiment № 1, except for the configuration of the impeller, since there are discharging holes in it. The experimental results are presented in tab. 2–4.

Table 2

Flow-pressure characteristics of EPU, pressure drop is 0.4 kgf/cm^2

Parameter name	Atmospheric pressure				Pressure of 1.2 kgf/cm^2			
	Holes		No holes		Holes		No holes	
	X = 0	X = 0.4	X = 0	X = 0.4	X = 0	X = 0.4	X = 0	X = 0.4
Pressure from the back of the electric motor, kgf/cm^2	–0.15	–0.1	0.24	0.24	0.05	0.06	0.43	0.423
EPU inlet pressure, kgf/cm^2	–0.08	–0.05	–0.05	–0.05	0.13	0.13	0.14	0.129
EPU outlet pressure, kgf/cm^2	0.32	0.35	0.35	0.35	0.53	0.53	0.54	0.529
Heat transfer fluid consumption, cm^3/s	0.32	0.35	0.35	0.35	0.53	0.53	0.54	0.529
Consumption current, A	>225	>225	228	>220	>225	>225	>228	>220
Heat transfer fluid temperature, ˚C	1.39	1.36	1.33	1.28	1.4	1.37	1.34	1.28

Table 3

Flow-pressure characteristics of EPU, pressure drop is 0.5 kgf/cm^2

Parameter name	Atmospheric pressure				Pressure of 1.2 kgf/cm^2			
	Holes		No holes		Holes		No holes	
	X = 0	X = 0.4	X = 0	X = 0.4	X = 0	X = 0.4	X = 0	X = 0.4
Pressure from the back of the electric motor, kgf/cm^2	–0.12	–0.07	0.27	0.28	0.08	0.1	0.47	0.465
EPU inlet pressure, kgf/cm^2	–0.06	–0.03	–0.03	0.027	0.15	0.15	0.16	0.15
EPU outlet pressure, kgf/cm^2	0.44	0.47	0.47	0.473	0.65	0.65	0.66	0.65
Heat transfer fluid consumption, cm^3/s	199	196	189	182	202	194	194	180
Consumption current, A	1.25	1,21	1.14	1.09	1.26	1.21	1.16	1.08
Heat transfer fluid temperature, ˚C	27.9	29.0	26.3	25.4	28.4	29.8	27.0	26.2

Table 4

Flow-pressure characteristics of EPU, pressure drop is 0.6 kgf/cm²

Parameter name	Atmospheric pressure				Pressure of 1.2 kgf/cm²			
	Holes		No holes		Holes		No holes	
	X = 0	X = 0.4	X = 0	X = 0.4	X = 0	X = 0.4	X = 0	X = 0.4
Pressure from the back of the electric motor, kgf/cm²	−0.08	−0.03	0.33	0.346	0.12	0.14	0.52	0.527
EPU inlet pressure, kgf/cm²	−0.03	0	−0.005	0.002	0.19	0.18	0.19	0.18
EPU outlet pressure, kgf/cm²	0.57	0.6	0.595	0.602	0.79	0.78	0.79	0.78
Heat transfer fluid consumption, cm³/s	121	122	116	95	121	119	114	94
Consumption current, A	1.01	0.99	0.93	0.83	1.02	0.99	0.92	0.83
Heat transfer fluid temperature, ˚C	28.0	29.2	26.4	25.6	28.2	29.9	27.1	26.3

Let us compare the results obtained for different values of the clearance X and the presence or absence of relief holes. Comparison will be applied to the value of pressure from the rear side of the electric motor, since the axial force arises from the pressure difference on both sides of the impeller, and the value of the axial force itself is characterized by the integral of pressure.

Study of the influence of the number and shape of the impeller blades. According to [8], the number of impeller blades should be 6–7 in order to obtain a stable flow-pressure characteristic. In accordance with [9], the rational number of blades for a low-flow pump is 4–6. The pressure pulsations excited during the operation of the EPU cause pressure fluctuations in adjacent cavities, thereby affecting the direction, magnitude and nature of the axial force. It was found that the geometrical and operating parameters have a significant effect on the frequency spectrum and amplitude of pressure pulsations [9]. It is assumed that an increase in the number of blades leads to a more uniform distribution of speeds in the impeller, which will entail a decrease in pressure pulsations, which will cause a change in the nature of the movement of the liquid in the impeller. The task was to determine the effect of the number of blades on the axial thrust.

In this part of the experiment, additive technologies were used. They allowed to reduce test time due to the rapid production of various solutions. A printer with DLP printing technology was used. The principle of operation of which consists in gradual hardening along the sections of the part by illuminating the photopolymer with ultraviolet light. This technology made it possible to manufacture EPU impellers without using additional soldering operations, which positively affected the time spent on the production of experimental parts [10]. Of all the available printing technologies, this one is the most suitable because it allows the complex geometry of the impeller. The printing error is equal to the error of a milling machine, on which such impellers are usually manufactured. In addition, this technology does not require auxiliary elements for printing (support), which are necessary when using, for example, FDM technology, which decisively affects the quality of the resulting part. For further confidence in the results obtained using this technology, an experiment was carried out. Measurements of flow-pressure characteristics and axial thrust were carried out for an impeller made of standard material (AMg6M) and an impeller of a similar design made of photopolymer, the results are presented in tab. 5.

It can be concluded that the impeller made of photopolymer shows flow-pressure characteristics lower than the impeller made of standard material, presumably due to the absence of sharp edges. However, we assume that this convergence is considered acceptable for a quick check of design solutions.

Experiment № 4. Investigation of the influence of the number of blades on the value of the axial force arising during the operation of the impeller in the EPU. With the help of the CAD - system, 3D models of EPU impellers were designed, presented below [11–15]. The shape of the blades was chosen on the basis of experimental experience, it provides the necessary blade frequency and allows you to obtain the flow-pressure characteristics presented in tab. 1. This result is the most suitable for the work of EPU. The subject of research in this work is the axial thrust arising from the functioning of the investigated impellers. The measurements were carried out using the setup shown in fig. 4, alternately in two types of enclosures shown in fig. 5. Vibration measuring information was obtained and analyzed on the electric motor DBE 63-25-6.3 with alternately installed impellers. Nominal parameters of EPU: the rotor speed of the electric motor during all tests was 5900 rpm. When registering vibration accelerations, the transducers were installed in accordance with fig. 5.

Registration of vibration acceleration signals was carried out using a set of means for multichannel recording of vibration parameters based on an LMS SCADAS Mobile measuring amplifier with the following recording parameters:

1) signal recording bandwidth – from 7 to 10240 Hz;
2) registration mode – continuous;
3) recording duration – 30 minutes;
4) sampling rate – 20480 Hz;
5) the sensor provides a three-axis measurement;
6) start mode – manual.

Signal processing was carried out using software LMS.Test.Xpress 5A (during signal recording) in order to

obtain the root mean square value (RMS) of vibration acceleration.

The cavity in which the impeller is located is filled with the power fluid LZ-TK-2. An axial force is created from the side of sensor 1. The electric motor is switched on. As the readings of the axial force on the sensor increase, it is gradually increased until it stops increasing or decreasing. When the force stops increasing, it means that the axial thrust from the sensor side is equal to the force from the impeller. The resulting value is the axial force acting from the impeller.

The axial thrust was measured under the following conditions:

1) the same flow path of the pump;

2) electric motor DBE 63-25-6.3;

3) the same position of the impellers relative to the spiral bend, discharging holes are present (in accordance with the calculation of dimensional chains X = 0). The choice is due to the result of experiment №1, according to which, at X = 0 and the presence of discharging holes, the pressure on the rear side of the electric motor decreased from 4 to 8 times;

4) power fluid LZ-TK-2.

Consider the options for the tested impellers.

16 blades, shortened in comparison with the ones of a standard impeller in fig. 2, axial thrust balancing discharging holes are present. Tab. 6, 7 show the test results of the impeller shown in fig. 6.

Impeller with 14 blades, which are shortened compared to the standard one, discharge holes for axial thrust compensation are present. Tab. 8–10 show the test results of the impeller shown in fig. 7.

Two tests were carried out:

1) discharge holes with a diameter of 2.2 mm;

2) discharge holes with a diameter of 3.2 mm.

After obtaining the results given in table 8, it was decided to widen the discharging holes in order to verify the calculations, according to which, with an increase of the discharging holes to a diameter of 3.2, the value of the axial thrust will decrease by 38 %.

Impeller with 14 straight blades. Tab. 11, 12 show the test results of the impeller shown in fig. 8.

Impeller with 14 long blades. Tab. 13, 14 show test results of the impeller shown in fig. 9.

Tab. 15 shows the results of measuring the axial thrust in the impellers above.

Table 5

Flow-pressure characteristics of an AMg6M impeller and a photopolymer impeller of a similar design

Impeller material	Head (ΔP), kgf/cm^2	Flow rate (Q), m^3/s	Rotational speed of the electric motor (n), rpm	Power fluid
AMg6M	0.61	110–150	5800	LZ-TK-2
Photopolymer	0.57	112	5800	LZ-TK-2
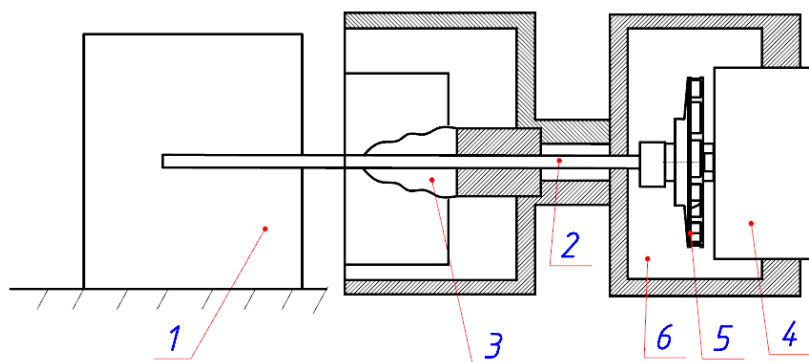
Fig. 4. Measurement circuitry:
1 – sensor; *2* – the rod; *3* – rubber gasket; *4* – motor; *5* – impeller;
6 – inner cavity with power fluid

Рис. 4. Схема измерения:
1 – датчик; *2* – шток; *3* – резиновое уплотнение; *4* – ЭД; *5* – рабочее колесо;
6 – внутренняя полость ЭНА, заполненная LZ-TK-2

Table 6

Test results, discharge holes Ø 2.2 mm

Pressure drop, kgf/cm^2	Consumption, cm^3/s	Axial force, N (g)	Electric motor speed, n, rpm
0,4	189	2.8 (290)	5900
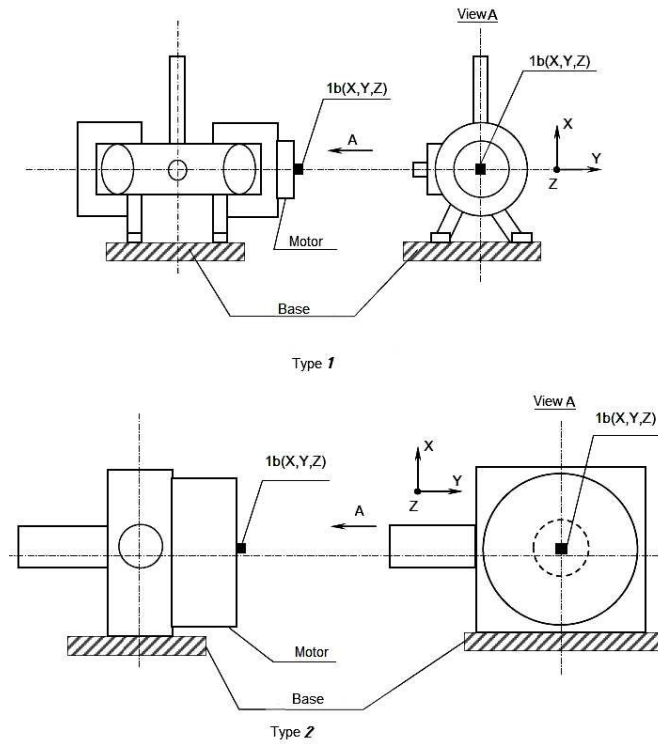
Fig. 5. Installation diagram of vibration transducers on the EPU electric motor

Рис. 5. Схема установки вибропреобразователей на ЭД ЭНА
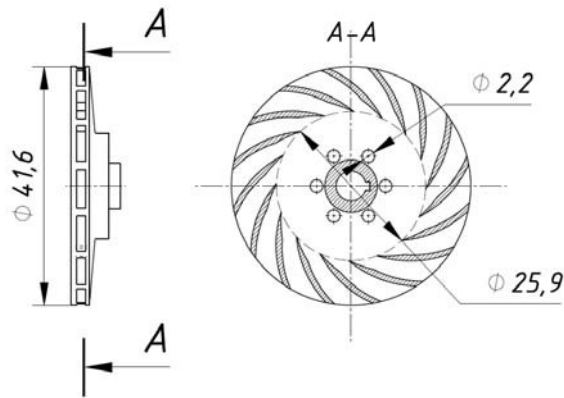
Fig. 6. Impeller with sixteen blades. The blades are shortened
in comparison to the ones of a standard impeller

Рис. 6. Рабочее колесо с 16 лопатками, укороченными
по сравнению со штатным

Table 7

RMS vibration acceleration of the impeller with 16 shortened blades

EPU type	Rotation speed, rpm	RMS by range 10–10240 Hz, m/s²			RMS by range 10–3200 Hz, m/s²			RMS by range 10-1000 Hz, m/s²			Average RMS vibration acceleration, m/s² (g)
		X	Y	Z	X	Y	Z	X	Y	Z	0.27 (0.026)
Type 2	5900	1.79	1.73	3.16	1.30	0.77	1.32	0.26	0.34	0.14	
Type 1		1.36	1.75	2.80	0.81	1.02	0.84	0.22	0.32	0.32	
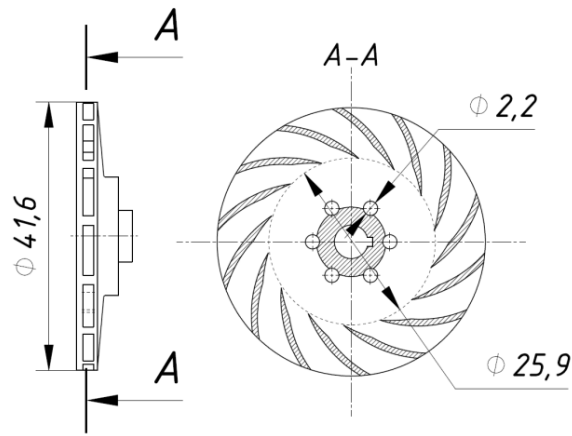
Fig. 7. An impeller with fourteen blades. The blades are shortened
in comparison to the ones of a standard impeller

Рис. 7. Рабочее колесо с 14 лопатками, укороченными
по сравнению со штатным
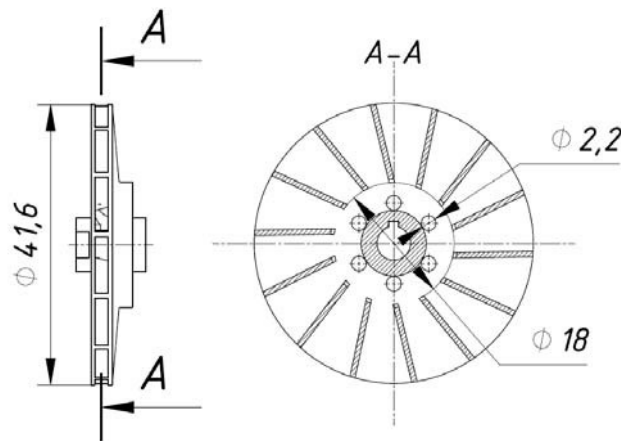
Fig. 8. Impeller with fourteen straight blades

Рис. 8. Рабочее колесо с 14 прямыми лопатками

Table 8

Test results, discharge holes Ø 2.2 mm

Pressure drop, kgf/cm^2	Consumption, cm^3/s	Axial force, N (g)	Electric motor speed, n, rpm
0.4	189	1.66 (170)	5900

Table 9

RMS vibration acceleration of the impeller with 14 shortened blades

EPU type	Rotation speed, rpm	RMS by range 10–10240 Hz, m/s^2			RMS by range 10–3200 Hz, m/s^2			RMS by range 10–1000 Hz, m/s^2			Average RMS vibration acceleration, m/s^2 (g)
		X	Y	Z	X	Y	Z	X	Y	Z	0.27 (0.026)
Type 2	5900	1.47	1.96	3.12	0.87	1.31	0.95	0.36	0.44	0.20	
Type 1		1.85	2.43	2.93	1.01	1.51	0.74	0.23	0.31	0.27	

Table 10

Test results, discharge holes Ø 3.2 mm

Pressure drop, kgf/cm^2	Consumption, cm^3/s	Axial force, N (g)	Electric motor speed, n, rpm
0.4	162	1.02 (105)	5900

Table 11

Test results, discharge holes Ø 2.2 mm

Pressure drop, kgf/cm^2	Consumption, cm^3/s	Axial force, N (g)	Electric motor speed, n, rpm
0.4	227	2.69 (275)	5900

Table 12

RMS vibration acceleration of the impeller with 14 straight blades

EPU type	Rotation speed, rpm	RMS by range 10–10240 Hz, m/s^2			RMS by range 10–3200 Hz, m/s^2			RMS by range 10–1000 Hz, m/s^2			Average RMS vibration acceleration, m/s^2 (g)
		X	Y	Z	X	Y	Z	X	Y	Z	0.41 (0.042)
Type 2	5900	2.79	2.73	3.46	2.23	1.73	1.19	0.40	0.56	0.28	
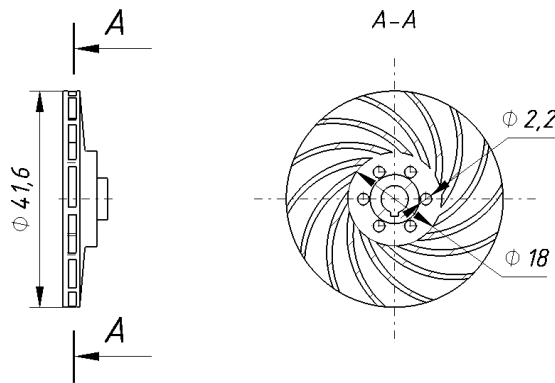
Fig. 9. Impeller with 14 long blades

Рис. 9. Рабочее колесо с 14 длинными лопатками

Table 13

Flow and pressure characteristics, axial thrust of impeller with 14 long blades, discharge holes Ø 2.2 mm

Pressure drop, kgf/cm^2	Consumption, cm^3/s	Axial force, N (g)	Electric motor speed, n, rpm
0.42	210	> 2.69 (> 275)	5900

Table 14

RMS vibration acceleration of the impeller with 14 long blades

EPU type	Rotation speed, rpm	RMS by range 10–10240 Hz, m/s^2			RMS by range 10–3200 Hz, m/s^2			RMS by range 10–1000 Hz, m/s^2			Average RMS vibration acceleration, m/s^2 (g)
		X	Y	Z	X	Y	Z	X	Y	Z	0.41 (0.042)
Type 2	5900	3.73	4.43	3.16	2.97	3.14	1.63	0.42	0.51	0.30	

Results of measuring the axial thrust in impellers with different blades

№	Impeller type	Axial thrust, N	Average RMS vibration acceleration, m/s^2 (g)
1	16 short blades	2.84	0.27 (0.026)
2	14 short blades	1.66/1.02	0.30 (0.029)
3	14 straight blades	2.69	0.41 (0.042)
4	14 long blades	> 2.69	0.41 (0.042)

Conclusion. With the same clearance and only from the presence of discharge holes, the value of the pressure acting from the rear side of the electric motor decreased approximately 2–3 times in the absence of pressure and up to four times in the presence of pressure of 1.2 kgf/cm^2. The introduction of discharging holes for reducing the magnitude of the axial force acting in the electric pump unit is a widespread measure due to its simplicity and efficiency, which is confirmed by this experiment.

There was no change in the magnitude of the pressure on the rear side of the electric motor when the clearance X was changed from 0 to 0.4. However, there is a small change in flow rate (from 7 to 21 cm^3/s) when the clearance X changes from 0 to 0.4 in the case of holes present. A similar phenomenon was not detected in the case of the absence of discharge holes.

When comparing the case with the presence of discharge holes and a clearance of X = 0 (case 1) with the case of the absence of discharge holes and a clearance of X = 0.4 (case 2), it was revealed that the pressure on the back of the electric motor decreased from 4 to 8 times in case 1 compared with case 2 in the presence of pressure of 1.2 kgf/cm^2. In the absence of a pressure of 1.2 kgf/cm^2, the pressure from the rear side of the electric motor decreased from 1.5 to 4 times.

The size of the discharge holes affects the amount of axial force that occurs when the impeller operates. With an increase in the diameter of the discharge holes by 45 %, the magnitude of the axial force decreased by 62 %. A further increase in the diameter of the discharge openings is considered impractical due to the increase in head losses.

According to the results of the analysis of vibration measurement information, for impellers with a different number of blades of the selected shape, the amplitudes of peaks above 1000 Hz prevail in the vibration acceleration spectra. This value is the most suitable for EPU operation.

With an increase in the number of blades from 14 to 16, the axial thrust increased by 4 %.

When changing the shape of the blade to a straight line (variant 3 of tab. 15), the value of the axial force increased by 62 %.

According to the results of the analysis of vibration measurement information for impellers with a different number of blades of the selected shape, the amplitudes of peaks above 1000 Hz prevail in the vibration acceleration spectra. This result is most suitable for the work of EPU.

The vibration acceleration spectra also show a significant predominance of the peak amplitudes in the range above 1000 Hz. The minimum parameters of the RMS vibration acceleration module are observed for the impeller with 16 short blades.

The use of additive DLP printing technology in this study significantly accelerated the testing process. Impellers made of photopolymer have flow-pressure characteristics close to those of impellers made of standard material.

References

1. Ley W., Wittman K., Hallmann W. Handbook of Space Technology, 2009, 884 p.

3. Sarafin T. P, Larson W. J. Spacecraft structures and mechanisms. From Concept to Launch, 2007, 850 p.

4. Lomakin A. A. *Tsentrobezhnye i osevye nasosy* [Centrifugal and axial pumps]. Moscow, Mashinostroenie Publ., 1996, 364 p.

4. Zimnitskiy V. A. et al. *Lopastnye nasosy* [Vane pumps]. Leningrad, Mashinostroenie Publ., 1986, 334 p.

5. Perevoshchikov S. I. *Konstruktsiya tsentrobezhnykh nasosov (obshchie svedeniya)* [The design of centrifugal pumps (general information)]. Tyumen, Tsogu Publ., 2013, 228 p.

6. Malyushenko V. V., Mikhaylov A. K. *Energeticheskie nasosy* [Energy pumps]. Moscow, Energoizdat Publ., 1981, 200 p.

7. Yarementko O. V. *Ispytaniya nasosov* [Pump Testing]. Moscow, Mashinostroenie Publ., 1976, 225 p.

8. Mikhaylov A. K., Malyushenko V. V. *Lopastnye nasosy. Teoriya, raschet i konstruirovanie*. [Vane pumps. Theory, calculation and construction]. Moscow, Mashinostroenie Publ., 1977, 288 p.

9. Kraev M. V., Lukin V. A., Ovsyannikov B. V. *Maloraskhodnye nasosy aviatsionnykh i kosmicheskikh sistem* [Low-flow pumps of aviation and space systems]. Moscow, Mashinostroenie Publ., 1985, 128 p.

10. Zlenko M. A., Nagaytsev M. V., Dovbysh V. M. *Additivnye tekhnologii v mashinostroenii. Posobie dlya inzhenerov* [Additive technologies in mechanical engineering. A manual for engineers]. Moscow, NAMI Publ., 2015, 220 p.

11. Baybakov O. V. *Primenenie EVM v raschetakh protochnoy polosti lopastnykh gidromashin* [The use of computers in the calculations of the flowing cavity of paddle hydraulic machines]. Moscow, MGTU im. N. E. Baumana Publ., 1982, 65 p.

12. Branshteyn L. Ya. *Spravochnik konstruktora gidroturbin* [Hydroturbine Designer Reference]. Moscow, Mashinostroenie Publ., 1971, 304 p.

13. Sazonov Yu. A., Mulenko V. V., Balaka A. Yu. [Computer modeling and development of a methodology for designing dynamic pumps and machines]. *Territoriya neftegaz.* 2011, No. 10, P. 34–36 (In Russ.).

14. Karelin V. Ya. *Kavitatsionnye yavleniya v tsentrobezhnykh i osevykh nasosakh* [Cavitation phenomena in centrifugal and axial pumps]. Moscow, Mashinostroenie Publ., 1976, 325 p.

15. Loytsyanskiy L. G. *Mekhanika zhidkosti i gaza* [Mechanics of fluid and gas]. Moscow, Drofa Publ., 2003, 840 p.

Библиографические ссылки

1. Ley W., Wittman K., Hallmann W. Handbook of Space Technology, 2009. 884 p.

2. Sarafin T. P, Larson W. J. Spacecraft structures and mechanisms. From Concept to Launch, 2007. 850 p.

3. Ломакин А. А. Центробежные и осевые насосы. М. : Машиностроение, 1996. 364 с.

4. Лопастные насосы : справочник / В. А. Зимницкий и др. Л. : Машиностроение, 1986. 334 с.

5. Перевощиков С. И. Конструкция центробежных насосов (общие сведения). Тюмень : ТюмГНГУ, 2013. 228 с.

6. Малюшенко В. В., Михайлов А. К. Энергетические насосы. М. : Энергоиздат, 1981. 200 с.

7. Ярементко О. В. Испытания насосов. М. : Машиностроение, 1976. 225 с.

8. Михайлов А. К., Малюшенко В. В. Лопастные насосы. Теория, расчет и конструирование. М. : Машиностроение, 1977. 288 с.

9. Краев М. В., Лукин В. А., Овсянников Б. В. Малорасходные насосы авиационных и космических систем. М. : Машиностроение, 1985. 128 с.

10. Зленко М. А., Нагайцев М. В., Довбыш В. М. Аддитивные технологии в машиностроению. М. : НАМИ, 2015. 220 с.

11. Байбаков О. В. Применение ЭВМ в расчетах проточной полости лопастных гидромашин. М. : МГТУ им. Н.Э. Баумана, 1982. 65 с.

12. Бранштейн Л. Я. Справочник конструктора гидротурбин. М. : Машиностроение, 1971. 304 с.

13. Сазонов Ю. А., Муленко В. В., Балака А. Ю. Компьютерное моделирование и развитие методологии конструирования динамических насосов и машин // Территория нефтегаз. 2011. № 10. С. 34–36.

14. Карелин В. Я. Кавитационные явления в центробежных и осевых насосах. М. : Машиностроение, 1976. 325 с.

15. Лойцянский Л. Г. Механика жидкости и газа. М. : Дрофа, 2003. 840 с.

Kuznetsova Zoya Alekseevna – category 3 design engineer; JSC Academician M. F. Reshetnev Information Satellite Systems. E-mail: u-z-a@yandex.ru.

Sinichenko Mikhail Ivanovich – head of department; JSC Academician M. F. Reshetnev Information Satellite Systems. E-mail: smi320@iss-reshetnev.ru.

Kuznetsov Artem Dmitrievich – category 2 design engineer; JSC Academician M. F. Reshetnev Information Satellite Systems. E-mail: tember63@mail.ru.

Kleshnina Irina Aleksandrovna – category 3 design engineer, JSC Academician M. F. Reshetnev Information Satellite Systems. E-mail: kleshninaia@iss-reshetnev.ru.

Sin'kovskiy Fedor Konstantinovich – Deputy director of the Industrial Center for Large-Sized Foldable Mechanical Structures; JSC Academician M. F. Reshetnev Information Satellite Systems. E-mail: sfk@iss-reshetnev.ru.

Кузнецова Зоя Алексеевна – инженер-конструктор третьей категории; АО «Информационные спутниковые системы имени академика М. Ф. Решетнева». E-mail: u-z-a@yandex.ru.

Синиченко Михаил Иванович – начальник сектора; АО «Информационные спутниковые системы» имени академика М. Ф. Решетнева». E-mail: smi320@iss-reshetnev.ru.

Кузнецов Артем Дмитриевич – инженер-конструктор второй категории; АО «Информационные спутниковые системы» имени академика М. Ф. Решетнева». E-mail: tember63@mail.ru.

Клешнина Ирина Александровна – инженер-конструктор третьей категории; АО «Информационные спутниковые системы» имени академика М. Ф. Решетнева». E-mail: kleshninaia@iss-reshetnev.ru.

Синьковский Федор Константинович – заместитель директора – главный конструктор отраслевого центра крупногабаритных трансформируемых механических систем; АО «Информационные спутниковые системы» имени академика М. Ф. Решетнева». E-mail: sfk@iss-reshetnev.ru.

ENERGY SAVING SIMULATION TEST COMPLEX FOR SPACECRAFT POWER SUPPLIES FULL-SCALE ELECTRICAL TESTS

D. K. Lobanov, E. A. Mizrah*, L. A. Samotik, S. B. Tkachev, N. V. Shtabel

Reshetnev Siberian State University of Science and Technology
31, Krasnoyarskii rabochii prospekt, Krasnoyarsk, 660037, Russian Federation
*E-mail: enis-home@mail.ru

The aim of this paper is to describe an energy saving automatized simulation test complex used for spacecraft power supplies full-scale electrical ground-based tests. The complex allows you to simulate the operation of solar array, lithium-ion-battery and spacecraft payload. The distinctive features of the test complex are a continuous and impulse control methods combination with an improved dynamic accuracy, and recuperation of consumed energy into its internal DC network for the better energy efficiency. Test complex operational time from uninterruptible power supply accumulator batteries is significantly increased due to the recuperation of excess power into the test complex internal DC network. The results are experimentally proved.

The authors of the paper analyzed dynamic accuracy improvement and energy saving during ground-based spacecraft power system electrical tests. The process of ground-based spacecraft electrical testing includs the following tasks:

– the accurate simulation of static and dynamic characteristics of spacecraft power system energy sources and loads;

– the utilization of energy produced by power system under load and during spacecraft battery charge simulation.

The paper deals with the description of energy saving automatized simulation test complex (ESAST) including complex subsystems structure and experimental study of the test complex characteristics.

Commercially available simulation test complexes usually use continuous or impulse control methods. The continuous control methods decrease energy efficiency, as the most part of energy is dissipated on the regulator, which requires massive heat sink, increasing weight and size. It makes difficult to produce high-power test complexes. The impulse control methods provide better energy efficiency, but limit dynamics and real devices fast response reproduction accuracy. The paper describes the combination of continuous and impulse control methods with the aim of taking the advantages of both.

The energy consumed by the test complex can be utilized either by the heat dissipation in the environment or by the recuperation into industrial AC grid. The heat dissipation reduces the energy efficiency, increases the testing room temperature (in case of high-power spacecraft power system) and an air conditioning system. The recuperation into AC grid is free of specified disadvantages, but it requires the recuperated excess energy parameters matching with AC grid requirements through the network of grid-tied inverters, which leads to the increase of weight and size of the test complex. Moreover, the recuperation into AC grid is difficult during grid emergency shutdown, which can result in long test failure. The paper describes the method of excess energy recuperation into the complex internal DC network. The method significantly reduced test complex energy consumption, which in case of powering test complex from uninterruptible power supply (UPS) notably increase operating time from UPS accumulator batteries during AC grid emergency shutdown.

In conclusion the main advantages of ESAST are given:
– more than twice wattage reduction of test complex main power supply;
– the ability to work during AC grid emergency shutdown with increased operating time from UPS;
– the significant reducing of ESAST main parts weight and size.

Keywords: solar array simulator, battery simulator, electronic load, power supply system, energy saving.

ЭНЕРГОСБЕРЕГАЮЩИЙ ИМИТАЦИОННО-НАТУРНЫЙ КОМПЛЕКС ДЛЯ ЭЛЕКТРИЧЕСКИХ ИСПЫТАНИЙ СИСТЕМ ЭЛЕКТРОПИТАНИЯ КОСМИЧЕСКИХ АППАРАТОВ

Д. К. Лобанов, Е. А. Мизрах*, Л. А. Самотик, С. Б. Ткачев, Н. В. Штабель

Сибирский государственный университет науки и технологий имени академика М. Ф. Решетнева
Российская Федерация, 660037, г. Красноярск, просп. им. газ. «Красноярский рабочий», 31
*E-mail: enis-home@mail.ru

В работе рассмотрен автоматизированный энергосберегающий имитационно-натурный комплекс, предназначенный для наземных испытаний систем электропитания космических аппаратов. Комплекс позволяет имитировать работу солнечной батареи, аккумуляторной батареи и бортовой нагрузки. Отличительной особенностью комплекса является комбинирование непрерывных и импульсных методов управления и использование рекуперации потребленной энергии в собственную сеть постоянного тока с целью повышения динамической точности и повышения коэффициента полезного использования энергии. Также рекуперация в сеть постоянного тока снижает энергопотребление комплекса, что при использовании источника бесперебойного питания (ИБП) позволяет увеличить время работы комплекса от аккумуляторов ИБП.

В статье рассматриваются вопросы повышения динамической точности и снижения энергопотребления при проведении наземных электрических испытаний систем электропитания (СЭП) космических аппаратов (КА). В ходе наземных электрических испытаний СЭП КА возникают следующие задачи:

– необходимо достаточно адекватно воспроизводить статические и динамические свойства как источников энергии СЭП КА, так и потребителей;

– при энергонагружении СЭП и имитации заряда бортовой аккумуляторной батареи (АБ) необходимо утилизировать потребленную энергию.

Статья представляет собой описание автоматизированного энергосберегающего имитационно-натурного комплекса (ЭИНК), структур его подсистем, экспериментальное подтверждение характеристик. Приведен внешний вид ЭИНК.

Промышленно выпускаемые имитационно-натурные комплексы, как правило, используют непрерывные или импульсные методы управления. Использование непрерывных методов управления снижает коэффициент полезного использования энергии, поскольку относительно большая часть энергии рассеивается в виде тепла на регулирующих элементах, а также приводит к увеличению массогабаритных показателей из-за необходимости применения теплоотводов. Это затрудняет создание мощных имитационно-натурных комплексов. Использование импульсных методов управления обеспечивает высокое значение коэффициента использования энергии, однако не позволяет получить высокого быстродействия и адекватного воспроизведения быстропротекающих процессов реальных устройств. В данной статье рассмотрено комбинирование непрерывных и импульсных методов управления, что позволяет объединить их преимущества.

Для утилизации избыточной энергии в промышленно выпускаемых имитационно-натурных комплексах используется или рассеивание энергии в виде тепла или рекуперация в промышленную сеть переменного тока. Сброс избыточной энергии в виде тепла снижает коэффициент полезного использования энергии, приводит к повышению температуры в помещении (при испытании мощных СЭП), может потребовать систем вентиляции и кондиционирования воздуха. Рекуперация энергии в сеть переменного тока лишена этих недостатков. Однако она требует согласования параметров рекуперируемой энергии с требованиями промышленной сети посредством ведомых сетью инверторов, что приводит к ухудшению массогабаритных показателей комплекса. Кроме того, рекуперация в сеть переменного тока затруднена при аварийном отключении сети. Это может привести к срыву длительных испытаний. В данной статье рассмотрен метод рекуперации избыточной энергии в собственную сеть постоянного тока комплекса. При этом снижается энергопотребление комплекса, что при использовании источников бесперебойного питания (ИБП) повышает время работы ЭИНК от аккумуляторов ИБП при аварийном отключении сети переменного тока.

В выводах статьи подчеркивается, что разработанный ЭИНК обладает следующими преимуществами:

– возможность уменьшения мощности источника электропитания комплекса минимум в два раза;

– сохранение работоспособности и увеличение длительности работы от источника бесперебойного питания при отключении промышленной сети переменного напряжения;

– существенное уменьшение массы и габаритов составных частей ЭИНК.

Ключевые слова: имитатор солнечной батареи, имитатор аккумуляторной батареи, нагрузочное устройство, система электропитания, энергосбережение.

Introduction. The automatized simulation test complex (AST)), which contain simulators of the primary energy source (solar battery), rechargeable battery (RB), and various load devices are used to carry out the ground-based tests of the power supply systems (PS) of the spacecraft (SC). To ensure the required test quality the simulators must reproduce the static and dynamic characteristics of the prototypes with a sufficiently high accuracy.

While creating AST of powerful (more than 10 kW) SC power systems and conducting long-term (resource) tests two problems arise:

– to ensure the required accuracy of simulating the static and dynamic characteristics of power sources of the PS, which is important for the adequacy of the tests performed;

– to save energy and reduce the heat generation of the complex subsystems , which is important for improving the functional and operational characteristics of the complex, its weight and dimension.

In the existing AST, the first problem is solved by applying continuous control laws [1–3], which leads to a low coefficient of electricity use (no more than 50 %) and, as a result, to a large heat emission.

While solving the second problem, the pulse control methods [4] and power recovery to the AC network are used. At the same time, the dynamic characteristics of simulators worsen, while meeting the requirements for the quality of electricity, the recuperator schemes become more complicated and their cost increases. To improve the quality of complex power supply the uninterruptible power supplies (UPS) have been used lately. But even in this case the significant disadvantage of this method is that, when the AC power is switched off in an emergency, recovery becomes impossible.

In this paper, we propose the solution of these problems: providing the required dynamic properties and increasing energy use in high-power AST

For the solution of the problems with the energy-saving AST (ESAST) developed by the authors the new approaches are used:

– the combination of pulse and continuous control methods for simulators of power installations and subsystems of PS, which allows to increase the coefficient of electricity use and provide the required dynamic properties of simulators;

– the recovery of excess power of the load devices in the DC circuit of the complex power supply system , which allows to increase the of electricity use rate, reduce power consumption from the AC mains and the capacity of the power source of ESAST and increase the working time of ESAST from the battery when you unplug the AC.

The proposed device structure. Fig. 1 shows a block diagram of the ESAST [5], which explains the use of the electricity recovery method in the DC network.

In the first mode of operation (the illuminated section of the SC flight path, the RB charge), the PS receives electricity from the SAS and supplies the load and the LibS charge. LDER sets the power loading mode of the PS and returns the consumed energy to the general DC power supply network of the ESAST. The LibS operates in the RB charge simulation mode and recovers excess energy to the general DC power supply network of the ESAST.

In the second mode of operation of the PS (the shadow section of the flight path of the SC), the SAS stops power supply to the PS. The LibS operates in the RB discharge simulation mode and provides power to the PS. LDER

sets the power loading mode of the PS and returns the consumed energy to the general DC power supply network of the ESAST.

In the third mode of operation (the illuminated section of the SC flight path, the peak power consumption), the PS is powered from the SAS and the LibS together. The LibS also, as in the previous case, operates in the RB discharge simulation mode. LDER sets the power loading mode of the PS and returns the consumed energy to the general DC power supply network of the ESAST.

The following advantages of the ESAST structure should be considered: a relatively simple implementation of LDER, recovering the consumed energy in single SAS and LibS power supply, and relatively high specific energy characteristics of LibS using a bidirectional switching converter (PC).

The combination of pulse and continuous simulators control methods, which allows providing high dynamic characteristics with relatively high energy efficiency, is as follows. Simulators (SAS, LibS and LDER) contain high-speed continuous regulators that regulate the output parameter of the simulator (voltage, current, power, etc.), and pulse regulators that limit the power dissipation on continuous regulators and increase the energy efficiency.

The solar array simulator. The basis of the SAS (fig. 2) is a continuous current stabilizer with the parallel control element (ACE) switching on. The CCS consists of the following devices: ACE, SA1, and CS1. To reproduce the required nonlinear current-voltage characteristics of the SB, the continuous current stabilizer (CCS) is covered by functional voltage feedback (FFD). The use of a pulsed current stabilizer (PCS) for the current flowing through the ACE allows us to limit the power dissipated by the ACE. The PCS consists of the following devices: PC, PWM, SA2, CS2, Vref.

The principle of operation of the SAS: SA1 compares the voltage with CS1, proportional to the output current of the SAS, with the voltage at the output of the FFD and generates a control signal for the ACE. The FFD generates a set point for the continuous current stabilizer in accordance with the specified current-voltage characteristic and the current voltage value measured by the VD. SA2 compares with the reference (Vref) voltage proportional to the current through the ACE obtained from the CS2, and generates a control signal for the PC proportional to the deviation of the current through the ACE from the required value.

The lithium-ion-battery simulator (LibS). The basis of the Lithium-ion-battery simulator structure (fig. 3) [6] is a continuous voltage stabilizer with parallel switching on the ACE. The continuous voltage stabilizer consists of the following devices: ACE, SA1, VD to reproduce the required nonlinear charge-discharge characteristics of the AB, the continuous voltage stabilizer is covered by functional current feedback (CS). The use of a pulsed current stabilizer for current flowing through the ACE allows you to limit the power dissipated by the ACE. Pulsed current stabilizer consists of the following devices: BPC, PWM, SA2, CS2, Vref.
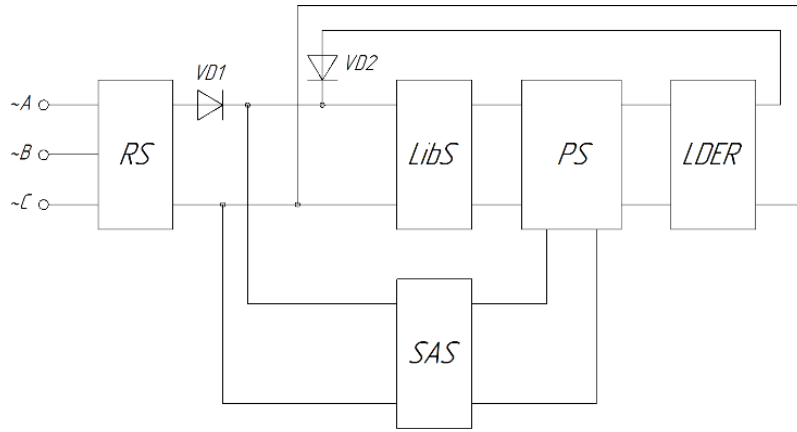
Fig. 1. ESAST structure:
RS – rectifier stabilizer; SAS – Solar array simulator;
PS – tested power supply; LDER – load device with energy
recuperation; LibS – Lithium-ion-battery simulator

Рис. 1. Структурная схема модуля ЭИНК:
ВС – выпрямитель-стабилизатор; ИСБ – имитатор солнечной
батареи; СЭП – испытываемая система электропитания;
НУРТ – нагрузочное устройство рекуперативного типа;
ИАБ – имитатор аккумуляторной батареи

Fig. 2. Solar array simulator structure (SAS):
PC – pulse converter; PWM – pulse width modulator; SA – summing amplifier;
Vref – voltage reference; ACE – analogue control element; FFD – functional feedback;
VD – voltage divider; CS – current sensor

Рис. 2. Структурная схема ИСБ:
ИП – импульсный преобразователь; ШИМ – широтно-импульсный модулятор;
УС – усилитель-сумматор; ИОН – источник опорного напряжения;
НРЭ – непрерывный регулирующий элемент; УФОС – устройство функциональной
обратной связи; ДН – датчик напряжения; ДТ – датчик тока

The operating principle of the LibS: SA1 compares the voltage with the VD, proportional to the output voltage of the LibS, with the voltage of the FFD and generates a control signal for the ACE. The FFD generates a set point for continuous voltage stabilizer in accordance with the specified charge-discharge characteristic (CDC) and the state of charge measured by the AHS. SA2 compares the voltage proportional to the current through the ACE obtained from the CS2 with the reference one and generates a control signal for the BPC proportional to the deviation of the current through the ACE from the required value.

Load device with energy recuperation. The LDER basis (fig. 4) is the continuous current stabilizer with parallel inclusion of the ACE. The continuous current stabilizer consists of the following devices: ACE, SA1, and CS1.

To reproduce the required nonlinear current-voltage characteristics of the simulated load, the CCS is covered by functional voltage feedback (FFD). The use of a pulsed current stabilizer (PCS) flowing through the ACE allows you to limit the power dissipated by the ACE. Pulsed current stabilizer consists of the following devices: PC, PWM, SA2, CS2, Vref.

The principle of operation of the LDER: SA1 compares the voltage with CS1, proportional to the input current of the LDER, with the voltage at the output of the FFD and generates a control signal for the ACE. The FFD generates a set point for the continuous current stabilizer in accordance with the specified VAC and the current voltage value measured by the VD. SA2 compares the voltage proportional to the current through the ACE obtained from the CS2 with the reference one and generates a control signal for the PC proportional to the deviation of the current value through the ACE from the required value.

Energy-saving simulation and full-scale complex. ESAST developed by the authors (fig. 5) contains: SAS, LibS, LDER, high-speed protection device (HSPD), spe-cialized hardware and software complex (HSC). The SAS module consists of 4 independent channels that allow both parallel, serial connection of two channels and mixed connections. Each channel provides: the no-load voltage changing from 20 to 200 V; the short-circuit current from 0.1 to 7 A changing; the VAC shape setting mathemati-cally, using a table, slopes for voltage and current branches and a non-linear transition zone; changing the output capacitance from 500 to 1000 nF with a step of 100 nF.

The module of the lithium-ion battery simulator (LibS) includes the following blocks: simulation of charge-discharge characteristics of the LibS; simulation of analog voltage sensors changes of each battery; simula-tion of analog temperature sensors.
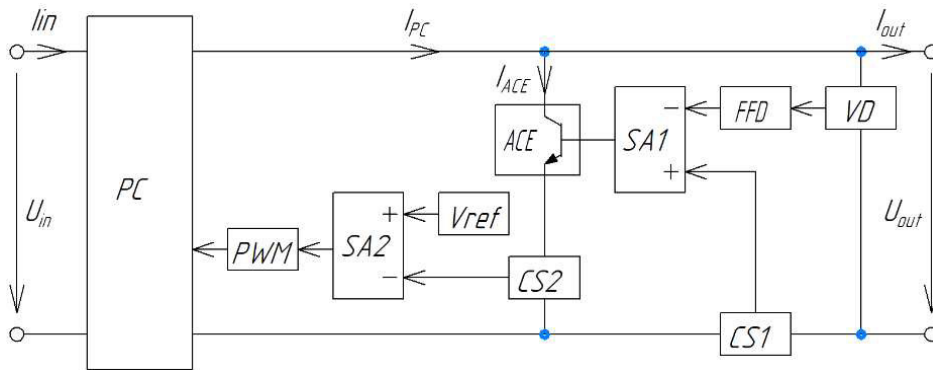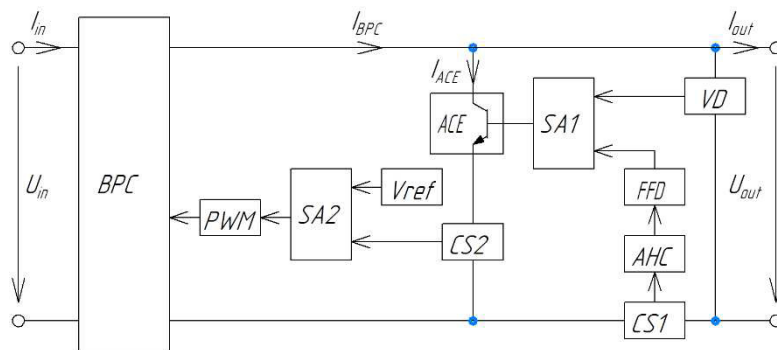

Fig. 3. Lithium-ion-battery simulator structure:
BPC – bi-directional pulse converter; PWM – pulse width modulation; SA – summing
amplifier; Vref – voltage reference; ACE – analogue control element; CS – current sensor;
VD – voltage divider; FFD – functional feedback; AHC – amp hours counter

Рис. 3. Структурная схема ИАБ:
ДИП – двунаправленный импульсный преобразователь; ШИМ – широтно-импульсный
модулятор; УС – усилитель-сумматор; ИОН – источник опорного напряжения;
ДТ – датчик тока; НРЭ – непрерывный регулирующий элемент; ДН – датчик напряжения;
УФОС – устройство функциональной обратной связи; САЧ – счетчик ампер-часов
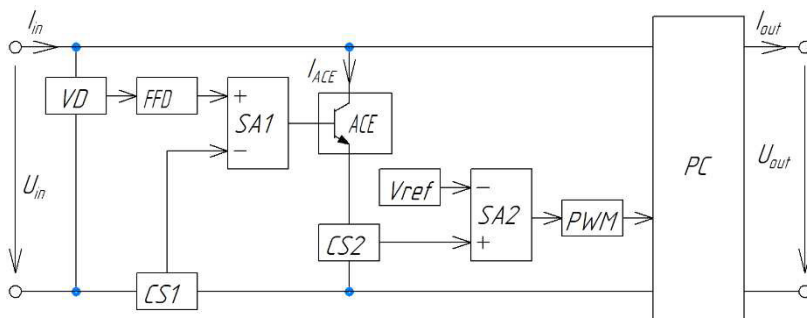
Fig. 4. Structure of load device with energy recuperation:
PC – converter; PWM – pulse width modulation; SA – summing amplifier;
Vref – voltage reference; ACE – analogue control element; FFD – functional feedback;
VD – voltage divider; CS – current sensor

Рис. 4. Структурная схема НУРТ:
ДН – датчик напряжения; ДТ – датчик тока; УФОС – устройство функциональной
обратной связи; УС – усилитель-сумматор; НРЭ – непрерывный регулирующий
элемент; ИОН – источник опорного напряжения; ШИМ – широтно-импульсный
преобразователь; ИП – импульсный преобразователь
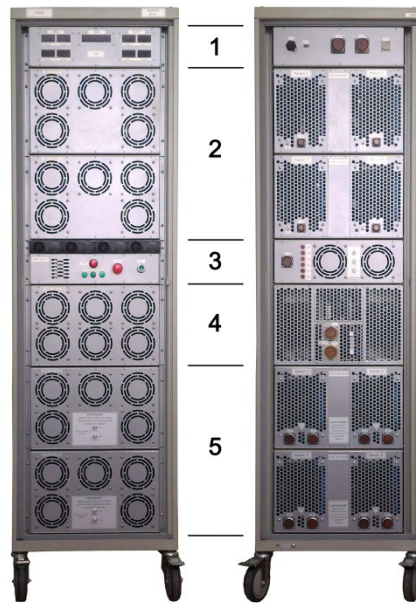
Fig. 5. ESAST:
1 – Hardware and software complex; *2* – Four SAS channels;
3 – PS; *4* – LibS; *5* – four LDER channels

Рис. 5. Внешний вид ЭИНК:
1 – АПК; *2* – четыре канала ИБС; *3* – источник электропитания;
4 – ИАБ; *5* – четыре канала НУРТ

The LibS module provides: changing the voltage from 10 to 105 V; changing the charge current from 0 to 25 A; the discharge current changing from 0 to 70 A; the shape of the charge discharge characteristics (CDC) setting mathematically, using a table; changing the active component of the internal resistance from 5 mohm to 50 mohm, the inductive component – from 8 mgN to 80 mgN.

The LDER module contains 4 independent channels that allow both parallel, serial connection of two channels and mixed connections. LDER provides: maximum channel power of 1500 W; voltage change from 20 to 120 V; current change from 0.1 to 20 A; guidance of harmonic interference with an amplitude of 5 A in the band up to 300 kHz.

To confirm the effectiveness of the pilot images of the main subsystems ESAST a comparative analysis of the technical and price characteristics of subsystems EINK modular characteristics of the subsystems of foreign companies [7–9] and energy saving subsystems of the test systems manufactured was carried out by NIIAM TUSUR (The Research Institute of Automation and Electro mechanics) [10–12], the testing equipment for spacecraft production leader in Russia.

It should be noted that the main advantages of the EINK with the recovery of excess electricity to the DC network of the power supply system of the complex are:

– the ability to reduce at least twice the power source force of the complex;

– keeping the operability and increasing the operation duration from an uninterruptible power supply when the industrial AC network is disconnected;

– the significant mass and dimension reduction of the ESAST components.

Tab. 1 shows the technical characteristics of lithium-ion battery simulators: BIAB-200LI [10], manufactured by NIIEM –TUSUR, Tomsk; LibS with two modules parallel connection, manufactured by Reshetnev Siberian State University of Science and Technology, Krasnoyarsk and a battery simulator manufactured by AMETEK [7], USA.

Tab. 1 shows that the main technical characteristics of the Libs developed by Reshetnev Siberian State University are at the same level, and in terms of weight and size characteristics it is even ahead.

Tab. 2 shows the technical characteristics of simulators of solar cells of comparable capacity: SAS-200/7-4 [11], produced by NIIEM –TUSUR, Tomsk; ISB-200-4K with parallel connection of two modules, produced by Reshetnev Siberian State University, Krasnoyarsk and E4360 Keysight Technologies [8] with parallel connection of four modules containing eight channels.

Tab. 2 shows that in terms of technical characteristics and functions the SAS developed by Reshetnev Siberian State University occupies the intermediate position between the SAS produced by TUSUR and Keysight Technologies. The Keysight Technologies SAS disadvantages are the greater heat capacity when working on the current branch WAC , the WAC insufficient slope on the branch voltage, determined by the value of series resistance RS, low voltage-170V.

Tab. 3 shows comparable in power load device simulators technical characteristics: BIN-100 [12], produced by NIIEM-TUSUR, Tomsk; NUK-120-4K with parallel

connection of two modules, produced by Reshetnev Siberian State University, Krasnoyarsk and EA-ELR 9250-70 Elektro-Automatik [9], Germany.

Elektro-Automatik load devices have good weight and size characteristics, but the reason is ,that the function of directing test sinusoidal and pulse currents on the buses of power sources is limited to a frequency band not exceeding several kilohertz by the use of pulse converters. It is necessary to increase the frequency band to hundreds of kilohertz and measure the impedance frequency characteristics of power sources in order to study the noise immunity, while the use of continuous load devices is required, which significantly worsens the weight and size characteristics of the devices. This is illustrated by the load devices production TUSUR and Reshetnev Siberian State University.

Table 1

Energy and mass-dimensional characteristics of lithium-ion battery simulators

№	Parameter	Dimention	BIAB-200LI NIIEM TUSUR	Libs Reshetnev Siberian State University	Battery String Simulator, AMETEK
1	Charge/ discharge voltage range	Volt	40–110	10–120	120
2	The maximum power in the discharge mode	Watt	12000	14700	18000
3	Discreteness of charge/discharge voltage adjustment	Volt	0.1	0.1	No data
4	The magnitude of the output voltage ripple, not more	мVolt	50	500	No data
5	Maximum charging current	Amp	30	50	50
6	Maximum chargig current	Amp	200 voltage not more than 60 Volt. 109 voltage 110 В	140 over entire voltage range	150
7	Charge/discharge characteristics simulation	---	no	yes	no
8	Recuperation in charge mode	---	no	yes	no
9	Voltage sensors simulation	---	yes	yes	yes
10	Temperature sensors simulation	---	yes	yes	yes
13	Specific volume	m^3/Watt	79.56×10^{-6}	16.46×10^{-6}	114.76×10^{-6}
14	Specific gravity	kg/Watt	33.33×10^{-3}	8.84×10^{-3}	31.25×10^{-3}

Table 2

Energy and mass-dimensional characteristics of lithium-ion battery simulators

№	Parameter	Dimention	SAS-200/7-4TUSUR	SAS-200-4К Reshetnev Siberian State University	E4360 Keysight Technologies
1	Control range Uxx	Volt	40–210	20–210	20–170
2	Adjustment discreteness	Volt	0.1	0.1	0.048
3	Single-channel icz current adjustment range	Amp	0-8	0–7	0–3.8
4	Icz current adjustment discretness	Amp	0.01	0.01	0.0012
5	VAC reproduction error	%	5	2	No data
6	Frequency band for admittance playback	Гц Hz	No data	100000	No data
7	Frequency band for admittance playback not more	%	No data	5	No data
8	Resistance serial RS minimum	Ом Om	0.3	0.3	1.72
9	Specific volume	m^3/Watt	87.71×10^{-6}	43.20×10^{-6}	30.36×10^{-6}
10	Specific gravity	kg/Watt	32.74×10^{-3}	16.43×10^{-3}	14.75×10^{-3}

Table 3

Energy and mass-dimensional characteristics of the regenerative-type load devices

№	Parameter	Dimention	BIN-100 TUSUR	NUK-120-4K Reshetnev Siberian State University	EA-ELR 9250-70 Elektro-Automatik
1	Maximum input voltage	Volt	100	120	250
2	Input current range	Amp	0–65	0–80	0–70
3	Adjustment discreteness	Amp	0.01	0.01	No data
4	Range of sinusoidal load test current	Amp	0–15	0–16	No data
5	Adjustment discreteness	Amp	0.1	0.1	No data
6	Frequency range of the test signal	кГц kHrz	0.02–100	0–300	No data
7	Constant resistance load simulation	---	no	yes	yes
8	Constant power load simulation	---	no	yes	yes
9	Recovery of excess energy	---	To the industrial AC network	To the DC network of the test complex	To the industrial AC network
10	The ability to work when disconnecting the commercial power supply AC voltage	---	No, without additional devices	yes	no
11	Specific volume	m^3/Watt	90.68×10^{-6}	40.32×10^{-6}	22.36×10^{-6}
12	Specific gravity	kg/Watt	33.85×10^{-3}	18.33×10^{-3}	9.72×10^{-3}

Conclusion: The main subsystems of the ESAT developed by Reshetnev Siberian State University in most parameters are at the world manufacturer technical characteristics level, and in a number of functions it is sometimes higher. In particular, it concerns the dynamic properties: the frequency band for reproducing the AB impedance, the SB admittance, the frequency range for inducing the test current of the sinusoidal form of the LDER, and the power utilization coefficient.

References

1. Keysight E4350B, E4351B Modular Solar Array Simulators Datasheet. Available at: https://www.keysight.com/ru/pc-1000000530%3Aepsg%3Apgr/e4350b-e4351b-solar-array-simulators?nid=-32610.0.00&cc=RU&lc=rus. (accessed 02.03.2020).

2. Elgar Solar Array Simulator. Available at: https://www.powerandtest.com/power/engineered-systems/solar-array-simulator (accessed 02.03.2020)

3. Haeberlin H. et al. Development of a fully automated PV array simulator of 100 kW. *23rd European Photovoltaic Solar Energy Conference*, Valencia, Spain, Sept. 2008

4. Martín-Segura G. et al. Development of a photovoltaic array emulator system based on a full-bridged structure. *Electrical Power Quality and Utilisation (EPQU) 9th International Conference on*. 2007, Vol. 4, Iss. 2, P. 1–6.

5. Mizrakh E. A., Balakirev R. V., Lobanov D. K., S. B. Tkachev, A. S. *Fedchenko. Kompleks dlya nazemnykh ispytaniy sistem elektropitaniya kosmicheskikh apparatov* [Groundbased test complex for spacecraft power supplies tests]. Patent RF, no. 159208, 2016.

6. Mizrakh E. A., Balakirev R. V., Lobanov D. K., Shtabel' N. V., Poymanov D. N. *Elektricheskiy imitator akkumulyatornoy batarei s zashchitoy po toku i napryazheniyu i ustroystvo zashchity elektricheskogo imitatora akkumulyatornoy batarei* [Electric battery simulator with current and voltage protection and protection device for electric battery simulator]. Patent RF, no. 2635897, 2017.

7. Elgar Battery String Simulators. Available at: https://www.powerandtest.com/power/engineered-systems/battery-string-simulator (accessed 02.03.2020)

8. Keysight E4360 Modular Solar Array Simulators. Available at: https://www.keysight.com/ru/pc-1367756/e4360-modular-solar-array-simulators?pm=LB&nid=-34612.0&c=181710.i.1&to=79830.g.0&cc=RU&lc=rus (accessed 02.03.2020)

9. Keysight E4360 Modular Solar Array Simulators. Available at: https://www.keysight.com/ru/pc-1367756/e4360-modular-solar-array-simulators?pm=LB&nid=-34612.0&c=181710.i.1&to=79830.g.0&cc=RU&lc=rus (accessed 02.03.2020)

10. *Nauchno-issledovatel'skiy institut avtomatiki i elektromekhaniki TUSUR. Blok imitatsii litiy-ionnoy akkumulyatornoy batarei BIAB-200LI* [Research Institute of Automatics and Electromechanics TUSUR. The simulation unit of the lithium-ion battery BIAB-200LI]. Available at: : http://niiaem.tomsk.ru/product/biab/biab-200li.html (accessed 02.03.2020).

11. Nauchno-issledovatel'skiy institut avtomatiki i elektromekhaniki TUSUR [Research Institute of Automatics and Electromechanics TUSUR.]. Available at: http://niiaem.tomsk.ru/product/ibs/ibs-200.htm (accessed 02.03.2020).

12. *Nauchno-issledovatel'skiy institut avtomatiki i elektromekhaniki TUSUR. Blok imitatsii nagruzki BIN-100* [Research Institute of Automatics and Electromechanics TUSUR. Load Simulation Unit BIN-100]. Available at: http://niiaem.tomsk.ru/product/in/bin-100.html (accessed 02.03.2020).

Библиографические ссылки

1. Keysight E4350B, E4351B Modular Solar Array Simulators Datasheet [Электронный ресурс]. URL: https://www.keysight.com/ru/pc-1000000530%3Aepsg%3Apgr/e4350b-e4351b-solar-array-simulators?nid=-32610.0.00&cc=RU&lc=rus. (дата обращения 02.03.2020).

2. Elgar Solar Array Simulator [Электронный ресурс]. URL: https://www.powerandtest.com/power/engineered-systems/solar-array-simulator (дата обращения 02.03.2020).

3. Development of a fully automated PV array simulator of 100 kW / H. Haeberlin, L. Borgna, D. Gfeller, P. Schaerf, U. Zwahlen // 23rd European Photovoltaic Solar Energy Conference, Valencia, Spain, Sept. 2008

4. Development of a photovoltaic array emulator system based on a full-bridged structure / G. Martín-Segura, J. López-Mestre, M. Teixidó-Casas, A. Sudrià-Andreu // Electrical Power Quality and Utilisation (EPQU) 9th International Conference on. 2007. Vol. 4, Iss. 2. P. 1–6.

5. Пат 159208 РФ. МПК G01R 31/00. Комплекс для наземных испытаний систем электропитания космических аппаратов / Мизрах Е. А., Балакирев Р. В., Лобанов Д. К., Ткачев С. Б., Федченко А. С. (RU) № No 2015145047/28 ; заявл. 20.10.15 ; опубл. 10.02.16, Бюл. No 4.

6. Пат 2635897 РФ. МПК G06G 7/48. Электрический имитатор аккумуляторной батареи с защитой по току и напряжению и устройство защиты электрического имитатора аккумуляторной батареи / Мизрах Е. А., Лобанов Д. К., Пойманов Д. Н., Балакирев Р. В., Копылов Е. А., Штабель Н. В. (RU) № No 20161489828 ; заявл. 13.12.16 ; опубл. 16.11.17, Бюл. No 32.

7. Elgar Battery String Simulators [Электронный ресурс]. URL: https://www.powerandtest.com/power/ engineered-systems/battery-string-simulator (дата обращения 02.03.2020).

8. Keysight E4360 Modular Solar Array Simulators [Электронный ресурс]. URL: https://www.keysight.com/ru/pc-1367756/e4360-modular-solar-array-simulators?pm=LB&nid=-34612.0&c=181710.i.1&to=79830.g.0&cc= RU&lc=rus (дата обращения 02.03.2020).

9. Keysight E4360 Modular Solar Array Simulators [Электронный ресурс]. URL: https://www.keysight.com/ru/pc-1367756/e4360-modular-solar-array-simulators?pm=LB&nid=-34612.0&c=181710.i.1&to=79830.g.0&cc=RU&lc=rus (дата обращения 02.03.2020).

10. Научно-исследовательский институт автоматики и электромеханики ТУСУР. Блок имитации литий-ионной аккумуляторной батареи БИАБ-200ЛИ. [Электронный ресурс]. URL: http://niiaem.tomsk.ru/product/biab/biab-200li.html (дата обращения 02.03.2020).

11. Научно-исследовательский институт автоматики и электромеханики ТУСУР. [Электронный ресурс]. URL: http://niiaem.tomsk.ru/product/ibs/ibs-200.htm (дата обращения 02.03.2020).

12. Научно-исследовательский институт автоматики и электромеханики ТУСУР. Блок имитации нагрузки БИН-100 [Электронный ресурс]. URL: http://niiaem.tomsk.ru/product/in/bin-100.html (дата обращения 02.03.2020).

Lobanov Dmitriy Konstantinovich – Cand. Sc., Automatic control systems department assistant professor; Reshetnev Siberian State University of Science and Technology. E-mail: u649@yandex.ru.

Mizrah Enis Avrumovich – Cand. Sc., Automatic control systems department professor; Reshetnev Siberian State University of Science and Technology. E-mail: enis-home@mail.ru.

Samotik Lyudmila Arkad'evna – postgraduate student, engineer; Reshetnev Siberian State University of Science and Technology. E-mail: antikodona@gmail.com.

Tkachev Stepan Borisovich – master student, lead engineer; Reshetnev Siberian State University of Science and Technology. E-mail: steep_st@mail.ru.

Shtabel Nikolay Vladimirovich – master student, lead engineer; Reshetnev Siberian State University of Science and Technology. E-mail: shtabnik@gmail.com.

Лобанов Дмитрий Константинович – кандидат технических наук, доцент кафедры систем автоматического управления; Сибирский государственный университет науки и технологий имени академика М. Ф. Решетнева. E-mail: u649@yandex.ru

Мизрах Енис Аврумович – кандидат технических наук, доцент, профессор кафедры систем автоматического управления; Сибирский государственный университет науки и технологий имени академика М. Ф. Решетнева. E-mail: enis-home@mail.ru.

Самотик Людмила Аркадьевна – аспирант, инженер научно-исследовательского управления; Сибирский государственный университет науки и технологий имени академика М. Ф. Решетнева. E-mail: antikodona@gmail.com.

Ткачев Степан Борисович – магистрант, ведущий инженер; Сибирский государственный университет науки и технологий имени академика М. Ф. Решетнева. E-mail: antikodona@gmail.com.

Штабель Николай Владимирович – магистрант, ведущий инженер; Сибирский государственный университет науки и технологий имени академика М. Ф. Решетнева. E-mail: shtabnik@gmail.com.

DETERMINATION OF THE DIGITAL CONTROLLER'S CHARACTERISTICS OF THE SWITCHED-MODE POWER CONVERTERS

A. A. Lopatin, A. A. Druzhinin*, A. S. Asochakov, A. V. Puchkov

JSC Academician M. F. Reshetnev Information Satellite Systems
52, Lenin St., Zheleznogorsk, Krasnoyarsk region, 662972, Russian Federation
*E-mail: Alex-Druzh@mail.ru

The development of spacecrafts equipment is on the way to digitalization. In particular, energy spacecraft conversion devices are being modernized by introducing digital automatic control systems instead of analog ones. This leads to an increase in the efficiency of the power supply system, but at the same time, there is a need to create methods to determine characteristics that will confirm with a high degree of accuracy and conformity of the manufactured sample with the technical requirements specified during its design. The article describes the features of functioning and methodology for determining digital control channel of a pulse voltage converter's characteristics. The proposed approach is a toolkit for verifying the correct implementation of both the hardware parts of the control channel and the controller, which is a program code implemented on digital control devices. The technique is based on determining the degree of responses correspondence to typical external influences of a hardware-implemented control channel and its model. Based on the transfer functions of the IIR and FIR digital filters, using standard built-in models, the control channel of the pulse voltage converter corresponding to the tested hardware-implemented device is simulated in the package Matlab Simulink. The basic principles of building the software architecture experiment are described. A block diagram of the test complex has been developed, including sources of external influence, control channel, and a test management tool (in this case, a personal computer). An example of applying such a technique to verify the parameters of the developed PID controller is given. Operability and accuracy of the proposed method to determine characteristics of the control channel by reaction to a sequence of rectangular pulses, and by constructing the AFCL are experimentally shown. Application of this verification method to production conditions will allow a complete check of individual central control units (CCU) of energy-converting equipment with closed feedbacks even at the stage of devices development, which will eliminate errors in the implementation of regulators in control loops.

Keywords: testing, pulse voltage converter, digital controller, reference model, response, typical input.

ОПРЕДЕЛЕНИЕ ХАРАКТЕРИСТИК ЦИФРОВЫХ РЕГУЛЯТОРОВ ИМПУЛЬСНЫХ ПРЕОБРАЗОВАТЕЛЕЙ НАПРЯЖЕНИЯ

А. А. Лопатин, А. А. Дружинин*, А. С. Асочаков, А. В. Пучков

АО «Информационные спутниковые системы» имени академика М. Ф. Решетнева»
Российская Федерация, 662972, г. Железногорск Красноярского края, ул. Ленина, 52
*E-mail: Alex-Druzh@mail.ru

Развитие космического приборостроения идет по пути цифровизации. В частности, энергопреобразующая аппаратура космических аппаратов модернизируется путем внедрения цифровых систем автоматического управления взамен аналоговых. Это приводит к повышению эффективности системы электропитания, но в то же время возникает необходимость в создании способов определения их характеристик, которые позволят с высокой степенью точности подтвердить соответствие изготовленного прибора заданным при проектировании требованиям технического задания. В статье описаны особенности функционирования и предложен способ определения характеристик цифрового канала управления импульсным преобразователем напряжения. Предложенный подход представляет собой инструментарий для проверки правильности реализации как аппаратных частей канала управления, так и самого регулятора, представляющего собой программный код, реали-

зованный на цифровых управляющих устройствах. Метод основан на определении степени соответствия откликов на типовые внешние воздействия аппаратно реализованного канала управления и его модели. На основе передаточных функций цифровых фильтров с бесконечной импульсной характеристикой и конечной импульсной характеристикой, с использованием типовых встроенных моделей, в пакете имитационного моделирования Matlab Simulink смоделирован канал управления импульсным преобразователем напряжения, соответствующий испытываемому аппаратно-реализованному устройству. Описаны основные принципы построения программной архитектуры обеспечения эксперимента. Разработана структурная схема испытательного комплекса, включающая источники внешнего воздействия, сам канал управления и средство управления проведением испытаний (в данном случае персональный компьютер). Приведен пример применения такой методики для верификации параметров разработанного пропорционально-интегрального дифференциального регулятора. Экспериментально показана работоспособность и точность предложенного способа определения характеристик канала управления по реакции на последовательность прямоугольных импульсов и путем построения логарифмической амплитудно-фазовой частотной характеристики. Применение такого метода верификации в условиях производства позволит обеспечить полную проверку отдельных цифровых управляющих устройств энергопреобразующей аппаратуры с замкнутыми обратными связями еще на этапе разработки приборов, что позволит исключить ошибки в реализации регуляторов в контурах управления.

Ключевые слова: тестирование, импульсный преобразователь напряжения, цифровой регулятор, эталонная модель, отклик, типовое воздействие.

Introduction. Operation of space technology devices has its own specific features, which combine high cost of failure, inability to repair, and a long period of continuous operation under conditions of outer space radiation exposure. In this regard, all devices that are designed for space technology go through a full cycle of checks and tests, which differ in terms of regulations, physical nature, and magnitude of disturbing effects. To ensure reliability and quality of the equipment produced, a multi-stage verification of the device is applied, which includes tests according to a hierarchical system [1]. This is how the parameters of all electrical components used are checked, tested for compliance with technical specifications requirements: first the individual units of the device, then the device autonomously as a part of the spacecraft (SC). Today, space technology is actively developing and modernizing. In this regard, development of methods for testing onboard equipment remains an important task.

One of the lines of space technology development is modernization of power supply system, and, in particular, energy-converting equipment. Improvements of microelectronics and electronic component base allowed to start introducing microprocessor systems to control the processes of voltage and current stabilization and regulation of the power bus. Digital control systems (CS) have a number of advantages over analog systems, among them the flexibility of setting parameters and independence of characteristics from external climatic influences [2], which is an important property for long-term operation in conditions of external impact factors of outer space.

Introduction of digital controllers in microprocessor systems sets the task of developing methods for determining their characteristics. Methods for characterizing analog regulators are widely known. Analog regulators are operational amplifiers with external feedback reactance. Elements used for regulators undergo input control of parameters and a series of electrical and temperature tests aimed at revealing the drift of parameters. The regulator is then subjected to electrical and functional tests. A digital controller, in contrast to an analogue one, is a program code for a digital control device (DCD), consisting of the operations of storing the values of variables, multiplications by constants and additions [3]. While a microprocessor system is used to control a pulse voltage converter, the input signal – a feedback signal (feedback) for a digital controller is converted using an analog-to-digital converter (ADC), and the output signal is formed using a digital pulse-width modulator (DPWM). Since the approach to the physical implementation of digital and analog controllers is significantly different, the test methods applied to the control channel of an analog system are not suitable for testing the microprocessor system.

In this regard, this work proposes a method for determining characteristics of a switched-mode power supply (SMPS) control channel. The proposed method was verified during IIT prototype testing.

First, a description of the test object will be given, which is a control channel of a SMPS, its features will be highlighted based on which the approach to its testing is developed. Next, the method for determining parameters is explained – which software is needed to implement the proposed method, and features of the test complex functioning are explained. The next step is results of experimental verification of the proposed method, by determining the degree of correspondence of the hardware-implemented control channel of the IIT characteristics with the results of simulation.

Test object. The object of testing is the channel of SMPS digital control system, which is shown in fig. 1.

The control channel consists of a sensor, an analog-to-digital converter, an error signal generator, a digital controller and a pulse-width modulator [4].

Operation of control channel can be described as follows. A signal representing the value of physical quantity is coming from the sensor. This signal is digitized by the ADC and fed to the input of the error signal generator. The digitized signal is subtracted from the reference signal, resulting in an error signal. The error signal is processed by a digital controller which calculates the control signal. The control signal goes to the digital pulse width modulator (DPWM).
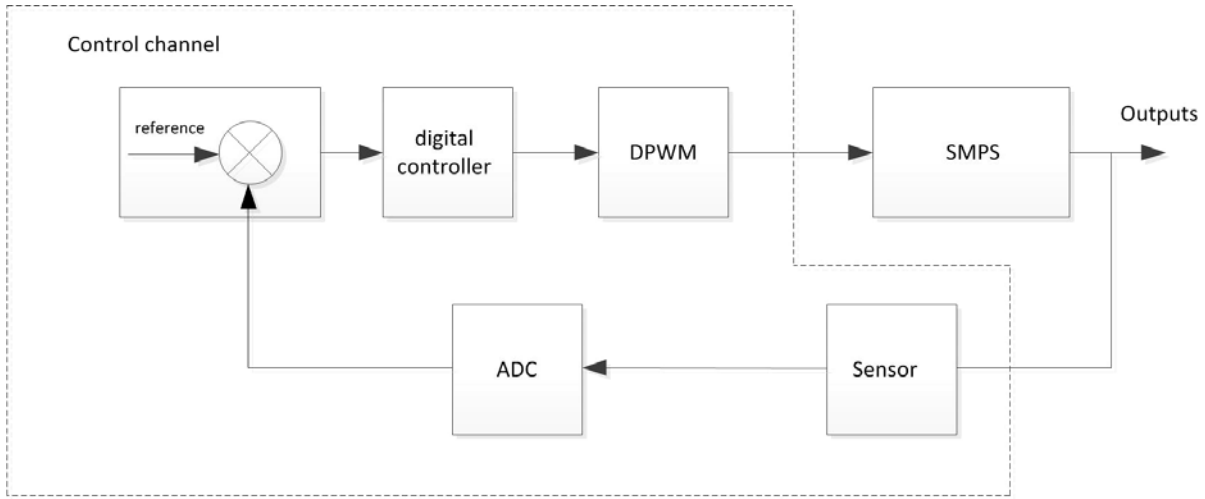
Fig. 1. Pulse converter control channel

Рис. 1. Канал управления импульсным преобразователем

There are several ways to implement a control channel [5]. It can be a microcontroller or digital signal processor (DSP) with built-in ADCs, regulators and DPWMs, or it can be a field-programmable gate array (FPGA) on which the regulator and DPWMs are made, and the ADC is an external device. However, the testing approach will be identical.

The main testing element is the digital regulator. As a mathematical object, the regulator is a digital filter with an infinite impulse response (IIR – filter), or a digital filter with a finite impulse response (FIR – filter) [6]. Formulas of transfer functions IIR (1) and FIR (2) filters in general form are given below.

$$D(z) = \frac{\sum\limits_{i=0}^{N-1} b_i \cdot z^{-i}}{1 + \sum\limits_{k=1}^{M-1} a_k \cdot z^{-k}}, \qquad (1)$$

$$D(z) = \sum\limits_{i=0}^{N-1} b_i \cdot z^{-i}, \qquad (2)$$

where b_i, a_k are regulator coefficients, z^{-i} is the delay element per cycle of the regulator operation.

The digital filter, depending on the structure and values of coefficients, has a number of static and dynamic characteristics that are unique for a given filter [7]. This property is well manifested by determining the response to typical inputs, including stepwise, impulse and harmonic effects. All outputs will also be unique to this filter. Based on this property, a methodology for checking the control channel will be built.

Since the controller is a program code consisting of the simplest arithmetic operations, it can be simulated in the Matlab Simulink simulation system. The methods for modeling digital filters in this program are well known and have shown their efficiency [8]. Also, with a given accuracy in this program, an ADC can be modeled in the

form of a transmission coefficient, and external typical disturbance signals. Thus, with the help of simulation, it is possible to obtain an accurate response of the digital filter to typical inputs.

According to the described hardware-implemented control channel, a model was developed in Matlab Simulink (fig. 2). In the model, a PID – regulator is used as a regulator, and the FPGA block designates a signal source that represents a signal received from the model of the IIT control channel.

The block diagram of the hardware measuring the response of a digital filter to typical inputs is shown in fig. 3.

The source of disturbance is a serial connection between a constant voltage source and a signal generator. In this case, the controller includes an integral component, therefore, the presence of a DC component in the error signal will lead to saturation of the digital controller, which will not allow obtaining a response to any action. Thus, for correct operation it is necessary to select a source voltage and a generator signal amplitude in such a way that relation [9] is fulfilled.

$$\int_0^T (Ref - Udsup - Udgen)dt = 0, \qquad (3)$$

here Ref is the reference signal, Udsup, Udgen are the digitized values of the voltage source and the generator signal, respectively, at the sensor input, T is the generator signal period.

In accordance with fig. 3, the total voltage of the source and generator is converted by the sensor and fed to the ADC input. The signal from the ADC output is used to receive the control error signal and is fed to the digital filter input. An interface connection is established between the digital control device, where the digital filter is implemented, and the personal computer [10]. Matlab is also used to obtain measurement results. Details about the program for the control center and its interaction with a personal computer will be described in detail in the next

section. As a result of the experiment on a personal computer in the Matlab environment, graphs are displayed that represent the input signal of the hardware-implemented controller and its response to this signal.

As a result, in one simulation environment responses to typical inputs of the designed control channel model and responses to similar typical actions obtained during testing of the hardware-implemented control channel will be obtained. By comparing the received signals, it is possible to make an unambiguous conclusion about whether the IIT control channel is correctly implemented. If the

control channel is working correctly, the signals must match.

Software. Digital control systems can be based on digital signal processors (DSP), universal microcontrollers or field-programmable gate array (FPGA).

Modern universal microcontrollers have ample opportunities for the formation of a control action and support digital signal processing (DSP) operations, which makes it possible to use them in control systems of power converters [11]. The most common general purpose microcontrollers are embedded 32-bit microcontrollers.
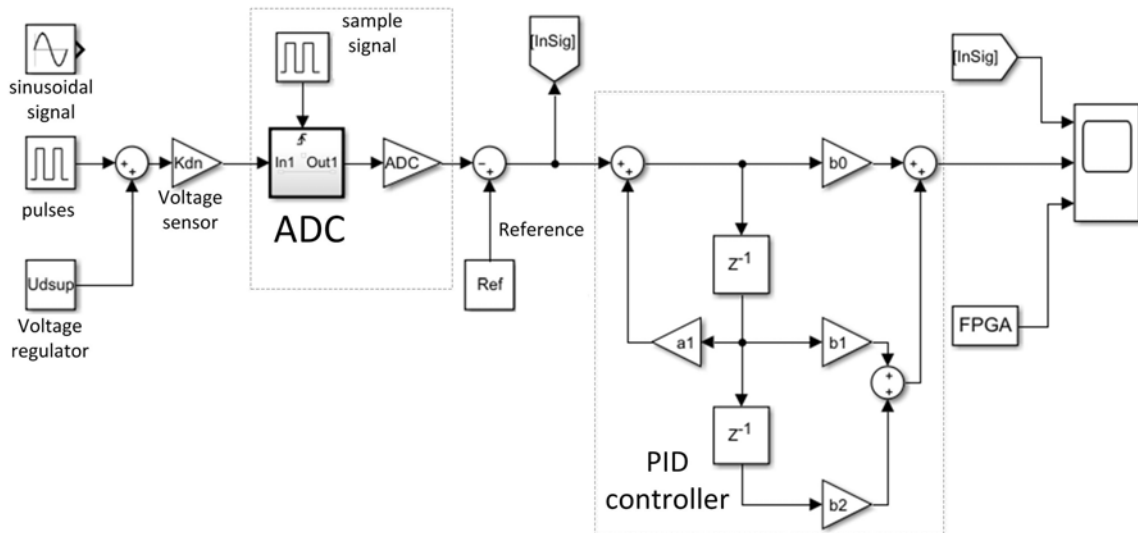

Fig. 2. Control channel model in Matlab Simulink

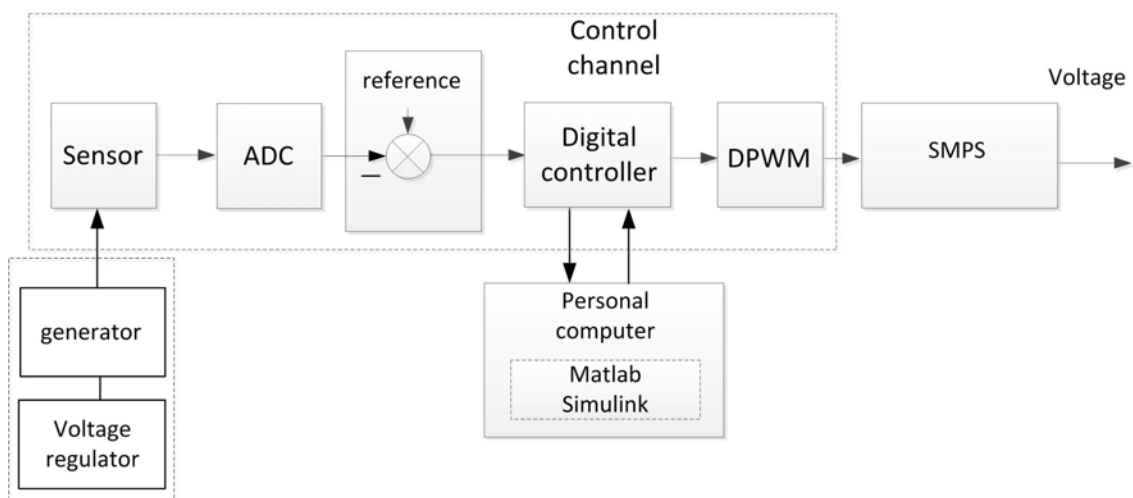Рис. 2. Модель канала управления в Matlab Simulink

Fig. 3. Scheme of experimental determination of control channel characteristics

Рис. 3. Схема экспериментального определения характеристик канала управления

These processors include the STMicroelectronics 32-bit STM32 microcontroller. In space technology, the Milandr 32-bit 1986BE8 microcontroller is widely used to provide resistance to external influences.

Digital signal processors, in comparison with general-purpose microcontrollers of general use, ensure to maximally speed up the execution of typical tasks of digital signal processing, such as digital filtering, Fourier transform, signal search, etc. [12]. Therefore, signal processors are optimized for speed to perform just such operations. DSP processors TMS320 or specialized microcontrollers UCD3138 from Texas Instruments are widely used in power converters.

FPGAs are well suited for devices such as radar systems, electronic intelligence systems, image processing systems, signal processing devices, etc. they are primarily intended for those devices in which signal processing and vector or matrix calculations are performed. Due to the ability to perform cumbersome parallel computations, FPGAs have become widely used in complex applications [13]. Operating at relatively low clock rates of the order of hundreds of MHz, they can perform tens of thousands of calculations per clock cycle and still consume much less power than microprocessors with the same performance.

FPGA cyclone IV (EP4CE22F17C6N) [14] from Altera, which is an indirect analogue of the domestic Rad-Hard FPGA 5578TS064 manufactured by VZPP-S, and a 12-bit ADC128S022 ADC with a digital SPI interface from Texas Instruments were used in the IIT layout. The FPGA implements an ADC control unit via the SPI interface and a regulator in structure and coefficients similar to the model.

The block diagram of the program is shown in fig. 4.

Since for calculating the controllers in the used FPGA it is necessary to perform floating point calculations, the FPGA used computing units according to the IEEE 754 standard [15].

With the frequency of 100 kHz, the values are captured from the ADC and the regulators are calculated. The ADC data and regulator responses are transferred to the FPGA's internal RAM.

After experiment completion the data is transferred to the computer via the UART interface to the Matlab simulation system and output to the virtual oscilloscope for comparison with similar signals measured in the simulation model.

In the course of the work, three types of controllers were implemented and their performance and resources used were evaluated when implemented on a specific FPGA (EP4CE22F17C6N). The parameters are presented in the tab. 1.

Experiment. A digital regulator has been developed for the SMPS. In this case, it is a proportional-integral-derivative (PID) controller made by the method of integration according to the Euler method. This regulator was converted into an IIR – filter, the structure corresponds to formula 1, and has the coefficients presented in tab. 2.

The response to rectangular pulses signal type makes it possible to assess the correspondence of the regulator coefficients in terms of the output signal overshoot, as a result of the response to a change in the level of the disturbing pulse, and in the rate of change in the regulator output signal as a result of integrating the control error. In this experiment a signal of the type of a sequence of pulses with a peak-to-peak value of 3 V (from 0 to 3 V), a frequency of 100 Hz and a duty cycle of 0.5 was selected as a disturbance signal. Thus, at the input of the PID-controller there will be a numerical equivalent of pulses with voltage from −1.5 to +1.5 V with a zero constant component, which is necessary to fulfill condition (3).

Fig. 5 shows the results of an experiment on a pulse sequence. The dashed line indicates the disturbance signal at the filter input, and the solid line indicates the response at the filter output. The top graph shows the signals obtained on the simulation model, and the bottom graph shows the signals obtained as a result of testing the hardware-implemented control channel.

As you can see from the graphs, the responses are identical with minor differences. The differences are explained by the presence of distortion and noise in the signal of the generator, as well as by the errors of the real ADC.

The controller in the feedback loop is designed based on the requirements for characteristics in frequency and time domains of the control object. It must adjust the frequency response of the open loop of the control object so that it meets a number of requirements, such as crossover frequency and phase margin. This means that the key characteristic of the designed controller is its Logarithmic Amplitude-Phase Frequency Response (LAFC). LAFC is determined from the response to harmonic influences at different frequencies. To construct the LAFC, harmonic signals with an amplitude of 1.5 V and frequencies of 100, 250, 500, 1000, 2500, 5000 and 10000 Hz were selected as disturbing influences. From the responses of the regulator, obtained as a result of tests for harmonic influences at the declared frequencies, a piecewise-linear IIR-filter LAFC was built and compared with the continuous theoretical characteristic of the developed regulator.

In fig. 6, the solid line with highlighted points denotes the frequency response obtained as a result of the experiment, and the dashed line – calculated from the TF of the controller.

According to fig. 6 it can be concluded that the dynamic properties in the investigated frequency range of the implemented controller correspond to the calculated ones with the required accuracy.

Thus, from the totality of the experiment results carried out comparing the responses to the typical inputs of the control channel model and the real tested control channel, we can make an unambiguous conclusion that the control channel is implemented correctly and its characteristics correspond to the calculated ones.
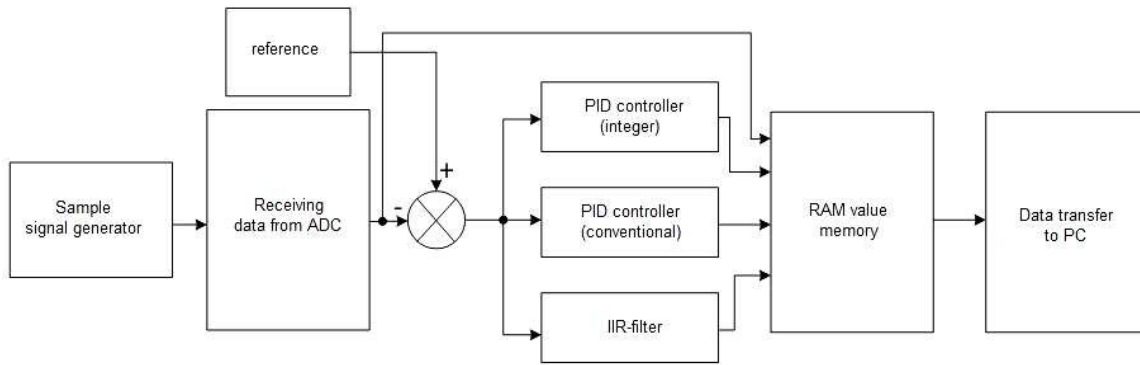
Fig. 4. Block diagrams of the program on the FPGA Cyclone IV

Рис. 4. Структурные схемы работы программы на ПЛИС Cyclone IV

Comparison table of implemented regulators

Parameters \ Controller	Integral controller	Standard PID-controller	IIR filter
Base frequency, MHz	40	40	40
Conversion time, ns	350	1500	2000
Number of occupied logical elements, pcs.	1393	2314	1452
The number of used DSP blocks, pcs.	10	7	7

IIR filter coefficient values

Coefficient	Value
a_1	−1
a_2	0
b_0	2.647745
b_1	−5
b_2	2.354
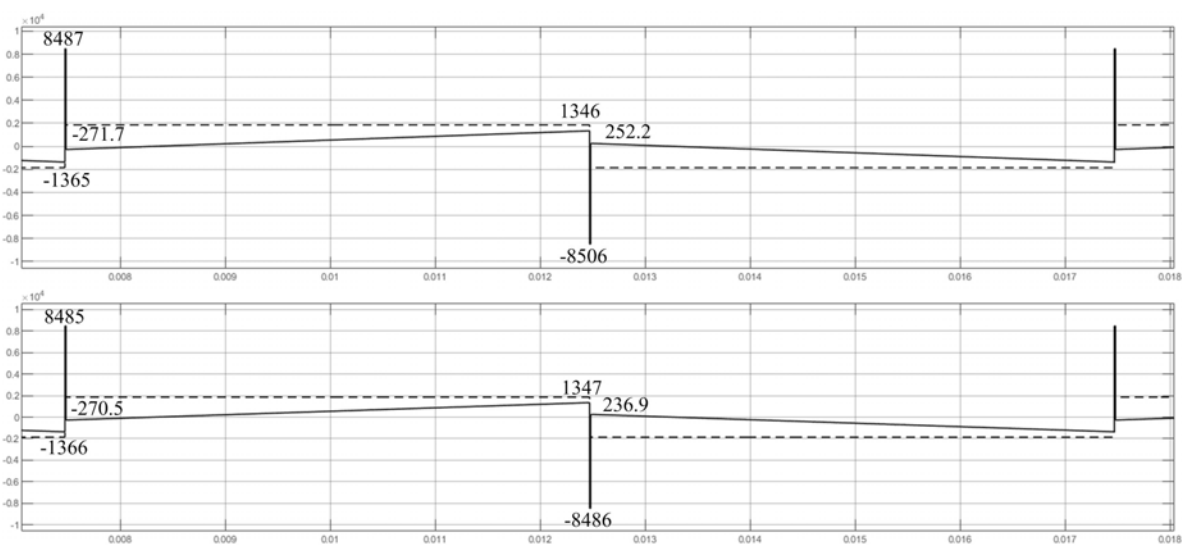
Fig. 5. Responses of the model and CCU to the impact of sequence of impulses type

Рис. 5. Отклики модели и ЦУУ на воздействие типа «последовательность импульсов»
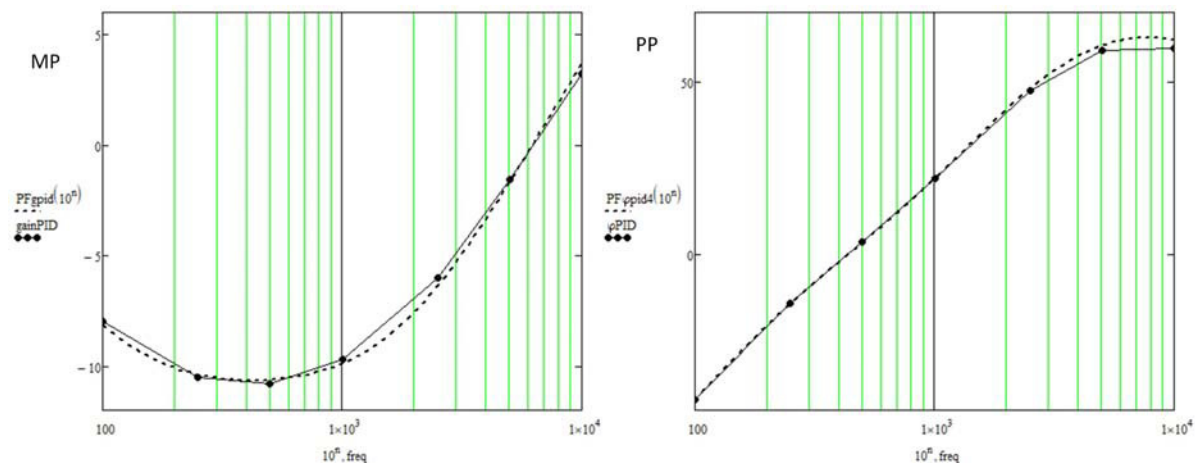
Fig. 6. Calculated from the TF filter, and obtained as a result of a full-scale experiment,
Log-magnitude and Phase diagrams

Рис. 6. Расчетные из ПФ фильтра и полученные в результате натурного эксперимента ЛАЧХ и ФЧХ

Conclusion. As a result of the work done, a method for determining the channel characteristics of a digital control system of a SMPS was proposed and tested, based on the comparison of control channel responses and its model to typical disturbance signals and LAFC removal. An example of the application of such a technique for verifying the parameters of the developed PID controller is given. In the course of the study of the CCU of the IIT layout, it was confirmed that the responses to the sequence of rectangular pulses coincide, and the LAFC of the model and the physical control channel also coincided.

The proposed technique can be used to test a digital control channel of not only switched-mode power supply, but also other control objects; for testing itself any necessary disturbance signals, including non-periodic signals of a complex shape, can be used.

Introduction of this testing technique in production conditions will allow a complete check of individual control centers of power converters with closed feedbacks before the final assembly of the device and power on, which will eliminate errors in the implementation of control loop regulators, leading to undesirable non-stationary modes of operation of power converters.

References

1. *GOST R 53711–2009. Izdeliya elektronnoj tekhniki. Pravila priemki* [State Standard R 53711-2009. Electronic products. Acceptance rules]. Moscow, 2009.

2. Olsson G., Piani D. *Cifrovye sistemy avtomatizacii i upravleniya* [Digital automation and control systems]. SPb., Nevskiy Dialekt Publ., 2001, 557 p.

3. Solodovnikov V. V. *Tekhnicheskaya kibernetika. Teoriya avtomaticheskogo regulirovaniya. Kniga 1 Matematicheskoe opisanie, analiz ustojchivosti i kachestva sistem avtomaticheskogo regulirovaniya* [Technical cybernetics. Theory of automatic regulation. Book 1 Mathematical description, analysis of stability and quality of automatic control systems.]. Moscow, Mashinostroenie Publ., 1967, 769 p.

4. Corradini L., Macsimovich D. Digital Control of high frequency Switched-Mode Power Converters. Hoboken, New Jersey, 2015. 356 p.

5. Meleshin V. I. *Tranzistornaya preobrazovatel'naya tekhnika* [Transistor Converter Technology]. Moscow, Tekhnosfera Publ., 2005, 632 c.

6. Ayficher E., Dzhervis B. *Cifrovaya obrabotka signalov: prakticheskiy podhod* [Digital Signal Processing: A Practical Approach]. Moscow, Vil'yams Publ., 2004, 992 p.

7. Belov G. A. *Dinamika impul'snyh preobrazovateley* [Dynamics of pulse power converters]. Cheboksary, 2001, 528 p.

8. Solonina A. I., Klionskij D. M., Merkucheva T. V., Perov S. N. *Cifrovaya obrabotka signalov i Matlab* [Digital Signal Processing and Matlab]. SPb., BHV-Peterburg, 512 p.

9. John Rice. Accelerating Power-Supply Compliance to Specification. Available at: http://www.ti.com/lit/ml/slup308/slup308.pdf (accessed 01.05.2020)

10. Denisenko V. V. *Komp'yuternoe upravlenie tekhnologicheskim processom, eksperimentom, oborudovaniem* [Computer control of a technological process, experiment, equipment.]. Moscow, Goryachaya liniya – Telekom Publ., 2009, 608 p.

11. Belyaev A., Solohina T., Yudincev V. [Modern digital signal processing devices. Together or apart?]. *Elektronika: Nauka, Tekhnologiya, Biznes.* 2009, No. 1(91), P. 28–35 (In Russ.).

12. Shtraus V. *Rynki DSP vysokogo klassa, raschitannye na bolee vysokiy dohod* [High-end DSP Markets for Higher Income]. 2006.

13. Markulov I. *Elektronnye komponenty.* 2011, No. 4, P. 3 (In Russ.).

14. *Rukovodstvo po ustrojstvu Cyclone IV* [Cyclone IV device manual]. Kompaniya Altera, 2016, 490 p.

15. *IEEE 754-2008 Standart dvoichnoy arifmetiki s plavayushchey tochkoy* [IEEE 754-2008 standard for binary floating-point arithmetic-Institute of Electrical and Electronics Engineers]. 2008, 23 p.

Библиографические ссылки

1. ГОСТ Р 53711–2009. Изделия электронной техники. Правила приемки. Утвержден и введен в действие приказом Федерального агентства по техническому регулированию и метрологии от 15 декабря 2009 г. № 1161-ст: дата введения 01.09.2010.

2. Олссон Г., Пиани Дж. Цифровые системы автоматизации и управления. СПб. : Невский Диалект, 2001. 557 с.

3. Солодовников В. В. Техническая кибернетика. Теория автоматического регулирования. Книга 1 Математическое описание, анализ устойчивости и качества систем автоматического регулирования. М. : Машиностроение, 1967. 769 с

4. Corradini L., Macsimovich D. Digital Control of high frequency Switched-Mode Power Converters. Hoboken, New Jersey, 2015. 356 p.

5. Мелешин В. И. Транзисторная преобразовательная техника. М. : Техносфера, 2005. 632 с.

6. Айфичер Э., Джервис Б. Цифровая обработка сигналов: практический подход : 2-е изд. ; пер. с англ. М. : Вильямс, 2004. 992 с.

7. Белов Г. А. Динамика импульсных преобразователей. Чебоксары : Изд-во Чуваш. ун-та, 2001. 528 с.

8. Цифровая обработка сигналов и Matlab / А. И. Солонина, Д. М. Клионский, Т. В. Меркучева, С. Н. Перов. СПб. : БХВ-Петербург, 2013. 512 с.

9. John Rice. Accelerating Power-Supply Compliance to Specification. [Электронный ресурс]. URL: http://www.ti.com/lit/ml/slup308/slup308.pdf (дата обращения 01.04.2020)

10. Денисенко В. В. Компьютерное управление технологическим процессом, экспериментом, оборудованием. М. : Горячая линия – Телеком, 2009. 608 с.

11. Беляев А., Солохина Т., Юдинцев В. Современные устройства цифровой обработки сигналов. Вместе или врозь? // Электроника: Наука, Технология, Бизнес. 2009. № 1(91). 28–35 с.

12. Штраус В. Рынки DSP высокого класса, рассчитанные на более высокий доход. DSP-FPGA.com. Руководство по ресурсам продукта, 2006.

13. Маркулов И. // Электронные компоненты. 2011. № 4. С. 3.

14. Руководство по устройству Cyclone IV – Компания Altera, 2016. 490 с.

15. IEEE 754-2008 Стандарт двоичной арифметики с плавающей точкой – Institute of Electrical and Electronics Engineers, 2008. 23 с.

Lopatin Aleksandr Aleksandrovich – Cand. Sc., head of design section power supply and conversion equipment; JSC Academician M. F. Reshetnev Information Satellite Systems. E-mail: lopatin@iss-reshetnev.ru.

Druzhinin Aleksandr Aleksandrovich – design engineer; JSC Academician M. F. Reshetnev Information Satellite Systems. E-mail: Alex-Druzh@mail.ru.

Asochakov Arseniy Stepanovich – design engineer; JSC Academician M. F. Reshetnev Information Satellite Systems. E-mail: arseniy.asochakov@yandex.ru.

Puchkov Aleksandr Vital'yevich – design engineer; JSC Academician M. F. Reshetnev Information Satellite Systems. E-mail: puchok_95@mail.ru.

Лопатин Александр Александрович – кандидат технических наук, начальник сектора разработки силовой бортовой аппаратуры; АО «Информационные спутниковые системы» имени академика М. Ф. Решетнева». E-mail: lopatin@iss-reshetnev.ru.

Дружинин Александр Александрович – инженер-конструктор; АО «Информационные спутниковые системы» имени академика М. Ф. Решетнева». E-mail: Alex-Druzh@mail.ru.

Асочаков Арсений Степанович – инженер-конструктор; АО «Информационные спутниковые системы» имени академика М. Ф. Решетнева». E-mail: arseniy.asochakov@yandex.ru.

Пучков Александр Витальевич – инженер-конструктор; АО «Информационные спутниковые системы» имени академика М. Ф. Решетнева». E-mail: puchok_95@mail.ru.

CFD METHODS FOR CAVITATION MODELING IN CENTRIFUGAL AND AXIAL PUMPS OF LRE

A. S. Torgashin*, D. A. Zhujkov, V. P. Nazarov, A. M. Begishev, A. V. Vlasenko

Reshetnev Siberian State University of Science and Technology
31, Krasnoyarskii rabochii prospekt, Krasnoyarsk, 660037, Russian Federation
*E-mail: ttarg23@yandex.ru

Currently, design and manufacture of liquid-propellant rocket engines (LRE) are imposed with ever greater reliability requirements. Accordingly, the standards for the design and manufacture of rocket engine units are raising. One of these units is a turbopump unit (TNA), which provides continuous supply of liquid components from combustion reaction to the combustion chamber of a rocket engine to create traction or other engine units. TNA is also the main source of pressure increase for these liquid components in front of the LRE combustion chamber. Important requirements are imposed on a turbopump unit (TNA): ensuring work performance and basic parameters for a given resource with the necessary possible pauses of a specified duration; providing all engine operating modes, supplying the fuel components of the required flow rate and pressure, guarantying a high degree of reliability with acceptable entire unit efficiency; providing high anti-cavitation characteristics of the pump in all modes. In the article, the authors summarize the latest results of the study on cavitation in turbopump units of liquid propellant rocket engines alongside with the relevant research in the field of hydraulics. The problems of cavitation in cryogenic liquids, simulation of stall characteristics, and usability of various models to simulate cavitation flow are observed. A solution to the problems of flow modeling was considered with respect to applicability to the following structural elements of LRE units: interscapular space of the screw centrifugal main and booster pumps, axial pre-pump. Particular attention is paid to the implementation of various numerical methods based on the use of various cavitation models, computational fluid dynamics in various CFD packages, and also comparison of results with the model. In summary, the authors draw conclusions about the possibility of applying these methods to solve the problems of the cavitation phenomenon research in LRE.

Keywords: Cavitation, TNA, LRE, CFD modeling.

МЕТОДЫ CFD МОДЕЛИРОВАНИЯ КАВИТАЦИИ В ЦЕНТРОБЕЖНЫХ И ОСЕВЫХ НАСОСАХ ЖИДКОСТНЫХ РАКЕТНЫХ ДВИГАТЕЛЕЙ

А. С. Торгашин*, Д. А. Жуйков, В. П. Назаров, А. М. Бегишев, А. В. Власенко

Сибирский государственный университет науки и технологии имени академика М. Ф. Решетнева
Российская Федерация, 660037, г. Красноярск, просп. им. газ. «Красноярский рабочий», 31
*E-mail: ttarg23@yandex.ru

В настоящее время к проектированию и производству жидкостных ракетных двигателей (ЖРД) предъявляются все большие требования по обеспечению надежности. В соответствии с этим повышаются требования по проектированию и изготовлению агрегатов ЖРД. Одним из таких агрегатов является турбонасосный агрегат (ТНА), обеспечивающий непрерывную подачу жидких компонентов реакции горения в камеру сгорания ракетного двигателя для создания тяги или в другие агрегаты двигателя. Также ТНА является основным источником повышения давления данных жидких компонентов перед камерой сгорания ЖРД. К ТНА предъявляются важные требования по обеспечению работоспособности основных параметров при заданном ресурсе с необходимыми возможными паузами установленной продолжительности; подачи компонентов топлива требуемого расхода и давления на всех режимах работы двигателя; высокой степени надежности с приемлемым КПД всего агрегата; высоким антикавитационным характеристикам насоса на всех режимах. В данной статье авторы обобщают последние результаты исследования кавитации в турбонасосных агрегатах ЖРД, а также применимые к ним исследования в области гидравлики. Рассмотрены проблемы кавитации в криогенных жидкостях, моделирование срывной характеристики, применение различных моделей к модели-

рованию кавитационного потока. Решение данных проблем моделирования течения рассматривалось относительно применяемости к следующим элементам конструкции агрегатов ЖРД: межлопаточного пространства шнекоцентробежного основного и бустерных насосов, осевого преднасоса. Особое внимание уделено реализации различных численных методов, основанных на использовании различных моделей кавитации, вычислительной гидрогазодинамики в различных CFD пакетах, а также сравнении результатов с модельными. Авторы делают выводы о возможности применения данных методов к решению вопросов исследования явления кавитации в ЖРД.

Ключевые слова: кавитация, ТНА, ЖРД, CFD моделирование.

Introduction. Cavitation in hydrodynamics is a special case of liquid boiling (phase transition of a liquid into a gas inside a liquid at a certain temperature and pressure), which occurs in moving liquid due to local pressure reductions to the level of saturated steam pressure. In hydrodynamics the phenomenon of cavitation plays a negative role as it causes violation of medium homogeneity. As a result, there may be bubbles in the flow that break when in contact with the blades, which can lead to a hydraulic shock that destroys the blades. It is important to take into account that the cavities connecting the units, movable parts of pumps and turbines, supply pipelines are elements of a complex spatial structure, geometry of which also affects the flow. In the working parts of the pump, the pressure reduction inside the flow part is connected with the streamlining of the blade profiles, where, as with the streamlining of any profile, a cavity of reduced pressure is formed at the inlet from the rear (non-working) side. This region of minimum pressure is the region of cavitation origin. The higher velocity of the flow, flowing around the blade is, the greater will be the discharge on the blade. Therefore, the most distant point from the axis of rotation of the blade leading edge may be the generation center of cavitation. Cavitation during TNA LRE operation can lead to three main negative consequences:

a) failure of TNA operation modes, i.e. sharp decrease of main output parameters – head, flow rate and, as a result, efficiency;

b) to the collapse of steam cavitation bubbles in the area of the blades, accompanied by strong blows, helps to destruct the blades of the machine impeller – erosion destruction. This phenomenon is usually manifested during long-term operation in cavitation mode, during the operation of the TNA LRE;

c) to occurrence of low-frequency self-oscillations due to possible unstable operation of TNA LRE [1].

To determine cavitation conditions in theoretical and experimental studies, the following non-dimensional parameter is used:

$$C_a = \frac{p - p_v}{\frac{1}{2}\rho U^2}, \qquad (1)$$

where p is flow pressure (for example, the input pressure), p_v is the saturated vapor pressure for the liquid, denominator is the dynamic pressure. This coefficient represents the pressure difference at a point of the body and in an undisturbed fluid at a certain distance from it and is proportional to the square of the velocity of the relative motion. The definition of the main condition for reducing the pressure to the minimum at which cavitation begins is also derived from it.

In 1917 Lord Rayleigh published the article "On the pressure, developing in a liquid when a spherical cavity" [2]. Rayleigh used the formulation of the problem on an empty cavity in a homogeneous liquid at constant pressure at infinity, proposed by Besant in 1859: "An infinitely large mass of a forced homogeneous incompressible fluid is at rest. The liquid inside a certain spherical surface instantly disappears. It is required to find the instantaneous change in pressure at any point of the liquid and the filling time of the cavity, assuming that the pressure at infinity is constant". The solution to this problem is based on the complete transformation of the work done by the mass when the cavity collapses into kinetic energy. The resulting equation:

$$\rho(RR_{TT} + \frac{3}{2}R_T^2) = -p, \qquad (2)$$

where p is the pressure at infinity, R is the bubble radius, ρ is the density of the fluid around the cavity, R_T and R_{TT} are the derivatives of the radius with respect to time. There is also a version of the Rayleigh equation for a gas-filled bubble, in which the condition is accepted that the gas does not exchange heat with the liquid, which means that its state is described by the Poisson pV^γ = const:

$$\rho(RR_{TT} + \frac{3}{2}R_T^2) = P_0\left(\frac{R_0}{R}\right)^{3k} - p, \qquad (3)$$

where κ is the polytropic index, P_0 is the atmospheric gas pressure in the bubble, and R_0 is the atmospheric radius of the bubble. Note that equations (1) and (2) do not take into account the influence of the gas cavity contents, surface tension, viscosity, and compressibility. Also, for these equations, it is assumed that the pressure at the distance from the bubble is also constant. At the moment, various generalizations of the Rayleigh equation are used to solve hydrodynamic problems.

Currently, significant work has been carried out on the study of the Rayleigh-Plesset model applicability for solving the problems of cavitation flow modeling in the channels of the LRE pumps. The Rayleigh-Plesset equation provides the basis for the flow equation that controls steam formation and condensation. The Rayleigh-Plesset equation describing the growth of a gas bubble in liquid is derived from the equations of moments:

$$R_B\frac{d^2 R_B}{dt^2} + \frac{3}{2}\left(\frac{dR_B}{dt}\right)^2 + \frac{2\sigma}{\rho_f R_B} = \frac{p_v - p}{\rho_f}, \qquad (4)$$

where R_B represents the bubble radius, p_v is the pressure in the bubble (it is assumed that this is the vapor pressure at the liquid temperature), p is the pressure in the liquid surrounding the bubble, ρ_f is the liquid density, and σ is the coefficient of surface tension between the liquid and the vapor. In the practices of cavitation flows modeling with various software packages simplified modifications of the Rayleigh-Plesset equation are usually used. For example, in the ANSYS CFX package, the second-order terms (which are suitable for low vibration frequencies) and surface tension are neglected [3].

In addition to numerical studies of cavitation flows in the pump, general solutions of the Rayleigh and Rayleigh-Plesset equations were obtained in [4] and [5], respectively.

Modern approaches to modeling the cavitation flow. Let us consider the approaches used for modeling the cavitation flow in pumps applied in various areas of hydraulic engineering. The main attention will be paid to a representative comparison with real tests with reference to the used cavitation models. Over the past several decades due to the growth of computational capacities many tests have been carried out the results of which allow to select the most suitable cavitation model for modeling the flow in the pump TNA LRE.

In [6] the authors consider the possibility of applying the Rayleigh-Plesset model to modeling the flow of cryogenic components. Since this work was carried out directly in application to the TNA LRE unit, it is also necessary to highlight the following comments and assumptions given by the authors:

– lack of consideration of thermal effects affecting the development of the cavity, development of which according to [6] is currently underway;

– insufficient amount of empirical data on cryogenic fluids;

– calculation used a model with three interscapular channels.

The work was carried out in the ANSYS CFX environment. Importantly, in addition to the cavitation equation discussed above, the ANSYS CFX model also includes a k-ω turbulence model, which also affects the numerical simulation results. Comparison in the article is based on the total volume of cavitation cavities. In contrast to the results discussed further, the text only mentions the results of full-scale tests of the screw, but no numerical data or percentage comparison is given. However, the authors note that despite the fact that heat effects are not taken into account in the Rayleigh – Plesset formula, good convergence of the data was obtained from numerical modeling. Also, the authors carried out a numerical simulation of the cavitation flow with an improved screw.

In [7] a technique for modeling a stalling cavitation flow in a booster turbopump unit is considered. In this article construction of a cavitation model is also based on the application of the Rayleigh-Plesset model. The work, as well as [4], was carried out in the ANSYS environment. The authors considered the method of setting the parameters for constructing computational grid, setting

initial conditions, and also compared the results obtained for models with and without a gap, as well as with field tests. The discrepancy with the model test for the model with a gap in the case of calculating the cavitation headroom was about 15 %, without a gap – 10 %. However, the clearance model showed better head convergence with the model tests. Also, the model without a gap does not take into account the vortex component of the flow. The authors conclude that the model with a gap is more applicable to modeling cavitation flow than without it.

Articles [8–12] were also considered in [7], where the authors compared the results obtained with the results of the authors of [8–12], however, it also seems necessary to consider cavitation models applicable in them and the authors' conclusions about the possible reasons for the discrepancies in the modeling results and model tests.

In the article [8], the authors consider development and application of numerical methods for cavitation modeling. The work was carried out in the CFX TASC flow 2.12 software environment. Currently the developers of this software environment are part of ANSYS. The constructed model was compared with the results obtained in model tests of the National Graduate School of Arts and Crafts. In the preface, the authors note that for flows with large accelerations, it is necessary to use a solution method based on solving the conservation equations for each of the phases and used in the development of non-equilibrium conditions for the exchange of heat, mass, momentum between phases. Moreover, the models will contain certain assumptions. The model used by the authors in [8] is based on the use of a non-equilibrium approximation in order to reduce the number of equations to be solved. According to the simulation data, in comparison with the real experiment, the results of the numerical model converge agree with the indicators of the ratio of expenses (current to nominal) from 0.91 to 1.09. In this work, a simplified Rayleigh – Plesset equation was used, which is similar to the equation used in the ANSYS CFX software environment.

The article [9] also discusses the problem of cavitation numerical simulation. The authors emphasize that at the time of 2003 the problem of flow optimization by reducing cavitation was rarely used and mainly suggested optimizing the flow angle at the pump input. This article discusses several software packages CFX-Tascflow, FLUENT and STAR-CD. FLUENT, like CFX-Tascflow, is currently part of the ANSYS package and allows the use of Zwart-Gerber-Belamri, Schnerr and Sauer and Singhal et al. The STAR-CD package is also in production today and uses the Rayleigh-Plesset cavitation model. At the time of this article writing, none of them take into account three-dimensional turbulent flow and viscosity effect. Based on the simulation results, the authors note that of the three selected programs, CFX-Tascflow shows the most accurate results in comparison with the model test. Also, the most accurate results obtained in CFX-Tascflow were compared with a simplified method based on the use of the initial shape of the cavitation cavity. This model is described in detail in [9]. Both methods are good at predicting the starting level and the percentage of head drop. Based on the comparison results, the authors

conclude that none of the proposed software packages at the time of 2003 justifies the time spent on the calculation, as compared to the achieved level of accuracy. However, CFX-Tascflow simulation data remains relatively accurate.

Article [10] addresses the issues of cavitation modeling in a diagonal centrifugal pump. In the article the authors employ the commercial package ANSYS CFX and clarify that they use the ANSYS CFX model without changes, that is, a model based on the VOF (volume of fluid) method. The aim of the study was to test the applicability of this commercial package as part of a standard engineering study. In terms of building a spatial model and a method of breaking it up into elements, the authors note that the hexahedral mesh is preferable to the tetrahedral one when modeling flows in turbopump units. Also in the model moving and stationary parts of the mesh are connected using the frozen-rotor interface. As in the work of previous authors, the studies also consider cavitation at higher, equal or lower than the nominal pump flow rate. In comparison with real tests the authors note that cavitation in the model begins with a lower number of cavitations and pressure drop is steeper. They attribute this to the lack of accounting for instability in the numerical model used. Under overload conditions at a flow rate of 1.25 of the nominal flow rate, the model showed the results that are closest to the real experiment. Analyzing the data obtained, the authors confirm that the model built in ANSYS CFX shows accurate results in terms of displaying the position, size of the cavitation cavity, and also emphasize the importance of using meshes based on hexahedral elements.

In the article [11], the authors consider numerical simulation of cavitating flow performed according to the standard model built into ANSYS CFX. The authors compared the results of numerical simulation with the standard model used in ANSYS CFX, as well as with the model with a modified k-ω turbulence model, which takes into account the cavity compressibility in the cavitation flow. Also, the Schnerr-Sauer cavitation model is used for the modified k-ω turbulence model. The comparison was also carried out with real model tests and showed that, despite discrepancies between the real cavitation curve and the one built on the basis of numerical simulation, the modified k-ω model gives results that are closer to real data. However, at a higher flow rate the pressure drop curves obtained using the two models have practically no differences. Apart from that, in comparison with model tests cavitation occurs with a lower number of cavitations and the total head is higher in both numerical models. The high head is explained by the imperfection of the model and the lack of accounting for flow losses that inevitably arise during the real pump operating. Based on the comparison results, the authors concluded that the use of the Schnerr-Sauer model can improve the accuracy of cavitation flow modeling.

In the article [12], the authors analyze the effect of cavitation flows on screws with different blade geometry. A number of studies have been carried out for each of the three geometry options. In their work, the authors used the Fluent software package. In the mass transfer model,

the cavitation rate is also based on the simplified Rayleigh-Plesset model. Before working with pumps, the authors did preliminary work in terms of studying cavitation, first in Venturi tubes, then in two-blade cascades and axial screws. The type of emerging cavitation and the development of cavitation during the test were determined for all of the above geometries. In terms of a more accurate behavior of the flow characteristics, considering the comparison of the stable flow of model tests and numerical modeling: similar to previous studies, the numerical model shows the onset of cavitation at large cavitation numbers for all three pumps tested by the authors. The authors also note that the results are in good agreement. The factors influencing the discrepancies between model tests and numerical modeling, according to the authors' conclusions, are: modeling of only one interscapular channel and, as a consequence, the lack of consideration of interactions between the channels, in comparison with the real geometry of the model is ideal without defects and deviations, as well as a numerical model does not take into account the radial clearance.

The article [13] presents the development and numerical simulation of cavitation flow based on a set of open source tools in OpenFOAMR, allowing the use of various cavitation models. The authors carried out work considering applicability of various cavitation models to the problem of cavitation flow modeling in the pump. In the article, the authors reviewed 4 models: Kunz et al, Merkle et al., Schnerr-Sauer-Yuan and Zwart et al. As in all previous studies, a 3 % head drop due to cavitation was modeled. Of the above models, the Zwart model first showed the best results on the airfoil and was then used to simulate cavitation flow. Comparison with model tests also showed high head values, but low values of the cavitation volume for the numerical model compared to the experimental one. The authors explain this discrepancy by the fact that the material used to create the impeller has a low stiffness and could deform during a real experiment, which cannot be taken into account in the numerical model; pump operation in a numerical model.

In article [14] the authors consider unsteady flow in the pump, as well as structural calculation of strength based on hydraulic calculation. Despite the fact that the main topic of this article is the analysis of the possibility of realizing the combination of interrelated strength and hydraulic calculations in the software package, the authors also carried out research in the field of cavitation modeling. When carrying out hydraulic calculations, a comparison of model tests and a numerical model was also carried out. The authors used the Zwart – Gerber – Belamri model, also based on the simplified Rayleigh – Plesset model. This model was also used by the authors of the article [13]. The results presented by the authors show good agreement with model tests. The numerical model of cavitation shows the onset of stalling at large cavitation numbers, in comparison with model tests, at a pump flow rate equal to the nominal (1.0 Q_d). Note that in this study, the values of the head during the real test and the results of the numerical model are close to each other.

The article [15] considers pump impeller optimization in order to increase productivity. The work was carried

out using the CFturbo 9.0 software. Despite the fact that the main topic of this article is the pump efficiency increase, the authors also carried out tests in terms of determining the cavitation characteristics. Prior to presenting test results with already optimized geometry, the authors also compared numerical and model tests results. Provided that a two-phase vapor-liquid model is used with a k-ε turbulence model and a constant mass fraction of gas, based on the already Rayleigh-Plesset equation, the numerical simulation data give almost identical results in comparison with model tests.

Conclusion. Having considered all the above works along with conclusions made by the authors, it is possible to define a number of factors that affect the accuracy of cavitation modeling in software packages, which must be taken into account:

– to increase the simulation accuracy it is necessary to take into account the working fluid leaks during the operation of the TNA pump;

– it is important to take into account the clearance between the blades and the casing wall in geometric models;

– when choosing a numerical model, it is necessary to consider both the model of cavitation and turbulence.

In summary, the results of [13] and [14] show good convergence of the numerical model and real experiment, which allows to conclude that the Zwart – Gerber – Belamri model, also based on the Rayleigh – Plesset model, is more applicable for cavitation flow simulating in a pump. This line of research is relevant, but insufficiently developed for application in engineering calculation methods and design of TNA LRE, especially for obtaining numerous options for more advanced designs at the initial stages of new models of rocket engines development.

References

1. Gahun G. G., Baulin. V. I., Volodin V. A. et al. *Konstrukciya i proektirovanie zhidkostnyh dvigateley* [Construction and design of liquid rocket engines]. Moscow, Mashinostroenie Publ., 1989, 424 p.

2. Lord R. On the pressure developed in a liquid during the collapse of a spherical cavity. *Phil. Mag.* 1917, No. 34 (200), P. 94–98.

3. ANSYS CFX Tutorial Guide. Chapter 28: Drop Curve for Cavitating flow in a Pump. ANSYS Inc. Release 15.0.

4. Kudryashov N. A., Sinelshchikov D. I. Analytical solutions of the Rayleigh equation for empty and gas-filled bubble. *J. Phys. A: Math. Theor.* 2014. No. 47. P. 405202.5.

5. Mancas Stefan C., Rosu Haret C. Cavitation of spherical bubbles: closed-form, parametric, and numerical solutions. Physics of Fluids. 2016.

6. Afanasyev A. A., Demyanenko Yu. V., Popkov A. N. [Application of the Rayleigh-Plesset cavitation model for studying the flow of cryogenic liquid in the paths of a screw-center-run pump]. *Vestnik voronezhskogo gos. tekhn. un-ta.* 2017, Vol. 12, No. 2, P. 44–49 (In Russ.).

7. Kazyonnov I. S., Kanalin Yu. I., Poletaev N. P., Chernysheva I. A. [Modeling of the breakdown cavitation characteristics of a booster turbopump unit and comparison of experimental and numerical results]. *Vestnik samarskogo gos. aerokosmich. un-ta im. ak. S. P. Koroleva (Nats. issled. un-ta).* 2014, No. 5-1 (47), P. 188–198 (In Russ.).

8. Bakir F., Rey R., Gerber A. G., Belamri T., Hutchinson B. Numerical and Experimental Investigations of the Cavitating Behavior of an Inducer. *International Journal of Rotating Machinery.* 2004, No. 10, P. 15–25.

9. Dupont P., Okamura T. Cavitating Flow Calculations in Industry. *International Journal of Rotating Machinery.* 2003, No. 9 (3), P. 163–170.

10. Pierrat D., Gros L., Couzinet A., Pintrand G. On the Leading Edge Cavitation In a Helico-centifugal Pump: Experimental and Numerical Investigations. *3rd IAHR International Meeting of the Workgroup on Cavitation and Dynamic Problems in Hydraulic Machinery and Systems.* October 14–16, 2009, Brno, Czech Republic.

11. Application of modified k-ω model to predicting cavitating flow in centrifugal pump / Hou-lin Liu*, Dong-xi Liu, Yong Wang, Xian-fang WU, Jian Wang // Water Science and Engineering. 2013, No. 6(3), P. 331–339.

12. Rafael Campos-Amezcua, Sofiane Khelladi, Zdzislaw Mazur-Czerwiec, Farid Bakir, Alfonso Campos-Amezcua and Robert Rey (2011). Numerical and Experimental Study of Mass Transfer Through Cavitation in Turbomachinery, Mass Transfer – Advanced Aspects, Dr. Hironori Nakajima (Ed.), InTech.

13. Hanimann L., Mangani L., Casartelli E., Widmer M. Cavitation modeling for steady-state CFD simulations. *IOP Conf. Ser.: Earth Environ.* 2016.

14. Denghao Wu, Yun Ren, Jiegang Mou, Yunqing Gu, Lanfang Jiang. Unsteady Flow and Structural Behaviors of Centrifugal Pump under Cavitation Conditions. Chinese. *Journal of Mechanical Engineering.* 2019.

15. Pei Ji1, Yin Tingyun1, Yuan Shouqi1, Wang Wenjie1, Wang Jiabin. Cavitation Optimization for a Centrifugal Pump Impeller by Using Orthogonal Design of Experiment. *Chinese Journal of Mechanical Engineering.* 2017, Vol. 30, No. 1, P. 103.

Библиографические ссылки

1. Конструкция и проектирование жидкостных ракетных двигателей / Г. Г. Гахун, В. И. Баулин, В. А. Володин и др. ; под общ. ред. Г. Г. Гахуна. М. : Машиностроение, 1989. 424 с.

2. Lord R. On the pressure developed in a liquid during the collapse of a spherical cavity // Phil. Mag. 1917. No. 34 (200). P. 94–98.

3. ANSYS CFX Tutorial Guide. Chapter 28: Drop Curve for Cavitating flow in a Pump. ANSYS Inc. Release 15.0.

4. Kudryashov N. A., Sinelshchikov D. I. Analytical solutions of the Rayleigh equation for empty and gas-filled bubble // J. Phys. A: Math. Theor. 2014. No. 47. P. 405202.

5. Mancas Stefan C., Rosu Haret C. Cavitation of spherical bubbles: closed-form, parametric, and numerical solutions. Physics of Fluids. 2016.

6. Афанасьев А. А., Демьяненко Ю. В., Попков А. Н. Применение кавитационной модели Релея – Плессета для исследования течения криогенной жидкости

в трактах шнекоцентробежного насоса // Вестник воронежского гос. техн. ун-та. 2017. Т. 12, № 2. С. 44–49.

7. Моделирование срывной кавитационной характеристики бустерного турбонасосного агрегата и сравнение экспериментальных и численных результатов / И. С. Казённов, Ю. И. Каналин, Н. П. Полетаев, И. А. Чернышева // Вестник самарского гос. аэрокосмич. ун-та им. ак. С. П. Королёва (Нац. исслед. ун-та). 2014. № 5-1 (47). С. 188–198.

8. Numerical and Experimental Investigations of the Cavitating Behavior of an Inducer / F. Bakir, R. Rey, A. G. Gerber, T. Belamri, B. Hutchinson // International Journal of Rotating Machinery. 2004. No. 10. P. 15–25.

9. Dupont P., Okamura T. Cavitating Flow Calculations in Industry // International Journal of Rotating Machinery. 2003. No. 9 (3). P. 163–170.

10. On the Leading Edge Cavitation In a Helicocentifugal Pump: Experimental and Numerical Investigations / D. Pierrat, L. Gros, A. Couzinet, G. Pintrand // 3rd IAHR International Meeting of the Workgroup on Cavitation and Dynamic Problems in Hydraulic Machinery and Systems, October 14–16, 2009, Brno, Czech Republic.

11. Application of modified k-ω model to predicting cavitating flow in centrifugal pump / Hou-lin Liu*, Dong-xi Liu, Yong Wang, Xian-fang WU, Jian Wang // Water Science and Engineering. 2013. No. 6(3). P. 331–339.

12. Rafael Campos-Amezcua, Sofiane Khelladi, Zdzislaw Mazur-Czerwiec, Farid Bakir, Alfonso Campos-Amezcua and Robert Rey (2011). Numerical and Experimental Study of Mass Transfer Through Cavitation in Turbomachinery, Mass Transfer – Advanced Aspects, Dr. Hironori Nakajima (Ed.), InTech.

13. Cavitation modeling for steady-state CFD simulations / L. Hanimann, L. Mangani, E. Casartelli, M. Widmer // IOP Conf. Ser.: Earth Environ. 2016.

14. Unsteady Flow and Structural Behaviors of Centrifugal Pump under Cavitation Conditions. Chinese / Denghao Wu, Yun Ren, Jiegang Mou, Yunqing Gu, Lanfang Jiang // Journal of Mechanical Engineering. 2019.

15. Cavitation Optimization for a Centrifugal Pump Impeller by Using Orthogonal Design of Experiment / Pei Ji1, Yin Tingyun1, Yuan Shouqi1, Wang Wenjie1, Wang Jiabin // Chinese Journal of Mechanical Engineering. a2017. Vol. 30, aNo. 1. P. 103.

Begishev Aleksey Mikhaylovich – graduate student; Reshetnev Siberian State University of Science and Technology. E-mail: alex-beg95@mail.ru.

Zhujkov Dmitrij Aleksandrovich – Cand. Sc., Docent of a department of Aircraft Engines; Reshetnev Siberian State University of Science and Technology. E-mail:d_zhuikov@sibsau.ru.

Nazarov Vladimir Pavlovich – Cand. Sc., Professor, Head of the Department of Aircraft Engines; Reshetnev Siberian State University of Science and Technology. E-mail:nazarov@sibsau.ru.

Torgashin Anatoliy Sergeevich – graduate student; Reshetnev Siberian State University of Science and Technology. E-mail: ttarg23@gmail.com.

Vlasenko Alesksey Vladimirovich – graduate student; Reshetnev Siberian State University of Science and Technology. E-mail: lesha.vlasenko.94@mail.ru.
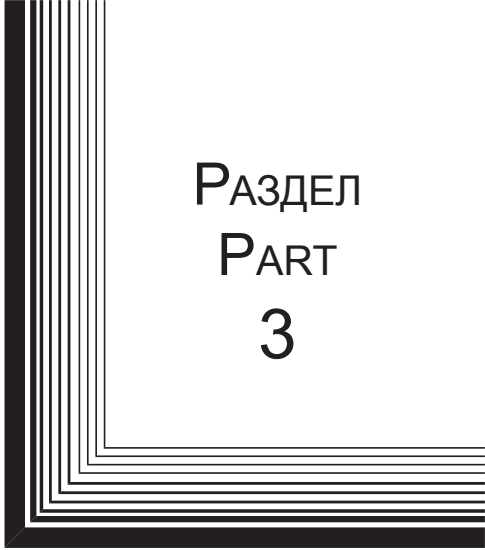
Бегишев Алексей Михайлович – аспирант; Сибирский государственный университет науки и технологий имени академика М. Ф. Решетнева. E-mail: alex-beg95@mail.ru.

Жуйков Дмитрий Александрович – кандидат технических наук, доцент кафедры двигателей летательных аппаратов; Сибирский государственный университет науки и технологий имени академика М. Ф. Решетнева. E-mail: d_zhuikov@sibsau.ru.

Назаров Владимир Павлович – кандидат технических наук, профессор, заведующий кафедрой двигателей летательных аппаратов; Сибирский государственный университет науки и технологий имени академика М. Ф. Решетнева. E-mail: nazarov@sibsau.ru.

Торгашин Анатолий Сергеевич – аспирант; Сибирский государственный университет науки и технологий имени академика М. Ф. Решетнева. E-mail: ttarg23@gmail.com.

Власенко Алексей Владимирович – аспирант; Сибирский государственный университет науки и технологий имени академика М. Ф. Решетнева. E-mail: lesha.vlasenko.94@mail.ru

ТЕХНОЛОГИЧЕСКИЕ
ПРОЦЕССЫ
И МАТЕРИАЛЫ

TECHNOLOGICAL
PROCESSES
AND MATERIALS SCIENCE

SIMULATION OF THE INDUCTION SOLDERING PROCESS OF WAVEGUIDE PATHS FROM ALUMINUM ALLOYS

O. A. Bocharova*, A. V. Murygin, A. N. Bocharov, R. V. Zaitsev

Reshetnev Siberian State University of Science and Technology
31, Krasnoyarskii rabochii prospekt, Krasnoyarsk, 660037, Russian Federation
*E-mail: shyx_89@mail.ru

A system of waveguide paths is a complex structure of various elements with various geometries. Induction soldering based on the induction heating method is one of the promising methods for waveguides fabricating. Induction soldering of waveguide paths has a number of technological features: the melting temperature of the base material AD31 (695–663 ^0C) slightly differs from the melting temperature of St. AK12 solder (577–580 ^0C) at an average induction heating rate of 20–25 ^0C / sec; a wide variety of standard sizes of waveguide paths elements complicates the development and subsequent reproduction of technological parameters of the induction soldering process; zones of maximum heating of waveguide paths elements do not coincide with zones of soldering. Therefore, to solve the problems of controlling the waveguides soldering process, it is necessary to simulate this process. The paper deals with the problem of simulating the process of heating a waveguide during induction soldering. Requirements for the process model have been formed. The model is built on the basis of the differential heat conduction equation. The formed model requirements take into account the geometric parameters of waveguides, the physical parameters of materials, the initial and boundary conditions, as well as the uneven distribution of eddy current density in the waveguide. It is proposed to use the finite difference method for the numerical solution of the heat conduction equation. The process of calculating the temperature at the grid nodes is shown. The authors propose a two-stage solution. At the first stage, at an intermediate time step, the temperature at the grid nodes along the X axis is calculated. At the second stage, the temperature at the grid nodes along the Y axis is calculated. The numerical solution of the difference equations along the X and Y axes is carried out by the sweep method. An algorithm for the numerical solution of the heat conduction equation has been developed.

Keywords: waveguide path, induction soldering, model of the waveguide heating process, differential heat conduction equation, finite difference method.

МОДЕЛИРОВАНИЕ ПРОЦЕССА ИНДУКЦИОННОЙ ПАЙКИ ВОЛНОВОДНЫХ ТРАКТОВ ИЗ АЛЮМИНИЕВЫХ СПЛАВОВ

О. А. Бочарова*, А. В. Мурыгин, А. Н. Бочаров, Р. В. Зайцев

Сибирский государственный университет науки и технологий имени академика М. Ф. Решетнева
Российская Федерация, 660037, г. Красноярск, просп. им. газ. «Красноярский рабочий», 31
*E-mail: shyx_89@mail.ru

Система волноводных трактов представляет собой сложную конструкцию из различных элементов с разнообразной геометрией. Одним из перспективных способов изготовления волноводов является индукционная пайка, основанная на методе индукционного нагрева. Индукционная пайка волноводных трактов обладает рядом технологических особенностей: относительно небольшая разница температуры плавления основного материла АД31 (695–663 ^0C) и припоя Св. АК12 (577–580 ^0C) при средней скорости индукционного нагрева 20–25 ^0C/сек; большое разнообразие типоразмеров элементов волноводных трактов представляет сложность при отработке и последующем воспроизведении технологических параметров процесса индукционной пайки; зоны максимального нагрева элементов волноводных трактов не совпадают с зонами пайки. Поэтому для решения задач управления процессом пайки волноводов необходимо провести моделирование данного процесса.

В статье рассмотрена задача моделирования процесса нагрева волновода при индукционной пайке. Сформированы требования к модели. Модель строится на основе дифференциального уравнения теплопроводности. Сформированные требования к модели учитывают геометрические параметры волноводов, физические параметры материалов, начальные и граничные условия, а также неравномерное распределение плотности вихревого тока в волноводе. Предлагается для численного решения уравнения теплопроводности использовать метод конечных разностей. Показан процесс расчета температуры в узлах сетки. Решение осуществляется в два этапа. На первом этапе на промежуточном временном шаге проводится расчет температуры в узлах сетки по оси X, на втором этапе вычисляется температура в узлах сетки по оси Y. Численное решение разностных уравнений по оси X и Y осуществляется методом прогонки. Разработан алгоритм численного решения уравнения теплопроводности.

Ключевые слова: волноводный тракт, индукционная пайка, модель процесса нагрева волновода, дифференциальное уравнение теплопроводности, метод конечных разностей.

Introduction. Systems of waveguide paths are widely used in spacecraft to ensure their functioning and transmission of electromagnetic energy in them [1].

A system of waveguide paths is a complex structure of various elements with various geometries (fig. 1).

Various methods are used to connect the structural elements of waveguide paths: argon-arc welding, soldering in salt baths, soldering using a laser source [2–5].

Induction soldering is one of the promising methods for waveguide paths fabricating [1; 3].

Induction soldering provides contactless, fast and local heating of the soldering point. It reduces the oxidation of current-carrying surfaces and waveguide warping. The equipment providing induction heating is rather compact and easily controlled, which allows automated controlling the soldering process [6].

However, induction soldering of waveguide paths has a number of features [7]:

1. The melting temperature of the base material AD31 (695–663 ^{0}C) slightly differs from the melting temperature of St. AK12 solder (577–580 ^{0}C) at an average induction heating rate of 20–25 ^{0}C / sec.

2. A wide variety of standard sizes of waveguide paths elements complicates the development and subsequent reproduction of technological parameters of the induction soldering process.

3. Zones of maximum heating of the waveguide paths elements do not coincide with zones of soldering.

Therefore, it is necessary to simulate the process of heating the waveguide before setting the problem of controlling the process of waveguide paths induction soldering.
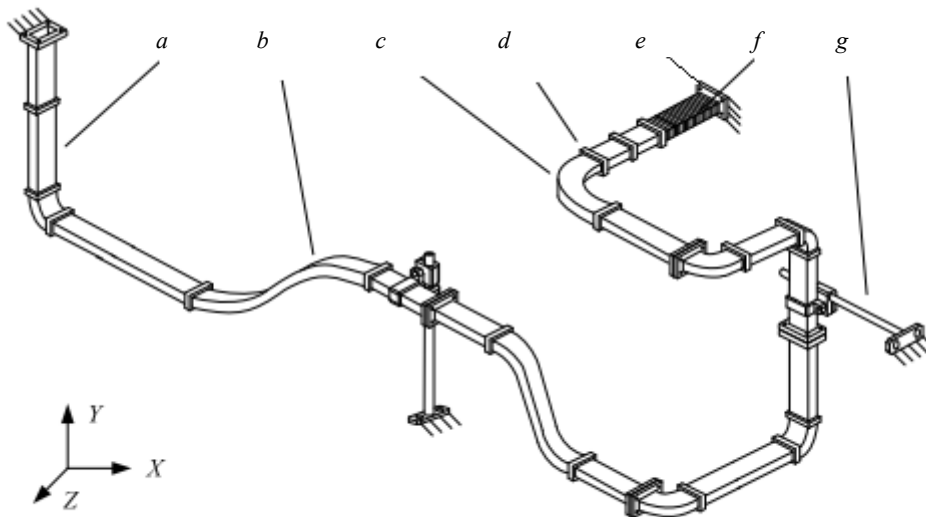

Fig. 1. An example of a section of a waveguide distribution system:
a – a direct element; *b* – a curved element with a variable radius of curvature;
c – a curved element with a constant radius of curvature; *d* – a coupling; *e* – a flange;
f – a flexible section; *g* – an intermediate support

Рис. 1. Пример участка волноводно-распределительной системы:
а – прямой элемент; *б* – криволинейный элемент с переменным радиусом кривизны;
в – криволинейный элемент с постоянным радиусом кривизны; *г* – соединительная муфта;
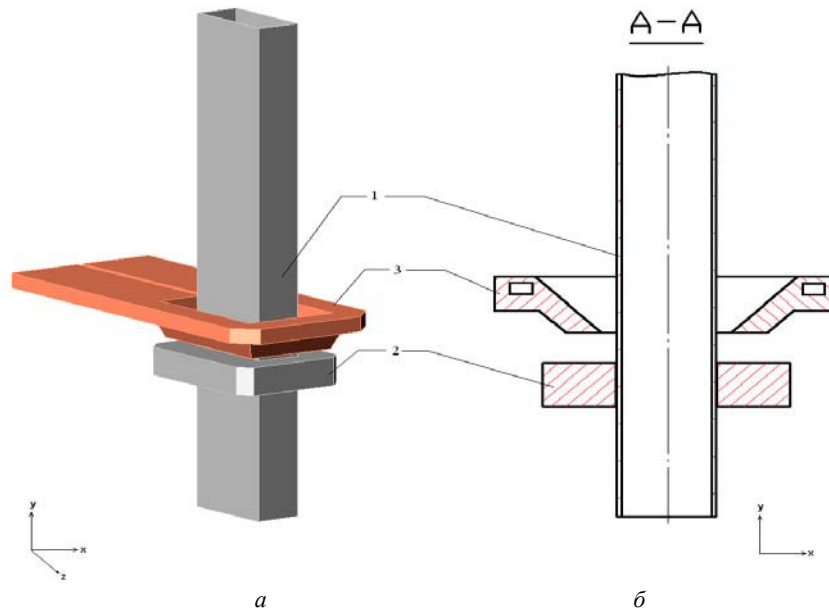*д* – фланец; *е* – гибкая секция; *ж* – промежуточная опора

Fig. 2. The researched system "inductor – waveguide":
1 – a waveguide pipe; *2* – a flange; *3* – an inductor

Рис. 2. Исследуемая система «индуктор – волновод»:
1 – волноводная труба; *2* – фланец; *3* – индуктор

Construction of a waveguide heating model. The connection of the straight section of the waveguide tube and the flange was chosen as a typical object for considering the process of induction heating (fig. 2).

The inductor (without considering the power part of the induction equipment) is a ring made of copper (fig. 2). The inductor is a source of alternating magnetic field, which forms eddy currents flowing in the waveguide. The calculation of a simplified two-dimensional waveguide-inductor circuit showed that the eddy currents in the waveguide are unevenly distributed [8–10].

Based on the above, it is possible to construct a mathematical model of heating the waveguide path during induction soldering, taking into account the following assumptions:

– the spatial configuration of the system allows us to restrict ourselves to a simplified two-dimensional model;

– a general model can be used to simulate a pipe-flange system, since the waveguide elements can be represented by plates in a simplified form.

For a generalized model of thermal processes occurring during induction soldering of waveguide paths, we take the differential equation of heat conduction [11]. Since the heating of the waveguide is due to eddy currents flowing in it, a permanent heat source is added to the formula:

$$\frac{\partial T(x,y,t)}{\partial t} =$$

$$= a\left(\frac{\partial^2 T(x,y,t)}{\partial x^2} + \frac{\partial^2 T(x,y,t)}{\partial y^2}\right) + q(x,y,t), \quad (1)$$

where a is the coefficient of thermal diffusivity of the material; T is temperature; t is time; x, y are Cartesian coordinates; $q(x, y, t)$ is a permanent source of heat.

Equation (1) describes a variety of options for the waveguide heating process flow. Therefore, in order to simulate the thermal processes occurring during induction soldering, it is necessary to add single-valued conditions to equation (1). Single-valued conditions may contain geometric, physical, initial and boundary conditions. These conditions are as follows:

– a simplified geometric two-dimensional model of the waveguide is adopted, shown in fig. 3;

– eddy currents are supposed to flow over the surface of the waveguide [12];

– it is taken into account that the eddy current density is distributed unevenly due to the shape of the waveguide and the location of the inductor relative to the waveguide [12];

– thermophysical characteristics of the waveguide material are constant;

– the initial temperature of the waveguide is the same along its entire length:

$$T(x,y) = T_i = \text{const};$$

– heat exchange with the environment (Newton's boundary condition) is carried out by the inner and outer surface of the pipe:

$$a\frac{\partial T(x,y,t)}{\partial x} = b(T(x,y,t) - Ten),$$

where b is the heat exchange coefficient; *Ten* is the temperature of the environment; $0 \le x \le l_p$ (inner side); $0 \le x \le l_p - h_f$ (outer side);
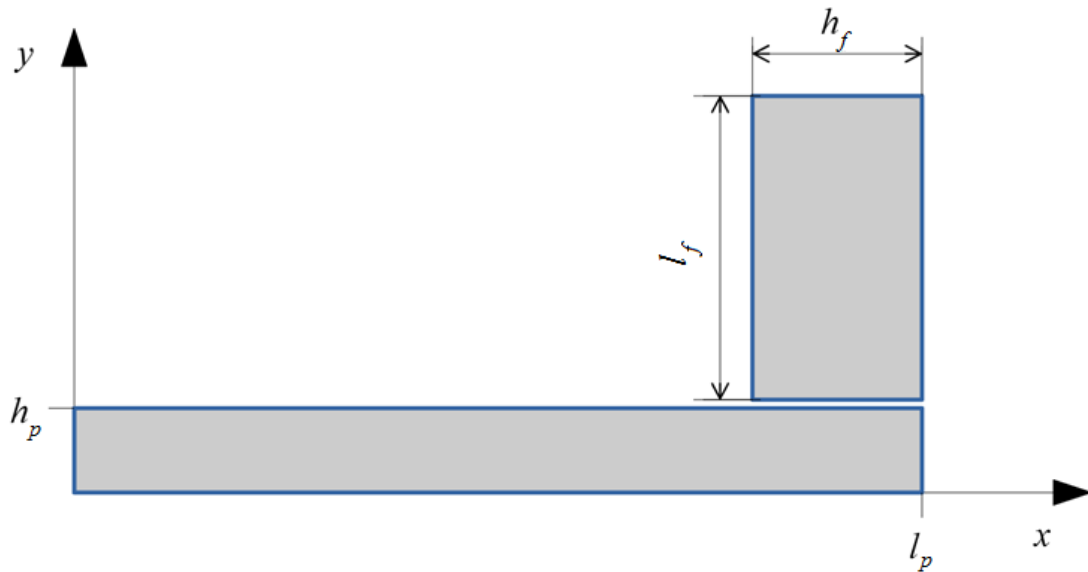
Fig. 3. A simplified geometric model of the waveguide:
l_p – length of a pipe; h_p – width of a pipe; h_f – width of a flange; l_f – length of a flange

Рис. 3. Упрощенная геометрическая модель волновода:
l_T– длина трубы; h_T – ширина трубы; h_f – ширина фланца; l_f – длина фланца
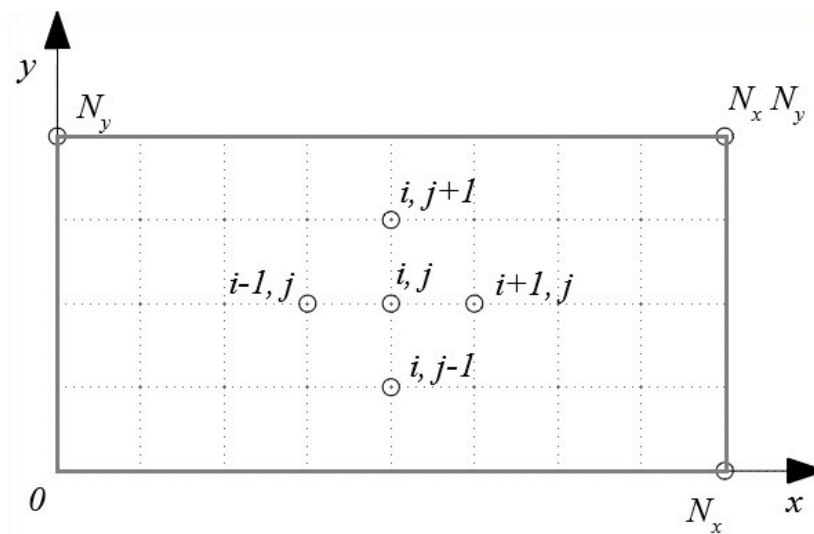

Fig. 4. A difference mesh of the solution domain

Рис. 4. Разностная сетка области решения

– heat exchange with the environment is carried out by the upper and side faces of the flange.

For the upper face:

$$a\frac{\partial T(x,y,t)}{\partial y} = b(T(x,y,t) - Ten),$$

where $h_p \leq y \leq h_p + l_f$.

For the side face:

$$a\frac{\partial T(x,y,t)}{\partial x} = b(T(x,y,t) - Ten),$$

where $l_p - h_f \leq x \leq l_p$;

– heating power remains constant $q(x,y,t) = \text{const}$;

– heat exchange between the pipe and the flange is assumed to be zero.

For the numerical solution of equation (1), we apply the finite difference method [13–15]. Let us consider the method applied to a waveguide tube.

To approximate equation (1) by the finite difference method, we represent the pipe as a set of nodes with coordinates (fig. 4): $x_i = i{\cdot}h_x$, $y_i = j{\cdot}h_y$, $t_k = k\tau$, where h_x, h_y is the step along the coordinate grid x, y; τ is the time step.

Let us sample equation (1) in two stages. At the first stage, at an intermediate time step $\tau / 2$, we carry out sampling along the *X* axis; at the second stage, we carry out sampling along the Y axis. We obtain equation (1) in the difference form [15]:

$$\frac{T_{ij}^{k+\frac{1}{2}} - T_{ij}^{k}}{\frac{t}{2}} = a\left(\frac{T_{i+1,j}^{k+\frac{1}{2}} - 2T_{ij}^{k+\frac{1}{2}} + T_{i-1,j}^{k+\frac{1}{2}}}{h_x^2}\right) + q_{ij}^{k+\frac{1}{2}}, \quad (2)$$

$$\frac{T_{i,j}^{k+1} - T_{i,j}^{k+\frac{1}{2}}}{\frac{t}{2}} = a\left(\frac{T_{i,j+1}^{k+1} - 2T_{i,j}^{k+1} + T_{i,j-1}^{k+1}}{h_x^2}\right) + q_{i,j}^{k+1}, \quad (3)$$

where $T_{ij}^k = T(x_i, y_j, t_k)$; $q_{i,j}^k = q(x_i, y_j, t_k)$.

Solving first equation (2), and then equation (3), we determine the temperature field at a whole time step.

Approximation of the boundary conditions for a pipe is as follows:

$$a\frac{T_{i,j+1}^k - T_{i,j}^k}{h_y} = b(T_{i,j}^k - Ten), \text{ if } 0 \leq i \leq N_x, j = 0,$$

$$a\frac{T_{i,j-1}^k - T_{i,j}^k}{h_y} = b(T_{i,j}^k - Ten), \text{ if } 0 \leq i \leq N_x, j = N_y.$$

The sweep method [14] is suitable for solving difference equations (2) and (3). Let us consider this method using the example of solving equation (2). We transform the equation (2) [14]:

$$\frac{T_{i,j}^{k+\frac{1}{2}}}{\frac{\tau}{2}} + a^2\left(\frac{T_{i,j}^{k+\frac{1}{2}}}{h_x^2}\right) = a\frac{T_{i+1,j}^{k+\frac{1}{2}}}{h_x^2} + a\frac{T_{i-1,j}^{k+\frac{1}{2}}}{h_x^2} + \frac{T_{i,j}^{k}}{\frac{\tau}{2}} + q_{i,j}^{k+\frac{1}{2}}.$$

Then

$$\left(\frac{1}{\frac{\tau}{2}} + \frac{2q}{h_x^2}\right)T_{i,j}^{k+\frac{1}{2}} = \frac{a}{h_x^2}T_{i+1,j}^{k+\frac{1}{2}} + \frac{a}{h_x^2}T_{i-1,j}^{k+\frac{1}{2}} + \frac{1}{\frac{\tau}{2}}T_{i,j}^{k} + q_{i,j}^{k+\frac{1}{2}}.$$

Hence we get

$$a_i T_{i,j}^{k+\frac{1}{2}} = b_i T_{i+1,j}^{k+\frac{1}{2}} + c_i T_{i-1,j}^{k+\frac{1}{2}} + d_i + q_{i,j}^{k+\frac{1}{2}}, \quad (4)$$

where

$$a_i = \frac{1}{\frac{\tau}{2}} + \frac{2q}{h_x^2}; \quad b_i = c_i = \frac{q}{h_x^2}; \quad d_i = \frac{1}{\frac{\tau}{2}}T_{i,j}^{k}.$$

For the boundary points 0 and N_x, we write equation (4) in the following form:

$$a_0 T_{0,j}^{k+\frac{1}{2}} = b_0 T_{i,j}^{k+\frac{1}{2}} + d_0, \quad (5)$$

$$a_N T_{N,j}^{k+\frac{1}{2}} = c_N T_{N-1,j}^{k+\frac{1}{2}} + d_N. \quad (6)$$

The sweep algorithm begins by writing equation (5) in the form:

$$T_{0,j}^{k+\frac{1}{2}} = P_0 T_{i,j}^{k+\frac{1}{2}} + Q_0, \quad (7)$$

where $P_0 = \frac{b_0}{a_0}$, $Q_0 = \frac{d_0}{a_0}$ are determined by the initial and boundary conditions of the simulation.

We substitute relation (7) into (4) for $i = 0$. Continuing the process of sequential substitution $T_{i,j}^{k+\frac{1}{2}}$ can be expressed through $T_{i+1,j}^{k+\frac{1}{2}}$:

$$T_{i,j}^{k+\frac{1}{2}} = P_i T_{i+1,j}^{k+\frac{1}{2}} + Q_i, \quad (8)$$

where P_i и Q_i are new coefficients obtained during the substitution process. Using expressions (8) and (4), we can obtain formulas for calculating P_i и Q_i:

$$P_i = \frac{b_i}{a_i - c_i P_i}, \quad (9)$$

$$Q_i = \frac{d_i + c_i Q_{i-1}}{a_i - c_i P_{i-1}}. \quad (10)$$

When calculating P_{N_x} and Q_{N_x} we get that $P_{N_x} = 0$, $b_{N_x} = 0$. Therefore, T_{N_x} will be equal to Q_{N_x}. Having calculated T_N in this way, one can start the backward-sweep process to obtain T_{N-1}, T_{N-2}, …, T_2, T_1, T_0 [9].

$$T_{i-1}^{k+\frac{1}{2}} = P_{i-1} T_{i-1,j}^{k+\frac{1}{2}} + Q_{i-1}. \quad (11)$$

Based on the above, we can formulate a solution algorithm:

1. We calculate P_0 and Q_0, the coefficients a_0, b_0, d_0 are determined using the initial and boundary conditions.

2. We calculate P_i and Q_i for $i = 1, 2, …, N_x$, using expressions (9) and (10).

3. We suppose $T_N = Q_N$.

4. We substitute T_N into formula (11) and determine T_{N-1}, T_{N-2}, …, T_2, T_1, T_0.

The algorithm for solving equation (3) is similar. The coefficients included in equation (3) will take the following form:

$$a_i = \frac{1}{\frac{\tau}{2}} + \frac{a}{h_y^2}, \quad b_i = c_i = \frac{a}{h_y^2}, \quad d_i = \frac{1}{\frac{\tau}{2}}T_{i,j}^{k+\frac{1}{2}}.$$

The sweep will be carried out on index *j*.

The Elcut software package was used to calculate the eddy current density distribution in the waveguide pipe and flange. The results confirm the previously accepted assumptions when setting the simulation problem. Fig. 5 and 6 show that the eddy current density increases sharply on the corner surfaces of the pipe and the waveguide flange. In addition, in fig. 5 the eddy current density decreases sharply in the thickness of the pipe and flange walls. Eddy current flow areas are well localized (fig. 6).

Fig. 7 shows the results of heating the waveguide according to the proposed model.

To check the simulation results, the temperature change at control points 1 and 2 was taken (fig. 7). The control points coincide with the points of temperature measurement during the process of heating the waveguide using induction equipment [16; 17].

As it can be seen from fig. 8 and 9, the simulation results quite accurately describe the process of the waveguide elements heating. Consequently, this model can be used to simulate an automated control system for soldering waveguide paths and analyzing control algorithms.
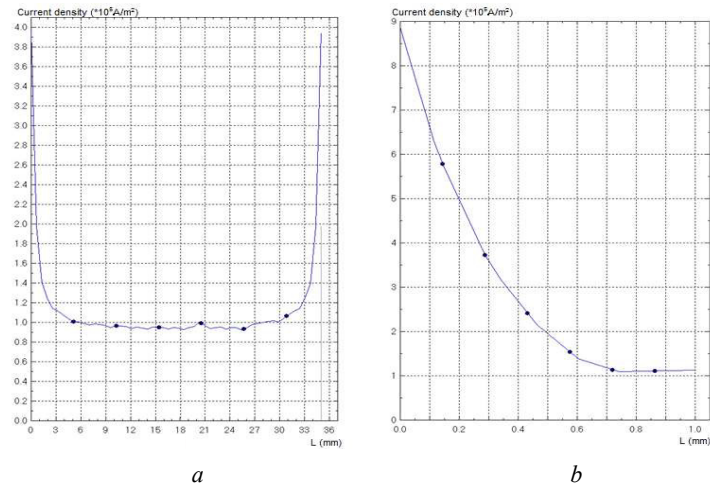
a   *b*

Fig. 5. The distribution of pipe eddy current density for the size 35×15 mm:
a – in the large side of the pipe; *b* – in the thickness of the pipe

Рис. 5. Распределение плотности вихревого тока трубы для типоразмера 35×15 мм:
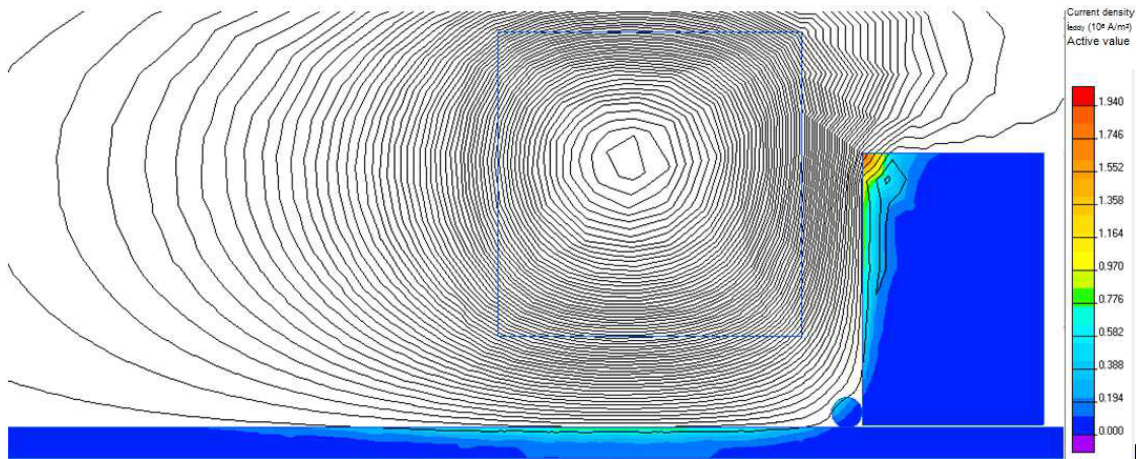*а* – по большой стороне трубы; *б* – по толщине трубы

Fig. 6. The distribution of eddy current density in the "inductor – waveguide" system for the size 35×15 mm

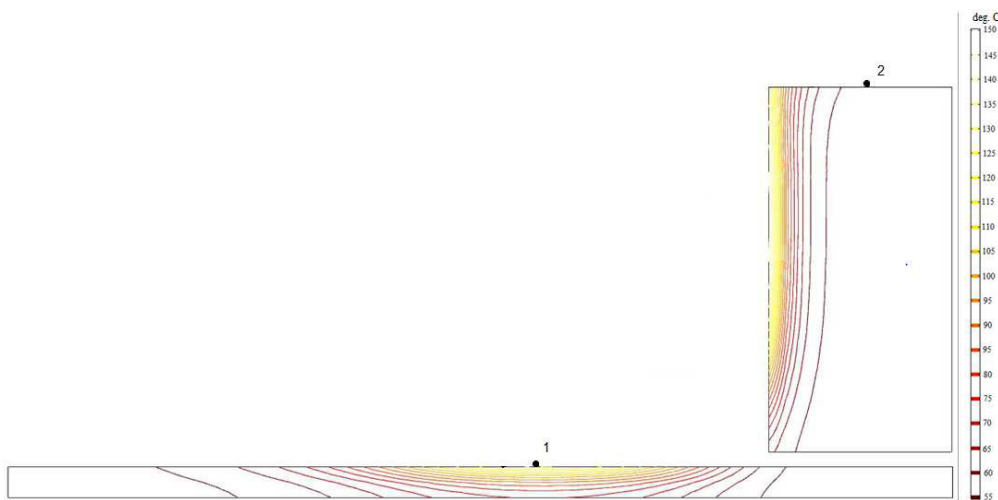Рис. 6. Распределение плотности вихревого тока в системе «индуктор – волновод» для типоразмера 35×15 мм

Fig. 7. Temperature fields of the waveguide during induction heating

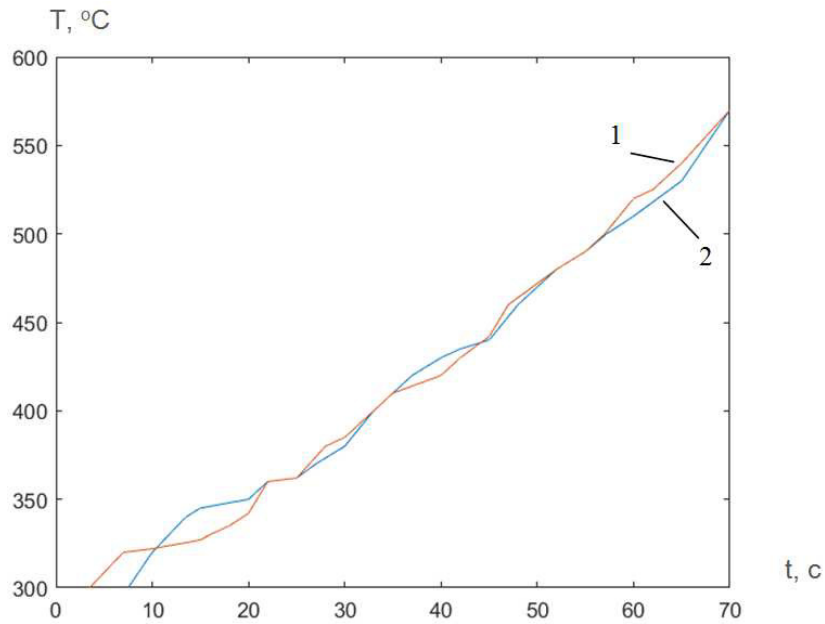Рис. 7. Температурные поля волновода при индукционном нагреве

Fig. 8. Heating of the 35 × 15 waveguide pipe:
1 – calculated values; *2* – measured data

Рис. 8. Нагрев трубы волновода типоразмера 35 × 15:
1 – расчетные значения; *2* – измеренные данные
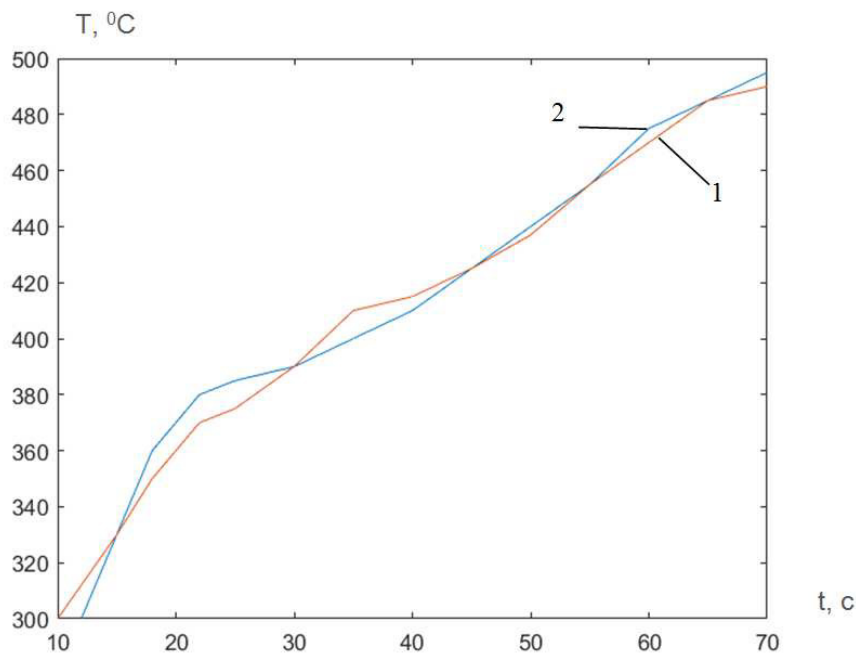
Fig. 9. Heating of the 35 × 15 waveguide flange:
1 – calculated values; *2* – measured data

Рис. 9. Нагрев фланца волновода типоразмера 35 × 15:
1 – расчетные значения; *2* – измеренные данные

Conclusion. 1. The process of induction soldering of waveguide paths has a number of features, which complicates the selection of process parameters for various types of waveguide paths and process control and suggests the need to simulate the heating of waveguides based on the differential equation of heat conduction.

2. To simulate the process of the pipe and the waveguide flange heating, it is most expedient to use the finite difference method.

Science, within the framework of the research project: "Mathematical and physical simulation of processes occurring during induction soldering of pipelines in protective environments", project № 18-48-242006.

References

1. Zlobin S. K., Mikhnev M. M., Laptenok V. D., Bocharov A. N., Dolgopolov B. B. [Features of production of waveguide-distribution paths of antenna-feeder devices of space vehicles]. *Vestnik SibGAU.* 2013, No 6, P. 196–201 (In Russ.).

2. Brovko A. V. [Problems of automatic welding of radar waveguides]. *Izvestiya vuzov: Mashinostroenie.* 2013, No. 1, P. 50–54 (In Russ.).

3. Bushminsky I. P. *Izgotovlenie ehlementov konstruktsii SVCh. Volnovody i volnovodnye ustroistva* [Manufacturing of elements of microwave structures. Waveguides and waveguide devices]. Moscow, Vysshaya shkola Publ., 1974, P. 304.

4. Full in-house production facilities. Available at: http://www.advancedmicrowave.com/our-facilities (accessed: 10.05.2020).

5. Pamin S. et al. Joining of aluminum waveguides using pulsed laser radiation. *Microwave Conference (APMC), 2015 Asia-Pacific. – IEEE*, 2015, vol. 3, P. 1–3.

6. Rapoport E., Pleshivtseva Y. Optimal Control of Induction Heating Processes. CRC Press, NY, 2007, 349 p.

7. Zlobin S. K. [Features of soldering elements of waveguide-distribution paths from aluminum alloys with the use of an induction heating source]. *Materialy XVI Mezhdunar. nauch. konf. "Reshetnevskie chteniya"* [Materials XVI Intern. Scientific. Conf "Reshetnev reading"]. Krasnoyarsk, 2012, Vol. 1, P. 16–17 (In Russ.).

8. Bocharova O. A., Tynchenko V. S., Bocharov A. N., Oreshenko T. G., Murygin A. V., Panfilov I. A. Induction heating simulation of the waveguide assembly elements. *Journal of Physics: Conference Series.* 2019, Vol. 1353, P. 012040.

9. Patidar B., Hussain M. M., Sanjoy Das, Mukherjee D, Tiwari A. P. Simulation and Experimental Validation of Induction Heating of MS Tube for Elevated Temperature. *NDT Application Excerpt from the Proceedings of the COMSOL Conference in Pune*, 2015, 6 p.

10. Rhein S., Tilman U., Knut G. Optimal control of induction heating processes using FEM software. *Conference: 2015 European Control Conference (ECC)*, 2015, P. 515–520.

11. Lykov A. V. *Teoriya teploprovodnosti* [Theory of thermal conductivity]. Moscow, Vysshaya shkola Publ., 1967, 599 p.

12. Babat G. I. *Induktsionnyi nagrev metallov i ego promyshlennoe primenenie* [Induction heating of metals and its industrial application]. Moscow – Leningrad, Energy Publ., 1965, 552 p.

13. Paskonov V. M., Polezhaev V. I., Chudov L. A. *Chislennoe modelirovanie protsessov teplo-massoobmena* [Numerical modeling of heat and mass transfer processes]. Moscow, Nauka Publ., 1984, 288 p.

14. Patankar S. V., Kalabin E. V., Yankov G. G. *Chislennoe reshenie zadach teploprovodnosti i konvektivnogo teploobmena pri techenii v kanalakh* [Numerical solution of problems of thermal conductivity and convective heat transfer during flow in channels]. Moscow, Mehi Publ., 2003, 312 p.

15. Samara A. A. *Teoriya raznostnykh skhem* [Theory of difference schemes]. Moscow, Nauka Publ., 1977, 388 p.

16. Zlobin S. K., Mikhnev M. M., Laptenok V. D., Seregin Yu. N., Bocharov A. N., Tynchenko V. S., Dubets Yu. P., Dolgopolov B. B. [Automated equipment and technology for soldering waveguide paths of spacecraft]. *Vestnik SibGAU.* 2014, No. 4 (56), P. 219–229 (In Russ.).

17. Murygin A. V., Tynchenko V. S., Laptenok V. D., Emilova O. A., Seregin Y. N. Modeling of thermal processes in waveguide tracts induction soldering. *IOP Conference Series: Materials Science and Engineering.* 2017, Vol. 173(1), P. 012026.

Библиографические ссылки

1. Особенности производства волноводно-распределительных трактов антенно-фидерных устройств космических аппаратов / С. К. Злобин, М. М. Михнев, В. Д. Лаптёнок и др. // Вестник СибГАУ. 2013. № 6. С. 196–201.

2. Бровко А. В. Проблемы автоматической сварки волноводов радиолокационных станций // Известия вузов: Машиностроение. 2013. № 1. С. 50–54.

3. Бушминский И. П. Изготовление элементов конструкций СВЧ. Волноводы и волноводные устройства. Учебное пособие для вузов. М. : Высшая школа, 1974. 304 с.

4. Full in-house production facilities [Электронный ресурс]. URL: http://www.advancedmicrowave.com/our-facilities (дата обращения: 10.05.2020).

5. Pamin S. et al. Joining of aluminum waveguides using pulsed laser radiation // Microwave Conference (APMC), 2015 Asia-Pacific. – IEEE, 2015. Vol. 3. P. 1–3.

6. Rapoport, E., Pleshivtseva Y. Optimal Control of Induction Heating Processes. CRC Press. N. Y., 2007.

7. Особенности пайки элементов волноводно-распределительных трактов из алюминиевых сплавов с применением источника индукционного нагрева / С. К. Злобин, М. М. Михнев, В. Д. Лаптёнок и др. // Решетневские чтения : материалы XVI междунар. научн. конф. : в 2 ч. Красноярск, 2012 . Ч. 1. С. 16–17.

8. Induction heating simulation of the waveguide assembly elements / O. A. Bocharova, V. S. Tynchenko, A. N. Bocharov et al. // Journal of Physics: Conference Series. IOP Publishing, 2019. Vol. 1353. P. 012040

9. Patidar, B. Simulation and Experimental Validation of Induction Heating of MS Tube for Elevated Temperature / B. Patidar, M. M. Hussain, Sanjoy Das et al. // NDT

Application Excerpt from the Proceedings of the COMSOL Conference in Pune. 2015.

10. Rhein S., Tilman U., Knut G. Optimal control of induction heating processes using FEM software // Conference: 2015 European Control Conference (ECC). 2015, P. 515–520.

11. Лыков А. В. Теория теплопроводности. М. : Высшая школа, 1967. 599 с.

12. Бабат Г. И. Индукционный нагрев металлов и его промышленное применение. М. – Л. : Энергия, 1965. 552 с.

13. Пасконов В. М., Полежаев В. И., Чудов Л. А. Численное моделирование процессов тепло-массообмена. М. : Наука, 1984. 288 с.

14. Патанкар С. В. Численное решение задач теплопроводности и конвективного теплообмена при течении в каналах : пер. с англ. Е. В. Калабина ; под ред. Г. Г. Янькова. М. : Изд-во МЭИ, 2003. 312 с.

15. Самарский А. А. Теория разностных схем. М. : Наука, 1977. 388 с.

16. Автоматизированное оборудование и технология для пайки волноводных трактов космических аппаратов / С. К. Злобин, М. М. Михнев, В. Д. Лаптенок и др. // Вестник СибГАУ. 2014. № 4(56). С. 219–229.

17. Modeling of thermal processes in waveguide tracts induction soldering / A. V. Murygin, V. S. Tynchenko, V. D. Laptenok et al. // IOP Conference Series: Materials Science and Engineering 173(1) 012026. 2017.

Bocharova Olesya Andreevna – senior lecturer of the department of Information and control systems; Reshetnev Siberian State University of Science and Technology. E-mail: shyx_89@mail.ru.

Murygin Aleksandr Vladimirovich – Dr. Sc., professor, head of the department of Information and control systems; Reshetnev Siberian State University of Science and Technology. E-mail: avm514@mail.ru.

Bocharov Aleksei Nikolaevich – Cand. Sc., docent of the department of Information and control systems; Reshetnev Siberian State University of Science and Technology. E-mail: sibalexbo@gmail.com.

Zaitsev Roman Viktorovich – a post-graduate student; Reshetnev Siberian State University of Science and Technology. E-mail: spoon27@yandex.ru.

Бочарова Олеся Андреевна – старший преподаватель кафедры информационно-управляющих систем; Сибирский государственный университет науки и технологий имени академика М. Ф. Решетнева. E-mail: shyx_89@mail.ru.

Мурыгин Александр Владимирович – доктор технических наук, профессор, заведующий кафедрой информационно-управляющих систем; Сибирский государственный университет науки и технологий имени академика М. Ф. Решетнева. E-mail: avm514@mail.ru.

Бочаров Алексей Николаевич – кандидат технических наук, доцент, доцент кафедры информационно-управляющих систем; Сибирский государственный университет науки и технологий имени академика М. Ф. Решетнева. E-mail: sibalexbo@gmail.com.

Зайцев Роман Викторович – аспирант; Сибирский государственный университет науки и технологий имени академика М. Ф. Решетнева. E-mail: spoon27@yandex.ru.

POINT DEFECTS IN NEMATIC LIQUID CRYSTAL MATERIALS WITH CONICAL ANCHORING AT THE INTERFACE

M. N. Krakhalev[1,2], V. F. Shabanov[3], V. Ya. Zyryanov[1*]

[1]Kirensky Institute of Physics, Federal Research Center KSC SB RAS
50/38, Akademgorodok, Krasnoyarsk, 660036, Russian Federation
[2]Institute of Engineering Physics and Radio Electronics, Siberian Federal University
79, Svobodny Av., Krasnoyarsk, 660041, Russian Federation
[3]Federal Research Center "Krasnoyarsk Science Center of the Siberian Branch of the Russian Academy of Sciences"
50, Akademgorodok St., Krasnoyarsk, 660036, Russian Federation
E-mail address: zyr@iph.krasn.ru

The topological point defects in nematic liquid crystal materials have been studied. The method of oblique light incidence has been proposed to determine an azimuthal director angle of an achiral nematic as well as a chiral nematic (cholesteric). The idea of the method is based on the dependence of the optical phase difference between ordinary and extraordinary light beams on the azimuthal director angle at the layer center at oblique incidence of light on a structure in which the polar director angle of a nematic liquid crystal is not equal to 0° or 90° (conical boundary conditions). It has been shown that the phase difference reaches a maximum at a zero azimuthal angle at the center of the layer regardless of the total twist angle of the director. The developed method has been used to analyze topological defects formed in the nematic and cholesteric layers under conical boundary conditions at the interface. The director field distributions of nematic and cholesteric near the surface point defects (boojums) with topological charges m = +1 and m = –1 have been drawn based on the experimental data. The proposed method of oblique light incidence can be used to analyze a wide class of the achiral and chiral liquid crystal media of various types: smectics, nematics, and cholesterics with tilted or hybrid boundary conditions.

Keywords: topological defect, orientational structure, nematic liquid crystal, optical phase difference.

ТОЧЕЧНЫЕ ДЕФЕКТЫ В НЕМАТИЧЕСКИХ ЖИДКОКРИСТАЛЛИЧЕСКИХ МАТЕРИАЛАХ С КОНИЧЕСКИМ СЦЕПЛЕНИЕМ НА ГРАНИЦЕ РАЗДЕЛА

М. Н. Крахалев[1,2], В. Ф. Шабанов[3], В. Я. Зырянов[1*]

[1] Институт физики им. Л. В. Киренского Сибирского отделения Российской академии наук – обособленное подразделение ФИЦ КНЦ СО РАН
Российская Федерация, 660036, г. Красноярск, Академгородок, 50/38
[2]Сибирский федеральный университет, Институт инженерной физики и радиоэлектроники
Российская Федерация, 660041, г. Красноярск, просп. Свободный, 79
[3]Федеральный исследовательский центр «Красноярский научный центр СО РАН»
Российская Федерация, 660036, г. Красноярск, Академгородок, 50
E-mail address: zyr@iph.krasn.ru

Исследованы топологические точечные дефекты в нематических жидкокристаллических материалах. Предложен метод наклонного падения света, позволяющий определять азимутальный угол директора ахирального нематика, а также закрученного нематика (холестерика). Суть метода состоит в том, что при наклонном падении света на структуру с отличным от 0° и 90° полярным углом директора нематического жидкого кристалла (конические граничные условия) оптическая разность фаз, возникающая между обыкновенным и необыкновенным лучами, определяется величиной азимутального угла директора в центре слоя. Показано, что максимальное значение разности фаз достигается при нулевом азимутальном угле в центре слоя независимо от полного угла закрутки директора. Разработанный метод был использован для анализа топологических дефектов, формирующихся в слоях нематика и холестерика с коническими граничными усло-

виями на межфазной границе. На основании полученных экспериментальных данных были построены распределения поля директора нематика и холестерика вблизи поверхностных точечных дефектов (буджумов) с топологическими зарядами *m = +1* и *m = –1*. Полученные результаты интересны для исследований структурированных материалов, анализа оптическими методами дефектов структур, а предложенный метод наклонного падения света может использоваться для анализа широкого класса ахиральных и хиральных жидкокристаллических сред различного типа: смектиков, нематиков и холестериков с наклонными или гибридными граничными условиями.

Ключевые слова: топологический дефект, ориентационная структура, нематический жидкий кристалл, оптическая разность фаз.

Introduction. Liquid crystals (LC) are anisotropic liquids with long-range orientational order of molecules. The orientation of LC molecules is characterized by the director n, which is a unit vector oriented along the preferred orientation of the long axes of the molecules [1]. A rich variety of forming configurations of the director's field is possible in an LC, depending on the boundary conditions (preferred orientation of the director at the interface), material parameters of the LC (elasticity constants, helix pitch), external electric or magnetic fields [2]. In this case, defects can be formed in the system, where significant distortions of the director field are observed. And vice versa, upon induction of strong distortions in the volume, for example, by magnetic (electric) fields or introduction of microparticles into the LC, topological defects are formed. The resulting distortions of the director field facilitate interaction between defects and particles which can be found in the effects of self-ordering of defects [3–5], colloidal [6; 7] and magnetic [8] particles, makes it possible to control the position of microparticles [9], and determines the group motion of defects in external electric field [10]. Thus, topological defects are an important feature that significantly affects the main characteristics of liquid crystal materials (optical, electro-optical, dynamic) which determine their prospects for various applications in modern information technologies.

Point bulk (hedgehogs) [11; 12] and surface (boojums) [13] defects, linear defects [14] and two-dimensional defects (walls) [2] can be formed in nematic LC. In the case of twisted nematic with the ratio $d / p \approx 1$ of the layer thickness d and the helix pitch p, soliton-like structures [15] or linear defects [16] can be formed in the system. The possibility of formation and stability of various types of defects is determined by the boundary conditions specified on the substrates. Thus, under degenerate tangential (planar) boundary conditions (the angle between the director and the normal to the surface is 90°), a schlieren texture is formed in the LC cell which consists of point and linear defects, the strength of which depends on the ratio of the LC elastic constants [17]. In the case of homeotropic anchoring (the angle between the director and the normal to the surface is 0°), there are initially no defects in the system, but the application of an electric field or a combination of electric and magnetic fields promote the formation of an ordered set of point defects [3], two-dimensional defects [2], or soliton-like structures in twisted nematic [15]. Under homeo-planar boundary conditions, the formation of point defects on a substrate with planar anchoring or a structure of domains with closed linear defects is possible in the system.

Conical boundary conditions (the director is oriented to the surface normal at an angle other than 0° and 90°) are more suitable for the occurrence of defects. For example, in a cell with a conical anchoring, point, linear, and two-dimensional defects are formed even when there are no external fields [18]. In the case of a twisted nematic with planar-conical anchoring, linear defects are formed [19] or domains bounded by a closed linear defect with a pair of point singularities [20]. At the same time, point defects in LC systems with conical anchoring have not been practically investigated to this date.

This work presents for the first time the results of studying the structures of point defects formed in nematic and twisted nematic under conical boundary conditions on both substrates.

Materials and methods. The studies were carried out for a nematic LN-396 mixture (Belarusian State Technological University) and LN-396 mixture doped with a left-handed chiral addition of cholesteryl acetate (Sigma Aldrich). The concentration of cholesteryl acetate was 0.2 % which determines the pitch of the cholesteric helix with a value of $p = 72.5$ μm [19]. The studies were carried out in LC cells consisting of two glass substrates assembled in such a way that a gap is formed between them which is filled with a liquid crystal (fig. 1, a). Glass substrates were coated by centrifugation with a poly(isobutyl methacrylate) film (Sigma Aldrich) which sets conical boundary conditions for the used nematic LN-396 with a polar angle $\theta_{d/2} = 40°$ [21]. The thickness d of the LC layer was set with glass balls and was measured by the interference method until the cell was filled with a liquid crystal. LC cells were filled at room temperature and kept for at least 24 hours before to the study. The studies were carried out using a polarizing microscope (POM) AxioImager.M1m (CarlZeiss) with a 20x / 0.22 long-focus objective in monochromatic light with a wavelength of $\lambda = 546$ nm. The refractive indices of LC LN-396 $n_\perp = 1.528$, $n_\parallel = 1.741$ ($\lambda = 546$ nm).

Oblique incidence light method. It is convenient to describe the distribution of the director field in the cell using the polar θ (x, y, z) and azimuthal φ (x, y, z) angles (fig. 1, b). In this case, the n-director is described by the following equation:

$$\begin{cases} n_x = \sin\left(\theta[x,y,z]\right)\cos\left(\varphi[x,y,z]\right), \\ n_y = \sin\left(\theta[x,y,z]\right)\sin\left(\varphi[x,y,z]\right), \\ n_z = \cos\left(\theta[x,y,z]\right). \end{cases} \quad (1)$$

Generally, the angles θ and φ can vary both over the thickness of the LC layer and in the plane of substrates.

This is more typical for the LC areas near defects, and the nature of the change in the angles is determined by the type of defect. Conversely, the nature of the change in the angles in the vicinity of the defect can be used to determine its parameters. In the case of point defects in nematics, the method of fluorescence microscopy is used [22]. In the case of an tilted orientation of the director in the bulk which is realized under conical boundary conditions, it is convenient to use the method of oblique incidence of light proposed and described below in order to characterize defects.

Consider a twisted nematic away from defects. In this case, we can assume that the polar angle of the director is constant and equal to the tilt angle of the director on substrates $\theta(x, y, z) = \theta_{d/2} = \theta_{-d/2}$, and the azimuthal angle $\varphi(x, y)$ depends on the coordinate z linearly:

$$\varphi(x, y, z) = \varphi_0(x, y) + \frac{\varphi_{TOTAL}}{d} z, \qquad (2)$$

where $\varphi_0(x, y)$ – azimuthal angle of the director at the center of the layer (at $z = 0$), φ_{TOTAL} is the difference between the azimuthal angles of the director on the upper ($z = +d/2$) and lower ($z = -d/2$) substrates (the total azimuthal angle of rotation of the director on the layer d-thickness). Consider the oblique incidence of the light beam on the LC layer in the *xOz* plane (fig. 1, *b*). The direction of the beam will be characterized by the unit vector $\boldsymbol{k}^0(\pm\sin\alpha, 0, \cos\alpha)$, where the plus sign corresponds to the zero azimuthal angle for the vector $\boldsymbol{k}^0$, the minus sign corresponds to the value of the azimuthal angle of the vector $\boldsymbol{k}^0$ equal to π. When Mauguin condition [23] is fulfilled, we can assume that two linear waves propagate in such a twisted structure, the phase difference between which in the case of oblique light incidence at an angle α is determined as:

$$\delta = \frac{2\pi d}{\lambda \cos\alpha}\left(\int_{-1/2}^{1/2} \frac{n_\perp n_\|}{\sqrt{n_\perp^2 + \left(n_\|^2 - n_\perp^2\right)\cos^2(\theta')}} dz' - n_\perp\right), \quad (3)$$

where $z' = z/d$, $\cos(\theta')$ equals:

$$\cos(\theta') = \boldsymbol{n}\boldsymbol{k}^0 = \pm\sin\alpha\sin\left(\theta_{d/2}\right)\cos\left(\varphi_0(x, y) + \varphi_{TOTAL}z'\right) + \\ + \cos\alpha\cos\left(\theta_{d/2}\right). \qquad (4)$$

Fig. 2 shows the dependences on the angle $\varphi_0(x, y)$ of the δ/d values calculated by equation (3) for several values of the total twist angle φ_{TOTAL} at an oblique incidence at an angle $\alpha = 5.33°$ (for the case shown in fig. 1, *b*), and polar angle $\theta_{d/2} = 40°$. It can be seen that one maximum is observed in the dependences only at the angle $\varphi_0(x, y) = 0°$, and an increase in the angle φ_{TOTAL} leads to a slight decrease in the difference $(\delta_{max} - \delta_{min})/d$ from a value of approximately 0.43 rad/μm to 0.27 rad/μm for angles φ_{TOTAL} 0° and 180 °, respectively. Such a difference in the phase differences observed for different azimuthal angles $\varphi_0(x, y)$ can be easily fixed for the commonly used LC cell thicknesses of about 10 μm. At the same time, the angle α used for calculation makes it easy to carry out observations with a polarizing microscope using a long-focus lens. The data presented in fig. 2 were obtained for positive angles φ_{TOTAL} (right-handed cholesteric), while due to the symmetry of the structure relative to the center of the layer, identical results are obtained for negative angles φ_{TOTAL} (left-handed cholesteric).

The above results were obtained from the assumption that the polar angle of the θ-director is constant and there is a simple linear dependence of the azimuthal angle φ on the coordinate z. In general, these conditions may not be met. For example, in a twisted nematic structure with significant pretilt angles of the director on substrates, the polar angle θ begins to depend on the z coordinate, while the dependence of the azimuthal angle of the director on the z coordinate deviates from the linear law [24]. Nevertheless, the results obtained for simple cases show that the maximum value of δ is reached at $\varphi_0(x, y) = 0°$ regardless of the values of the angle $\theta_{d/2}$ and φ_{TOTAL}.
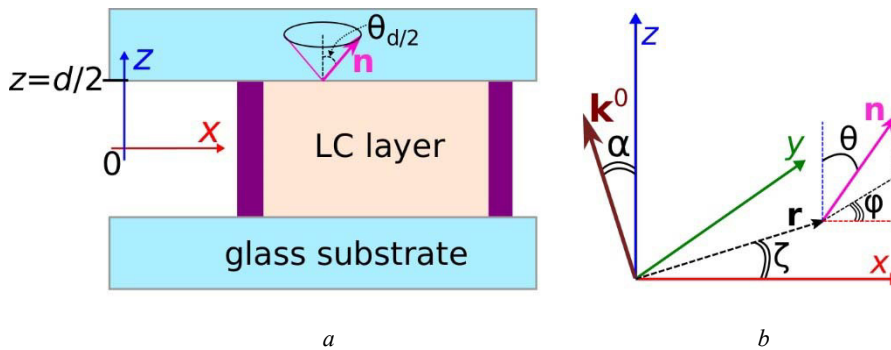

Fig. 1. Scheme of LC cell (*a*) and the coordinate system used to calculate
the optical phase difference at oblique light incidence and the director
field around the boojums (*b*)

Рис. 1. Схематическое представление ЖК ячейки (*a*) и система координат,
используемая для расчетов оптической разности фаз в случае наклонного
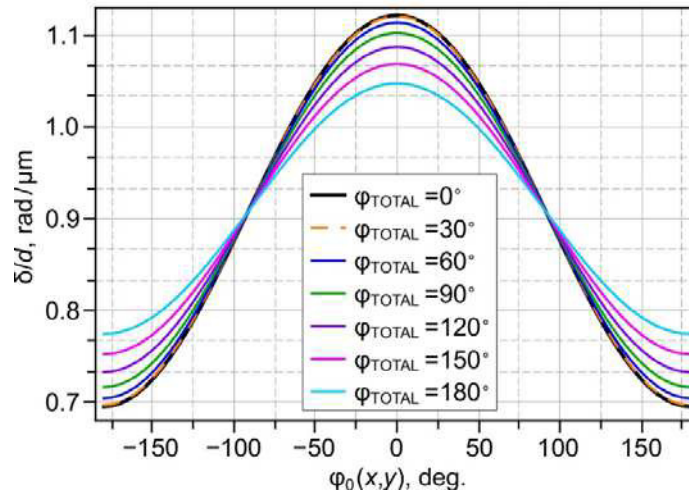падения света и поля директора вокруг буджумов (*b*)

Fig. 2. Dependences of the ratio δ/d on the angle $\varphi_0(x, y)$ calculated
for some twist angles φ_{TOTAL}. The data have been calculated for the angles
$\alpha = 5.33°$, $\theta(x, y, z) = \theta_{d/2} = 40°$, the wavelength $\lambda = 546$ nm and the refractive
indices corresponding to LC LN-396

Рис. 2. Зависимости отношения δ/d от угла $\varphi_0(x, y)$, рассчитанные
для нескольких углов закрутки φ_{TOTAL}. Расчет сделан для углов $\alpha = 5,33°$,
$\theta(x, y, z) = \theta_{d/2} = 40°$, длины волны света $\lambda = 546$ нм и показателей
преломления, соответствующих ЖК ЛН-396

Thus, this conclusion can be extended to the case of an inhomogeneous slope and an uneven twist angle in the case when the director distribution in the bulk is symmetric about the center of the layer. It is this situation that is realized in LC cells under the same boundary conditions in the absence of external influences (for example, an electric field). Further, this method will be applied to analyze boojums that form in nematic and twisted nematic under conical boundary conditions.

Boojums in nematic. In the absence of a given orientation of the director on the substrates (degenerate tangential or conical boundary conditions), point defects on the surface (boojums) are formed in the system. Near boojums, the orientation of the director on the surface (plane $z = d/2$) can be described as [25]

$$\begin{cases} n_x = \sin\left(\theta_{d/2}\right)\cos\left(m\zeta + \xi\right), \\ n_y = \sin\left(\theta_{d/2}\right)\sin\left(m\zeta + \xi\right), \\ n_z = \cos\left(\theta_{d/2}\right). \end{cases} \qquad (5)$$

where ζ is the angle in the polar coordinate system (fig. 1, b), m is the surface topological charge (strength) of the defect, $-\pi \le \xi < \pi$ is the twist angle of the boojum. The strength of the defect m and the angle ξ are used to classify boojums (as well as topological defects of other types), and, accordingly, the determination of these two parameters is sufficient to characterize the properties of topological defects. The LC cell has two substrates and the appearance of a boojum on one of the substrates (for example, the upper one at $z = d/2$) should be accompanied by the formation of a point defect on the second (lower one at $z = -d/2$) substrate. The identical distribu-

tion of the director near the boojums on the upper and lower substrates (escaped state) will correspond to the minimum of elastic energy. To determine the charge m, the sample is observed in the geometry of crossed linear polarizers (LP). In this case, extinction lines emerge from the defect, the number of which N is related to the charge of the defect by a simple relationship: $N = |m| \cdot 4$ (fig. 3, a). The m sign can be determined by rotating the polarizers relative to the sample or by observing in circular polarizers (CP). In the case of boojums with $m = +1$, the interference pattern observed in the geometry of circular polarizers near defects will have radial symmetry, while for boojums with $m = -1$, due to the inequality of splay, band, and twist LC elastic constants, the interference pattern will have lower symmetry (fig. 3, b). In the case of a nematic, the total twist angle of the director is $\varphi_{TOTAL} = 0$; accordingly, the azimuthal angle of the director turns out to be independent of the coordinate z and is equal to $\varphi_0(x, y)$. Since in the vicinity of boojums the azimuthal angle of the director varies in the range $-180° \le \varphi(x, y) = m\zeta + \xi \le 180°$, the twist angle ξ can be determined using the method of oblique incidence of light. In this case, when implementing the scheme shown in fig. 2 δ_{max} is observed under the condition $(m\zeta + \xi) = 0$, and δ_{min} corresponds to the condition $(m\zeta + \xi) = \pi (-\pi)$. It is convenient to use circular polarizers for this method.

The fig. 3 shows boojums with $|m| = 1$ which can be seen from observations in the geometry of crossed linear polarizers. When observed in the geometry of crossed circular polarizers, the observed interference pattern is determined only by the phase difference between the ordinary and extraordinary waves. It can be seen that the interference pattern in the vicinity of the boojums corresponds to the case when the phase difference increases from zero to $\delta > 4\pi$ as we move from the boojum to the

periphery, which fits well with the parameters of the LC cell with the LC layer thickness $d = 14.6$ μm and the director tilt angle $\theta_{d/2} = 40°$, for which the value $\delta = 4.17\pi$ is obtained from equation (3) at $\alpha = 0°$ and $\varphi_{TOTAL} = 0$. This corresponds to the situation described above, when the boojums on the upper and lower substrates are located opposite one another (escaped state). In the geometry of crossed linear polarizers from the boojum with $m = +1$ (fig. 3, the first row) four extinction bands emerge parallel to the polarizers. When observed in circular polarizers, the interference pattern is symmetric in the case of normal incidence of light ($\alpha = 0°$) (fig. 3, *b*, the first row). In the case of oblique incidence of light at an angle $\alpha = 5.33°$, the symmetry of the interference pattern is broken (fig. 3, *c*, the first row). Based on the change in the brightness of the observed interference pattern, it can be concluded that the maximum phase difference δ_{max} corresponds to the extinction line oriented at an angle $\zeta = -90°$, and δ_{min} corresponds to the value of the angle $\zeta = +90°$. This means that the twist angle of the boojum on the upper substrate $\xi = 90°$ (fig. 3, *d*, the first row). Similarly, we can determine the twist angle of a boojum with a charge $m = -1$ (fig. 3, the second row). In the geometry of crossed linear polarizers (at $\alpha = 0°$), the extinction bands form a straight cross oriented at an angle of 15° to the direction of the linear polarizer LP. From the interference pattern observed at an oblique ($\alpha = 5.33°$) incidence of light in the geometry of circular polarizers, it can be seen that δ_{max} corresponds to an extinction band oriented at an angle $\zeta = -75°$ which corresponds to a boojum twist angle on the upper substrate $\xi = -75°$ (fig. 3, *d*, the second row).

It should be noted that the sample contains boojums with the charge $m = +1$ and the twisting angle ξ close to $\pm 90°$. Thus, the boojum with $m = +1$ and $|\xi| = 90°$ is energetically most favorable for LC LN-396 in the case of the director tilt angle $\theta_{d/2} = 40°$. For boojums with a charge $m = -1$, different twist angles ξ are observed. This is a consequence of the fact that the distribution of the director field near the boojum with $m = -1$ at different angles ξ differs only in the orientation of the symmetry axes, i. e., the boojum with the angle ξ can be obtained by rotating the entire structure (coordinate system) of the director field with $\xi_0 = 0$ around the *Oz* axis by an angle $\xi/2$ [25]. Thus, the total free energy of the nematic director field near the boojums with $m = -1$, in contrast to the boojums with $m = +1$, does not depend on the twisting angle ξ.

Boojums in twisted nematic (cholesteric). The cholesteric structures were studied for a cell with a thickness of $d = 12.7$ μm which corresponds to the ratio $d/p = 0.18$. In this case, extinction bands are observed for an angle of 58° between the analyzer and the polarizer which corresponds to the director twisting angle $\varphi_{TOTAL} = -32°$ (fig. 4, *a* and 5, *a*).
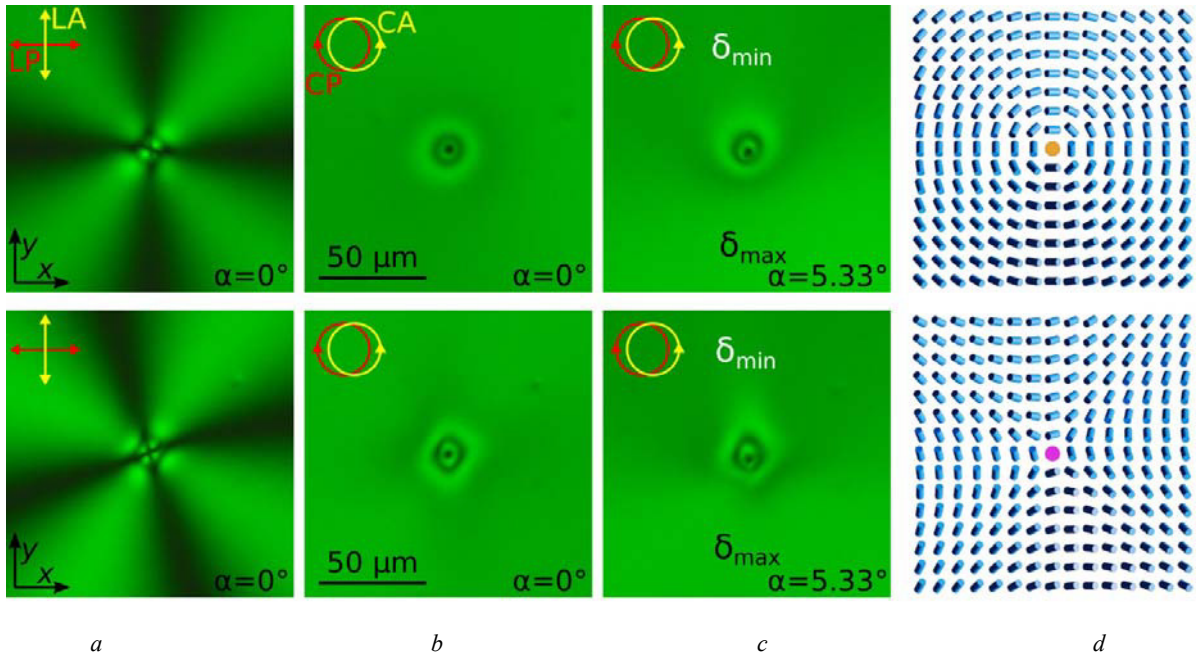

Fig. 3. POM photos of the sample areas of nematic with boojums of $m = +1$ strength and the twisting angle $\xi = 90°$ (the first row), $m = -1$ and $\xi = -75°$ (the second row). The photos were taken in the monochromatic light ($\lambda = 546$ nm) for the crossed linear polarizer (LP) and analyzer (LA) at the polarizer orientation LP 0° (*a*), for the crossed circular polarizer (CP) and analyzer (CA) at the light incidence angle $\alpha = 0°$ (*b*) and $\alpha = 5.33°$ (*c*). The corresponding director field distributions on the top substrate calculated by eq. (5) (*d*)

Рис. 3. POM фотографии участков образца нематика с буджумами, имеющими силу $m = +1$ и угол закрутки $\xi = 90°$ (первый ряд), $m = -1$ и угол закрутки $\xi = -75°$ (второй ряд). Фотографии сделаны в монохроматическом свете ($\lambda = 546$ нм) в геометрии скрещенных линейных поляризатора (LP) и анализатора (LA) для ориентации поляризатора LP 0° (*a*), скрещенных циркулярных поляризатора (CP) и анализатора (CA) для углов падения света $\alpha = 0°$ (*b*) и $\alpha = 5,33°$ (*c*). Рассчитанные по уравнению (5) соответствующие распределения поля директора на верхней подложке (*d*)
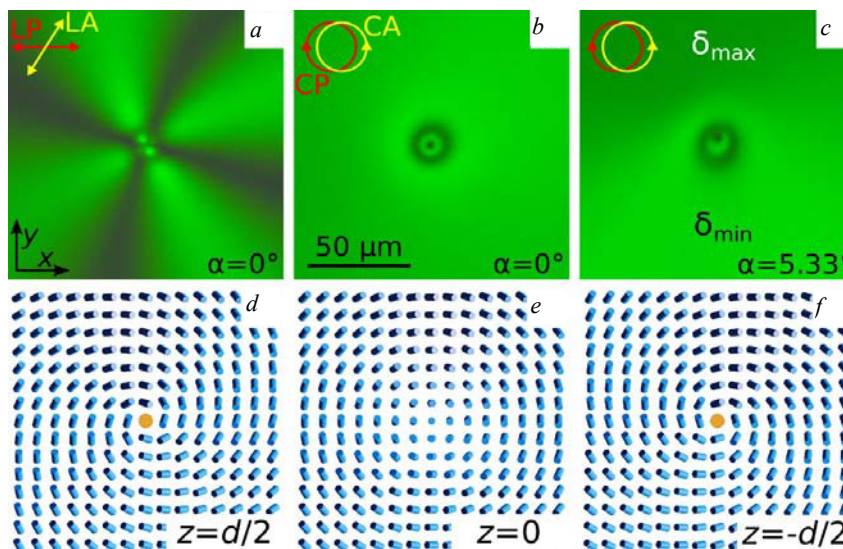
Fig. 4. POM photos of the sample area of cholesteric with boojum of $m = +1$ strength and the twisting angle on the top substrate $\xi = -106°$ taken in the monochromatic light ($\lambda = 546$ nm) for the crossed at 58° angle linear polarizers at the polarizer orientation LP 0° (*a*), for the crossed circular polarizers at the light incidence angle $\alpha = 0°$ (*b*) and $\alpha = 5.33°$ (*c*). The corresponding director field distributions on the top substrate (*d*), at the layer center (*e*) and on the bottom substrate (*f*) calculated by equation (5) considering the conditions (2)

Рис. 4. POM фотографии участка образца холестерика с буджумом, имеющими силу $m = +1$ и угол закрутки на верхней подложке $\xi = -106°$, сделанные в монохроматическом свете ($\lambda = 546$ нм) в геометрии скрещенных под углом 58° линейных поляризаторов для ориентации поляризатора LP 0° (*a*), скрещенных циркулярных поляризаторов для углов падения света $\alpha = 0°$ (*b*) и $\alpha = 5,33°$ (*c*). Рассчитанные по уравнению (5) с учетом условия (2) соответствующие распределения поля директора на верхней подложке (*d*), в центре слоя (*e*) и на нижней подложке (*f*)
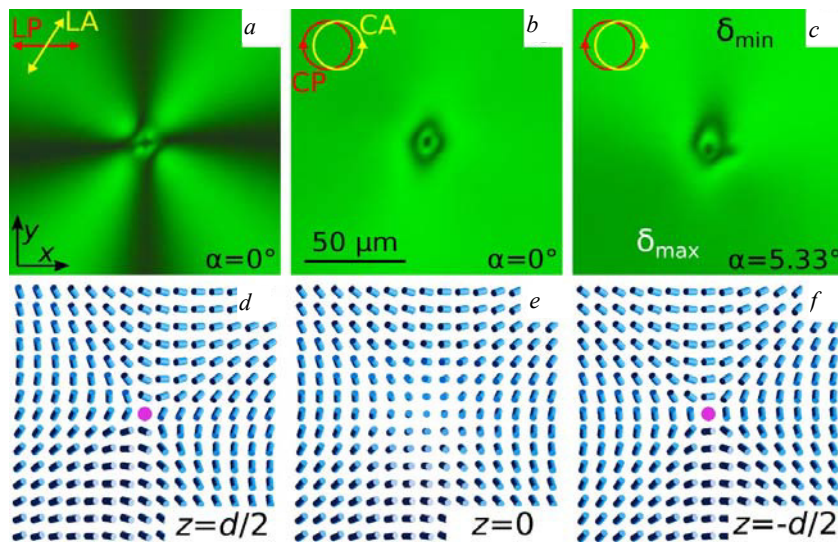

Fig. 5. POM photos of the sample area of cholesteric with boojum of $m = -1$ strength and the twisting angle on the top substrate $\xi = -116°$ taken in the monochromatic light ($\lambda = 546$ nm) for the crossed at 58° angle linear polarizers at the polarizer orientation LP 0° (*a*), for the crossed circular polarizers at the light incidence angle $\alpha = 0°$ (*b*) and $\alpha = 5.33°$ (*c*). The corresponding director field distributions on the top substrate (*d*), at the layer center (*e*) and on the bottom substrate (*f*) calculated by equation (5) considering the conditions (2)

Рис. 5. POM фотографии участка образца холестерика с буджумом, имеющими силу $m = -1$ и угол закрутки на верхней подложке $\xi = -116°$, сделанные в монохроматическом свете ($\lambda = 546$ нм) в геометрии скрещенных под углом 58° линейных поляризаторов для ориентации поляризатора LP 0° (*a*), скрещенных циркулярных поляризаторов для углов падения света $\alpha = 0°$ (*b*) и $\alpha = 5,33°$ (*c*). Рассчитанные по уравнению (5) с учетом условия (2) соответствующие распределения поля директора на верхней подложке (*d*), в центре слоя (*e*) и нижней подложке (*f*)

Fig. 4 shows a boojum with $m = +1$, for which the extinction bands form a straight cross rotated at an angle of $-16°$ with respect to the direction of the polarizer. Observations with oblique incidence of light on the cell (fig. 4, *c*) show that δ_{max} and, consequently, the value $\varphi_0(x, y) = 0$, is observed at an angle $\zeta \approx 90°$. In this case, in the approximation of the linear dependence of the azimuthal angle of the director on the coordinate *z* (equation (2)), the twisting angle of the boojum on the upper substrate can be found from the relation ($+1\cdot90° + \xi = \varphi_{TOTAL}/2$), whence $\xi_{d/2} = -106°$ (fig. 4, *d*), while on the lower substrate $\xi_{-d/2} = -74°$ (fig. 4, *f*). The orientation of the four extinction lines corresponds to the condition when $\varphi_{-d/2}$ equals $0°$, $\pm 90°$ and $-180°$, which corresponds to angles $74°$, $164°$, $-16°$, $-106°$ and is consistent with the orientation of extinction bands observed in the geometry of crossed polarizers (fig. 4, *a*).

The twisting angle of boojums with $m = -1$ (fig. 5) can be determined in a similar manner. The cross that forms the extinction bands is oriented at an angle of approximately $5°$ to the polarizer (fig. 5, *a*), while δ_{max} is reached at an angle of $\zeta \approx -100°$ (fig. 5, *c*). This corresponds to the twisting angle of the boojum on the upper substrate which is found from the relation ($-1\cdot(-100°) + \xi = \varphi_{TOTAL}/2$), whence $\xi_{d/2} = -116°$ (fig. 5, *d*). On the lower substrate, it corresponds to a boojum with $\xi_{-d/2} = -84°$ (fig. 5, *f*).

Conclusion. In this work we propose a method of oblique incidence of light on an LC cell which makes it possible to determine the polar and azimuthal angles of the director orientation in the case of conical boundary conditions. The capabilities of this method were demonstrated by the example of point topological defects-boojums that form in nematic with a director tilt angle at the boundary $\theta_{d/2} = 40°$, for which the defect strength *m* and twisting angles ξ were first determined. It is shown that in the used nematic liquid crystal LN-396, there is a tendency for the formation of boojums with $m = +1$, having a twisting angle $\xi = \pm 90°$. This method is also applicable for a twisted cholesteric structure. In this case, if the Mauguin regime is fulfilled, the maximum phase difference δ_{max} between the ordinary and extraordinary beams is achieved at the azimuthal orientation of the director at the center of the layer $\varphi_0(x, y) = 0$, regardless of the total angle of rotation of the director φ_{TOTAL}. Using the proposed method, we determined the orientational structure of boojums, formed on the upper and lower substrates specifying conical anchoring for the liquid crystal. The results obtained are of interest for studies of structured materials, analysis of defect structure by optical methods, and the developed method of oblique incidence of light can potentially be used to analyze a wide class of optically anisotropic and chiral media, such as smectics, nematics and cholesterics with tilted or hybrid boundary conditions.

It is necessary to note the applied significance of the research results, since liquid crystal media today remain the most competitive functional materials for use in opto-electronic devices requiring low weight and dimensions, low-voltage control and low power consumption which, for example, is very important for use in space technologies.

References

1. Gennes P. G. de, Prost J. The physics of liquid crystals. 2. ed., Reprint. Oxford: Clarendon Press, 1998. 597 p.

2. Oswald P., Pieranski P. Nematic and cholesteric liquid crystals: concepts and physical properties illustrated by experiments. Boca Raton: Taylor & Francis, 2005. 618 p.

3. Sasaki Y. et al. Large-scale self-organization of reconfigurable topological defect networks in nematic liquid crystals. *Nature Communications*. 2016, Vol. 7, No. 1, P. 13238.

4. Kim M., Serra F. Tunable dynamic topological defect pattern formation in nematic liquid crystals. *Advanced Optical Materials*. 2020, Vol. 8, No. 1, P. 1900991.

5. Kim M., Serra F. Topological defect arrays in nematic liquid crystals assisted by polymeric pillar arrays: effect of the geometry of pillars. *Crystals*. 2020, Vol. 10, No. 4, P. 314.

6. Senyuk B. et al. Topological colloids. *Nature*. 2013, Vol. 493, No. 7431, P. 200–205.

7. Nych A. et al. Assembly and control of 3D nematic dipolar colloidal crystals. *Nature Communications*, 2013, Vol. 4, No. 1, P. 1489.

8. Medle Rupnik P. et al. Field-controlled structures in ferromagnetic cholesteric liquid crystals. *Science Advances*. 2017, Vol. 3, No. 10, P. 1701336.

9. Lavrentovich O. D. Transport of particles in liquid crystals. *Soft Matter*. 2014, Vol. 10, No. 9, P. 1264–1283.

10. Sohn H. R. O., Liu C. D., Smalyukh I. I. Schools of skyrmions with electrically tunable elastic interactions. *Nature Communications*. 2019, Vol. 10, No. 1, P. 4744.

11. Sengupta A. Microbial active matter: A topological framework. *Front. Phys. Frontiers*. 2020, Vol. 8, P. 184.

12. Nabarro F. R. N. Singular lines and singular points of ferromagnetic spin systems and of nematic liquid crystals. *Journal de Physique*. 1972, Vol. 33, No. 11–12, P. 1089–1098.

13. Meyer R. B. Point disclinations at a nematic-isotropic liquid interface. *Molecular Crystals and Liquid Crystals*. 1972, Vol. 16, No. 4, P. 355–369.

14. Kleman M., Friedel J. Disclinations, dislocations, and continuous defects: A reappraisal. *Rev. Mod. Phys.* 2008, Vol. 80, No. 1, P. 61–115.

15. Oswald P., Baudry J., Pirkl S. Static and dynamic properties of cholesteric fingers in electric field. *Physics Reports*. 2000, Vol. 337, No. 1, P. 67–96.

16. Smalyukh I. I., Lavrentovich O. D. Three-dimensional director structures of defects in Grandjean-Cano wedges of cholesteric liquid crystals studied by fluorescence confocal polarizing microscopy. *Phys. Rev. E*. 2002, Vol. 66, No. 5, P. 051703.

17. Madhusudana N. V., Pratibha R. Studies on high strength defects in nematic liquid crystals. *Molecular Crystals and Liquid Crystals*. 1983, Vol. 103, No. 1–4, P. 31–47.

18. Ryschenkow G., Kleman M. Surface defects and structural transitions in very low anchoring energy nematic thin films. *Journal of Chemical Physics*. 1976, Vol. 64, No. 1, P. 404–412.

19. Krakhalev M. N. et al. Nematic and cholesteric liquid crystal structures in cells with tangential-conical boundary conditions. Crystals. 2019, Vol. 9, No. 5, P. 249.

20. Krakhalev M. N. Electrically induced transformations of defects in cholesteric layer with tangential-conical boundary conditions. *Scientific reports*. 2020. Vol. 10. P. 4907.

21. Krakhalev M.N. et al. Director configurations in nematic droplets with tilted surface anchoring. *Liquid Crystals*. 2017, Vol. 44, No. 2, P. 355–363.

22. Ohzono T. Uncovering different states of topological defects in schlieren textures of a nematic liquid crystal. *Scientific reports*. 2017, Vol. 7, P. 16814.

23. Yeh P., Gu C. Optics of liquid crystal displays. New York, Wiley, 1999, 438 p.

24. Lien A. The general and simplified Jones matrix representations for the high pretilt twisted nematic cell. *Journal of Applied Physics*. 1990, Vol. 67, No. 6, P. 2853–2856.

25. Harth K., Stannarius R. Topological point defects of liquid crystals in quasi-two-dimensional geometries. *Front. Phys. Frontiers.* 2020, Vol. 8, P. 112.

Krakhalev Mikhail Nikolaevich – Cand. Sc., senior researcher, Laboratory of molecular spectroscopy, Kirensky Institute of Physics, Federal Research Center KSC SB RAS, Associate Professor at the Department of General Physics, Institute of Engineering Physics and Radio Electronics, Siberian Federal University. E-mail: kmn@iph.krasn.ru.

ShabanovVasilyPhilipovich – Dr. Sc., Professor, Academician, Scientific director of Federal Research Center "Krasnoyarsk Science Center of the Siberian Branch of the Russian Academy of Sciences". E-mail: shabanov@ksc.krasn.ru.

Zyryanov Victor Yakovlevich – Dr. Sc., Professor, Head of the scientific direction and Laboratory of molecular spectroscopy, Kirensky Institute of Physics, Federal Research Center KSC SB RAS. E-mail: zyr@iph.krasn.ru.

Крахалев Михаил Николаевич – кандидат физико-математических наук, старший научный сотрудник лаборатории молекулярной спектроскопии, Институт физики им. Л. В. Киренского Сибирского отделения Российской академии наук – обособленное подразделение ФИЦ КНЦ СО РАН; доцент кафедры общей физики, Институт инженерной физики и радиоэлектроники Сибирского федерального университета. E-mail: kmn@iph.krasn.ru.

Шабанов Василий Филиппович – доктор физико-математических наук, профессор, академик РАН, научный руководитель; Федеральный исследовательский центр «Красноярский научный центр СО РАН». E-mail: shabanov@ksc.krasn.ru.

Зырянов Виктор Яковлевич – доктор физико-математических наук, профессор, руководитель научного направления, заведующий лабораторией молекулярной спектроскопии; Институт физики им. Л. В. Киренского Сибирского отделения Российской академии наук – обособленное подразделение ФИЦ КНЦ СО РАН. E-mail: zyr@iph.krasn.ru.

ELECTRONIC STRUCTURE CHANGE AT CATIONIC SUBSTITUTION OF MANGANESE SULFIDE BY ELEMENTS WITH VARIABLE VALENCE

O. B. Romanova[1*], S. S. Aplesnin[1,2], L. V. Udod[1,2]

[1]Kirensky Institute of Physics, Federal Research Center KSC SB RAS
50/38, Akademgorodok, Krasnoyarsk, 660036, Russian Federation
[2]Reshetnev Siberian State University of Science and Technology
31, Krasnoyarskii rabochii prospekt, Krasnoyarsk, 660037, Russian Federation
*E-mail: rob@iph.krasn.ru

Cation-substituted solid solutions $Yb_XMn_{1-X}S$ were prepared by the melt method from polycrystalline sulfide powders. The synthesized samples are antiferromagnetic semiconductors and, according to the results of X-ray structural analysis, have an FCC structure of the NaCl type. Structural, electrical, optical, and acoustic properties of the chalcogenide system $Yb_XMn_{1-X}S$ were studied in the temperature range 80–500 K. The effect of variable valence elements on the electronic structure of cationic substitution of manganese sulfide has been studied. The change in the electronic structure in the $Yb_XMn_{1-X}S$ system occurs due to the electron-phonon interaction. Samples with variable valence have anomalous compressibility, which is confirmed by the data on the thermal expansion coefficient and the change in the attenuation coefficient. As a result of inelastic interaction with d- electrons, the density of states at the Fermi level changes, this is reflected in the temperature dependence of the conductivity. The positions of the f-level and two electronic transitions were determined from the IR spectra. A zone of temperatures and concentrations was found, where a correlation of structural, electrical, optical and acoustic properties is observed. To explain the experimental results, the electronic structure of the semiconductor is considered and a model is proposed that qualitatively describes the experiment.

Keywords: elements with variable valence, structure, IR spectroscopy, attenuation coefficient, conductivity, electronic structure.

ИЗМЕНЕНИЕ ЭЛЕКТРОННОЙ СТРУКТУРЫ ПРИ КАТИОННОМ ЗАМЕЩЕНИИ СУЛЬФИДА МАРГАНЦА ЭЛЕМЕНТАМИ С ПЕРЕМЕННОЙ ВАЛЕНТНОСТЬЮ

О. Б. Романова[1*], С. С. Аплеснин[1,2], Удод[1,2] Л. В.

[1] Институт физики имени Л. В. Киренского Сибирского отделения Российской академии наук – обособленное подразделение ФИЦ КНЦ СО РАН
Российская Федерация, 660036, г. Красноярск, Академгородок, 50, стр. 38
[2]Сибирский государственный университет науки и технологий имени академика М. Ф. Решетнева
Российская Федерация, 660037, г. Красноярск, просп. им. газ. «Красноярский рабочий», 31
*E-mail: rob@iph.krasn.ru

Методом расплава из поликристаллических порошков сульфидов приготовлены катион замещенные твердые растворы $Yb_XMn_{1-X}S$. Синтезированные образцы являются антиферромагнитными полупроводниками и согласно результатам рентгеноструктурного анализа имеют ГЦК структуру типа NaCl. Проведены исследования структурных, электрических, оптических и акустических свойств халькогенидной системы $Yb_XMn_{1-X}S$ в интервале температур 80–500 К. Исследовано влияние на электронную структуру элементов переменной валентности при катионном замещении сульфида марганца. Изменение электронной структуры в системе $Yb_XMn_{1-X}S$ происходит за счет электрон-фононного взаимодействия. Образцы с переменной валентностью обладают аномальной сжимаемостью, что подтверждается данными коэффициента теплового расширения и изменением коэффициента затухания. В результате неупругого взаимодействия с d-электронами меняется плотность состояний на уровне Ферми, что отражается на температурной зависимости проводимости. Из ИК спектров определены положения f-уровня и два электронных перехода. Обнаружена область темпера-

тур и концентраций, где наблюдается корреляция структурных, электрических, оптических и акустических свойств. Для объяснения экспериментальных результатов рассмотрена электронная структура полупроводника и предложена модель, качественно описывающая эксперимент.

Ключевые слова: элементы с переменной валентностью, структура, ИК-спектроскопия, коэффициент затухания, проводимость, электронная структура.

Introduction. Recently, active research has been carried out in the field of spin electronics or spintronics, which is one of the priority areas of modern electronics [1–3]. In spintronics, not only the charge degree of freedom of the electron, but also the spin is used to convert an electrical signal, which makes it possible to create fundamentally new spintronic devices based on materials with a magnetoresistive effect. These substances include the cation-anionic semiconductors which we investigate, and which are synthesized on the basis of manganese chalcogenides and they demonstrate phase transitions, and a number of effects associated with changes in the electronic structure under the influence of external factors [4–10]. A similar correlation of changes in the electronic and crystal structures was observed in bismuth pyrovskites [11–13]. The study of these phenomena in manganese chalcogenides seems to be relevant, both from the point of view of technical applications and from the point of view of fundamental physics.

Manganese monosulfide, on the basis of which the studied compound $Yb_XMn_{1-X}S$ was synthesized, is an antiferomagnetic (T_N = 150 K) p-type semiconductor [14; 15]. It has an fcc structure of the NaCl type with the unit cell parameter a = 5.22 nm and undergoes a number of structural distortions at temperatures below the Néel temperature [16]. It reveals the anisotropy of the electrical resistance, which in the (111) plane is two orders of magnitude greater than in the (100) plane and depends on the applied magnetic field. The negative magnetoresistance found in the (111) plane for MnS was – 12 % in a magnetic field of 10 kOe at T = 230 K [17].

When manganese cations are replaced by ytterbium ions, the pressure exerted by the nearest environment will lead to a change in the valence of ytterbium ions and to the formation of a metal bond. This was observed in YbS compounds under pressure [18]. Substitution of ytterbium for manganese will cause an f-level shift. Several options are possible here, the f-level falls into the conduction band, and the electron passes from the f-to the d-level of the rare-earth ion, or remains below the bottom of the conduction band, and bound to the donor. The transition of an electron from the f-level to the t_{2g} state will lead to electronic degeneracy, which can be lifted due to the spin-orbit or Jahn–Teller interaction. In the work [19], the effect of a magnetic field on the electrical and magnetic properties in $Yb_XMn_{1-X}S$ (0.05 < X < 0.2) was studied. A change in the type of conductivity from the Poole–Frenkel law to the Mott law was found from the current-voltage characteristics and a change in the sign of the current carriers, both in temperature and in concentration. The effect of prehistory under the action of a magnetic field on the conductivity, impedance, and magnetic susceptibility was found in a wide temperature range. The trivalent state of ytterbium ions from EPR was found. The experimental data are satisfactorily explained by the

condensation of lattice polarons with the formation of orbital glass with successive freezing of interstitial orbital angular momentum and with orbital angular momentum at the site.

In solid solutions with a disordered arrangement of ytterbium ions, a situation is possible when ions of different valences occupy crystallographically equivalent positions, but the exchange of electrons between them turns out to be relatively slow and is associated with thermally activated hopping with emission and absorption of phonons. At high temperatures, the exchange between ions of different valence occurs rather quickly, which causes an increase in conductivity, and with decreasing temperature, the characteristic times increase sharply and the situation becomes close to static. This will manifest itself in the study of acoustic properties, in softening and splitting of sound vibration modes, in particular, in damping of acoustic phonons, which is sensitive to valence fluctuations and to local deformations accompanying them. Acoustic properties which main parameters are elastic moduli and ultrasound damping are very sensitive to the defect structure of the crystal [20]. In studies of high-temperature superconductors [21–23], it was found that the structure (grain size, presence of pores, etc.), as well as defects of the grain itself, can largely determine the acoustic characteristics of ceramics. The experience with ceramic compounds has shown that acoustic measurements make it possible to effectively control the quality of synthesized samples. In the work [24], a new method was proposed for studying the metal-insulator transition using acoustic effects. They were measured by successive irradiation of the sample in the absence of a magnetic field and in a magnetic field of 6 T at 4.2 K. By successive irradiation of the n-GaAs/AlGaAs heterostructure, the conductivity can be increased fivefold. The absorption of ultrasound in metals has been studied for a long time [25]. This phenomenon is closely related to electron-phonon heat exchange [26], which determines the possible scale of violation of thermodynamic equilibrium of the electron gas and phonons and the lattice.

Thus, the aim of this work is to establish possible phase transitions and changes in the electronic structure caused by the substitution of manganese by ytterbium ions as a result of a comprehensive study of optical, electrical, structural and acoustic properties. It should be noted that optical and acoustic studies are sensitive to local distortions of the structure; therefore, the selected methods will allow obtaining detailed information on phase transitions in $Yb_XMn_{1-X}S$ systems.

Experimental results and discussion. *Synthesis and experimental technique.* Cation-substituted solid solutions of the $Yb_XMn_{1-X}S$ system with a substitution concentration (0 ≤ X ≤ 0.2) were grown in a quartz reactor from a melt of polycrystalline sulfide powders. A reactor with a charge in glassy carbon crucibles was pulled through

a single-turn inductor of the HF unit. High-purity argon was used as an inert medium [7]. Determination of the phase composition and crystal structure of the synthesized samples was carried out at 300 K on a DRON-3 X-ray facility using CuK_α radiation after their preparation and measurements of their acoustic and optical properties. The electrical resistance measurements were carried out by a four-probe direct current compensation method in the temperature range of 77÷1000 K. IR spectroscopy studies of $Yb_XMn_{1-X}S$ samples by IR spectroscopy were performed on an 2202 IR Fourier spectrometer (FSM) with a spectral resolution of 1 cm^{-1} in a temperature range of 80–500 K and frequencies of 400–7000 cm^{-1} on a polycrystalline sample in the form of tablets with a diameter of 13 mm in a KBr matrix. Acoustic properties were measured directly on the tablets with two piezoelectric sensors glued with silver paste to the tablet planes, one of which was a generator, the other was a receiver of ultrasonic waves. The sound propagation time was $\tau = 10(-6)$ seconds at a frequency of 5 MHz, the sample thickness was 0.4 cm. The sound wave attenuation coefficient was calculated by the formula: $\alpha = \ln(U_0/U)/d$, where U and U_0 are the voltage amplitudes recorded by the generator and the receiver of vibrations, d is the thickness of the tablet.

X-ray structural analysis. According to the results of X-ray structural analysis, the synthesized $Yb_XMn_{1-X}S$ samples with a low substitution concentration $X \leq 0.05$ have a cubic lattice of the NaCl type, characteristic of α-MnS (fig. 1, *a*). With an increase in concentration to $X = 0.2$, along with diffraction reflections of the cubic structure, very weak reflections of the impurity Yb_2S_3 phase with a cubic structure (space group *Ia3*) are observed, which do not disappear upon heat treatment (fig. 1, *b*). The result of exposure to temperature is redistribution of the intensity of diffraction reflections on X-ray diffraction patterns. The main peak [200] in the X-ray diffraction pattern for the $Yb_XMn_{1-X}S$ solid solution splits into two with increasing X, which is possibly associated with the cooperative Jahn – Teller effect and a decrease in cubic symmetry. Cationic substitution with ytterbium leads to a linear increase in the unit cell parameter in accordance with an increase in the radius of the substituting element ($r = 0.91$ nm for Mn and $r = 0.101$ nm for Yb). The concentration dependence of the lattice parameter for the ytterbium-substituted system is shown in the inset to fig. 1, *a*.

Investigation of samples by IR spectroscopy and acoustic method. The substitution of ytterbium for manganese in the $Yb_XMn_{1-X}S$ system leads to structural distortions accompanied by a change in the electronic spectrum, which can be established using IR spectroscopy. Distortion of octahedra, due to the Jahn-Teller effect, was observed in the IR spectra in the form of splitting of the intensity lines shown in fig. 2. In the frequency range of 900–1100 cm^{-1} in $Yb_{0.15}Mn_{0.85}S$, a splitting of the absorption peak into two maxima at frequencies $\omega_1 = 953$ cm^{-1} and $\omega_2 = 994$ cm^{-1} was found. When heated to $T > 200$ K, the first maximum detected at the frequency ω_1 disappears, and the intensity of the second one decreases several times and disappears at 400 K. With increasing temperature, ω_1 and ω_2 shift by 3 cm and 12 cm, respec-

tively. Substitution of manganese by ytterbium ions leads to the formation of electrons in the t_{2g} subsystem and to the degeneracy of electronic states, which are removed due to the Jahn-Teller effect. Two electronic transitions were found from the IR spectra for $X = 0.15$, one disappears at 200 K and the other at 400 K, which are caused by the successive growth of the octahedral symmetry and the splitting of the t_{2g} states of the ions in the zone with electronic phase separation.

Studies of the magnetic properties of the $Yb_XMn_{1-X}S$ system presented in [19] showed that the synthesized compounds are antiferromagnets with T_N decreasing with increasing concentration from 150 K for $X = 0.05$ to 102 K for $X = 0.2$. In the paramagnetic region, two features were observed in the temperature behavior of the magnetization measured in the magnetic field of 8.6 kOe, associated with the local minimum $d\sigma/dT$ at T_1 and T_2, the values of which are in the ranges 224 K $< T <$ 234 K and at 336 K $< T <$ 386 K. Above T_2, the temperature dependence of the magnetic susceptibility is described by the Curie–Weiss law with a negative paramagnetic Curie temperature θ, which sharply decreases when manganese is replaced by ytterbium ions. This can be explained by the formation of superparamagnetic clusters with a strong ferromagnetic interaction between manganese ions, which are the nearest neighbors of the ytterbium ion.

The anomalous behavior of the attenuation coefficient (α) shown in fig. 3 for the sample $Yb_{0.05}Mn_{0.95}S$ is observed in two temperature regions (in the magnetic ordering region and paramagnetic one). The first temperature region correlates with the temperatures of structural distortions (100, 120, 150 K) observed in the initial matrix of manganese monosulfide [27] and with the data of the temperature dependence of the thermal expansion coefficient measured for samples of the $Yb_XMn_{1-X}S$ system [19]. According to which anomalies in the temperature range of the magnetic phase transition 110K $\leq T \leq$ 140 K are established on the temperature dependence of the coefficient of thermal expansion. This is due to the fact that when moving to a magnetically ordered region, the lattice begins to contract anomaly, as a result of magnetoelastic interaction.

Above 150 K, the α (T) curve reaches a plateau. An exponential decrease in the value of the attenuation coefficient is observed at $T = 220$ K; at this temperature, the first local minimum of magnetization was detected. The anomalous behavior of the attenuation coefficient in the high temperature range above 400K correlates with the temperatures detected in the IR spectra and is most likely connected with the rearrangement of the electronic spectrum due to the Jahn–Teller effect.

Fig. 4, *a*, *b* illustrates the behavior of the frequency dependence of the sound attenuation coefficient in samples $Yb_{0.05}Mn_{0.95}S$ and $Yb_{0.2}Mn_{0.8}S$ measured at a pulse sequence t = 50 sec in the temperature range 300–450 K. At temperatures of 300 and 320 K for concentrations 0.05 and 0.2, respectively, the α (ω) curves are almost linear. With increasing temperatures, maxima were found on the frequency dependences of the attenuation coefficient. For both the $Yb_{0.05}Mn_{0.95}S$ and $Yb_{0.2}Mn_{0.8}S$ samples, the frequency range 5–5.5 MHz for which anomalies are ob-

served at $T = 350$ and 400 K coincides (fig. 4, *a*, *b*). A further increase in temperature to 450K results in a step on the α (ω) curve in the low-frequency region at 3 MHz for $Yb_{0.05}Mn_{0.95}S$ and 2.5 MHz for $Yb_{0.2}Mn_{0.8}S$. It is assumed that energy absorption in the room temperature region is caused by internal friction, and the approach to 400 K is due to scattering on crystallographic domains.

When acoustic waves propagate in polycrystalline solid media, reflection, refraction, and transformation occur at grain boundaries, domain boundaries, and structure inhomogeneities. Thus, attenuation is due to both absorption and dissipation of energy. In solids, absorption can be caused by: internal friction (in this case, the sound attenuation coefficient α is proportional to the frequency ω); thermal conductivity (α is proportional to ω^2); elastic effects (α is proportional to ω).

Electrical property. The rearrangement of the electronic structure at the Mn-Yb interface as a result of lowering the local crystal structure and splitting the t_{2g} levels will manifest itself as a result of the study of electrical properties, namely, conductivity. The temperature dependence of the conductivity for solid solutions of $Yb_{0.15}Mn_{0.85}S$ is shown in fig. 5. It has a typical semiconductor type and does not differ qualitatively from the temperature dependence $\sigma(T)$ for the initial manganese monosulfide. A correlation is found between the temperatures at which anomalies are detected in the IR spectra, the attenuation coefficient, and the temperature dependence of the conductivity (σ). The first jump in the curve $\sigma(T)$ is observed in the room temperature region. Further along the temperature, a slight increase in conductivity is observed, which turns into a sharp increase in the region of 400 K. This behavior of σ correlates with anomalies detected in the frequency and temperature dependences of the attenuation coefficient and IR spectroscopy data, which confirms the assumptions made above about changes in the electronic structure during cationic substitution of manganese with ytterbium. In the high temperature range of $880 < T < 1020$ K, a small maximum in electrical resistance is detected (inset in fig. 3).
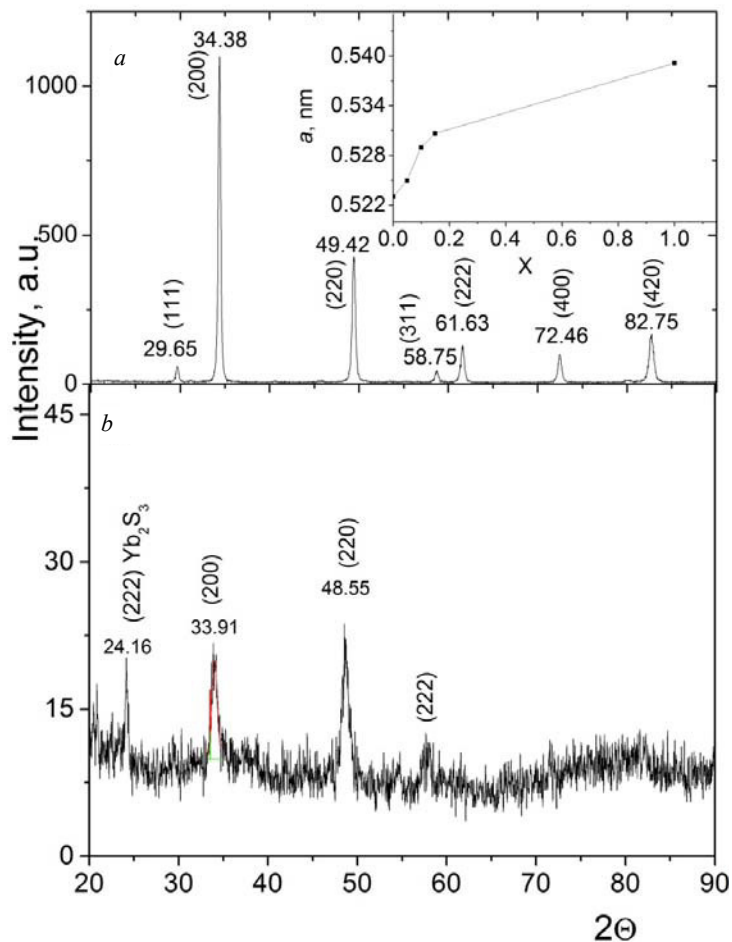

Fig. 1. X-ray diffraction patterns of $Yb_{0.05}Mn_{0.95}S$ (*a*) and $Yb_{0.2}Mn_{0.8}S$ (*b*) samples. The inset shows the concentration dependence of the lattice parameter of the system $Yb_XMn_{1-X}S$

Рис. 1. Рентгенограммы образцов $Yb_{0.05}Mn_{0.95}S$ (*a*) и $Yb_{0.2}Mn_{0.8}S$ (*b*). На вставке концентрационная зависимость параметра решетки системы $Yb_XMn_{1-X}S$
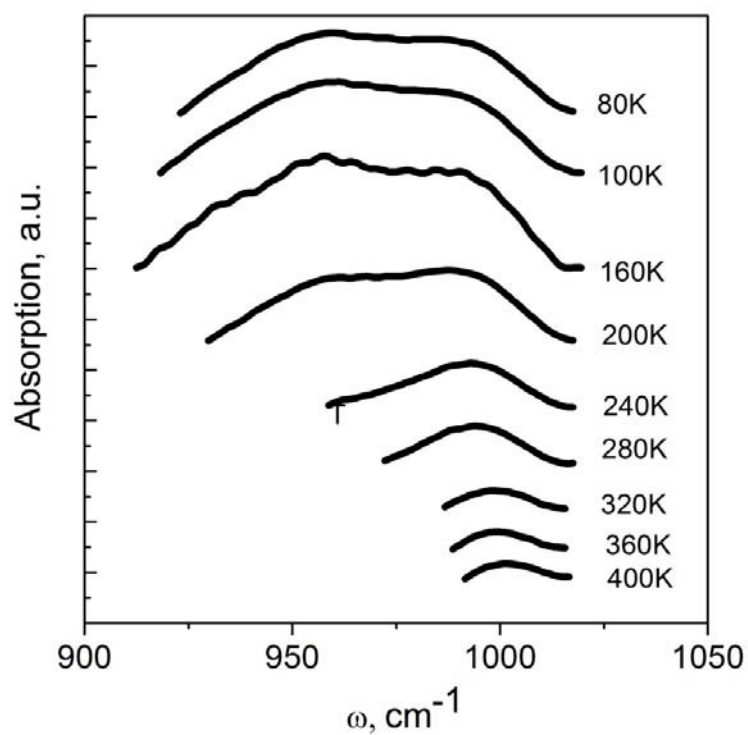
Fig. 2. Temperature dependences of the intensity of the IR spectra
of the sample $Yb_{0.15}Mn_{0.85}S$

Рис. 2. Температурные зависимости интенсивности ИК
спектров образца $Yb_{0.15}Mn_{0.85}S$
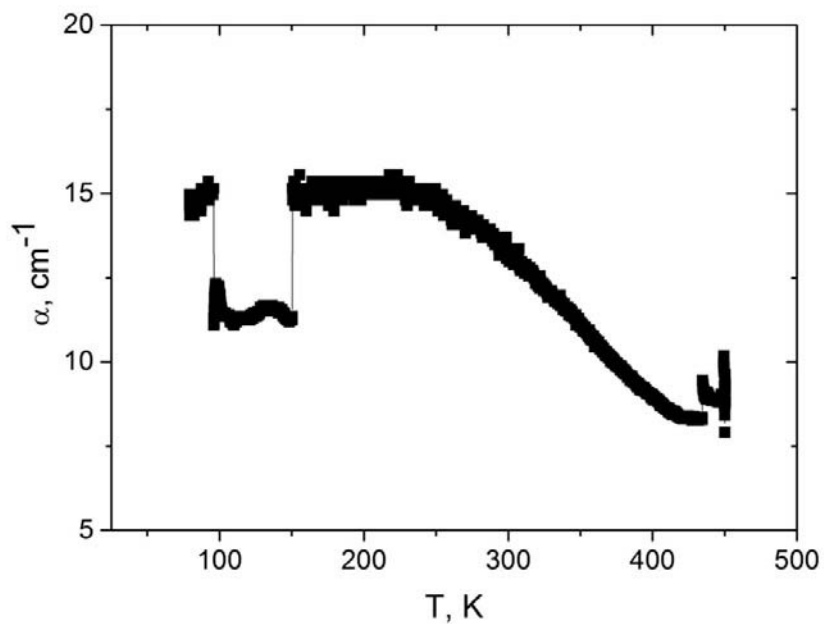

Fig. 3. Temperature dependence of the attenuation coefficient
for the sample $Yb_{0,05}Mn_{0,95}S$

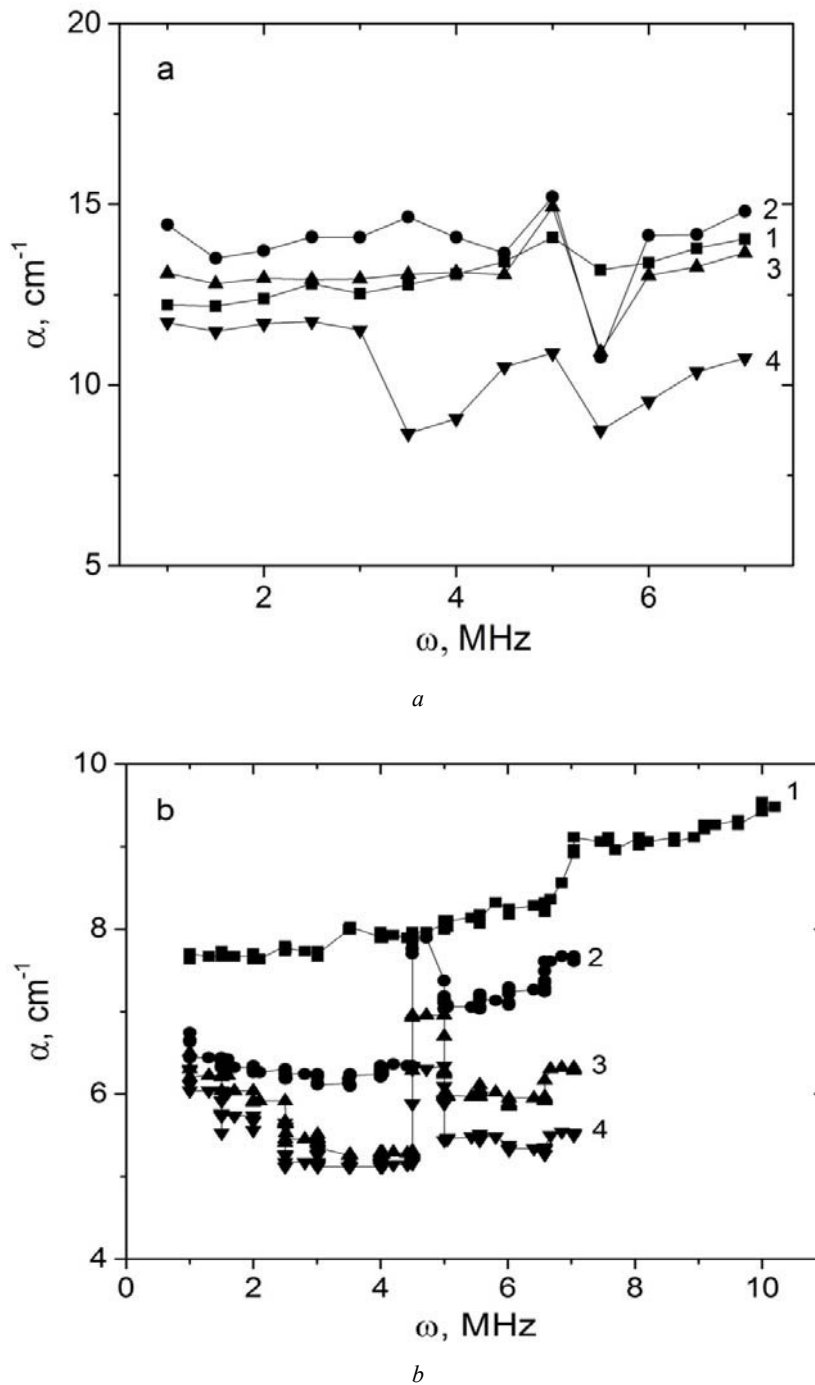Рис. 3. Температурная зависимость коэффициента затухания
для образца $Yb_{0,05}Mn_{0,95}S$

a

b

Fig. 4. Frequency dependence of the sound attenuation coefficient for
$Yb_{0.05}Mn_{0.95}S$ (*a*) measured at $T = 300$ K (*1*); 350 K (*2*); 400 K (*3*); 450 K (*4*)
and for $Yb_{0.2}Mn_{0.8}S$ (*b*) at $T = 320$ K (*1*); 360 K (*2*); 400 K (*3*); 440 K (*4*)

Рис. 4. Частотная зависимость коэффициента затухания звука
для $Yb_{0.05}Mn_{0.95}S$ (*a*), измеренного при $T = 300$ K (*1*); 350 K (*2*); 400 K (*3*); 450 K (*4*)
и для $Yb_{0.2}Mn_{0.8}S$ (*b*) при $T = 320$ K (*1*); 360 K (*2*); 400 K (*3*); 440 K (*4*)

This maximum is due to the coincidence of the 4f-level with the chemical potential when it is shifted from the bottom of the conduction band to the middle of the band gap.At low temperatures, the 4f-level is filled and located below the chemical potential, and at high temperatures, electrons are scattered at the f − centers as a result of df-exchange, which leads to a maximum in resistance. It should be noted that with an increase in the concentration to $X = 0.2$, a jump in the electrical resistance is observed at $T = 700$ K and the reason for this is the electron-phonon interaction, which induces splitting of the 4f subband. Another reason is the presence of ytterbium ions of different sizes (+2 and +3) with different (up to 10–15 %) ion radii. The electron-lattice interaction

consists of the interaction of electrons with a homogenous strain and with phonons at a given strain.

To explain the experimental results obtained for solid solutions of $Yb_XMn_{1-X}S$, we consider the electronic structure shown in fig. 6. In the band gap below the bottom of the conduction band is the donor level corresponding to 4f ytterbium electrons. The electron concentration at the 4f-level is equal to the concentration of ytterbium ions. In the temperature range 390–440 K, condensation of local octahedral modes is possible, i. e., sulfur ions shift from octahedral positions in the direction of manganese at the Mn-Yb boundary.
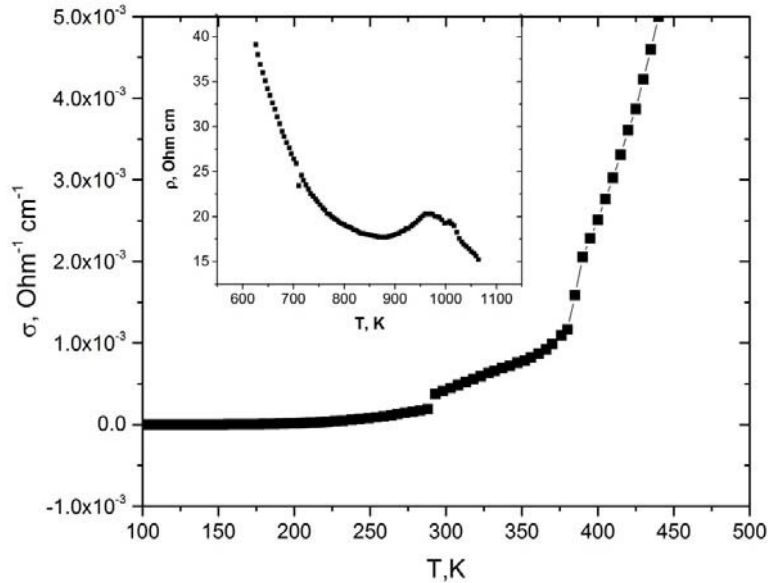

Fig. 5. Temperature dependence of conductivity for the $Yb_{0.15}Mn_{0.85}S$ sample. Inset: temperature dependence of electrical resistivity for the same concentration

Рис. 5. Температурная зависимость проводимости для образца $Yb_{0.15}Mn_{0.85}S$. На вставке: температурная зависимость удельного электросопротивления для этой же концентрации
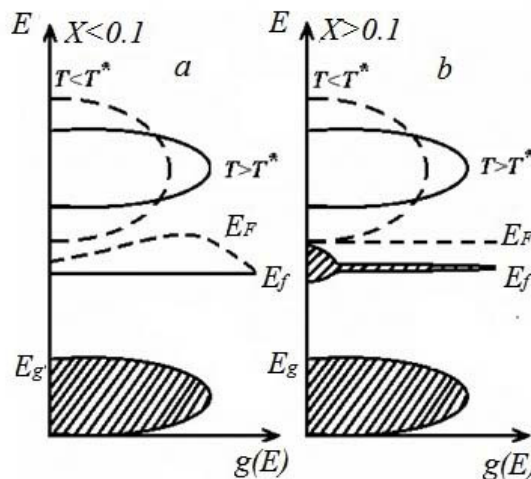

Fig. 6. Temperature dependence of the 4f-level energy E_f and Fermi energy E_F. T^* – temperature at which the activation energy increases, taken from the data on electrical resistance

Рис. 6. Температурная зависимость энергии 4f-уровня E_f и энергии Ферми E_F. T^* – температура, при которой энергия активации увеличивается, взята из данных по электросопротивлению

The bending mode of the octahedron is likely to lead to splitting of the t_{2g} states of electrons and to a shift in the conduction band, as well as a decrease in the energy interval between the f-level and the bottom of the conduction band. There is a shift of the f-level relative to the bottom of the conduction band, which leads to a rearrangement of the electronic structure. At high temperatures, the Fermi energy and the 4f-level intersect at high temperatures for all concentrations.

Conclusion. Cation-substituted solid solutions of $Yb_X Mn_{1-X} S$ ($0 \leq X \leq 0.2$) were synthesized, which mainly have a face-centered cubic lattice of the NaCl type according to the results of x-ray diffraction analysis. An increase in the substitution concentration $X = 0.2$ leads to splitting of the main peak on the x-ray image, which is associated with the cooperative Jahn–Teller effect and a decrease in cubic symmetry. Structural changes and rearrangements of the electronic spectrum were confirmed by IR spectroscopy. Two electron transitions were detected from the IR spectra, one of which disappears at 200 K and the other at 400 K. These transitions are caused by a sequential increase in the symmetry of the octahedron and with the splitting of the t_{2g} states of the ions. A structural transition for $X = 0.05$ is detected in the magnetically ordered phase, which is accompanied by compression of the crystal lattice and minima on the temperature dependence of the attenuation coefficient. A temperature range is found in which the correlation of structural, magnetic, electrical, optical, and acoustic properties is observed. Comparison of acoustic parameters with the behavior of the temperature dependence of the thermal expansion coefficient of the sample, IR spectroscopy, x-ray diffraction data, and conductivity in the paramagnetic region allows us to assume that the detected anomalies indicate the existence of both structural phase transitions and changes in the electronic structure in the sample. The change in the electronic structure as a result of substitution of manganese with elements of variable valence is caused by a shift in the bottom of the conduction band with an increase in temperature as a result of electron-phonon interaction

References

1. Zvezdin A. K., Pyatakov A. P. [Phase transitions and giant magnetoelectric effect in multiferroics]. *UFN.* 2004, Vol. 174, P. 465–470 (In Russ.).

2. Manfred Fiebig. Revial of the magnetoelectric effect. *J. Phys. D: Appl. Phys.* 2005, Vol. 38, P. R123–R152.

3. Volkov N. V. [Spintronics: magnetic tunneling structures based on manganites]. *UFN.* 2012, Vol. 182, P. 263–285 (In Russ.).

4. Romanova O. B., Aplesnin S. S., Udod L. V., Sitnikov M. N., Kretinin V. V., Yanushkivich K. I., Velikanov D. A. Magnetoresistance, magnetoimpedance, magnetothermopower and photoconductivity in silver-doped manganese sulfides. *J. Appl. Phys.* 2019, Vol. 125, P. 175706-9.

5. Aplesnin S. S., Sitnikov M. N., Kharkov A. M., Masyugin A. N., Kretinin V. V., Fisenko O. B., Gorev M. V. Influence of induced electrical polarization on the magnetoresistance and magnetoimpedance in the spin-disordered $Tm_X Mn_{1-X} S$ solid solution. *Phys. Stat. Sol. B.* 2019, P. 1900043-10.

6. Aplesnin S. S., Sitnikov M. N. [Magnetotransport effects in the paramagnetic state in $Gd_X Mn_{1-X} S$]. *JETP.* 2014, Vol. 100, P. 104–110 (In Russ.).

7. Aplesnin S. S., Ryabinkina L. I., Romanova O. B., Sokolov V. V., Pichugin A. Yu., Galyas A. I., Demidenko O. F., Makovetskiy G. I., Yanushkevich K. I. [Magnetic and electrical properties of cation-substituted sulfides $MeXMn1-XS$ (Me = Co, Gd)]. *Sol. St. Phys.* 2009, Vol. 51, P. 661–664 (In Russ.).

8. Aplesnin S. S., Kharkov A. M., Sitnikov M. N., Sokolov V. V. Spin reduction in the $Ho_X Mn_{1-X} S$ solid solution. *JMMM*, 2013, Vol. 347, P. 10–13.

9. Aplesnin S. S., Romanova O. B., Yanushkevich K. I. Magnetoresistance effect in anion-substituted manganese chalcogenides. *Phys. Stat. Sol. B,* 2015. Vol. 252, P. 1792–1798.

10. Romanova O. B., Ryabinkina L. I., Sokolov V. V., Pichugin A. Yu., Velikanov D. A., Balaev D. A., Galyas A. I., Demidenko O. F., Makovetskii G. I., Yanushkevich K. I. Magnetic properties and the metal-insulator transition in $Gd_X Mn_{1-X} S$ solid solutions. *Sol. St. Comm.* 2010, Vol. 150, P. 602–604.

11. Aplesnin S. S., Udod L. V., Sitnikov M. N., Velikanov D. A., Gore M. V., Molokeev M. S., Galyas A. I., Yanushkevich K. I. Magnetic and electrical properties of bismuth cobaltite $Bi_{24}(CoBi)O_{40}$ with charge ordering. *Phys. Sol. Stat.* 2012, Vol. 54, P. 2005–2014.

12. Aplesnin S. S., Udod L. V., Sitnikov M. N., Shestakov N. P. $Bi_2(Sn_{0.95}Cr_{0.05})_2O_7$: Structure, IR spectra, and dielectric properties. *Ceram. Int.*, 2016, Vol. 42, P. 5177–5183.

13. Udod L. V., Aplesnin S. S., Sitnikov M. N., Romanova O. B., Molokeev M. N. Phase transitions in bismuth pyrostannate upon substitution of tin by iron ions. *J. Alloys Compd.* 2019, Vol. 804, P. 281–287.

14. Heikens H. H., Wiegers G. A., van Bruggen C. F. On the nature of a new phase transition in $\alpha - MnS$. *Solid State Comm.* 1977, Vol. 24, P. 205–209.

15. Aplesnin S. S., Romanova O. B., Demidenko O. F., Yanushkevich K. I., *Magnitnyye fazovyye perekhody i kineticheskiye svoystva khal'kogenidov 3d-metallov* [Magnetic phase transitions and kinetic properties of 3d-metal chalcogenides.]. Krasnoyarsk, 2017, 208 p.

16. Morosin B. Exchange striction effects in MnO and MnS. *Phys. Rev. B.* 1970, Vol. 1, P. 236–243.

17. Aplesnin S. S., Ryabinkina L. I., Abramova G. M., Romanova O.B., Vorotynov A. M., Velikanov D. A., Kiselev N. I., Balaev A. D. Conductivity, weak ferromagnetism, and charge instability in an α-MnS single crystal. *Phys. Rev. B.* 2005, Vol. 71, P. 125204–125212.

18. Cava R. J., Batlogg B., van Dover R. B., Ramirez A. P., Krajewski J. J., Peck W. F., Rupp L. W. Trivalent rare earths in layered $(LX)_{1.15}NbX_2$ chalcogenides. *Phys. Rev. B.* 1994, Vol. 49, P. 6343–6345.

19. Aplesnin S. S., Kharkov A. M., Romanova O. B., Sitnikov M. N., Eremin E. V., Gorev M. V., Yanushkevich K. I., Sokolov V. V., Pichugin A. Yu. Spin state of cations and magnetoelastic effect in $Mn_{1-X}Yb_XS$. *JMMM.* 2014, Vol. 352, P. 1–5.

20. Nikanorov S. P., Kardashev B. K. *Elasticity and dislocation inelasticity of crystals* [Uprugost' i dislokatsionnaya neuprugost' kristallov]. Moscow, Nauka Publ.,1974, 254 p.

21. Lebedev A. B., Burenkov Yu. A., Ivanov V. I. [Amplitude and temperature dependences of ultrasound absorption and Young's modulus of elasticity for superconducting ceramics $YBa_2Cu_3O_{7-x}$]. *Sol. St. Phys.* 1989, Vol. 31, P. 300–303 (In Russ.).

22. Golyandin S. N., Kardashev B. K., Kustov S. B., Nikanorov S. P., Devos P., Cornelis J., De Batist R. Low temperature cross – over effect in ultrasonic damping in YBCO ceramics. *Phys. Stat. Sol. (a).* 1995, Vol. 147, P. 111–118.

23. Kardashev B. K., Burenkov Yu. A., Smirnov B. I., Shpeizman V. V., Stepanov V. A., Chernov V. M., Singh D., Goretta K. C. [Elasticity and inelasticity of ceramic specimens of graphite-like boron nitride]. *Sol. St. Phys.* 2001, Vol. 43, P. 1048–1052 (In Russ.).

24. Drichko I. L., Dyakonov A. M., Smirnov I. Yu., Toropov A. I. [Light-induced metal-insulator transition in a heterostructure n-GaAs/AlGaAs. Acoustic research methods]. *Sol. St. Phys.* 2006, Vol. 40, P. 1449–1456 (In Russ.).

25. Schmid A. Electron-phonon interaction in an impure metal. *Zeitschrift für Physik.* 1973, Vol. 259, P. 421–436.

26. Shtyk A. V., Feigel'man M. V., Kravtsov V. E. Magnetic field-indiced giant enhancement of electron-phonon energy transfer in striongly disordered conductors. *Phys. Rev.Lett.* 2013, Vol. 111, P. 166603-5.

27. Aplesnin S. S. *Magnetic and electrical properties of heavily doped magnetic semiconductors* [Magnitnyye i elektricheskiye svoystva sil'nodegirovannykh magnitnykh poluprovodnikov]. Moscow, Nauka Publ., 2013, 176 p.

Библиографические ссылки

1. Звездин А. К., Пятаков А. П. Фазовые переходы и гигантский магнитоэлектрический эффект в мультиферроиках // УФН. 2004. Т. 174. С. 465–470.

2. Manfred Fiebig Revial of the magnetoelectric effect // J. Phys. D: Appl. Phys. 2005. Vol. 38. P. R123–R152.

3. Волков Н. В. Спинтроника: магнитные туннельные структуры на основе манганитов // УФН. 2012. Т. 182. С. 263–285.

4. Magnetoresistance, magnetoimpedance, magnetothermopower, and photoconductivity in silver-doped manganese sulfides / O. B. Romanova, S. S. Aplesnin, L. V. Udod et al. // J. Appl. Phys. 2019. Vol. 125. P. 175706-9.

5. Influence of induced electrical polarization on the magnetoresistance and magnetoimpedance in the spin-disordered $Tm_XMn_{1-X}S$ solid solution / S. S. Aplesnin, Sitnikov M. N., Kharkov A.M. et al. // Phys. Stat. Sol. B. 2019. P. 1900043-10.

6. Аплеснин С. С., Ситников М. Н. Магнитотранспортные эффекты в парамагнитном состоянии в $Gd_XMn_{1-X}S$ // ЖЭТФ. 2014. Т. 100. С. 104–110.

7. Магнитные и электрические свойства катион замещенных сульфидов $Me_XMn_{1-X}S$ (Me = Co, Gd) / С. С. Аплеснин, Л. И. Рябинкина, О. Б. Романова и др. // ФТТ. 2009. Т. 51. С. 661–664.

8. Spin reduction in the $Ho_XMn_{1-X}S$ solid solution / S. S. Aplesnin, A. M. Kharkov, M.N. Sitnikov et. al. // JMMM. 2013. Vol. 347. P. 10–13.

9. Magnetoresistance effect in anion-substituted manganese chalcogenides / S. S. Aplesnin, O. B. Romanova, K. I. Yanushkevich // Phys. Stat. Sol. B. 2015. Vol. 252. P. 1792–1798.

10. Magnetic properties and the metal-insulator transition in $Gd_XMn_{1-X}S$ solid solutions / O. B. Romanova, L. I. Ryabinkina, V. V. Sokolov et al. // Sol. St. Comm. 2010. Vol. 150. P. 602–604.

11. Magnetic and electrical properties of bismuth cobaltite $Bi_{24}(CoBi)O_{40}$ with charge ordering / S. S. Aplesnin, L. V. Udod, M. N. Sitnikov et al. // Phys. Sol. Stat. 2012. Vol. 54. P. 2005–2014.

12. $Bi_2(Sn_{0.95}Cr_{0.05})_2O_7$: Structure, IR spectra, and dielectric properties / S. S. Aplesnin, L. V. Udod, M. N. Sitnikov et al. // Ceram. Int. 2016. Vol. 42. P. 5177–5183.

13. Phase transitions in bismuth pyrostannate upon substitution of tin by iron ions / L. V. Udod, S. S. Aplesnin, M. N. Sitnikov et al. // J. Alloys Compd. 2019. Vol. 804. P. 281–287.

14. On the nature of a new phase transition in α-MnS / H. H. Heikens, G. A. Wiegers, van C. F. Bruggen // Solid State Comm. 1977. Vol. 24. P. 205–209.

15. Магнитные фазовые переходы и кинетические свойства халькогенидов 3d-металлов / С. С. Аплеснин, О. Б. Романова, О. Ф. Демиденко, К. И. Янушкевич ; Сиб. гос. аэрокосмич. ун-т. Красноярск, 2017. 208 с.

16. Morosin B. Exchange striction effects in MnO and MnS // Phys. Rev. B. 1970. Vol. 1. P. 236–243.

17. Conductivity, weak ferromagnetism, and charge instability in an α-MnS single crystal / S. S. Aplesnin, L. I. Ryabinkina, G. M. Abramova et. al. // Phys. Rev. B. 2005. Vol. 71. P. 125204–125212.

18. Trivalent rare earths in layered $(LX)_{1.15}NbX_2$ chalcogenides / R. J. Cava, Batlogg B., van Dover R. B. et. al. // Phys. Rev. B. 1994. Vol. 49. P. 6343–6345.

19. Spin state of cations and magnetoelastic effect in $Mn_{1-X}Yb_XS$ / S. S. Aplesnin, A. M. Kharkov, O. B. Romanova et al. // JMMM. 2014. Vol. 352. P. 1–5.

20. Никаноров С. П., Кардашев Б. К. Упругость и дислокационная неупругость кристаллов. М. : Наука, 1985. 254 с.

21. Амплитудные и температурные зависимости поглощения ультразвука и модуля упругости Юнга сверхпроводимой керамике $YBa_2Cu_3O_{7-x}$ / А. Б. Лебедев, Ю. А. Буренков, В. И. Иванов и др. // ФТТ. 1989. Т. 31. С. 300–303.

22. Low temperature cross –over effect in ultrasonic damping in YBCO ceramics / S. N. Golyandin, B. K. Kardashev, S. B. Kustov et al. // Phys. Stat. Sol. (a). 1995. Vol.147. P. 111–118.

23. Упругость и неупругость керамических образцов графитоподобного нитрида бора / Б. К. Кардашев, Ю. А. Буренков, Б. И. Смирнов и др. // ФТТ. 2001. Т. 43. С. 1048–1052.

24. Индуцированный светом переход металл-диэлектрик в гетероструктуре n-GaAs/AlGaAs. Акустические методы исследования / И. Л. Дричко, А. М. Дьяконов, И. Ю. Смирнов, А. И. Торопов // ФТТ. 2006. Т. 40. С. 1449–1456.

25. Schmid A. Electron-phonon interaction in an impure metal // Zeitschrift fȯr Physik. 1973. Vol. 259. P. 421–436.

26. Shtyk A. V., Feigel'man M. V., Kravtsov V. E. Magnetic field-indiced giant enhancement of electron-phonon energy transfer in striongly disordered conductors // Phys. Rev. Lett. 2013. Vol. 111. P. 166603-5.

27. Аплеснин С. С. Магнитные и электрические свойства сильнодегированных магнитных полупроводников. М. : Наука, 2013. 176 с.

Romanova Oksana Borisovna – Cand. Sc., Researcher; Kirensky Institute of Physics, Federal Research Center KSC SB RAS. E-mail: rob@iph.krasn.ru.

Aplesnin Sergey Stepanovich – Dr. Sc., Professor, Head of the Department of Physics; Reshetnev Siberian State University of Science and Technology. E-mail: aplesnin@sibsau.ru, apl@iph.krasn.ru.

Udod Lubov Viktorovna – Cand. Sc., Researcher; Kirensky Institute of Physics, Federal Research Center KSC SB RAS. E-mail: luba@iph.krasn.ru.

Романова Оксана Борисовна – кандидат физико-математических наук, научный сотрудник; Институт физики имени Л. В. Киренского Сибирского отделения Российской академии наук – обособленное подразделение ФИЦ КНЦ СО РАН. E-mail: rob@iph.krasn.ru.

Аплеснин Сергей Степанович – доктор физико-математических наук, профессор, заведующий кафедрой физики; Сибирский государственный университет науки и технологий имени академика М. Ф. Решетнева. E-mail: aplesnin@sibsau.ru, apl@iph.krasn.ru.

Удод Любовь Викторовна – кандидат физико-математических наук, научный сотрудник; Институт физики имени Л. В. Киренского Сибирского отделения Российской академии наук – обособленное подразделение ФИЦ КНЦ СО РАН. E-mail: luba@iph.krasn.ru.

INFLUENCE OF THE MAGNETIC FIELD ON TRANSPORT PROPERTIES OF HOLMIUM – MANGANESE SULFIDE

M. N. Sitnikov[1], A. M. Kharkov[1*], S. S. Aplesnin[1], O. B. Romanova[2]

[1]Reshetnev Siberian State University of Science and Technology
31, Krasnoyarskii rabochii prospekt, Krasnoyarsk, 660037, Russian Federation
[2]Kirensky Institute of Physics, Federal Research Center KSC Siberian Branch Russian Academy of Sciences
660036, Krasnoyarsk, Akademgorodok 50, bld. 38
*E-mail: khark.anton@mail.ru

Holmium-manganese sulfide with giant magnetoresistance refers to new magnetic sulfide compounds of holmium and manganese that have the effect of giant magnetoresistance (i. e., with special magnetoelectric properties), which can be used as components of sensor technology, magnetic memory, and spintronics. The technology of manufacturing polycrystals $Ho_XMn_{1-X}S$ grown by crystallization from the melt of the obtained powdered sulfides with a purity not lower than 99,9 %, in glass-carbon crucibles and a quartz reactor in an argon atmosphere is presented. According to the results of x-ray diffraction analysis, $Ho_XMn_{1-X}S$ holmium-manganese sulfides have a HCC structure of the NaCl type. As the degree of cationic substitution increases, the unit cell parameter increases linearly with the concentration. No concomitant impurity phases are detected in the synthesized samples. To determine the state of the spin glass, magnetic moment measurements are conducted at several frequencies $\omega = 1$ kHz, 10 kHz and 100 kHz. The dependence of magnetic characteristics on the frequency of measurements is found. The damping of the magnetic moment and its increase with a decrease in temperature is reviled, which is connected with the formation of metastable States. Measurements of electrical resistance without a field and in a magnetic field are conducted. Anomalies in the temperature dependence of the conductivity are found. A change in the magnetoresistance sign is detected with the increase of temperature below and above room temperature.

Keywords: solid solutions, resistance, magnetic permeability, the effect of giant magnetoresistance.

ВЛИЯНИЕ МАГНИТНОГО ПОЛЯ НА ТРАНСПОРТНЫЕ СВОЙСТВА ГОЛЬМИЙ-МАРГАНЦЕВОГО СУЛЬФИДА

М. Н. Ситников[1], А. М. Харьков[1*], С. С. Аплеснин[1], О. Б. Романова[2]

[1]Сибирский государственный университет науки и технологий имени М. Ф. Решетнева
Российская Федерация, 660037, г. Красноярск, просп. им. газ. «Красноярский рабочий», 31
[2]Институт физики им. Л. В. Киренского Сибирского отделения Российской академии наук – обособленное подразделение ФИЦ КНЦ СО РАН
Российская Федерация, 660036, г. Красноярск, Академгородок, 50, стр. 38
*E-mail: khark.anton@mail.ru

Гольмий-марганцевый сульфид с гигантским магнитосопротивлением относится к новым магнитным сульфидным соединениям гольмия и марганца, обладающим эффектом гигантского магнитосопротивления, то есть с особыми магнитоэлектрическими свойствами, которые могут быть использованы в качестве составляющих компонент сенсорной техники, магнитной памяти для спинтроники. Приведена технология изготовления поликристаллов $Ho_XMn_{1-X}S$, выращенных кристаллизацией из расплава полученных порошковых сульфидов чистотой не ниже 99,9 % в стеклоуглеродных тиглях и кварцевом реакторе в атмосфере аргона. Согласно результатам рентгеноструктурного анализа, гольмий-марганцевые сульфиды $Ho_XMn_{1-X}S$ имеют ГЦК структуру типа NaCl. С увеличением степени катионного замещения параметр элементарной ячейки линейно увеличивается с концентрацией. Сопутствующих примесных фаз в синтезированных образцах не обнаружено. Для установления состояния спинового стекла проведены измерения магнитного момента на нескольких

частотах ω = 1, 10 и 100 kHz. Обнаружена зависимость магнитных характеристик от частоты измерений. Найдено затухание магнитного момента и его увеличение с понижением температуры, что связывается с образованием метастабильных состояний. Проведены измерения электросопротивления без поля и в магнитном поле. Найдены аномалии в температурной зависимости проводимости. Обнаружена смена знака магнитосопротивления с ростом температуры ниже и выше комнатной температуры.

Ключевые слова: твердые растворы, электросопротивление, магнитная проницаемость, эффект гигантского магнитосопротивления.

Introduction. The microelectronics element base, functioning on the basis of the magneto resistive effect [1], can operate under extreme conditions. Materials with the effect of giant magnetoresistance (GMR) can be used as components of sensor technology [2], magnetic memory [3] and are able to change their electrical resistance in several times under external magnetic field application [4–7].

Summing up, it is possible to say that all currently known GMR substances are complex (oxide) phases based on manganese oxides, the ferromagnetism of ions of which is responsible for the GMR effect emerging [8]. Oxide compounds of manganese type $La_{1-x}A_xMnO_3$ (A = Ca, Sr, Ba, etc.) and methods for their preparation [8; 9] are known. The maximum amplitude of this effect is observed in the immediate vicinity of the transition to the ferromagnetic state, at high values of the Curie temperature $T_C \sim 250 \div 400$ K and opens up broad prospects of their technological application.

The drawback of these substances is the high sensitivity of lanthanum manganite to concentration of a divalent impurity, a high melting point $T \sim 1800–1900$ °C, the cost of their constituent elements and realization of the GMR effect in a narrow temperature interval near the magnetic transition temperature. NaCl-type fcc lattice.

The vanadium chromium disulfide – copper $CuV_XCr_{1-X}S_2$ is also known (rhombohedral structure, space group R3m), which belongs to the class of mixed electron-ion semiconductors and is an antiferromagnetic with critical temperatures of superionic (T_{su} = 670 K) and magnetic ($T_N \sim 40$ K) transitions [10]. The effect of negative magnetoresistance in this compound is observed at 77 K in a magnetic field of 10 kOe and is – 40 %. This effect is observed only in polycrystalline samples but not in single-crystal samples with a copper deficiency.

The drawback of disulfides $CuV_XCr_{1-X}S_2$ is not a simple layered structure, the complexity of the crystal growth technology because of the high mobility of copper ions and low temperatures at which negative magnetoresistance arises. NaCl-type fcc lattice

In the initial manganese monosulfide α-MnS (an antiferromagnetic with NaCl-type fcc lattice), anisotropy of the electrical resistivity for two crystallographic directions [111] and [100] in the temperature range of 77–300 K [11–13] was found. A negative magnetoresistance was also found, the value of which in a field of 10 kOe is –12 % and most clearly showed in the (111) plane [14]. With an increase of the magnetic field, the magnitude of the magnetoresistance does not change, but the minimum shifts to the low temperature range.

The main drawbacks of manganese monosulfide are the small magnitude of the magneto resistive effect, the energy consumption of the synthesis technology, and the

low operating temperatures of magneto resistive elements on the basis on such materials.

The technically closest to the claimed invention is ferromanganese sulfide $FeXMn_{1-X}S$ [15–17], containing components in the following ratio, atom%: Fe 12.5–20; Mn 30–37.5 and S-50 and having a simple cubic structure such as NaCl. With an increase in the degree of cationic substitution (X) in the $FeXMn_{1-X}S$ system, a semiconductor – semimetal transition with Xc = 0.4 and an increase in magnetization are observed, with the Néel temperature increasing from 150 K for X = 0 and to 210 K for X = 0.2. Ferromanganese sulfide has GMR in the temperature range of 50 K – 250 K with the maximum development of the HMS effect (δ_H = –83 %) at 160 K in the magnetic field H = 10 kOe and δ_H = –450 % at 50 K in the field H = 30 kOe.

The drawback of the known ferromanganese sulfides $FeXMn_{1-X}S$ is the poor repeatability of the compounds obtained, the complexity and duration of the synthesis.

The aim of this work is to obtain magnetic compounds of holmium – manganese sulfides with a cubic NaCl lattice type, which have a stable and repeating effect of giant magnetoresistance in a wide temperature range.

Experimental results and their discussion. *Obtaining method and radiograph.* Three compositions of $HoXMn_{1-X}S$ were prepared; they are shown in tab. 1 in atomic%.

$HoXMn_{1-X}S$ crystals were grown by crystallization from a melt of the obtained powder sulfides with a purity of at least 99.9 %, in glassy carbon crucibles and a quartz reactor in an argon atmosphere; NH_4CNS was used as sulfiding reagents. The calculated mixture of oxides in a glassy carbon boat was placed in a quartz tube. After the air was displaced by argon and the decomposition products of ammonium thiocyanate, the furnace was turned on from a separate reactor. The synthesis was carried out in two stages: heating the mixture to 500 °C with keeping at this temperature for 1 hour; after grinding – repeated sulfiding for 3 hours at 7500–8000 °C. For completeness of sulfiding and homogenization of the resulting powder sulfide, annealing was carried out for 30 hours in a sulfiding atmosphere at 800 °C with repeated grinding of sulfides. The completeness of sulfidation was controlled by X-ray phase analysis and weight control.

For crystallization from sulphide melt, high-frequency heating of a graphite crucible 10 mm in diameter filled with 6–7 g of sulphide powder was used. A quartz reactor with a crucible was pulled at a speed of 0.5 to 1 cm / h through a single-turn inductor. The inert atmosphere in the reactor was maintained with argon. To obtain a sulphide melt, the necessary parameters of the power supplied to the inductor were determined experimentally. As a result of the synthesis, substances were obtained in the

form of dense ingots. The obtained samples were homogeneous in composition and were used for physical measurements.

According to the results of X-ray diffraction analysis, the holmium-manganese sulfides HoXMn1-XS have a NaCl-type fcc lattice [18]. With an increase of the degree of cationic substitution, the unit cell parameter *a* increases (fig. 1). No accompanying impurity phases were found in the synthesized samples.

Magnetization and magnetoresistance. The replacement of manganese with holmium ions leads to a significant change of the magnetic properties of the samples of the holmium-manganese system HoXMn1-XS. A sharp decrease in the paramagnetic Curie temperature as a result of the competition of exchange interactions and a decrease in the effective magnetic moment occurs. The microscopic mechanism of a decrease of exchange and magnetic moment is associated with a change in the electronic structure of manganese ions interacting with holmium ions. Ferromagnetic exchange interaction between manganese and holmium ions leads to an increase in the magnetic susceptibility with decrease of the temperature.

The competition of exchange interactions results in two possible variants: the disappearance of long-range magnetic order with the formation of a spin glass state [19; 20], or preservation of magnetic order in one of the spin components and with frozen transverse spin components (asperromagnetic state) [21; 22]. To determine the nature of this state, we are to measure the magnetic moment at several frequencies.

In the spin glass state, the time during which thermodynamic equilibrium is set depends on the temperature; the magnetic characteristics depend on the measurement frequency. The magnetic moment in an alternating magnetic field, shown in fig. 2, below $T = 30$ K depends on the frequency. Thus, the relative change of Re $(M (\omega = 10$ kHz$) - M (\omega = 100$ Hz$)) /$ Re $(M (\omega = 100$ Hz$))$ increases with the holmium concentration growth and Re $(M (T))$ reveals its maximum at $T = 5$ K, which is missing in HoS.

Table 1

Composition	Ho, %	Mn, %	S, %
I	10	40	50
II	17.5	32.5	50
III	20	30	50

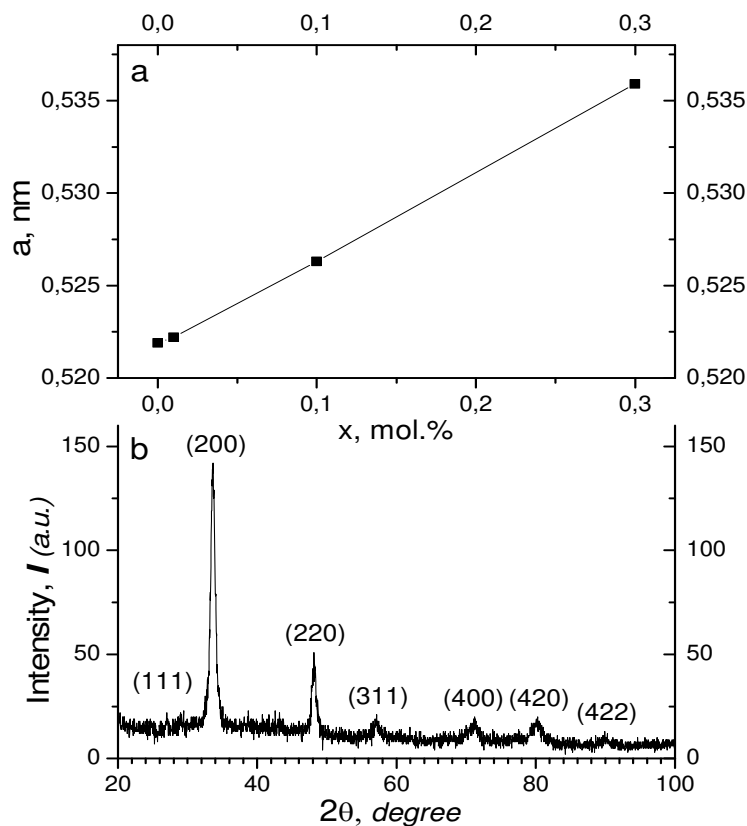Fig. 1. The lattice constant of holmium-manganese sulfide Ho$_X$Mn$_{1-X}$S versus concentration and *x*-ray for *x* = 0.3

Рис. 1. Постоянная решетки гольмий-марганцевого сульфида Ho$_X$Mn$_{1-X}$S от концентрации и рентгенограмма для *x* = 0,3

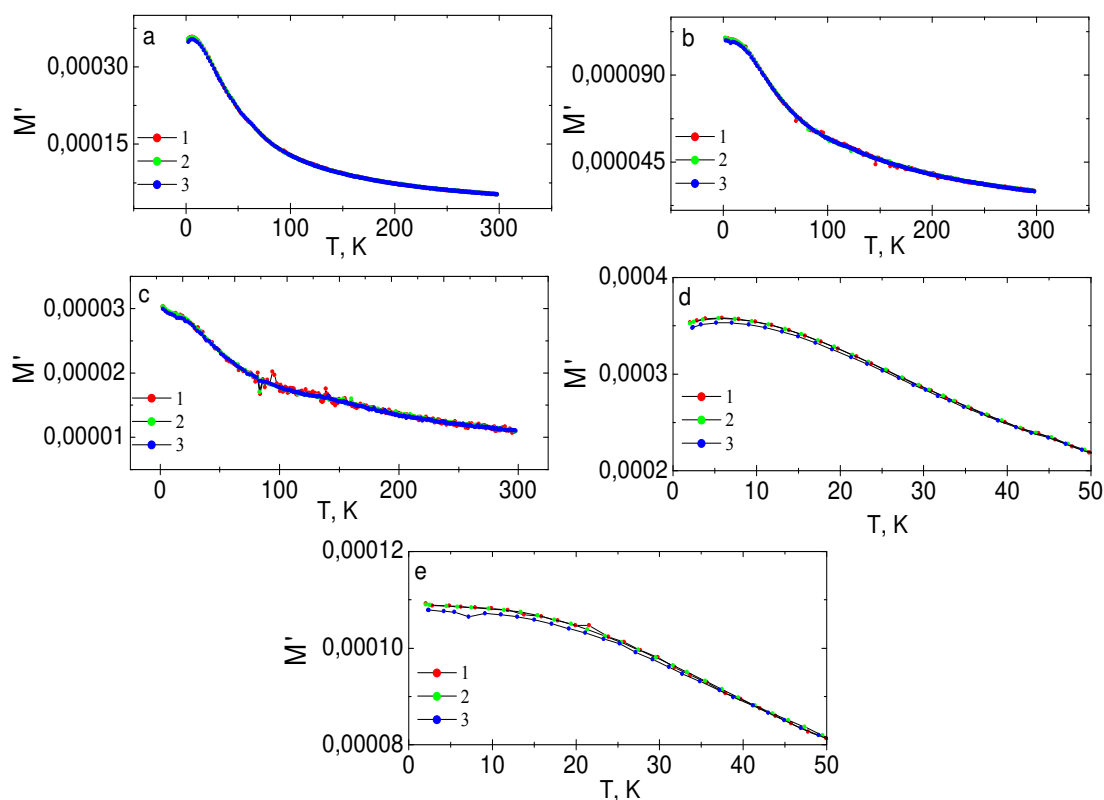Fig. 2. The Real part of the magnetic permeability (*a*, *b*, *c*) and the imaginary part (*d*, *e*) of the temperature
for Ho$_X$Mn$_{1-X}$S with *x* = 0.3 (*a*, *d*), 0.1 (*b*, *e*), 0.05 (*c*) at three frequencies ω = 1 kHz (*1*), 10 kHz (*2*), 100 kHz (*3*)

Рис. 2. Реальная часть магнитной проницаемости (*a*, *b*, *c*) и мнимая часть (*d*, *e*) от температуры
для Ho$_X$Mn$_{1-X}$S с *x* = 0,3 (*a*, *d*), 0,1 (*b*, *e*), 0,05 (*c*) на трех частотах ω = 1 kHz (*1*), 10 kHz (*2*), 100 kHz (*3*)

The imaginary part is practically independent from temperature and has the value Im (M (*T*)) ~ 10–7 for concentrations *x* ≤ 0.1 and Im (M (*T*)) is qualitatively different in the low-temperature range (fig. 2, *d*) for a composition with *x* = 0.3. The quantity Im (M (*T*)), which characterizes the decay of the magnetic moment, increases with temperature decreasing, and the derivative dIm (M) / dT passes through a maximum at *T* = 39 K at a frequency of ω = 1 kHz, at *T* = 44 K for ω = 10 kHz. An increase in the temperature of the maximum of the derivative of the imaginary part of the magnetic moment with frequency increasing is also connected with the formation of metastable states and is a characteristic feature of spin-glass behavior. It is possible that the spin relaxation mechanism is connected with the exchange interaction of localized and delocalized electrons, and the energy from the spin system is converted into the kinetic energy of current carriers [23; 24].

Replacement of manganese with a rare earth element in ReXMn$_{1-X}$S (Re = Gd, Sm, Ho) compounds [25; 26] will result in a shift of the f-level. Several variants are possible in this case, the f-level falls into the conduction band, and the electron passes from the Re ion not to the d-level of the rare-earth ion, but to the conduction band, remaining connected with the donor. If the concentration of such centers is low, less than the critical concentration for impurity band or the percolation threshold formation, then the substance will remain a semiconductor. If the f-level is located in the forbidden band near the chemical potential, extremum may appear in the temperature dependence of the resistance when the chemical potential is shifted with temperature increase [27; 28].

Substitution of manganese by a trivalent ion will cause electron doping and may induce orbital ordering [29–31], which will result in the splitting of the electron density of states. Depending on the location of the Fermi level relative to the split density of states, the electrical resistivity can change several times [32; 33].

In fig. 3, 4 the temperature dependences of the electrical resistance measured without and in a magnetic field are shown. The magnetoresistance is determined by the formula,

$$\delta_H^{ex} = \frac{\rho(H \neq 0) - \rho(H = 0)}{\rho(H \neq 0)} \cdot 100\,\% ,$$

where ρ (H = 0)) is the electrical resistance in a zero magnetic field, ρ (H ≠ 0) is the electrical resistance in a given magnetic field.

The magnetoresistance for compositions with *x* = 0.05 and *x* = 0.1 indicates that in the synthesized substances in the temperature range 100 K – 300 K, the effect of giant negative magnetoresistance is observed with the maximum effect of GMR in a magnetic field *H* = 8 kOe; the value of δ$_H$, % is –100 and –80 %, respectively.

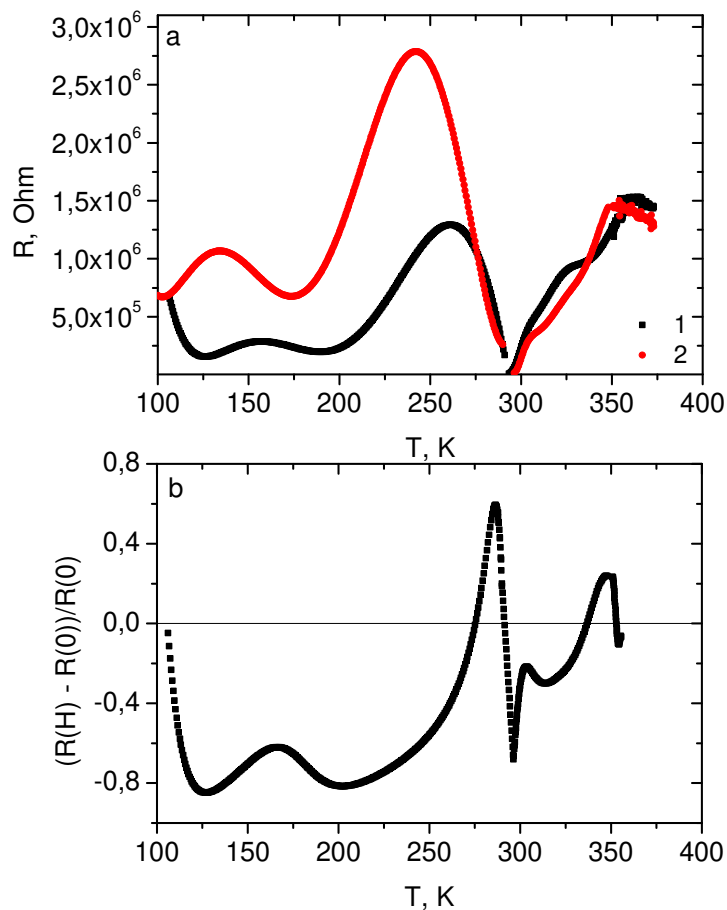Tab. 2 shows the main physical characteristics of the HoXMn$_{1-X}$S holmium-manganese sulfide system.

Fig. 3. Resistance Ho$_X$Mn$_{1-X}$S with $x = 0.1$ measured without a field (*2*)
and in a magnetic field $H = 8$ kOe (*1*) (*a*). Magnetoresistance at temperature (*b*)

Рис. 3. Сопротивление Ho$_X$Mn$_{1-X}$S с $x = 0,1$, измеренное без поля (*2*) и в магнит-
ном поле $H = 8$ kOe (*1*) (*a*). Магнитосопротивление от температуры (*b*)

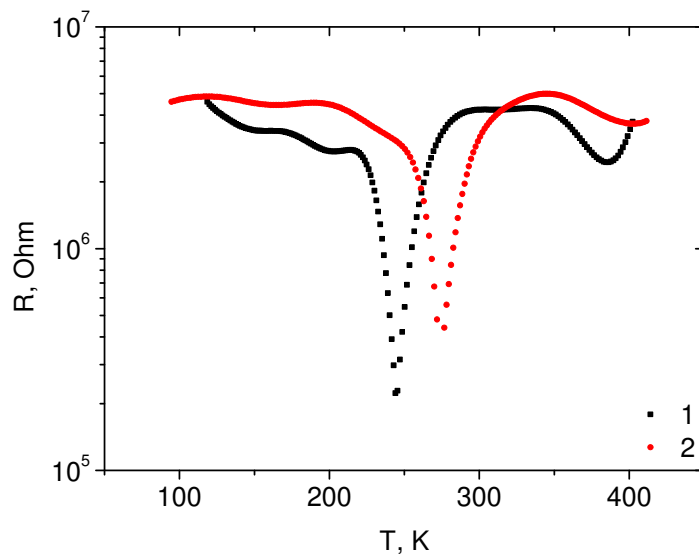Fig. 4. Resistance Ho$_X$Mn$_{1-X}$S with $x = 0.05$ measured without
a field and in a magnetic field $H = 8$ kOe

Рис. 4. Сопротивление Ho$_X$Mn$_{1-X}$S с $x = 0,05$, измеренное
без поля и в магнитном поле $H = 8$ kOe

Table 2

Ho$_X$Mn$_{1-X}$S	a, nm	$-\Theta$, K	T_N, K	δ_H, % $(H = 8$ kOe$)$	ρ, Ом·см $T = 300$ K $H = 0$
I ($X = 0.05$)	0.5242	140	145	100	$2 \cdot 10^7$
II ($X = 0.1$)	0.5256	100	134	80	$3 \cdot 10^5$
III ($X = 0.2$)	0.5303	60	112	30	10^4

Where a, nm is the crystal lattice parameter; Θ, K – paramagnetic Curie temperature; Ea, eV – activation energy; T_N, K is the Neel temperature; δ_H, % – magnetoresistance; ρ, Ohm cm – resistivity at 300 K.

Conclusion. The replacement of manganese with holmium leads to a sharp decrease in the paramagnetic Curie temperature as a result of the competition of exchange interactions in the solid solution and to a reduction of the effective magnetic moment in the concentration range $0 < X < 0.1$. The microscopic mechanism of exchange and magnetic moment decrease is connected with the change of the electronic structure of manganese ions interacting with holmium ions. Ferromagnetic exchange interaction between manganese and holmium ions causes an increase of the magnetic susceptibility with decreasing temperature in the magnetically ordered phase. The frequency dependence of the magnetic permeability at low temperatures and the maximum of the imaginary part of the magnetic permeability for $X = 0.3$, which is connected with freezing of the transverse spin components, is found.

In solid solutions HoXMn1-XS, a sharp maximum in the conductivity with respect to temperature is found, which shifts towards low temperatures in a magnetic field. A change in the sign of the magnetoresistance is reviled with an increase in temperature below and above room temperature. The results obtained can be used as perspective materials for spintronic, as components of sensor technology, magnetic memory based on the GMR effect for a wide range of temperatures and magnetic fields.

References

1. Fert A. Nobel Lecture: Origin, development, and future of spintronics. *Rev. Mod. Phys.* 2008, Vol. 80, P. 1517.

2. Barthelemy, A. Handbook of Magnetic Materials / A. Barthelemy, A. Fert, F. Petroff; ed. by K.H.J. Buschow. *Amsterdam: North Holland.* 1999, Vol. 12, P. 1–96.

3. Volkov N. V. [Spintronics: magnetic tunnel structures based on manganites]. *UFN.* 2012, Vol. 182, P. 263 (In Russ.).

4. Romanova O. B., Aplesnin S. S., Udod L. V., Sitnikov M. N., Kretinin V. V., Yanushkevich K. I., Velikanov D. A. Magnetoresistance, magnetoimpedance, magnetothermopower, and photoconductivity in silver-doped manganese sulfides. *J. Appl. Phys.* 2019, Vol. 125, P. 175706.

5. Aplesnin S. S., Sitnikov M. N., Kharkov A. M., Masyugin A. N., Kretinin V. V., Fisenko O. B., Gorev M. V. Influence of induced electrical polarization on the magnetoresistance and magnetoimpedance in the spin-disordered Tm$_x$Mn$_{1-x}$S solid solution. *Phys. Stat. Sol. B.* 2019, P. 1900043.

6. Bebenin N. G., Zainullina R. I., Ustinov V. V. [Manganites with colossal magnetoresistance]. *UFN.* 2018, Vol. 188, P. 801–820 (In Russ.).

7. Aplesnin S. S., Sitnikov M. N. [Magnetotransport effects in the ferromagnetic state in Gd$_x$Mn$_{1-x}$S]. *ZhETF.* 2014, Vol. 100, P. 104–110 (In Russ.).

8. Nagaev E. L. [Lanthanum manganites and other magnetic semiconductors with giant magnetoresistance]. *UFN.* 1996, Vol. 166, No. 8, P. 796–857 (In Russ.).

9. Kagan M. U., Kugel K. I. [Inhomogeneous charge states and phase separation in manganites]. *UFN.* 2001, Vol. 171, P. 577–596 (In Russ.).

10. Abramova G. M., Petrakovsky G. A., Vtyurin A. N., Vorotynov A. M., Velikanov D. A., Krylov A. S., Gerasimova Yu., Sokolov V. V., Bovina A. F. Magnetic properties, magnetoresistance, and Raman spectra CuV$_X$Cr$_{1-X}$S$_2$. *FTT.* 2009, Vol. 51, Vol. 3, P. 500–504.

11. Aplesnin S. S., Petrakovskii G. A., Ryabinkina L. I., Abramova G. M., Kiselev N. I., Romanova O. B. Influence of magnetic ordering on the resistivity anisotropy of α-MnS single crystal. *Solid State Communications.* 2004, Vol. 129, Iss. 3, P. 195–197.

12. Aplesnin S. S., Ryabinkina L. I., Romanova O. B., Sokolov V. V., Pichugin A. Y., Galyas A. I., Demidenko O. F., Makovetski G. I., Yanushkevich K. I. Magnetic and electrical properties of cation-substituted sulfides Me$_X$Mn$_{1-X}$S (Me = Co, Gd). *Physics of the Solid State.* 2009, Vol. 51, Iss. 4, P. 698–701.

13. Aplesnin S. S., Ryabinkina L. I., Abramova G. M., Romanova O. B., Vorotynov A. M., Velikanov D. A., Kiselev N. I., Balaev A. D. Conductivity, weak ferromagnetism, and charge instability in an α-MnS single crystal. *Phys. Rev. B.* 2005, Vol. 71, No. 1, P. 125204–125212.

14. Aplesnin S. S., Ryabinkina L. I., Romanova O. B. et al. [Magnetoresistance properties of solid solutions MnSe$_{1-x}$Te$_x$]. *FTT.* 2007, Vol. 49, P. 1984 (In Russ.).

15. Petrakovskii G. A., Loseva G. V., Ryabinkina L. I., Aplesnin S. S. Metal insulator transition and magnetic properties in disordered systems of solid solutions Me$_x$Mn$_{1-x}$S. *JMMM.* 1995, Vol. 140, P. 147–148.

16. Aplesnin S. S., Kharkov A. M., Sokolov V. V. Gigantic magnetocapacitive effect into Yb$_x$Mn$_{1-x}$S. *Abstract for Euro-Asian Symposium "Trends in magnetism", EASTMAG, Vladivostok.* 2013, P. 33–34.

17. Aplesnin S. S., Moskvin A. I. [The influence of strong electron correlations and interactions of electrons with the lattice on the electron orbital ordering]. *ZhETF.* 2010, Vol. 92, No. 4, P. 254–259 (In Russ.).

18. Aplesnin S. S., Kharkov A. M., Sitnikov M. N., Sokolov V. V. Spin reduction in the $Ho_XMn_{1-X}S$ solid solution. *JMMM*. 2013, Vol. 347, P. 10–13.

19. Aplesnin S. S. [Role of fluctuation relations for the transport properties in manganites and nichelato]. *ZhETF*. 2007, Vol. 131, No. 5, P. 878–884 (In Russ.).

20. Aplesnin S. S., Ryabinkina L. I., Romanova O. B., Bandurina O. N., Gorev M. V., Balaev A. D., Eremin E. V. [Spin-glass effects in solid solutions $Co_XMn_{1-X}S$]. *Izvestiya RAN. Seriya fizicheskaya*. 2009, Vol. 73, P. 1021–1023 (In Russ.).

21. Aplesnin S. S., Ryabinkina L. I., Romanova O. B., Sokolov V. V., Pichugin A. Yu., Galyas A. I., Demidenko O. F., Makovetskii G. I., Yanushkevich K. I. [Magnetic and electric properties of the cation-substituted sulfides $Me_xMn_{1-x}S$ (Me = Co, Gd)]. *FTT*. 2009, Vol. 51, P. 661–664 (In Russ.).

22. Aplesnin S. S. *Magnitnye i elektricheskie svoystva sil'nokorrelirovannykh magnitnykh poluprovodnikov s chetyrekhspinovym vzaimodeystviem i s orbital'nym uporyadocheniem.* [Magnetic and electrical properties of strongly correlated magnetic semiconductors with four-spin interaction and orbital ordering]. Moscow, Fizmatlit Publ., 2013, 172 p.

23. Aplesnin S. S. Influence of spin-phonon coupling on the magnetic moments in 2D spin-1/2 antiferromagnet. *Phys. Lett. A*. 2003, Vol. 313, P. 122–125.

24. Petrakovskii G. A., Ryabinkina L. I., Velikanov D. A., Aplesnin S. S., Abramova G. M., Kiselev N. I., Bobina A. F. Low-temperature electronic and magnetic transitions in the antiferromagnetic semiconductor $Cr_{0.5}n_{0.5}S$. *Phys. Sol. Stat.* 1999, Vol. 41, Iss. 9, P. 1520–1524.

25. Aplesnin S. S., Kharkov A. M., Eremin E. V., Romanova O. B., Balaev D. A., Sokolov V. V., Pichugin A. Yu. Nonuniform Magnetic States and Electrical Properties of Solid Solutions. *IEEE Transactions on magnetics*. 2011, Vol. 47, P. 4413–4416.

26. Aplesnin S. S., Romanova O. B., Kharkov A. M., Balaev D. A., Gorev M. V., Vorotinov A. M., Sokolov V. V., Pichugin A. Yu. Metal-semiconductor transition in $Sm_xMn_{1-x}S$ solid solutions. *J. Phys. Status Solidi (b).* 2012, Vol. 249, P. 812.

27. Aplesnin S. S., Romanova O. B., Kharkov A. M., Galyas A. I. [Study the transport properties of cation-substituted solid solutions $Yb_XMn_{1-X}S$]. *FTT*. 2015, Vol. 57, P. 872–876 (In Russ.).

28. Aplesnin S. S., Udod L. V., Sitnikov M. N., Velikanov D. A., Gorev M. V, Molokeev M. S., Galyas A. I., Yanushkevich K. I. Magnetic and electrical properties of bismuth cobaltite $Bi_{24}(CoBi)O_{40}$ with charge ordering. *Phys. Sol. Stat.* 2012, Vol. 54, Iss. 10, P. 2005–2014.

29. Aplesnin S. S., Moskvin A. I. Magnetic structures upon ordering of eg orbitals in a square lattice. *J. Phys.: Condens. Matt.* 2008, Vol. 20, P. 325202–325203.

30. Werner P., Gull E., Troyer M., Millis A. J. Spin Freezing Transition and Non-Fermi-Liquid Self-Energy in a Three-Orbital Model. *Phys. Rev. Lett.* 2008, Vol. 101, P. 166405.

31. Kugel K. I., Rakhmanov A. L., Sboychakov A. O., Khomskii D. I. Doped orbitally ordered systems: Possible mechanism for phase separation. *Phys. Rev. B.* 2008, Vol. 78, P. 155113.

32. Aplesnin S. S., Romanova O. B., Yanushkevich K. I. Magnetoresistance effect in anion-substituted manganese chalcogenides. *Phys. Stat. Sol. B. Basic Research*. 2015, Vol. 252, Iss. 8, P. 1792–1798.

33. Peters R., Kawakami N. Orbital order, metal-insulator transition, and magnetoresistance effect in the two-orbital Hubbard model. *Phys. Rev. B*. 2011, Vol. 83, P. 125110.

Библиографические ссылки

1. Fert A. Nobel Lecture: Origin, development, and future of spintronics // Rev. Mod. Phys. 2008. Vol. 80. P. 1517.

2. Barthelemy A. Handbook of Magnetic Materials / A. Barthelemy, A. Fert, F. Petroff; ed. by K. H. J. Buschow. Amsterdam : North Holland, 1999. Vol. 12. P. 1–96.

3. Волков Н. В. Спинтроника: магнитные туннельные структуры на основе манганитов // УФН. 2012. Vol. 182. P. 263.

4. Magnetoresistance, magnetoimpedance, magneto-thermopower, and photoconductivity in silver-doped manganese sulfides // O. B. Romanova, S. S. Aplesnin, L. V. Udod et al. / J. Appl. Phys. 2019. Vol. 125. P. 175706.

5. Influence of induced electrical polarization on the magnetoresistance and magnetoimpedance in the spin-disordered $Tm_xMn_{1-x}S$ solid solution / S. S. Aplesnin, M. N. Sitnikov, A. M. Kharkov et al. // Phys. Stat. Sol. B. 2019. P. 1900043.

6. Бебенин Н. Г., Зайнуллина Р. И., Устинов В. В. Манганиты с колоссальным магнетосопротивлением // УФН. 2018. Т. 188. С. 801–820.

7. Аплеснин С. С., Ситников М. Н. Магнитотранспортные эффекты в парамагнитном состоянии в $Gd_xMn_{1-x}S$ // ЖЭТФ. 2014. Т. 100. С. 104–110.

8. Нагаев Э. Л. Манганиты лантана и другие магнитные полупроводники с гигантским магнитосопротивлением // УФН, 1996. Т. 166, № 8. С. 796–857.

9. Каган М. Ю., Кугель К. И. Неоднородные зарядовые состояния и фазовое расслоение в манганитах // УФН. 2001. Т. 171. С. 577–596.

10. Магнитные свойства, магнитосопротивление и спектры комбинационного рассеяния $CuV_XCr_{1-X}S_2$ / Г. М. Абрамова, Г. А. Петраковский, А. Н. Втюрин и др. ФТТ. 2009. Т. 51, В. 3. С. 500–504.

11. Influence of magnetic ordering on the resistivity anisotropy of α-MnS single crystal / S. S. Aplesnin, G. A. Petrakovskii, L. I. Ryabinkina et al. // Solid State Communications. 2004. Vol. 129, Iss. 3. P. 195–197.

12. Магнитные и электрические свойства катион-замещенных сульфидов $Me_XMn_{1-X}S$ (Me = Co, Gd) / С. С. Аплеснин, Л. И. Рябинкина, О. Б. Романова и др. // ФТТ. 2009. Т. 51, В. 4. С. 661–664.

13. Conductivity, weak ferromagnetism, and charge instability in an α-MnS single crystal / S. S. Aplesnin, L. I. Ryabinkina, G. M. Abramova et al. // Phys. Rev. B. 2005. Vol. 71, No. 1. P. 125204–125212.

14. Магниторезистивные свойства твердых растворов $MnSe_{1-x}Te_x$ / С. С. Аплеснин, Л. И. Рябинкина, О. Б. Романова и др. // ФТТ. 2007. Т. 49. С. 1984.

15. Metal insulator transition and magnetic properties in disordered systems of solid solutions $Me_xMn_{1-x}S$ /

G. A. Petrakovskii, G. V. Loseva, L. I. Ryabinkina, S. S. Aplesnin // JMMM. 1995. Т. 140. С.147–148.

16. Gigantic magnetocapacitive effect into $Yb_xMn_{1-x}S$ / S. S. Aplesnin, A. M. Kharkov, V. V. Sokolov // Abstract for Euro-Asian Symposium "Trends in magnetism". EASTMAG. Vladivostok, 2013. P. 33–34.

17. Аплеснин С. С., Москвин А. И. Влияние сильных электронных корреляций и взаимодействия электронов с решеткой на орбитальное упорядочение электронов // ЖЭТФ. 2010. Т. 92, № 4. С. 254–259.

18. Spin reduction in the $Ho_xMn_{1-x}S$ solid solution / S. S. Aplesnin, A. M. Kharkov, M. N. Sitnikov, V. V. Sokolov // JMMM. 2013. Vol. 347. P. 10–13.

19. Аплеснин С. С. Роль флуктуации связей на транспортные свойства в манганитах и никелатах // ЖЭТФ. 2007. Т. 131, № 5. С. 878–884.

20. Спин-стекольные эффекты в твердых растворах $Co_xMn_{1-x}S$ / С. С. Аплеснин, Л. И. Рябинкина, О. Б. Романова и др. // Известия РАН. Серия физическая. 2009. Т. 73. С. 1021–1023.

21. Магнитные и электрические свойства катион-замещенных сульфидов $Me_xMn_{1-x}S$ (Me = Co, Gd) / С. С. Аплеснин, Л. И. Рябинкина, О. Б. Романова и др. // ФТТ. 2009. Т. 51. С. 661–664.

22. Аплеснин С. С. Магнитные и электрические свойства сильнокоррелированных магнитных полупроводников с четырехспиновым взаимодействием и с орбитальным упорядочением. М. : Физматлит, 2013. 172 с.

23. Aplesnin S. S. Influence of spin-phonon coupling on the magnetic moments in 2D spin-1/2 antiferromagnet // Phys. Lett. A. 2003. Vol. 313. P. 122–125.

24. Low-temperature electronic and magnetic transitions in the antiferromagnetic semiconductor $Cr_{0.5}n_{0.5}S$ / G. A. Petrakovskii, L. I. Ryabinkina, D. A. Velikanov et al. // Phys. Sol. Stat. 1999. Vol. 41, Iss. 9. P. 1520–1524.

25. Nonuniform Magnetic States and Electrical Properties of Solid Solutions / S. S. Aplesnin, A. M. Kharkov, E. V. Eremin et al. // IEEE Transactions on magnetics. 2011. Vol. 47. P. 4413–4416.

26. Metal-semiconductor transition in $Sm_xMn_{1-x}S$ solid solutions / Aplesnin S.S., Romanova O.B., Kharkov et al. // J. Phys. Stat. Sol. B. 2012. Vol. 249. P. 812.

27. Исследование транспортных свойств катион-замещенных твердых растворов $Yb_xMn_{1-x}S$ / С. С. Аплеснин, О. Б. Романова, А. М. Харьков, А. И. Галяс // ФТТ. 2015. Т. 57. С. 872–876.

28. Magnetic and electrical properties of bismuth cobaltite $Bi_{24}(CoBi)O_{40}$ with charge ordering / S. S. Aplesnin, L. V. Udod, M. N. Sitnikov et al. // Phys. Sol. Stat. 2012. Vol. 54, Iss. 10. P. 2005–2014.

29. Aplesnin S. S., Moskvin A. I. Magnetic structures upon ordering of eg orbitals in a square lattice // J. Phys.: Condens. Matt. 2008. Vol. 20. P. 325202–325203.

30. Spin Freezing Transition and Non-Fermi-Liquid Self-Energy in a Three-Orbital Model. Werner P., Gull E., Troyer M., Millis A. J. // Phys. Rev. Lett. 2008. Vol. 101. P. 166405.

31. Doped orbitally ordered systems: Possible mechanism for phase separation / K. I. Kugel, A. L. Rakhmanov, A. O. Sboychakov, D. I. Khomskii // Phys. Rev. B. 2008. Vol. 78. P. 155113.

32. Aplesnin S. S., Romanova O. B., Yanushkevich K. I. Magnetoresistance effect in anion-substituted manganese chalcogenides // Phys. Stat. Sol. B. Basic Research. 2015. Vol. 252, Iss. 8. P. 1792–1798.

33. Peters R., Kawakami N. Orbital order, metal-insulator transition, and magnetoresistance effect in the two-orbital Hubbard model // Phys. Rev. B. 2011. Vol. 83. P. 125110.

Sitnikov Maxim Nikolaevich – Cand. Sc., associate Professor of the Department of physics; Reshetnev Siberian State University of Science and Technology. E-mail: kineru@mail.ru

Kharkov Anton Mikhailovich – Cand. Sc., associate Professor of the Department; Reshetnev Siberian State University of Science and Technology. E-mail: khark.anton@mail.ru.

Aplesnin Sergey Stepanovich – Dr. Sc., Professor of the Department; Reshetnev Siberian State University of Science and Technology. E-mail: aplesnin@sibsau.ru , apl@iph.krasn.ru

Romanova Oksana Borisovna – Cand. Sc., Senior researcher; Kirensky Institute of Physics, Federal Research Center KSC Siberian Branch Russian Academy of Sciences. E-mail: rob@iph.krasn.ru.

Ситников Максим Николаевич – кандидат физико-математических наук, доцент кафедры физики; Сибирский государственный университет науки и технологий имени академика М. Ф. Решетнева. E-mail: kineru@mail.ru.

Харьков Антон Михайлович – кандидат физико-математических наук, доцент кафедры физики; Сибирский государственный университет науки и технологий имени академика М. Ф. Решетнева. E-mail: khark.anton@mail.ru.

Аплеснин Сергей Степанович – доктор физико-математических наук, профессор, заведующий кафедрой физики; Сибирский государственный университет науки и технологий имени академика М. Ф. Решетнева. E-mail: aplesnin@sibsau.ru, apl@iph.krasn.ru.

Романова Оксана Борисовна – кандидат физико-математических наук, старший научный сотрудник; Институт физики им. Л. В. Киренского Сибирского отделения Российской академии наук – обособленное подразделение ФИЦ КНЦ СО РАН. E-mail: rob@iph.krasn.ru.